UNIVERSITY OF OXFORD

Heterogeneity in Ewing sarcoma

Submitted for the Degree of Doctor of Philosophy

By

Harriet Alice Branford White

Lincoln College
Oxford
Michaelmas 2013

Heterogeneity in Ewing Sarcoma

Submitted for degree of Doctor of Philosophy
By
Harriet Branford White
Lincoln College
Oxford
Michaelmas 2013

Thesis Abstract

Ewing sarcoma, an aggressive primary bone and soft tissue tumour is characterised by the expression of the chimeric transcription factor EWS-FLI1 in 90% of patients. This alters expression of many genes including activation of the Insulin Growth Factor (IGF) pathway via IGFBP3 supression. Phase I/II trials with an IGF-1 inhibitor have demonstrated tumour regression in a modest number of Ewing sarcoma patients.

The aim of this thesis was to identify mechanisms contributing to the heterogeneity of resistance in Ewing sarcoma following inhibition with OSI-906, a dual kinase inhibitor of IGF-1 (IGF-1R) and Insulin (IR) receptors. The hypothesis was that mechanisms of resistance relate to heterogeneity of responses to signalling pathway activation and inhibition. Through selection, disruption of the pathway would identify subpopulations of cells both sensitive and resistant in their response allowing for interrogation of resistance mechanisms.

A genome wide approach was taken to model the resistance profile of cell lines. Through developing a method of unbiased quantification, a panel of validated Ewing sarcoma cell lines (EuroBoNet) were imaged and segmented to assess the responses of biomarkers on signalling pathway activation. Heterogeneity was confirmed between cell lines. The application to diagnostic biopsies led to the identification of prognostic classifiers and cellular subpopulations with clinical prognostic significance. The distribution of Ki67 was found to be predictive of survival and cells with lower levels of CD99 in the cytoplasm were most discriminative. Parallel sequencing strategies (RNA-seq, whole exome sequencing, and aCGH/ SNP array) for genome-wide screening was carried out for point mutations, copy number changes and rearrangements. Systematic detection was used to characterise genomic rearrangements and functional validation performed. Resistant clones, formed via ENU mutagenesis of cell lines, were sequenced in order to demonstrate the resistance profile of OSI-906.

In summary heterogeneity of Ewing sarcoma at the genomic and proteomic level can influence the signalling dependency of tumours and response to inhibitors. Genomic and proteomic profiling of tumour cells may be relevant to future developments of novel therapies.

Acknowledgements

Firstly thanks must go to Professor Bass Hassan who gave me an amazing opportunity not only to carry out this work but also learn so much about cancer biology of which I knew very little. Rarely do you meet someone with such infectious enthusiasm or dedication to their profession and it has been a privilege to work alongside him for the past few years.

My experience in the Hassan Lab has been brilliant and I have enjoyed my time there very much. I have laughed and learnt a lot and been blessed with great colleagues who are now good friends. In particular Dr David Barnes who has been so kind providing endless support, the answers to a million questions, and who has never wavered in his patience of me. Also huge thanks goes to Dr Claudia Bühnemann with whom I have spent many hours sat at a microscope and beyond helping me with imaging, has been a lovely friend.

I would like to acknowledge Joint Action Research, and Biomedical research centre for their financial support and also the Sir William Dunn School of Pathology for further funding. Thanks must also be given to all the collaborators I have worked with: the EuroBoNet and EuroSarc networks who provided cell lines and vital opportunities to meet other European groups working in related fields, and all those at OGT who performed the sequencing of cell lines.

Finally, I would like to offer gratitude to those suffering from Ewing sarcoma, who are so brave, face so much, and yet are selfless enough to consent to trials, extra blood tests, biopsy samples, scans, and hospital appointments which allow for work such as this to be carried out. Every day, for the past three years I have cycled past the home of Alice Liddell and the setting of the Mad Hatter's tea party and I hope that, unlike Alice, the answer to the riddle which lies behind the cure for Ewing sarcoma is a little closer to being solved.

"Have you guessed the riddle yet?" the Mad Hatter said, turning to Alice again.
"No, I give it up," Alice replied: "What's the answer?"
"I haven't the slightest idea," said the Hatter.

Extract from Alice's Adventures in Wonderland, Lewis Carroll.

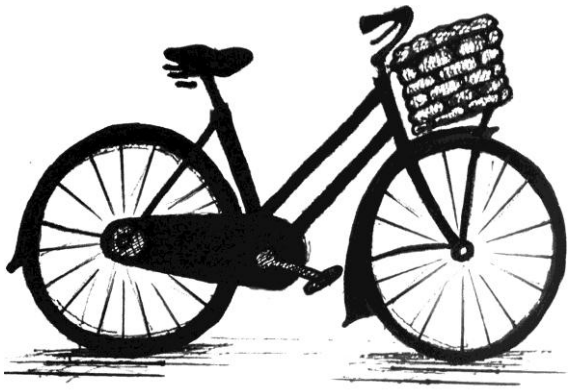


Table of Contents

Table of Figures x
Table of Tables xii
1 Introduction 1
1.1 Ewing sarcoma and the patient 1
1.1.1 Clinical presentation 1
1.1.2 Diagnostic tools 2
1.1.3 Treatment 3
1.1.4 Outcome 3
1.2 EWS-FLI1 translocation 4
1.2.1 Ewing sarcoma cell of origin 6
1.3 Insulin-like growth factor pathway in Ewing sarcoma 11
1.3.1 Insulin-like growth factor 1 receptor 14
1.3.2 Insulin-like growth factor inhibitors 14
1.3.3 Clinical experience of IGF-1R in Ewing sarcoma 15
1.4 Tumour heterogeneity 18
1.5 Next generation sequencing and its role in targeted therapy 18
1.5.1 Sanger vs. Next Generation Sequencing 20
1.6 Aims 23
2 Materials and Methods 24
2.1 Cell Lines 24
2.2 Cell culture 24
2.3 Immuno-labelling 24
2.4 RNA extraction, reverse transcription and quantitative real-time PCR 27
2.4.1 RNA extraction 27
2.4.2 RNA quantity and quality assessment 27
2.4.3 Reverse transcription of RNA 27
2.4.4 Quantitative real-time reverse transcription PCR 28
2.4.5 RT-qPCR primers and probes 30
2.4.6 qPCR reactions 32
2.4.7 Reaction efficiencies 32
2.4.8 RT-qPCR analysis 33
3 Quantification of the heterogeneity of prognostic cellular biomarkers in tumour tissues 34
3.1 Introduction 34
3.1.1 Confocal Microscopy 36

3.1.2 Image analysis 37
3.1.3 Segmentation 38
3.1.4 Validation 38
3.2 Chapter Aims 40
3.3 Methods 41
3.3.1 Cell culture conditions 41
3.3.2 Immuno-labelling of Ewing cell lines grown on coverslips 41
3.3.3 Paraffin-embedded cell cores 41
3.3.4 Tissue Microarrays (TMAs) 42
3.3.5 Immuno-labelling of TMAs 43
3.3.6 Image acquisition 43
3.3.7 Image segmentation 43
3.4 Results 45
3.4.1 Developing an unbiased method to assess for heterogeneity in Ewing sarcoma cell lines and biopsy tissue 45
3.4.2 Intracellular biomarker localisation changes in response to IGF-2 45
3.4.3 Validation of image analysis in Ewing sarcoma cell lines 48
3.4.4 Heterogeneity of signalling is seen in Ewing sarcoma cell lines 51
3.4.5 FoxO3a translocation in response to IGF-2 is heterogeneous in Ewing cell lines 53
3.4.6 pS6 increases in intensity when Ewing cell lines are exposed to IGF-2 53
3.4.7 Egr1 translocates from 1 out 10 of Ewing cell lines on exposure to the ligand 53
3.4.8 Application of image segmentation algorithm to Ewing sarcoma cell cores 56
3.4.9 Unbiased quantification can be applied to Ewing sarcoma biopsies 56
3.5 Discussion 60
3.5.1 Development of a method of unbiased quantification confirms heterogeneity in Ewing sarcoma cell lines 60
3.5.2 Heterogeneity of signalling responses between Ewing sarcoma cell lines ... 61
3.5.3 Application of validated algorithm to Ewing sarcoma tissue biopsies 62
3.5.4 A subpopulation of cells with high Ki67 expression are identified as a potential prognostic marker 62
4 Characterisation of Ewing sarcoma cell lines and response to OSI-906, a dual kinase inhibitor 64
4.1 Introduction 64
4.1.1 OSI-906, dual kinase inhibitor 64
4.1.2 Cancer stem cells and heterogeneity in Ewing sarcoma 65
4.1.3 ABC transporters and drug resistance 67

4.2 Chapter Aims 68
4.3 Materials and Methods 69
4.3.1 Cell labelling with Aldefluor assay 69
4.3.2 qPCR of sorted aldefluor cells 69
4.3.3 Colony forming assay of cell lines 69
4.3.4 Preparation of OSI-906 70
4.3.5 Cell viability assay 70
4.3.6 SDS-PAGE electrophoresis and immunoblotting 70
4.3.7 EdU labelling 71
4.3.8 Measurement of apoptosis 72
4.3.9 Cell cycle analysis 73
4.3.10 Flow cytometry analysis 74
4.4 Results 75
4.4.1 Ewing sarcoma cell lines vary in their expression of IR and IGF-1R genes 75
4.4.2 Cell surface expression of IGF-1R and IR protein varies within cell lines 75
4.4.3 Proliferation of Ewing sarcoma cell lines increases in response to IGF-2 79
4.4.4 Ewing sarcoma cell lines have a subpopulation of cells with high expression of aldehyde dehydrogenase 79
4.4.5 Expression of stem cell genes is not related to ALDH expression in Ewing sarcoma cell lines 83
4.4.6 Colony formation is increased in the ALDH high fraction of Ewing sarcoma cells 85
4.4.7 RD-ES and STA-ET1 express ABC transporter genes most highly 87
4.4.8 Ewing sarcoma cell lines confer overall sensitivity to OSI-906 89
4.4.9 OSI-906 inhibits IGF stimulated IGF-1R phosphorylation and downstream pathways in Ewing sarcoma cell 91
4.4.10 Proliferation of Ewing sarcoma cell lines is decreased by OSI-906 91
4.4.11 OSI-906 induces apoptosis in A673, CHP-100 and SK-N-MC 95
4.4.12 Cell cycle is not altered by OSI-906 95
4.5 Discussion 98
4.5.1 Ewing sarcoma cell lines differentially express IGF-1R and IR 98
4.5.2 OSI-906 is inhibitory to Ewing sarcoma cell lines 99
4.5.3 ALDH and Ewing sarcoma stem cells 99
4.5.4 Expression of ABC transporters in Ewing sarcoma 100
5 Genome wide analysis of Ewing sarcoma cell lines 102
5.1 Introduction 102
5.1.1 Clinical application of NGS 102

5.1.2 RNA-sequencing 105
5.2 Chapter Aims 107
5.3 Methods 108
5.3.1 Preparation of samples for RNA-seq , whole exome sequencing, and CNV 108
5.3.2 NGS Analysis 108
5.3.3 Primer design for expression of RP 11-680G10.1-GSE1 translocation 116
5.3.4 Etoposide 116
5.3.5 Cisplatin 116
5.3.6 Olaparib 117
5.3.7 Retinoic Acid 117
5.3.8 Imatinib 117
5.4 Results 118
5.4.1 NGS of a panel of Ewing sarcoma cell lines 118
5.4.2 RNA-seq of panel of Ewing sarcoma cell lines identifies translocations 120
5.4.3 Novel translocations and fusion protein identified in Ewing sarcoma cell lines 128
5.4.4 A673 demonstrates relative resistance to etoposide 131
5.4.5 CHP-100 has a gain of 1q 131
5.4.6 Copy number of CDKN2A is decreased in cell lines 133
5.4.7 c-Myc is over-expressed in CHP-100 133
5.4.8 p53 mutations are present in CHP-100, SK-N-MC and STA-ET1 133
5.4.9 Common 46 genes gained and 47 genes lost across panel of cell lines 139
5.4.10 Specific gene mutations reported on whole exome sequencing and RNA-seq 139
5.5 Discussion 151
5.5.1 Use of NGS in genomic analysis of Ewing sarcoma cell lines 151
5.5.2 RD-ES was not confirmed as a Ewing sarcoma cell line 151
5.5.3 RNA-seq reveals presence of RP11680G10.1-GSE1 fusion protein generated by intergenic deletion 152
5.5.4 Etoposide sensitivity varies between cell lines 153
5.5.5 CDKN2A has a loss of copy number in most cell lines 153
5.5.6 Ewing sarcoma cell lines are sensitive to PARP inhibitors 154
5.5.7 Identification of potentially actionable mutations 154
6 Actionable target in Ewing sarcoma 156
6.1 Introduction 156
6.2 Connector enhancer of kinase (CNK) suppressor of Ras 156

6.2.1 CNK2 158
6.2.2 CNK1 158
6.3 Chapter Aims 161
6.4 Methods 162
6.4.1 qPCR expression of CNKSR2 and CNKSR1 162
6.4.2 RNA extraction and RT-PCR from FFPE fixed Ewing sarcoma patient tumours 162
6.4.3 siRNA knockdown CNKSR2 162
6.4.4 Knockdown of CHP-100 and SK-N-MC with siRNA CNKSR2 and OSI-906 treatment 163
6.4.5 Immunofluorescence of CNKSR1 and CNKSR2 on exposure to OSI-906 163
6.5 Results 165
6.5.1 Expression of CNKSR2 is elevated in cell line SK-N-MC 165
6.5.2 Expression of KIF1B-CNKSR2 fusion gene in samples from 62 patients, taken from 3 European cohorts 165
6.5.3 Calculation of siRNA knockdown using qPCR analysis 169
6.5.4 siRNA knockdown of CNKSR2 was optimal at 24 hours 169
6.5.5 Sensitivity of SK-N-MC to OSI-906 is reduced with siRNA knockdown of CNKSR2 171
6.5.6 Knockdown of CHP-100 infers increased resistance to OSI-906 171
6.5.7 CNKSR1 is elevated in A673, CHP-100, and RM-82 173
6.5.8 CNKSR1 localises to the cytoplasm and CNKSR2 to the nucleus shown by immunofluorescence 173
6.6 Discussion 179
6.6.1 CNKSR1 is expressed in Ewing sarcoma cell lines 179
6.6.2 CNKSR2 may act as a lineage survival factor in SK-N-MC 179
6.6.3 Summary 181
7 Use of N-ethyl-N-nitrosourea (ENU) mutagenesis to identify potential mechanisms of resistance to OSI-906 182
7.1 Introduction 182
7.1.1 Methods to generate resistant mutations 184
7.1.2 N-ethyl-N-nitrosourea (ENU) 185
7.2 Chapter Aims 187
7.3 Methods 188
7.3.1 Transformation of competent cells with pRetroQ-mCherry-N1 Vector 188
7.3.2 Puromycin dose for antibiotic selection of transfected cells 188
7.3.3 Retroviral Transduction of Ewing sarcoma cell lines with pRetroQ-mCherry-N1 Vector 189

7.3.4 Preparation of ENU 189
7.3.5 Establishing optimal ENU dose 190
7.3.6 Mutagenesis screen for SK-N-MC and STA-ET1 190
7.3.7 Mutagenesis screen for A673 and CHP-100 191
7.3.8 Resistance Screen 192
7.4 Results 193
7.4.1 Determination of the optimal dose of puromycin for selection of pRetroQ-mCherry-N1 Vector transduced Ewing cell lines 193
7.4.2 Transduction of Ewing sarcoma cell lines with pRetroQ-mCherry-N1 was confirmed by flow cytometry 193
7.4.3 The optimal dose of ENU for the mutagenesis screen was determined to be 1mM 195
7.5 Discussion 201
8 Discussion and future work 203
8.1.1 The potential importance of genetic heterogeneity in Ewing sarcoma 203
8.1.2 IGF signalling pathway heterogeneity and its effect on responses in Ewing sarcoma cell lines 205
8.1.3 Next generation sequencing has a role in the future understanding of Ewing sarcoma 206
8.1.4 Drug resistance in Ewing sarcoma 208
8.1.5 Testing resistance at a single cell level 210
8.1.6 Summary 211
9 Appendix 213
10 References 215

Table of Figures

Figure 1-1. Schematic of EWS-FLI1 translocation.. 10
Figure 1-2. Schematic of IGF pathway. 13
Figure 3-1. Strategy of work and antibody localisation 47
Figure 3-2. Signalling responses were quantified after treatment with IGF-2. 50
Figure 3-3. Responses of cell lines to IGF-2. 52
Figure 3-4. Signalling pathway activity was quantified by image analysis. 55
Figure 3-5. Confocal images of agar pellets of EWS-FLI1 positive Ewing sarcoma cell lines were used to optimise image segmentation..... 58
Figure 3-6. Random forest machine learning predicts a correlation between survival and cells which have low cytoplasmic labelling of CD99 and Ki67 positive cells..... 59
Figure 4-1. Ewing sarcoma cell lines vary in their expression of IR and IGF-1R genes. .76
Figure 4-2. Expression of IGF-1R and IR in Ewing sarcoma cell lines measured by flow cytometry. 77
Figure 4-3. Proliferation in Ewing sarcoma cell lines increases in response to IGF-2 in a dose dependent manner. 78
Figure 4-4. CHP-100 cells show ALDH expression which is inhibited by DEAB. 81
Figure 4-5. Illustration of cell population (CHP-100 in this example) sorted for ALDH, a marker of stemness. 82
Figure 4-6. ALDH high cell populations do not increased expression of stem cell genes..84
Figure 4-7. ALDH sorted cells show variation in colony forming potential..... 86
Figure 4-8. ABC transporter genes have varied expression in Ewing sarcoma cell lines...88
Figure 4-9. Ewing sarcoma cell lines respond to treatment with OSI-906..... 90
Figure 4-10. PhosphoIGF-1R/IR is inhibited by OSI-906. 92
Figure 4-11. Treatment with OSI-906 results in blockade of phosphoMAPK and AKT.... 92
Figure 4-12. OSI-906 decreases proliferation of Ewing sarcoma cell lines. 93
Figure 4-13. Proliferation of Ewing sarcoma cell lines is inhibited by OSI-906. 94
Figure 4-14. Representation of apoptosis analysis by FAM-FLICA™ assay. 96
Figure 4-15. Apoptosis was shown in cell lines in response to OSI-906. 96
Figure 4-16. The effect of OSI-906 on cell cycle. 97
Figure 5-1. Workflow of enrichment and library preparation for whole exome sequencing. 110
Figure 5-2. Preparation of DNA for whole exome sequencing with SureSelect Target Enrichment..... 111
Figure 5-3. Illustration of mapping and alignment of whole exome sequencing. 112
Figure 5-4. Preparation of samples for RNA-seq. 114
Figure 5-5. RNA-seq analysis pipeline..... 115
Figure 5-6. Circos plots of somatic modifications in Ewing sarcoma cell lines. 119
Figure 5-7. The novel fusion of RP11-GSE1 does not result in increased expression of GSE1..... 129
Figure 5-8. A673 is resistant to etoposide in comparison to other Ewing sarcoma lines..130
Figure 5-9. CHP 100 has gained copies of 1q. 132
Figure 5-10. CDKN2A is lost in 3 Ewing sarcoma cell lines..... 135
Figure 5-11. c-Myc is over-expressed in a panel of cell lines. 136
Figure 5-12. Cell lines have gains and losses in copy number. 137
Figure 5-13. Gains and losses shared by A673, CHP-100, SK-N-MC and STA-ET1..... 138
Figure 5-14. SK-N-MC and STA-ET1 demonstrated sensitivity to cisplatin. 146
Figure 5-15. STA-ET1 shows increased sensitivity to the PARP inhibitor olaparib. 146

Figure 5-16. Ewing sarcoma cell lines appear to be resistant to exposure to retinoic acid. 149
Figure 5-17. Ewing sarcoma cell lines are resistant to the effect of imatinib. 150
Figure 6-1. Schematic representation of CNK pathway. 159
Figure 6-2. Schematic depiction of CNK proteins. 160
Figure 6-3. Schematic of KIF1B-CNKSR2 fusion protein as a result of the translocation identified in SK-N-MC. 160
Figure 6-4. Expression of CNKSR2 is elevated in SK-N-MC which harbours a translocation of KIF1B-CNKSR2.. 166
Figure 6-5. CNKSR2 gene expression is elevated in SK-N-MC 166
Figure 6-6. Expression of KIF1B-CNKSR2 fusion gene is analysed in patient sample from three European centres.....167
Figure 6-7. Sanger sequencing confirms the presence of the KIF1B-CNKSR2 translocation in a patient sample.. 168
Figure 6-8. Knockdown of CNKSR2 confers 4.5 fold increase in sensitivity to OSI-906 in SK-N-MC and a decrease of 1.5 fold in CHP-100. 172
Figure 6-9. CNKSR1 expression is elevated in A673, CHP-100 and RM-82.....175
Figure 6-10. Representative confocal microscopy images showing cytoplasmic CNKSR1 with and without treatment with OSI-906 in Ewing sarcoma cell lines. 176
Figure 6-11. CNKSR2 shows nuclear localisation in Ewing sarcoma cell lines. 177
Figure 6-12. Cellular localisation of CNKSR1 and CNKSR2 in response to OSI-906 in Ewing sarcoma cell lines. 178
Figure 7-1. Ewing sarcoma cell lines were transduced with pRetroQ-mCherry-N1 retrovirus followed by puromycin selection. 194
Figure 7-2. ENU kill curves for Ewing sarcoma cell lines. 194
Figure 7-3. Initial strategy for formation of resistant clones using ENU mutagenesis. 196
Figure 7-4. Amended method for ENU mutagenesis to generate resistant clones for cell lines SK-N-MC and STA-ET1. 197
Figure 7-5. Mutant clones viewed under an inverted light microscope at x4 magnification following 3 weeks growth. 198
Figure 7-6. Resistant clones are generated in the ENU mutagenesis screen. 199
Figure 7-7. Principle of ENU mutagenesis used to re-sensitise resistant cell lines A673 and CHP-100 to OSI-906.. 200
Figure 9-1. Standard curves for Actin, B2M and BMI1 genes. 213
Figure 9-2. Standard curve for ALDH, CD99 and EWS-FLI1 primer/probes. 214

Table of Tables

Table 1-1. Response of IGF-1R inhibitors used in clinical trials 17
Table 2-1. Primary antibodies with dilutions 26
Table 2-2. Secondary fluorescent antibodies with dilutions 26
Table 2-3. Reverse transcription mastermix 29
Table 2-4. RT-qPCR mastermix 29
Table 2-5. qPCR primer sequences and corresponding probe/ SYBR. 31
Table 3-1. Cell lines obtained from EuroBoNet. 46
Table 3-2. Validation of cell line nuclear segmentation. 49
Table 3-3. Survival data from 118 patients from three separate European cohorts which correlate to biopsy samples analysed. 59
Table 5-1. Quality control metrics for CNV by CGH/SNP arrays. 113
Table 5-2. RNA from cell lines A673 (top) and CHP-100 (bottom) were sequenced by Illumina NGS and fusion genes identified. 121
Table 5-3. RNA-seq to a read depth of $4x10^7$ paired end reads confirms the presence of EWS-FLI1 translocation in SK-N-MC and STA-ET1. 122
Table 5-4. RNA-seq did not demonstrate the presence of the expected EWS-FLI1 translocation in RD-ES. 123
Table 5-5. RM-82 and STA-ET10 are confirmed to express atypical translocations of EWSR1-ERG and EWSR1-FEV respectively. 124
Table 5-6. Quality control metrics for whole exome sequencing. 141
Table 5-7. All variants identified by whole exome sequencing. 142
Table 5-8. SK-N-MC and STA-ET1 both harbour potentially harmful mutations of BRCA1. 145
Table 6-1. siRNA knockdown of CNKSR2 is most abundant at 24 hours. 170

Abbreviations

ABC	ATP-binding cassette transporter
AKT	Protein Kinase B
C	Celsius
CGH	Comparative genomic hybridization
DAPI	4',6-diamidino-2-phenylindole
DNA	Deoxyribonucleic acid
EdU	5-ethynyl-2'-deoxyuridine
EGF	Epidermal growth factor
ERK	Extracellular signal regulated kinases
ENU	N-ethyl-N-nitrosourea
FACS	Fluorescence activated cell sorting
FCS	Foetal calf serum
FFPE	Formalin fixed paraffin embedded
IGF	Insulin growth factor
IgG	Immunoglobulin G
IR	Insulin receptor
IRS	Insulin receptor substrate
LOH	Loss of heterozygosity
mAb	Monoclonal antibody
MAPK	Mitogen-activated protein kinase
MEK	Mitogen-activated protein kinase kinase
MOS	Median overall survival
NGS	Next generation sequencing
PBS	Phosphate buffered saline
PCR	Polymerase chain reaction
PFS	Progression free survival
PI3K	Phosphoinositide 3-kinase
PIP2	Phosphatidylinositol (4,5) triphosphate
PIP3	Phosphatidylinositol (3,4,5) triphosphate
PNET	Primitive neuroectodermal tumours
QPCR	Quantitative polymerase chain reaction
RNA	Ribonucleic acid
RT	Reverse transcription
SDS	Sodium dodecyl sulphate
SEM	Standard error of mean
TBS	Tris buffered saline
TBST	Tris buffered saline plus tween
TKI	Tyrosine kinase inhibitor
UPL	Universal probe library
VEGF	Vascular endothelial growth factor

1 Introduction

In 1921 James Ewing first recognised the presence of a malignant small cell tumour of bone. He described "broad sheets of small polyhedral cells with pale cytoplasm, small hyper chromatic nuclei, well-defined cell borders and complete absence of inter cellular material". This typical small cell appearance represents classical Ewing sarcoma, Askin's tumour and primitive neuroectodermal tumours (PNET). The more recent 2013 WHO classification describes "A small, round cell sarcoma showing pathognomonic molecular findings, and varying degrees of neuroectodermal differentiation by light or electron microscopy or immunohistochemistry" (Fletcher 2013).

1.1 Ewing sarcoma and the patient

1.1.1 Clinical presentation

Ewing sarcoma is the second most common primary bone sarcoma of children and young adults comprising 39% of cases after osteosarcoma which makes up 54% of cases. The incidence of Ewing sarcoma in the United Kingdom is 13 per million 0-24 year olds per year (Cotterill, Ahrens et al. 2000, Siddle 2011). The incidence is most common in children of 10-14 years of age as it is believed the incidence of tumours peaks during puberty when bones are experiencing rapid growth (Eyre, Feltbower et al. 2009). The median age at presentation is 14 years and there is a slight male to female predominance of 3:2. It is known to have a lower incidence amongst black and Asian populations (Parkin, Stiller et al. 1993, Postel-Vinay, Véron et al. 2012).

Most commonly it arises in the diaphysis or meta-diaphyseal region of the long bones and plain radiographs demonstrate osteolytic, permeative lesions often with the characteristic "onion-skin" appearance of the periosteum on radiographs. Poor prognostic factors include

older patient age, high tumour volume, pelvic location, and poor response to chemotherapy (Baldini, Demetri et al. 1999, Seddon and Whelan 2008). It most commonly metastasises to the lungs (50%) followed by bone (25%) (Grier 1997).

The majority of patients with Ewing sarcoma present with pain or a palpable mass. Following plain radiographs and a chest x-ray patients go on to have whole limb (or compartment) MRI before receiving an image guided biopsy (either Ultrasound or CT). The biopsy should be undertaken following discussion with the operating surgeon in order to ensure that all possible reconstructive options remain available by preventing contamination of unnecessary tissue compartments (Balamuth and Womer 2010). Once this is made, patients will go on to need a bone scan and CT imaging of the chest in order to exclude pulmonary metastatic disease.

1.1.2 Diagnostic tools

Histologically Ewing sarcoma shows the presence of undifferentiated small round cells with scant cytoplasm which are also a feature of a larger group of tumours such as rhabomyosarcoma, neuroblastoma, small cell osteosarcoma, poorly differentiated synovial sarcoma, non-Hodgkins lymphoma, and mesenchymal chondrosarcoma so diagnosis can be difficult. Many can be distinguished by conventional immunohistology however molecular diagnostics such as PCR or FISH can be used to identify specific translocations (Bovée and Hogendoorn 2010). Considering ultrastructure, Ewing sarcoma cells are fairly uniform in size although their profiles are polygonal due to being closely packed. Nuclei are oval with small nucleoli, relatively few organelles, with cell cytoplasms which contain lakes of glycogen (Suh, Ordóñez et al. 2002).

Improved radiology and the advent of molecular markers have redefined the process of diagnosis for Ewing sarcoma. A useful diagnostic tool is the gene product of MIC2. This is

a pseudoautosomal gene localised on the short arm of chromosomes X and Y which codes for CD99, a 32kDa transmembrane glycoprotein (Gelin, Aubrit et al. 1989). CD99 is highly expressed on haematopoietic cells (T lymphocytes) and Ewing sarcoma cells. High serum lactate dehydrogenase levels have been shown to demonstrate a lower overall survival in patients in a systematic review of molecular and biological markers in the Ewing sarcoma family (Riley, Burchill et al. 2003).

1.1.3 Treatment

Typically treatment initially involves cytoreduction with chemotherapy in order to reduce the chance of micrometastatic spread and facilitate local control (ie negative resection margins). Definite local control is achieved most commonly through surgical resection (and reconstruction when required) however occasionally radiation may be used should surgery present a significant risk to the patient. Following post operative recovery and wound healing, patients undergo adjuvant chemotherapy in order to minimise the risk of recurrence.

1.1.4 Outcome

Amongst 19 European countries there has been an improvement in 5 year survival from 34% to 66% in the period between 1979-1982 and 1993-1997 respectively (Stiller, Bielack et al. 2006). This was supported by Eyre et al. who found that in a study of childhood bone cancer in northern England and the West Midlands between 1981-2002, there was also an improvement in survival with rates being 37.5% between 1981-1987, 66% between 1988-1994, and 70% for cases diagnosed in 1995-2000 (Eyre, Feltbower et al. 2009). This is most likely to be due to the dramatic change occurring in the late 1970s and early 1980s when treatment for such patients went from local therapy alone (ie surgery or radiotherapy) to local treatment plus systemic dose intensive chemotherapy (Balamuth and

Womer 2010). However, despite aggressive chemotherapy, surgical reconstruction and dose intensive radiotherapy for local control, the survival for Ewing sarcoma remains 60-70% at 5 years. Moreover, this survival comes at some cost, including late morbidity due to chemotherapy and radiotherapy (infertility, cardiac toxicity, secondary malignancy), as well as reconstructive surgery and psychological morbidity thereby supporting the role for tailoring therapeutic approaches to patients' needs.

The presence of metastatic disease at diagnosis worsens patient survival to around 30% at five years suggesting that those with metastatic or recurrent disease require a distinct approach compared to simply that of local control (Carvajal and Meyers 2005).

1.2 EWS-FLI1 translocation

In 1983 the presence of a specific genetic translocation, EWS-FLI1 t(11;22)(q24;q12) was identified in Ewing sarcoma and is believed to be present in around 85-90% of patients (Aurias, Rimbaut et al. 1983, Turc-Carel, Philip et al. 1983). The EWS gene on chromosome 22 encodes a widely-expressed and highly conserved RNA-binding protein (Figure 1-1). The amino terminus of EWS is fused with the DNA-binding domain of FLI1, a member of the ETS (erythroblastalis transforming-virus-1) family of transcription factors which are involved with cell proliferation and development. In approximately 10% of patients, EWS fuses with ERG, another member of the ETS family with other fusion partners such as ETV1, ET4, or FEV being more rare fusion types (<1% each). Due to a clear association of the expression of EWS-ETS fusion proteins with Ewing sarcoma it is considered that the fusion is the key to the development. Previously retrospective studies using cohorts of less than 100 patients suggested that different fusions had an association with prognosis of the disease and could influence patient management (de Alava, Kawai et al. 1998). The recent prospective Euro-E.W.I.N.G.99 trial which included 565 patients did

not support this (Le Deley, Delattre et al. 2010). Variability in the breakpoint of the fusion causes the formation of RNA which translates into different proteins. Such break points most commonly occur in EWS introns 7 or 8 and FLI1 introns 5 or 4 leading, in 51% of cases, to a type 1 fusion, or EWS exon 7 to FLI1 exon 6 or exon 5, known as a type 2 fusion which occurs in 27% of cases. Previous studies suggested that those with a type 1 fusion had a prognostic advantage over others. The Euro-E.W.I.N.G.99 study did not confirm this to be the case, nor any other advantage for other fusion type (Zoubek, Dockhorn-Dworniczak et al. 1996, de Alava, Kawai et al. 1998, Le Deley, Delattre et al. 2010).

Due to a clear association of the expression of EWS-ETS fusion proteins with Ewing sarcoma it is considered that the fusion is key to the development of the disease and functions as an aberrant transcription factor. Inhibition of EWS-FLI1 leads to loss of transformation in tumour cells, whilst re-expression rescues the phenotype (Kovar, Aryee et al. 1996, Smith, Owen et al. 2006, Takigami, Ohno et al. 2011). *In vivo* models have demonstrated that expression of EWS-FLI1 in mice results in a poorly differentiated sarcoma and in zebrafish leads to the development of tumours resembling those in Ewing sarcoma (Leacock, Basse et al. 2012). The EWS-FLI1 fusion protein would therefore be an excellent candidate for therapeutic targeting as its expression is limited to tumour cells however siRNA against EWS-FLI1 has not yet been fully developed into a therapeutic treatment due to a lack of a suitable delivery system (Chansky, Barahmand-Pour et al. 2004, Lin, Pandey et al. 2008, DuBois, Krailo et al. 2009, Leacock, Basse et al. 2012). Several EWS-FLI1 target genes have been implicated in tumour progression including MYC2, IGF-1, CAV1, and IGFBP3 which is repressed by the fusion protein (Figure 1-1) (Riggi, Cironi et al. 2007). NR0B1, a transcriptional coregulator, is upregulated by EWS-FLI1 and has been shown to physically interact with EWS-FLI1 mediating the transformed

phenotype of Ewing sarcoma (García-Aragoncillo, Carrillo et al. 2008, Kinsey, Smith et al. 2009). Using an NR0B1 reporter, Grohar et al. screened 50,000 compounds for inhibition of EWS-FLI1 and identified mithramycin as a potential inhibitor in Ewing sarcoma (Grohar, Woldemichael et al. 2011). Another study identified FoxO1 as an EWS-FLI1 suppressed regulator orchestrating a major subset of EWS-FLI1-repressed genes. Restoration of nuclear FoxO1 expression in Ewing sarcoma cells was found to impair proliferation and significantly reduced clonogenicity. Further investigation through gene-expression profiling revealed a significant overlap between EWS-FLI1-repressed and FoxO1-activated genes (Niedan, Kauer et al. 2013).

Although there is a substantial amount of research based on the EWS-FLI1 translocation it is also apparent that secondary genetic alterations may contribute to the clinical phenotype. Using array CGH, 67 tumour samples were analysed and copy number alterations recognised. These included chromosome 8 gain, 12p gain, and most frequently 1q gain which was present in 31% of patients. With increasing proportions of genome altered there was a decrease in survival and 1q gain alone was the copy number alteration associated with the most significant detrimental effect (Mackintosh, Ordóñez et al. 2012).

1.2.1 Ewing sarcoma cell of origin

In order to understand further the how Ewing sarcoma develops and the role in which the fusion protein EWS-FLI1 has, research has focused heavily in establishing a cell of origin of the disease and even since its recognition in 1921 this has been the subject of much debate. Unlike some other malignancies there are no known precursor states, preventing the analysis of precancerous cells and that, combined with its varied site of presentation (in bones and soft tissues) and undifferentiated appearance histologically has led to little clue of its origin (Tirode, Laud-Duval et al. 2007, Torchia, Boyd et al. 2007). An

impediment to understanding this is the lack of transgenic mice models. Attempts to force expression of EWS-FLI1 in mesenchymal cells have either induced leukaemia rather than sarcoma or have caused abnormal limb development rather tumour in developing limb buds (Torchia, Boyd et al. 2007, Lin, Pandey et al. 2008). The characteristic translocation of Ewing sarcoma is seen in other tumours such as neuroblastoma and primitive neuroectodermal tumours, and along with Ewing also expressing neural markers, has led many to believe that it has a neuroectodermal progenitor (McKeon, Thiele et al. 1988, Lizard-Nacol, Lizard et al. 1989).

In order to address the question of origin, research has focussed on attempts to express EWS-FLI1 in different cell types and its effect. It was shown that when expressed in mouse fibroblast cells (NIH3T3) there was cellular transformation to a phenotype similar to Ewing sarcoma and accelerated tumourgenesis however the gene expression pattern was different to those of Ewing sarcoma datasets (Braunreiter, Hancock et al. 2006). In addition some known target genes of EWS-FLI1 such as NR0B1 and NKX2.2 are not induced by the fusion protein in NIH3T3 so there is likely to be different mechanisms acting to those in Ewing sarcoma (Owen, Kowalewski et al. 2008, Kinsey, Smith et al. 2009). Unfortunately the EWS-FLI1 oncoprotein is toxic to human cell lines, so has added to the challenge of its investigation (Thompson, Teitell et al. 1999, Braunreiter, Hancock et al. 2006, Miyagawa, Okita et al. 2008). When marrow derived mesenchymal progenitor cells have EWS-FLI1 introduced in to them, they go onto generate tumours which have a small cell phenotype, and expression of Ewing markers, and interestingly IGF-1 dependency (Riggi, Cironi et al. 2005).

Further work has compared the gene expression profile of Ewing sarcoma to other tissues but results have been varied with some concluding Ewing cells to be most similar to those of neural origin and others to mesenchymal stem cells (Staege, Hutter et al. 2004, Kauer,

Ban et al. 2009, Riggi, Suvà et al. 2010). Groups such as Tirodes et al. worked backwards from the problem, inhibiting EWS-FLI1 with siRNA and making the assumption that cells would regain some of the characteristics of the primary cell which gave rise to Ewing sarcoma. With gene expression analysis it was found that cells regained markers and the differentiation ability of mesenchymal stem cells (Tirode, Laud-Duval et al. 2007). Potikyan et al. inhibited EWS-FLI1 in Ewing cell lines and then performed expression analysis. At least 162 genes were recognised which were altered by this inhibition, some being upregulated and some being downregulated. Amongst such genes there was increased expression of NR0BI, SOX2, IGFBP, IGF-1. Using a database of the gene expression of some 6900 samples and comparing that of the Ewing cell lines, it was found that they were most similar to IMR-90 cells (fibroblasts derived from human fetal lungs) again implying that the cell of origin is mesenchymal in its nature (Potikyan, France et al. 2008). When EWS-FLI1 was induced in human mesenchymal stem cells colonies formed which resembled the small cell histology of Ewing sarcoma. These were CD99 positive and had a gene expression pattern similar to Ewing sarcoma which included those of neural origin suggesting that the malignancy does originate from mesenchymal stem cells (Riggi, Suvà et al. 2008).

A growing number of tumours have been shown to contain a subpopulation of cells which possess stem cell like properties such as self-renewal. These are known as cancer stem cells (CSC) and it is believed that such cells may have elements of resistance to chemotherapy and therefore may allow tumours to reform. Experiments have demonstrated that EWS-FLI1 can alter the expression of miRNA145 and SOX2, a transcription factor usually found in embryonic stem cells which can reprogram mesenchymal stem cells towards these specific CSC with their unique properties (Riggi, Suvà et al. 2010). In summary, this information now means that specific molecular targeting of the Ewing

sarcoma cell of origin may have additional therapeutic advantages in terms of minimising systemic toxicity to non-tumour stem cells such as those in bone marrow, hair follicles and germ cells.

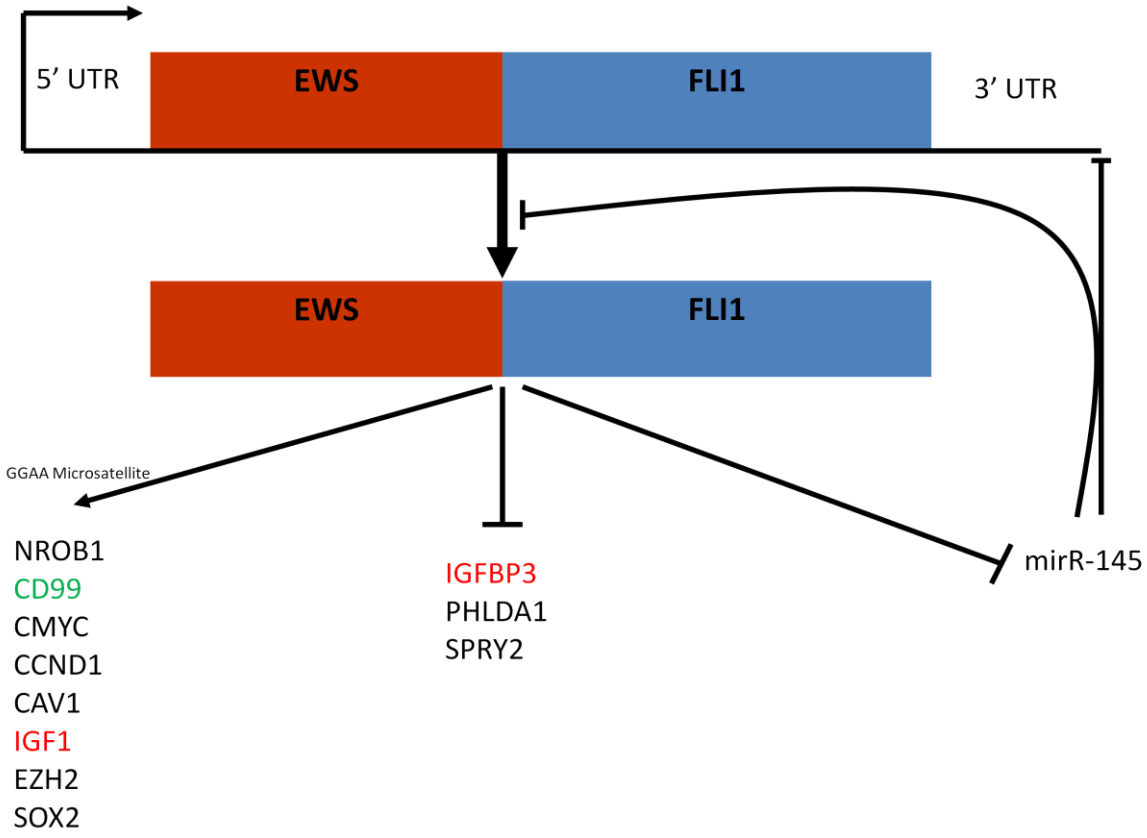


Figure 1-1. Schematic of EWS-FLI1 translocation. The resultant fusion protein leads to increase in activation of genes such as NR0B1, CD99, IGF-1 and SOX2 and inhibition of IGFBP3 and PHLDA1. mirR-145 which is believed to modulate FLI1 3’UTR is repressed by the fusion protein (Ban, Jug et al. 2011).

1.3 Insulin-like growth factor pathway in Ewing sarcoma

The EWS-FLI1 protein has been shown to deregulate the insulin-like growth factor pathway which is known to be tumour promoting in many malignancies including breast and prostatic carcinomas (Hankinson, Willett et al. 1998, Durai, Yang et al. 2005). Forced expression of EWS-FLI1 in mesenchymal stem cells resulted in transformation to a phenotype similar to that of Ewing sarcoma. Cells transformed by the fusion gene expressed high levels of IGF-1 and were dependent on the insulin like growth factor type 1 receptor (IGF-1R) for proliferation and survival (Torchia, Jaishankar et al. 2003). Both IGF-1 and IGF-2 bind via the IGF-1R, and IGF-2 to Insulin receptor-A (IR-A), leading to downstream intra-cellular activation of both phosphoinositol 3 kinase (PI3K) and MEK/ERK pathways resulting in promotion of growth, differentiation, and proliferation of the cell (Brognard and Hunter 2011, Poulikakos and Rosen 2011) (Figure 1-2). Several adaptor proteins such as the insulin receptor substrates (IRS1-4) and Src homology 2 domain-containing protein (Shc) are recruited to phosphorylation sites in the cytoplasmic domain which activate two major transduction pathways. IRS couples the receptor to the PI3K pathway whilst Shc couples it to the MAPK pathway. In the PI3K pathway, binding of IRS to PI3K causes the conversion of phosphatidylinositol-4,5-biphosphate to phosphatidylinositol-3,4,5-triphosphate causing activation of phosphoinositide-dependent-kinase-I (PDKI). PDKI phosphorylates the serine/threonine kinase Akt which has numerous substrates including transcription factors (FoxO, NF-κB) and kinases (mTOR and GSK3β). These cause cell cycle arrest, stress resistance, and lead to cell proliferation and survival. mTOR stimulates protein synthesis and cell growth via two downstream targets, 4E-binding protein-1 and S6 kinase (Hennessy, Smith et al. 2005). In the MAPK pathway, Shc, growth factor receptor bound protein 2 (Grb2) and son of sevenless (Sos) cause activation on Ras leading on to the activation of Raf. This protein phosporylates the

MAPK/ERK kinases (MEK1 and MEK2), which phosphorylates and activates extracellular signal-regulated kinase1 and 2 (ERK1 and ERK2). ERK has targets in both the nucleus and cytoplasm which regulate processes such as proliferation, survival, differentiation and migration (Rikhof, de Jong et al. 2009).

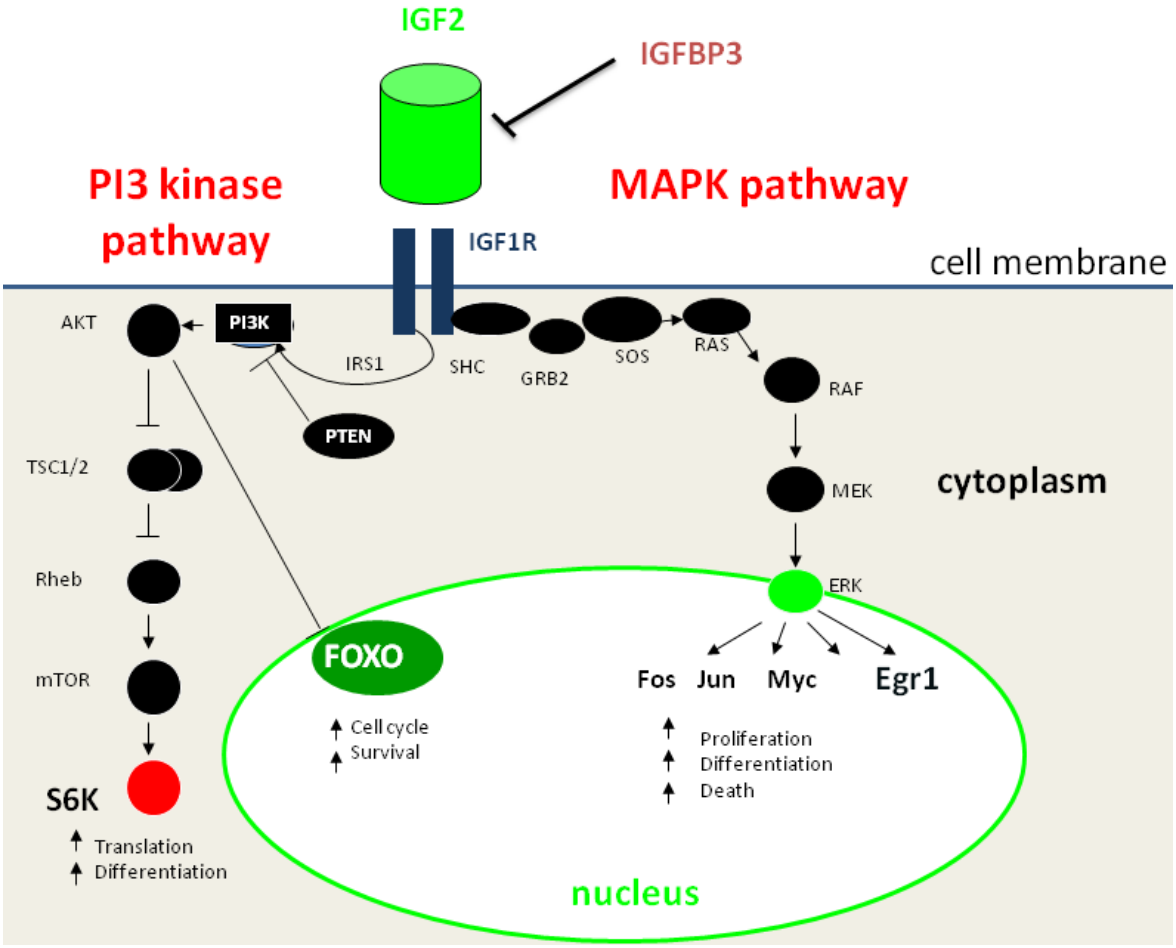


Figure 1-2. Schematic of IGF pathway. Activation of IGF-1R by the ligand IGF-2 results in activation of the PI3K and MAPK pathways which promotes cell proliferation and survival.

1.3.1 Insulin-like growth factor 1 receptor

IGF-1R is a transmembrane tyrosine receptor with approximately 50% homology to the insulin receptor (Rikhof, de Jong et al. 2009). It has an extra-cellular ligand-binding domain, a transmembrane region and a cytoplasmic domain that contains a tyrosine kinase. Both IGF-1 and IGF-2 are bound to IGFBP3 which negatively regulates their interaction with IGF-1R. EWS-FLI1 has been shown to limit levels of IGFBP3 resulting in increased levels of IGF-1 which in combination with autocrine production of IGF-1 by tumour cells leads to increased activation of the IGF-1 pathway (Prieur, Tirode et al. 2004).

The evidence described above supports a role for drugs targeting IGF-1R signalling in Ewing sarcoma. Blockade of IGF-1R has been shown to cause inhibition of cancer cell proliferation, survival and anchorage-independent growth *in vitro*, to inhibit tumorigenesis, block tumour invasion and metastasis and to sensitise cancer cells to chemotherapy and radiotherapy (Zeng, Zhang et al. 2011). In support of this, Sharma et al. demonstrated that a drug tolerant subpopulation of non-small cell lung cancer cells can be successfully ablated by treatment with an IGF-1R inhibitors there by supporting a therapeutic opportunity in targeting IGF-1R in resistant cells (Sharma, Lee et al. 2010).

1.3.2 Insulin-like growth factor inhibitors

It is important to investigate fully the potential targets of EWS-FLI1 as the fusion protein is unique to tumour cells. To achieve this aim, a large number of targeted therapeutic approaches have been evaluated in Ewing sarcoma models, both *in vitro* and *in vivo*. Among the various strategies used to interfere with IGF-1R function in preclinical studies, monoclonal antibodies (mAbs) and small molecule tyrosine kinase inhibitors represent the best candidates for clinical development (Scotlandi, Benini et al. 1998, Martins, Mackintosh et al. 2006, Carboni, Wittman et al. 2009, Kurmasheva, Dudkin et al. 2009).

IGF-1R inhibitors are currently undergoing evaluation in clinical trials with relatively modest responses of 10-30% (Table 1-1) (Juergens, Daw et al. 2011, Pappo, Patel et al. 2011). The cause of such response in only a subset of patients is still to be determined but could be due to an IGF-IR independent mechanism of growth by overexpression of alternative signalling pathways (Huang, Greer et al. 2009, Olmos, Postel-Vinay et al. 2010, Juergens, Daw et al. 2011, Pappo, Patel et al. 2011).

1.3.3 Clinical experience of IGF-1R in Ewing sarcoma

As previously mentioned IGF-1R has been shown *in vitro* to be directly involved with proliferation and survival in Ewing sarcoma (Scotlandi, Benini et al. 1996, Scotlandi, Benini et al. 1998). Works such as these have led to Phase I/II clinical trials of IGF-1R monoclonal antibodies. Juergens et al. treated 107 patients suffering refractory Ewing sarcoma with figitumumab, an IGF-1R antibody and found 14% had a partial response whilst 30% of patients had stable disease. The median progression free survival (PFS) for the population was unfortunately poor at 1.9 months and median overall survival (MOS) 8.9 months. It was observed that patients in whom blood levels of IGF-1 was elevated at baseline had a significant advantage in survival compared with those with lower IGF-1 levels (10.5 months to 4.5 months respectively) (Juergens, Daw et al. 2011).

Pappo et al. trialed R1507, also a monoclonal antibody to IGF-1R, in 111 Ewing sarcoma patients and noted a modest response in 10% of patients (median overall survival 7.6 months). The cause of such response in only a subset of patients has not been determined but could be due to an IGF-1R independent mechanism of growth by overexpression of alternative signalling pathways (Huang, Greer et al. 2009, Olmos, Postel-Vinay et al. 2010, Juergens, Daw et al. 2011, Pappo, Patel et al. 2011).

One mechanism to account for the variation in response to IGF-1R inhibitors, could be due to upregulation of IR signalling. This possible switch from IGF-1R to IR continues to maintain proliferation and survival which could lead to the lack of response to IGF-1R inhibitors and supports the rationale for co-targeting both receptors. Both IGF-1R and IR share complete homology at the ATP-binding pocket and 84% homology within the intracellular kinase domain and similarly activate PI3K and MAPK pathways (Garofalo, Mancarella et al. 2012). Subtle differences do exist in the recruitment of certain docking proteins and intracellular mediators resulting in the predominant metabolic effects elicited by IR activation and the predominant mitogenic, transforming, and non-metabolic effects elicited by IGF-IR (Siddle 2011). Both receptors, including the foetal isoform IR-A which is prevalent in tumours (Frasca, Pandini et al. 1999), can be activated by both IGF and insulin thus overcoming specificity in intracellular signalling pathways. It has been suggested that there is a compensatory role of IR-A when IGF-1R is disrupted (Buck, Gokhale et al. 2010, Ulanet, Ludwig et al. 2010). Garofalo et al. developed Ewing sarcoma cell lines resistant to IGF-1R antibody and showed an increase in expression of IR-A receptor and circulating levels of IGF-2 suggesting an IR-A dependent pathway (Garofalo, Manara et al. 2011). It could be postulated therefore that targeting IGF-1R signalling alone in patients, particularly those with high levels may inadvertently abrogate any potential response. Therefore by co-targeting IGF-1R and IR-A could be advantageous.

Reference	Drug	Phase	Response (proportion of patients)
Pappo et al. (2011)	R1507	II	11/115
Juergens et al. (2011)	Figitumumab	I-II	15/106
Malempati et al. (2012)	Cixutumumab	II	2/35
Tap et al. (2012)	Ganitumab	II	1/18

Table 1-1. Response of IGF-1R inhibitors used in clinical trials (Juergens, Daw et al. 2011, Pappo, Patel et al. 2011, Malempati, Weigel et al. 2012, Tap, Demetri et al. 2012).

1.4 Tumour heterogeneity

Tumour heterogeneity, the existence of subpopulations of cells with distinct genotypes and phenotypes within a primary tumour, may have profound implications for drug therapy in cancer. Tumour heterogeneity can be due to genetic factors causing resistance to drugs targeting specific mutations or signalling pathways (Greaves and Maley 2012), and non-genetic mechanisms such as epigenetic changes, posttranslational modifications and alterations in cell differentiation hierarchy thereby influencing cell-cell variability within a tumour adding to the complexity of a given cancer (Kreso, O'Brien et al. 2013).

Targeted therapy, which attempts to exploit a tumour's dependence on a critical proliferation or survival pathway, has significantly improved patient outcomes in a range of solid tumour types, but despite clinical benefit, may be only for a limited duration (Gore and Larkin 2011). With the advent of deep sequencing techniques, the extent and prevalence of tumour heterogeneity can be examined. Initially evidence that multiple subclones of differing genetic status existed within the same tumour were provided by G-banding karyotyping and fluorescent *in situ* hybridisation (FISH) studies. These demonstrated discrete patterns of chromosomal rearrangements and copy number alterations of representative genomic loci (Navin and Hicks 2010). Increasingly next generation sequencing (NGS) technologies are adding new evidence of genetic diversity both within and between common tumours by comprehensively and systematically determine both nucleotide sequence and copy number of genomic loci.

1.5 Next generation sequencing and its role in targeted therapy

There is now extensive literature and knowledge across many tumour types on genomic disruptions which influence treatment options in cancer. Increasingly treatments are being tailored to individuals based on their personal genomic blueprint. For three decades the

testing of breast cancer patients for Oestrogen Receptor (ER) positivity has determined the use of hormonal therapies in such patients ((EBCTCG) 2005). Following this, the human epidermal growth factor receptor gene (HER2), has been found to be amplified (17q12 amplicon) in 25-30% of breast cancers resulting in an aggressive form of the disease (Slamon, Godolphin et al. 1989). Trastuzumab (Herceptin), a monoclonal antibody which acts against the receptor, has been shown to be effective in prolonging survival in metastatic disease when used in combination with chemotherapeutics in a Phase III clinical trial (Slamon, Leyland-Jones et al. 2001).

Similarly in lung cancer sufferers who have an activating mutation of the Epidermal Growth Factor Receptor (EGFR) it has been shown that tyrosine kinase inhibitors such as erlotinib bind specifically to the mutant receptor at high affinity (Lynch, Bell et al. 2004). Being able to identify abnormalities which confer specificity to the tumour (such as mutations as in EGFR or amplifications in HER2) compared with normal cells allows for specific and relevant treatments to be administered with high therapeutic index.

Somatic base-pair mutations have been identified in many human genes through targeted DNA sequencing efforts (Forbes, Bhamra et al. 2008). Although analysing individual genes or mutations is clearly of value for some patients, it does not provide information about interwoven cell signalling pathways and the complex environment of malignant disease. Through interactions between genes and loci the cellular phenotype can be affected (epistasis) which can contribute to malignancy. In breast cancer, Sapkota et al. identified single nucleotide polymorphisms (SNP) related to DNA repair, modification, and metabolism pathway genes which in isolation had weak statistical significance in their effects but by acting as two-way or multi-way SNP-SNP interactions contributed to breast cancer risk. This led them to postulate that cross talk among members of multiple cancer

related pathways may exist contributing to the complexity of disease (Sapkota, Mackey et al. 2013).

The drive for the development of multigene assays such as gene arrays and next generation sequencing (NGS) is due to the need for a more comprehensive genomic analysis of patient samples performed as a single test which will have the ability to identify aberrations within the heterogeneous genomic landscape of tumours (Gerlinger, Rowan et al. 2012). NGS now allows, through extraction of patient DNA and RNA, for a profile of copy number variation of genes and chromosomal aberrations, for single nucleotide analysis and identification of mutations at this level and the presence of abnormal fusion genes via RNA sequencing (RNA-seq).

In addition, patient data can be archived in a digital format for future reference allowing for a genome forward and backward approach to clinical strategies.

1.5.1 Sanger vs. Next Generation Sequencing

The first generally applicable method for sequencing DNA was developed by Frederick Sanger and colleagues in 1977 and has been widely used for sequencing continuous reads of DNA of up to approximately 900 base pairs (Sanger, Nicklen et al. 1977). Developed using knowledge of DNA replication it uses a mixture of natural nucleotides and labelled (originally radioactively, now fluorescently) dideoxyribonucleotides (ddNTPS) to generate the DNA sequence. Dideoxyribonucleotides lack the presence of a 3'OH group which prevents DNA polymerase from extending the synthesis of a replicate DNA strand. When a DNA sequence is generated in the presence of natural dNTPs and one of four labelled ddNTPs, fragments of random length are generated. These fragments are then separated by size using electrophoresis and their fluorescence detected by a laser, with each fragment labelled with the specific ddNTP which prevented the strand elongation.

Sanger sequencing can produce long read lengths with reliable results but can only realistically be used as a small scale method of identifying mutations. Developments in molecular targeted therapies means that it is necessary to sequence larger panels or entire genomes in cancers to allow the best therapies to be chosen.

The concepts behind NGS are similar to Sanger sequencing. The bases of small fragments of DNA are sequentially identified from signals emitted as each fragment is re-synthesised from a DNA template strand. A key difference is that this process occurs across millions of reactions in parallel rather than being limited to a single or few DNA fragments. This advantage allows for rapid sequencing of large stretches of DNA base pairs spanning entire genomes with a single sequencing run producing hundreds of gigabases of data in a clinically useful time frame.

A single genomic DNA (gDNA) sample is first fragmented into a library of small segments which can be sequenced in millions of parallel reactions. The newly identified strings of bases, called reads, are then reassembled using a known reference genome as a scaffold resulting in the entire read of a sample of DNA. One of the leading platforms in the field is the Illumina genome analyser (Metzker 2010). Genomic DNA is sheared to form fragments of 75-150bp and amplified by bridge amplification. Upon addition of the terminating nucleotide, DNA polymerase and primers, a fluorescent signal is emitted which is captured and denotes the type of base incorporated in the sequence. The sequencing cycle is replayed one base at a time generating a series of images with each image representing a single base in the priming sequence. Read depth is a reflection of how often a specific region of the genome has been sequenced. Most technologies aim for a median coverage in DNA of 30-fold (30X) at >90% of bases allowing for proper alignment and to differentiate between errors and true variants (Ulahannan, Kovac et al. 2013). Accuracy of Illumina NGS sequencer is reported as having a phred score of Q30

compared with Sanger-sequencing which scores Q20 (phred quality score: $Q = -10 \log_{10} P$ where P is base calling error probability) (Ewing and Green 1998). This translates to the chance of a base-call error being 1 in 1,000 (Kamalakaran, Varadan et al. 2013). Although there are advantages of NGS over Sanger sequencing in terms of its high throughput nature, the amount of data generated can cause challenges for data analysis and requires significant informatics input (Margulies, Egholm et al. 2005). Reads are mapped to a reference genome (in this study, human genome 19) and this can be challenging due to the presence of repeated sequences within the genome or large-scale polymorphisms. This requires a large amount of computing capacity and informatics expertise to ensure accuracy (of the mapping) and sensitivity (the proportion of the reads mapped to the reference genome).

1.6 Aims

The aim of this work is to identify mechanisms contributing to the heterogeneity of resistance in Ewing sarcoma following IGF-1R/IR pathway inhibition. The hypothesis is that mechanisms of resistance relate to heterogeneity of responses to signalling pathway activation and inhibition. Through selection, disruption of the pathway will identify subpopulations of cells both sensitive and resistant in their responses allowing for interrogation of resistance mechanisms. Heterogeneity is most likely due to a combination of genetic (Xu, Hou et al. 2012), epigenetic (Irish, Hovland et al. 2004, Sharma, Lee et al. 2010), phenotype (Turtoi, Blomme et al. 2013) and germline factors (Hudler, Kocevar et al. 2014), but what has most bearing on cancer phenotype is protein abundance (expression), activation status (phosphorylation) and subcellular localisation. The specific aims of this project are to:

1. Develop a method of unbiased quantification using confocal microscopy and fluorescent immunohistochemistry, to ascertain levels of heterogeneity within the IGF-1R signalling pathway in Ewing sarcoma cell lines and tumour tissue.

2. To characterise a panel of Ewing sarcoma cell lines and assess the heterogeneity of response to a dual kinase inhibitor, OSI-906.

3. To analyse genomic rearrangements via a single platform in Ewing sarcoma cell lines through next generation sequencing technologies.

4. To validate findings from genome wide analysis through functional experiments.

5. To develop and apply a mutagenesis screen in order to identify and characterise subpopulations of cells resistant to OSI-906.

2 Materials and Methods

2.1 Cell Lines

Cells were derived from ATCC or different partner institutes (Ottaviano, Schaefer et al. 2010) and regular mycoplasma testing carried out (MycoAlert Kit, Lonza). No contamination was identified. Short tandem repeat (STR) testing was not carried out as cell lines had been directly obtained from the EuroBoNet consortium.

2.2 Cell culture

Cell lines were grown in RPMI 1640 (PAA Laboratories GmbH, Austria) supplemented with 1% Penicillin-Streptomycin (P/S) (PAA Laboratories GmbH, Austria) and 10% Foetal Calf Serum (FCS) (Biosera, UK). Three cell lines (STA-ET2.1, STA-ET10, WE-68) needed to be cultivated in gelatine-coated culture flasks to allow cells to attach. For growth factor experiments cell lines were grown on coverslips (d=13mm) in 24-well plates (Costar, USA) with $4x10^4$ cells per well. After adaptation for 2 days cells were serum-starved in RPMI 1640 supplemented with 1% P/S only for 24 hours and treated with IGF-2 (50ng ml^{-1}, R&D systems) for 1 hour at 37°C. Following exposure, cells were fixed in 4% formaldehyde (in PBS) for 15 minutes at room temperature, washed twice in PBS, and stored at 4°C until needed.

2.3 Immuno-labelling

Cells on coverslips were washed in TBS for 5 x 3 minutes, permeabilised and blocked in 0.5% Triton X-100/10% goat serum for 1 hour and incubated with the primary antibody at the described concentrations diluted in TBS/0.3% Triton and 10% serum and left at 4°C overnight (Table 2-1).

After 2 washing steps cells were incubated with a secondary goat anti-rabbit Alexa Fluor® 594 (Invitrogen, UK) for 2 hours at room temperature (Table 2-2). The fluorescent stain Phalloidin Alexa 488 (Invitrogen, UK) was used in order to probe the actin cytoskeleton of Ewing sarcoma cells. Cells were incubated with Phalloidin Alexa 488 (1:50) for 2 hours at room temperature following 3 x 3 minute washes in TBS. Nuclei were detected with the DNA stain 4',6-diamidino-2-phenylindole (DAPI) (Sigma, UK) 1:10,000. Coverslips were mounted with Prolong Gold Antifade (Invitrogen, UK).

Antibody	Species raised	Manufacturer (catalogue)	Optimised dilution
CD99	Mouse IgM	Leica (CD99)	1:100
Egr1	Rabbit IgG	Cell signaling (#4154)	1:50
FoxO3a	Rabbit IgG	Cell signaling (#2497)	1:100
Ki67	Rabbit IgG	Thermo Scientific (RM9106)	1:300
p-MAPK	Rabbit IgG	New England Biolabs (#4370)	1:50
pS6	Rabbit IgG	Cell signaling (#4857)	1:100

Table 2-1. Primary antibodies with dilutions

Antibody	Species raised in	Manufacturer (catalogue)	Optimised dilution
Alexa-488	Goat (anti-rabbit)	Invitrogen (A21426)	1:300
Alexa-555	Goat (anti-mouse)	Invitrogen (A11008)	1:300
Alexa-594	Goat (anti-rabbit)	Invitrogen (A11037)	1:300
Alexa-647	Goat (anti-mouse)	Invitrogen (A21240)	1:300

Table 2-2. Secondary fluorescent antibodies with dilutions

2.4 RNA extraction, reverse transcription and quantitative real-time PCR

2.4.1 RNA extraction

The RNeasy Plus Mini Kit (Qiagen Cat no. 74134) was used for the extraction of RNA from cell lines. Cells were grown in 10cm petri dishes until 80-90% confluent and lysed with RLT buffer containing β-mercaptoethanol as per manufacturer's protocol. General measures to minimise the risk of RNase contamination were used throughout including the use of designated "RNAase free" pippettes and tips, RNase free plasticware and the preparation of surfaces with RNaseZAP (Sigma).

Extraction was continued as per documented protocol with elution of RNA in 50µl of RNAse free water.

2.4.2 RNA quantity and quality assessment

A Nanodrop 2000 spectrophotometer (Thermo Fisher) was used to quantify extracted RNA. The Nanodrop measures absorbance of a sample at 260nm (A_{260}) and 280nm (A_{280}). Each measurement was normalised against the absorbance of ultrapure RNAse free water. Quantification of RNA amount is automated by the instrument using the Beer-Lambert equation which correlates the calculated absorbance with concentration (A_{260}=1=40µg of RNA per ml). RNA purity was assessed by the A_{260}/A_{280} ratio with a value of 1.8-2.1 deemed suitable for further analysis.

2.4.3 Reverse transcription of RNA

Where possible RNA samples were reverse transcribed immediately after extraction. A random priming approach was used to reverse transcribe RNA to DNA. All reverse transcription (RT) reactions had a no-RT duplicate reaction performed which was identical aside from the addition of the reverse transcriptase enzyme and RNAse inhibitor. The protocol followed was as per the manufacturer's instructions (The Applied Biosystems

High Capacity cDNA kit with RNase inhibitor). For each reaction 5µg made up in 25µl RNAse-free water was added to 25µl of prepared master mix in a PCR tube, mixed, and briefly spun down by microfuge (Table 2-3). Samples were run in a Bio-Rad MyCycler Thermal Cycler using the following conditions: 25°C for 10 minutes; 37°C for 120 minutes; 85°C for 5 minutes and then held at 4°C. At completion, assuming 100% efficiency of the reverse transcription, the DNA was diluted 1:5 with RNAse-free water resulting in a final concentration of 20ng μl^{-1}.

2.4.4 Quantitative real-time reverse transcription PCR

Quantitative real-time reverse transcription PCR (RT-qPCR) reactions were all performed using the SensiFast NoRef kit reagents. Dependent on Primer design either the Roche Universal Assay design centre using the Roche Universal Probe Library or the SensiFast SYBR green assay were used (Table 2-4, Table 2-5). A Corbett liquid handling robot was used to pipette samples for RT-qPCR.

Reagent	Volume per reaction (µl) : RT	Volume per reaction (µl) : no RT
10x RT buffer	5	5
25x dNTP mix (100mM)	2	2
10x RT random primers	5	5
Multiscribe reverse transcriptase	2.5	0
RNase inhibitor (40units/ul)	0.625	0
RNase-free water	9.875	13
Total volume per reaction	25	25

Table 2-3. Reverse transcription mastermix

Reagent	Roche primer/probe: volume per reaction (µl)	SYBR green: volume per reaction (µl)
SensiFast Solution	12.5	10
ddH20	0.25	3.4
Primer Forward	1	0.8
Primer Reverse	1	0.8
Probe	0.25	-
Total volume per reaction	15	15

Table 2-4. RT-qPCR mastermix

2.4.5 RT-qPCR primers and probes

The Roche Universal Probe Library system and ProbeFinder software were used to determine optimal probe and primer combinations (Table 2-5). This system uses probes which are 8-9 nucleotides long and are labelled at the 5' end with fluoroscein (FAM) and at the 3' end with a quencher dye. The ProbeFinder Assay Design Software displays the target-specific primer and the matching Universal Probe Library probe (http://www.roche-appliedscience.com/shop/CategoryDisplay?catalogId=10001&tab=&identifier=Universal+Probe+Library). The software selects probe/primer combinations based on melting temperature of primers (59-61°C), primer length (18-27 nucleotides), optimal amplicon length (60-150 nucleotides) and intron spanning assays (to reduce the risk of false positives from gDNA contamination of reactions) (Table 2-5).

Gene	Probe/ SYBR	Forward (F) primer sequence	Reverse (R) primer sequence	Intron spanning
CNKSR1	80	CTGACAGATCTGAGCATGTGG	TCCTCTGCTTCGGTCTCACT	Yes
CNKSR2	SYBR	GCAGTGT CTCCCATTCGCAAGA	GCAGGTGGCATTTCTGAGTTGGC	Yes
KIF1B-CNKSR2	SYBR	TTTGCCTATGGGCAGACTGG	ACTTCATCGCCAGCATGGAT	No
GSE1	25	AACCAAAACCGTGAATGGTG	TCCACAATGAGGCGTTCC	Yes
RP11-GSE1	SYBR	CGGGAGGAGGACGGACCAGA	AGCGAAGGGGACTTGGGCTC (ex2) CGGAGAGGACACGGGGGACG (ex3)	No
ABCA2	22	CGCCATCATCGACACTTTT	TGCTCAATGACAAACAGGAAGT	Yes
ABCB1	78	AGCTGCTGTCTGGGCAAA	TGCCAAGACCTCTTCAGCTAC	Yes
ABCC1	56	GGGCACGTGGCTATCAAG	GACATCCAAAAAGGATGTTTTCTC	Yes
ABCG2	40	TGGCTTAGACTCAAGCACAGC	TCGTCCCTGCTTAGACATCC	Yes
Actin, beta	64	CCAACCGCGAGAAGATGA	CCAGAGGCGTACAGGGATAG	Yes
IGF-1R	22	GGGAGAGAGCCTCCTGTGA	TGATGATGCGATTCTTCGAC	Yes
IGF-1R	SYBR	GAGCAGCTAGAAGGGAATTAC	AAGTTCTGGTTGTCGAGGA	Yes
IR-A	SYBR	GTTTTCGTCCCCAGGCCATC	CCAACATCGCCAAGGGACCT	Yes
IR-B	SYBR	CACTGGTGCCGAGGACCCTA	GACCTGCGTTTCCGAGATGG	Yes
ALDH	79	TCTCCACGTGGCATCTTTAAT	TGTAGGCCCATAACCAGGAA	Yes
HPRT	22	TGATAGATCCATTCCTATGACTGTAGA	CAAGACATTCTTTCCAGTTAAAGTTG	Yes
EWS-FLI1	57	GGGCACAAAGGATCAGTAAGA	GCTAGGCGACTGCTGGTC	Yes
CD99	21	ATGGAGAGCCACCGGAAT	CTGCCGACAATCTTCTATTTCTC	Yes
B2M	42	TTCTGGCCTGGAGGCTATC	TCAGGAAATTTGACTTTCCATTC	Yes
OCT4	78	TGCCGTGAAACTGGAGAAG	GCTTGGCAAATTGTCGAGT	Yes
BMI1	63	TTCTTTGACCAGAACAGATTGG	GCATCACAGTCATTGCTGCT	Yes
GAPDH	60	AGCCACATCGCTCAGACAC	GCCCAATACGACCAAATCC	Yes

Table 2-5. qPCR primer sequences and corresponding probe/ SYBR.

2.4.6 qPCR reactions

qPCR reactions were carried out on a Rotor Gene Q (Qiagen) using the following cycling conditions:

1. 95°C for 15 minutes
2. 60°C for 1 minute
3. 95°C for 15 seconds
4. Repeat points 2 and 3 for a total of 40 cycles

For each sample duplicate reactions were performed and a no-RT control.

2.4.7 Reaction efficiencies

For each gene a standard curve was performed to check the efficiency of the primer and probe combination and calculate a Ct threshold which would be subsequently used for future experiments. cDNA was prepared in 6 serial dilutions, standard curves generated by Rotor Gene software, and the reaction efficiencies calculated.

Genorm was used to determine the most stable reference (housekeeping) genes from a set of 4 tested candidate reference genes; GAPDH, ACTIN, B2M and HPRT. The software is based on principles and formulas described by Vandesompele et al. They demonstrated that normalising to a single reference gene could lead to large errors and they suggested that using the geometric mean of carefully chosen reference genes is more accurate (Vandesompele, De Preter et al. 2002). Genorm automatically excludes the housekeeping genes with the highest "M" value, the internal control gene-stability measure. This is an average of pairwise variations of a particular gene with all other control genes so those with the lowest "M" value are most stably expressed.

Genorm analysis was carried out separately for 3 cell lines; CHP-100, SK-N-MC, and RD-ES as well as for the combined dataset. It was found that all M values were <1.5 implying

that all housekeeping genes were stably expressed in these cell lines however of the 4 genes tested, ACTIN was the highest value so was excluded from further analysis.

2.4.8 RT-qPCR analysis

The average of duplicate Ct values from an experiment was used for the gene of interest. The ΔCt was calculated and normalised to the geometric mean of three housekeeping genes (GAPDH, HPRT, and B2M) unless otherwise stated. Results were calculated in excel and analysed and illustrated using Graphpad prism.

3 Quantification of the heterogeneity of prognostic cellular biomarkers in tumour tissues

3.1 Introduction

Tumours, like all tissues, differ by site of origin, histological appearance and mechanistic hallmarks (Hanahan and Weinberg 2011). Even within stratified clinical cohorts, for example by a specific diagnostic genotype, further sub-classifications can easily be identified by genome wide analysis and the differential response to drugs (Gerlinger, Rowan et al. 2012, Yap, Gerlinger et al. 2012). Within the same tumour, complex genomic heterogeneity between single cells can also be readily detectable, but it remains unclear what the prognostic significance is of these observations without clinically applied and unbiased approaches to quantify cellular heterogeneity *in situ* (Hou, Song et al. 2012, Xu, Hou et al. 2012).

Histopathological analysis of tissue samples is needed for cancer diagnosis and prognosis (Gurcan, Boucheron et al. 2009). Historically biomarker assessments have been based on localisation of protein epitopes in paraffin embedded, formalin fixed tissue (FFPE) using immunohistochemistry. This confines data to one biomarker which is semi-quantitative (1+, 2+, 3+), timely, open to inter and intra observer variation, and lacks the cellular localisation provided by immunofluorescence (Ginty, Adak et al. 2008) .

A number of quantitative methods can be applied to assessing signalling pathway activation of frozen unfixed tissue including Western blot, reverse protein lysate arrays and mass spectrometry (O'Neill, Bhamidipati et al. 2006). However to quantify signalling in small fixed core biopsies a novel approach is required. The rapidly labile (nanoseconds) and reversible nature of protein (tyrosine/serine) phosphorylation events make accurate observation and quantification difficult. In contrast nuclear transport events tend to happen

at a much slower time-scale (minutes, hours) and involve much larger concentration changes, so are significantly easier to observe (Camp, Chung et al. 2002, Baker, Dragovich et al. 2005). Optimisation of fluorescent imaging coupled with automated analysis algorithms offer an alternative solution to simultaneous protein detection and cell classification. For example, automated quantitative analysis utilises epitope localisation with cellular and tumour masks and statistical analysis of cut-point determination that maximises the significance values based on thresholds (Camp, Chung et al. 2002). Multiple-ligand epitope cartography utilises automated fluorescent tagging and sequential bleaching approaches and is a technique that can be applied to the screening of multiple biomarkers in a single section (Schubert, Bonnekoh et al. 2006, Friedenberger, Bode et al. 2007). Although such approaches offer significant technical advances, they remain prone to bias and fail to address the quantification of heterogeneity at the cellular level.

Ewing sarcoma currently has no prognostic biomarkers that have been prospectively validated and can be routinely applied in clinical risk stratification (de Alava, Antonescu et al. 2000, Mackintosh, Ordonez et al. 2012, van Maldegem, Hogendoorn et al. 2012). Ki67, a proliferative biomarker has been shown to be of potential prognostic significance in some large series using semi-quantitative techniques (Lopez-Guerrero, Machado et al. 2011). Other biomarkers are also of potential significance, as early phase clinical trials in relapsed Ewing sarcoma patients have exploited the EWS-FLI1 induced insulin-like growth factor (IGF) signalling pathway dependency. Biomarker assays to initially select patients more likely to respond to IGF pathway inhibition remain unavailable, and drug development programmes have been curtailed as a result (Juergens, Daw et al. 2011, Pappo, Patel et al. 2011).

There is therefore a need for a validated, automated, unbiased method of measuring relevant image features which may confirm the extent of variation and heterogeneity in

pathway activation within the same and similarly genotyped tumours. By developing a quantitative multi-fluorescence based assay in Ewing sarcoma cell lines using confocal microscopy and high content image analysis the distribution of signalling pathway activation can be illustrated prior to application in biopsy samples.

3.1.1 Confocal Microscopy

Confocal microscopy was first employed in the mid-1950s by Marvin Minsky and was developed further to be used in the examination of fluorescent biological specimens throughout the 1980s (Minsky 1988, Amos and White 2003). Fluorescence microscopy is commonly used in life science research as it can provide two types of information: spatial which can be used to calculate measurements such as distance and area, and intensity, which can be used to determine the number of fluorophores in a specimen. It allows individual components at the molecular level to be labelled with different markers in order that behaviour and interactions of proteins within a cell can be studied more closely.

Fluorescence occurs when a molecule, also known as a fluorophore, at a particular energy state, absorbs a photon. The molecule gains energy (excited) and moves to a higher energy state rendering it less stable and causing it to emit a photon of a particular wavelength. The difference in wavelengths is due to Stokes' shift, a loss of vibrational energy which allows excitation light to be separated from the observed emitted light.

Modern confocal microscopes are electronic systems which consist of an optical microscope, a computer (for image display, processing, and storage) and a laser system. The advantage of confocal microscopy is the ability to produce thin (0.5-1.5μm) optical sections through specimens with reduced background fluorescence (Sandison and Webb 1994). Confocal microscopes work by emitting light from a laser source. This should have an illumination wavelength which will optimally excite the fluorophore and therefore

collect as many of the emission photons as possible. The light passes through a pinhole aperture which is situated in a conjugate plane (confocal) and is reflected by a dichromatic mirror. The laser is scanned across the specimen in a defined plane and secondary fluorescence is emitted from points on the specimen. This passes back through the mirror and is focused as a confocal point at the detector pinhole aperture. Fluorescence emission which occurs at points above and below the focal plane is not confocal with the pinhole and therefore is not detected. Refocusing the objective on a microscope moves the excitation and emission points on a specimen to a new plane which is then confocal with the pinholes (Claxton, Fellers et al. , Waters and JR 2008).

Digital images enable quantitative analysis of data. They occur when the optical image of a specimen is recorded on a detector using a two-dimensional grid of equally sized pixels. Each pixel represents a finite sized part of a specific area of the image. Whilst obtaining the image, the intensity value of a pixel is related to the number of fluorophores present at that specific pixel (Pawley).

3.1.2 Image analysis

Once captured, images need to be analysed in an efficient, quantitative and unbiased fashion. Automatic image analysis allows this to occur with the development of computer algorithms. The advantages lie not only in the increase in efficiency but also the precise identification of the location of markers within multi-labelled images. Segmentation of images needs to be carried out in order that geometric features and temporal parameters be analysed. The main challenges are related to the non predictable size and shape of nuclei in both terms of morphological and chromatic features (Di Cataldo, Ficarra et al. 2009). There are several methods of segmentation which include level set and “Voronoi” watershed segmentation.

3.1.3 Segmentation

3.1.3.1 Level Set Segmentation

Level set segmentation is widely used in medical image segmentation (Alilou, Kovalev et al. 2013). It is a boundary based approach which starts from initializing the evolution of a curve (for example within a nuclei) subject to constraints for a given image such as intensity, in order to achieve an optimal state and therefore a boundary (Kass, Witkin et al. 1988).

3.1.3.2 Watershed Segmentation

The watershed method of segmentation is a morphology based partitioning tool based on imaging intensities as equivalents to heights of a surface. Watershed methods are fast, and have some capability of handling multiple touching objects, though in practice they suffer from over-segmentation (Malpica, de Solórzano et al. 1997). A variant of watershed methods are those based on a generalised Voronoi diagram, which provides an estimation of cell boundaries based on the equal distance between neighbouring nuclei.

3.1.4 Validation

This is essential in the process of developing a new algorithm in order to ensure that meaningful data is being gained from it. In a perfect situation the performance of any segmentation algorithm should be compared against ground truth however in biomedical imaging this is usually not possible so the algorithm has to be compared against the results of expert observers. Three examples of validation tests used in this work are; receiver operating characteristic (ROC), Bland-Altman analysis, and Hausdorff distance. ROC is used to illustrate the performance of a binary classifier, for example the number of nuclei identified. Bland-Altman test is a measure used to analyse agreement between two

different assays and the Hausdorff distance calculates how far two subsets of a metric space are from each other, which can be presented statistically.

3.2 Chapter Aims

Understanding functional heterogeneity is key to the successful treatment of Ewing sarcoma. Tumour tissues are typically heterogeneous, yet unbiased quantitative methods are rarely used to analyse heterogeneity at the protein level. The aim was to develop, validate, and apply automated image segmentation to confocal microscope images of multiple biomarkers in Ewing sarcoma cell lines and generate distributions of biomarkers between, and within, each cell. Using validated Ewing sarcoma cell lines, confocal images would be segmented using level sets and watershed algorithms. Each cell's nucleus and cytoplasm, identified in relation to DAPI and CD99, respectively, and protein biomarkers (e.g. Ki67, pS6, FoxO3a, Egr1, MAPK) localised relative to nuclear and cytoplasmic regions of each cell would be analysed in order to generate image feature distributions. This validated algorithm would then be applied to Ewing sarcoma biopsy tissue from three separate European cohorts and integrated with patient clinical outcomes using a random survival forests machine learning algorithm.

3.3 Methods

3.3.1 Cell culture conditions

Ten validated Ewing sarcoma cell lines were obtained from the EuroBoNet consortium (Table 3-1). All lines were grown in RPMI 1640 with L-Glutamine which was supplemented with 10% FCS and 1% Penicillin/Streptomycin. Conditions of incubation were at 37°C in a humidified atmosphere containing 5% CO_2. Cell lines were regularly screened for mycoplasma contamination.

3.3.2 Immuno-labelling of Ewing cell lines grown on coverslips

The method was carried out as previously described. In brief, cell lines were seeded at a density of $4x10^4$ cells per well in to 24 well plates with a coverslip in the base. 24 hours later, once adhered, growth medium was replaced with serum free media. The plates were incubated for a further 24 hours before half the plates were treated with 50ng ml^{-1} IGF-2 and the other half a vehicle only control and left for 1 hour (time point optimised by lab member previously) prior to fixation with 4% formaldehyde. Following permeabilisation and blocking, coverslips were incubated overnight at 4°C with a primary antibody in TBS/0.3% Triton and 3% serum (Table 2-1). After washing, coverslips were incubated with a secondary antibody for 2 hours prior to counterstaining with DAPI 1:10,000 and mounting on slides (Table 2-2).

3.3.3 Paraffin-embedded cell cores

Four Ewing cell lines each harbouring the EWS-FLI1 translocation, (A673, CHP-100, RD-ES, SK-N-MC) were grown in petri-dishes (d=14cm) for 2 days prior to 24 hours of serum starvation. After treatment with IGF-2 (50ng ml^{-1}) for 1 hour cells were trypsinised (TrypLE Express, Invitrogen, UK) and centrifuged at 1,000rpm for 5 minutes. Cells were resuspended in 4% neutral buffered formaldehyde and fixed for 1 hour at room

temperature. After centrifugation at 1,300rpm for 2 minutes, cells were re-suspended in 2% v/v agarose/4% formaldehyde warmed to 60°C, centrifuged at 2,000rpm for 20 seconds and kept on ice for 30 minutes to set. The agarose block containing the cell pellet was dehydrated in a descending alcohol series and embedded in paraffin. Five micrometer slices were cut and transferred to Polysin slides. Slides were dried overnight at 37°C and kept at 4°C until needed.

3.3.4 Tissue Microarrays (TMAs)

Tissue Microarrays (TMAs) have become a standard means by which prognostic biomarkers in tumours such as Ewing sarcoma are assessed. They comprise of a single paraffin block containing multiple duplicate cores (in this series 2mm) constructed from selected blocks of tumour tissue. They allow for a uniform approach to multiple samples which is economical in time, tissues, and cost (Hsu, Nielsen et al. 2002).

Ewing sarcoma tissue microarrays (TMA) were derived from three cohorts: the Institute of Pathology, University of Valencia (cohort a); the Institute of Pathology, University Medical Centre, Düsseldorf (cohort b); and the Department of Pathology, Leiden University Medical Centre (cohort c) in collaboration with EuroBoNet. Importation of annonymised tissue was approved under UK HTA licence and local ethical review to the Sarcoma component of the Oxford Research Biobank (HTA 12217, REC 09/H0606/5). A total of 314 formalin fixed and paraffin embedded pre-treatment biopsies were analysed with each TMA containing one (d=2mm, cohort a), three (d=2mm, cohort b) or two (d=1mm, cohort c) representative cores for each case respectively. 5µm sections of each TMA were processed.

3.3.5 Immuno-labelling of TMAs

TMA sections were deparaffinised in xylene (Fisher, 2x5 minutes), then rehydrated in an ethanol series (100% x2, 95%, 80%, 70%, 50% for 3 minutes each). After washing twice in deionised water, slides were permeabilised with TBS/0.5% Tween for 30 minutes at room temperature and washed several times in distilled water. For antigen de-masking slides were immersed in citrate buffer (pH6.0) and antigen retrieval was performed in a pressure cooker (Biocare Medical, UK) for 2 minutes at 125°C followed by 10 minutes at 85°C. Non specific binding was prevented by blocking in TBS/Tween20 (0.5%) and 10% goat serum for 1 hour at room temperature. Primary antibodies rabbit anti-Ki67, rabbit anti-Egr1, rabbit anti-FoxO3a and rabbit anti-pMAPK were incubated simultaneously with mouse anti-CD99 in a humidified chamber overnight at 4°C.

Slides were washed 3 times and then incubated for 2 hours at room temperature with a cocktail of 2 secondary antibodies; Alexa Fluor® 488 goat anti-rabbit and Alexa Fluor® 555 goat anti-mouse.

3.3.6 Image acquisition

Fluorescent images were obtained using an Olympus FVC1000 confocal microscope and a 60x oil objective (NA:1.35). Each image had a size of 2048 x 2048 pixels, a horizontal and vertical dimension of 211µm x 211µm and a thickness of 1.292µm. Between 1 and 6 images per patient were captured.

3.3.7 Image segmentation

Through collaboration with biomedical engineers (Yu, Li) a method of image segmentation was developed to identify DAPI stained nuclei with level set algorithms. For cytoplasmic segmentation a Voronoi tesselation was calculated based on equidistant partitioning between neighbouring and segmented nuclei, followed by a marker controlled

watershed method to find the inner boundaries based on the intensity gradient of CD99 alongside representative antibodies of the IGF pathway. Sample images were validated prior to unbiased quantification using Matlab software and presented as cumulative frequency plots before and after ligand exposure.

3.4 Results

3.4.1 Developing an unbiased method to assess for heterogeneity in Ewing sarcoma cell lines and biopsy tissue

From a panel of 10 Ewing sarcoma cell lines (EuroBoNet, Table 3-1) an assay was developed and optimised using immunolabelling and a customised image segmentation algorithm (developed by collaborators Yu and Li) involving level sets and Voronoi watershed partitioning. These were applied to cell lines to assess for activation of the IGF pathway once stimulated by the ligand IGF-2.

Following application to cell lines, the assay was applied to cell line cores. These were Ewing sarcoma cell lines which were formalin fixed and paraffin embedded as a core with the aim that they would mimic Ewing sarcoma tissue. Once validated the algorithm was applied to Ewing sarcoma TMAs obtained from EuroBoNet and unbiased quantification of biomarkers performed (Table 3-1).

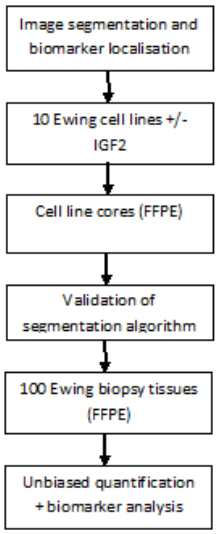
3.4.2 Intracellular biomarker localisation changes in response to IGF-2

Localisation of phosphoproteins in response to treatment with IGF-2 was assessed in cell lines. Cells were grown on coverslips and exposed to IGF-2 or a vehicle only control for 1 hour (this time point had been observed to be optimal in previous work performed by a lab colleague). Using immuno-labelling, pS6, a downstream biomarker of mTORC1 involved in growth signalling, showed an increase in cytoplasmic intensity in cells exposed to IGF-2. Similarly, pAkt shows an increase in intensity in the cytoplasm whereas transcription factors FoxO3a and Egr1 change in their localisation translocating from the nucleus to the cytoplasm, or cytoplasm to nucleus respectively (Figure 3-1).

Cell Line	Diagnosis	Source	Age	Sex	Translocation	Type of Fusion	p53
A673	ES	Muscle	15	F	t(11;22)	7/6	c.551_552insCA
CHP-100	pPNET	Mediastinum	12	F	t(11;22)	_	Wt
RD-ES	ES	Humerus	19	M	t(11;22)	7/5	p.Arg273Cys
RM-82	ES	Femur	8	M	t(21;22)	7/6	p.Arg273His
SK-N-MC	pPNET	Supraorbital	14	F	t(11;22)	_	c.170_572del
STA-ET1	pPNET	Humerus	13	F	t(11;22)	_	Wt
STA-ET2.1	pPNET	Fibula	15	M	t(11;22)	_	p.Cys277tyr
STA -ET10	ES	Muscle (paraspinal)	2	F	t(2;22)	_	Wt
TC71	ES	Humerus	22	M	t(11;22)	7/5	p.Arg213X
WE-68	ES	Fibula	19	F	t(11;22)	7/6	Wt

Table 3-1. Cell lines obtained from EuroBoNet. All cell lines were grown in RPMI (10% FCS, 1%PS) and regularly tested for mycoplasma. Cell line data obtained from EuroBoNet publication described diagnosis, Ewing sarcoma (ES) or peripheral primitive neuroectodermal tumours (pPNET), anatomical location of tumour, age and gender of donor, translocation and fusion type, and p53 status (Ottaviano, Schaefer et al. 2010).

A



B

antibodies	IGF2 dependent. Localisation or Intensity
pS6(Ser235/236)	Increase in intensity
Fox03a	Nucleus → cytoplasm
pAkt	Increase in intensity
Egr1	Cytoplasm → nucleus
CD99	Membrane

C

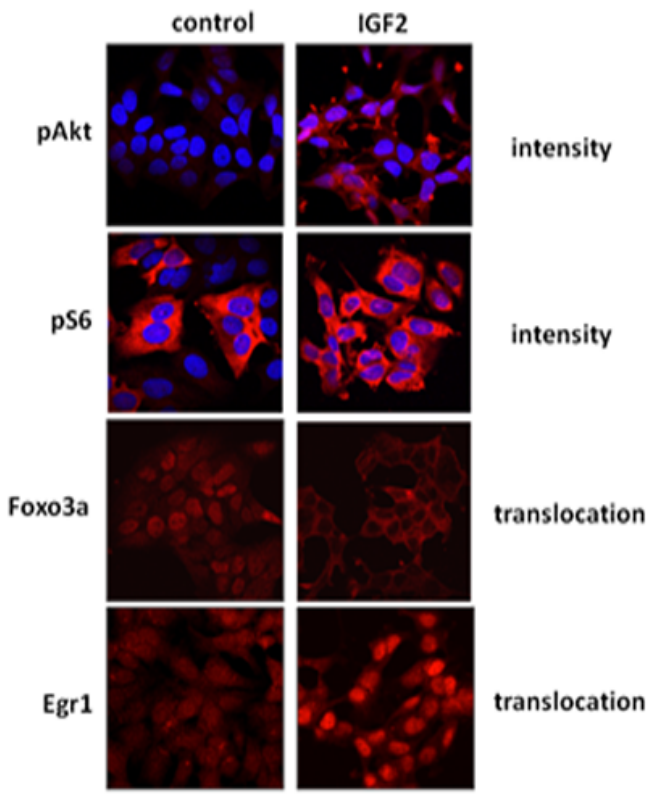


Figure 3-1. Strategy of work and antibody localisation. **A** - identification of antibody localisation and development of computer generated image segmentation was carried out, and then applied to 10 Ewing sarcoma cell lines prior to cell lines embedded in a paraffin core. Following validation against manual segmentation it was applied to TMAs before biomarker analysis and quantification. **B** – antibodies were tested and changes in localisation or intensity recorded of proteins in the IGF pathway. CD99 was identified in the membrane of cells. **C** - pS6 and pAKT (protein labelled red) both showed an increase in intensity to IGF-2 ligand exposure. FoxO3a and Egr1 show a change in localisation with increased cytoplasmic fluorescence and nuclear fluorescence respectively.

3.4.3 Validation of image analysis in Ewing sarcoma cell lines

Sample segmented images were validated relative to three experts who had undergone training and practice on manual segmentation (HBW, CB, HY). This demonstrated that nuclear segmentation performed manually compared with that calculated by the computer algorithm had a specificity of 89.8% (Table 3-2). Hausdorff distance (the number of pixels between manual and computer generated segmentation of the nucleus) in the majority of cases was less than 10 pixels (0.8μm). This was confirmed by Bland-Altman analysis highlighting similarities of segmentation. DNA content between the treated and untreated groups was unchanged (Figure 3-2).

Image	Over-segmentation	Well segmented nuclei	Under segmentation	Fake nuclei	Manual segmentation	Computer segmentation
A673_1	0	17	0	2	17	19
A673_2	0	24	0	0	24	24
A673_3	0	24	0	0	24	24
RD-ES_1	1	18	0	0	21	23
RD-ES_2	0	21	0	0	21	21
RD-ES_3	0	20	0	1	20	21
SK-N-MC_1	0	33	6	0	43	40
SK-N-MC_2	0	23	5	0	27	25
SK-N-MC_3	1	31	9	1	41	28
SK-N-MC_4	1	17	0	0	18	19

Table 3-2. Validation of cell line nuclear segmentation. The manual segmentation was carried out by 3 independent scientists and an average of their scores per image taken. Comparison was made with data produced by the computer algorithm. A specificity of 89.8% was observed.

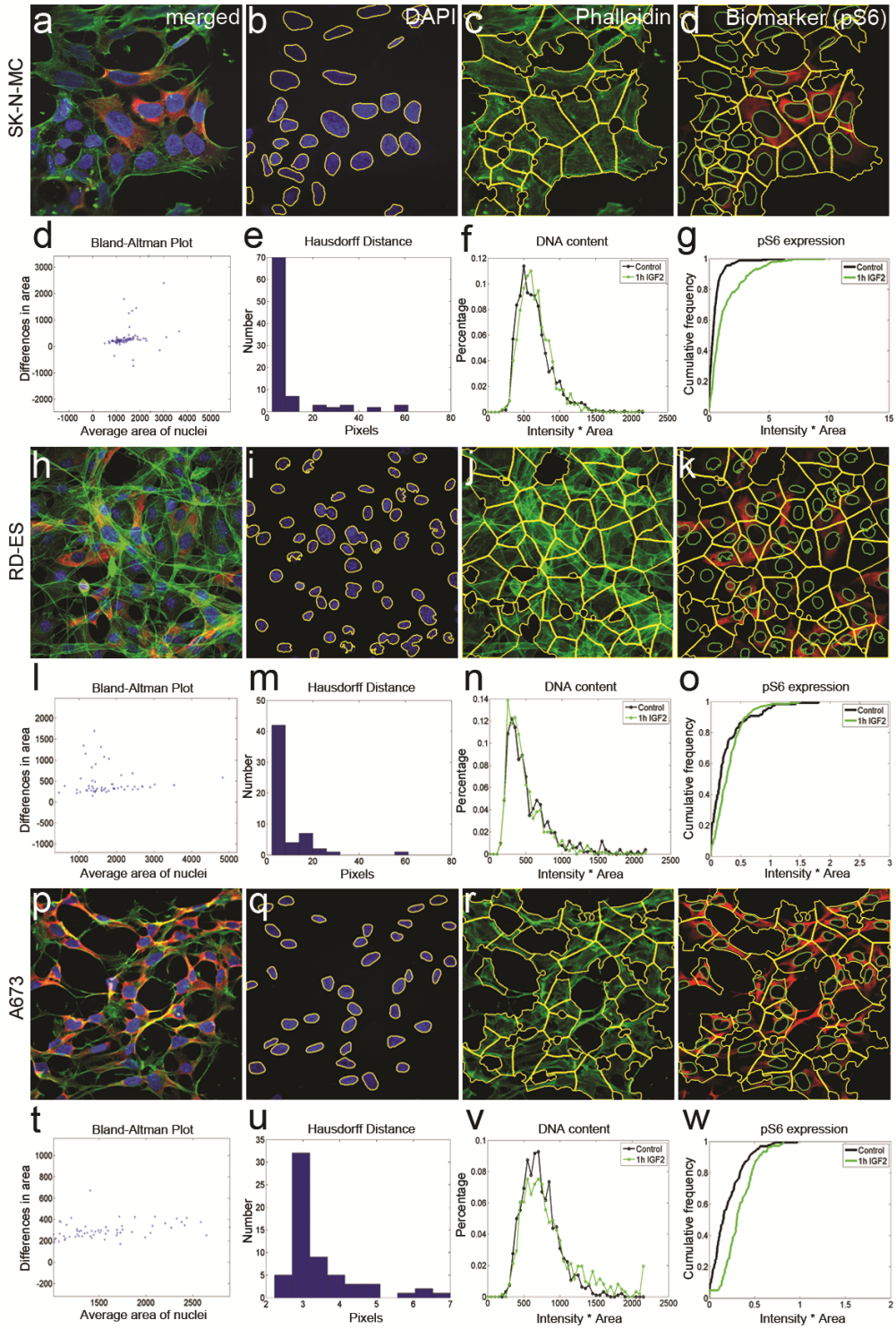


Figure 3-2. Signalling responses were quantified after treatment with IGF-2. SK-N-MC a-g, RD-ES h-o, and A673 p-w, Ewing sarcoma cell lines were incubated with IGF-2 for 1h after 24h serum starvation. The images were captured with confocal microscopy and segmented with a combination of nuclear DAPI and cytoplasmic phalloidin. The activation of the IGF pathway was revealed by an increase in the expression intensity of the ribosomal protein pS6 in the cytoplasm, with distribution of nuclear DNA and pS6 shown with Bland-Altman and Hausdorff validation.

3.4.4 Heterogeneity of signalling is seen in Ewing sarcoma cell lines

In order to dissect the heterogeneity of response of the IGF pathway to the ligand IGF-2 the customised algorithm was applied to a panel of Ewing sarcoma cell lines and simultaneous fluorescent detection of phalloidin, DAPI, signalling biomarkers pS6, FoxO3a and Egr1 were imaged by multi-spectral confocal microscopy. Cumulative frequency plots were generated to illustrate the cell line specific effects of biomarker nuclear-cytoplasmic localisation distributions (Figure 3-2). These demonstrate heterogeneity between cell lines in their overall response to IGF-2 stimulation despite each having a EWS-FLI1 based translocation. In particular, variation in response of pS6 and FoxO3a was particularly striking confirming that there is biomarker heterogeneity (Figure 3-3). In addition the cumulative frequency plots illustrate that although derived from an assumed clonal cell line, individual cells show a distribution in nuclear to cytoplasmic ratio with IGF-2 stimulation.

By measuring intensity of DAPI, DNA content was calculated for each cell line. It was observed that DNA content between untreated and IGF-2 treated cells were equivalent, however there was variation overall between the different Ewing sarcoma cell lines (Figure 3-4).

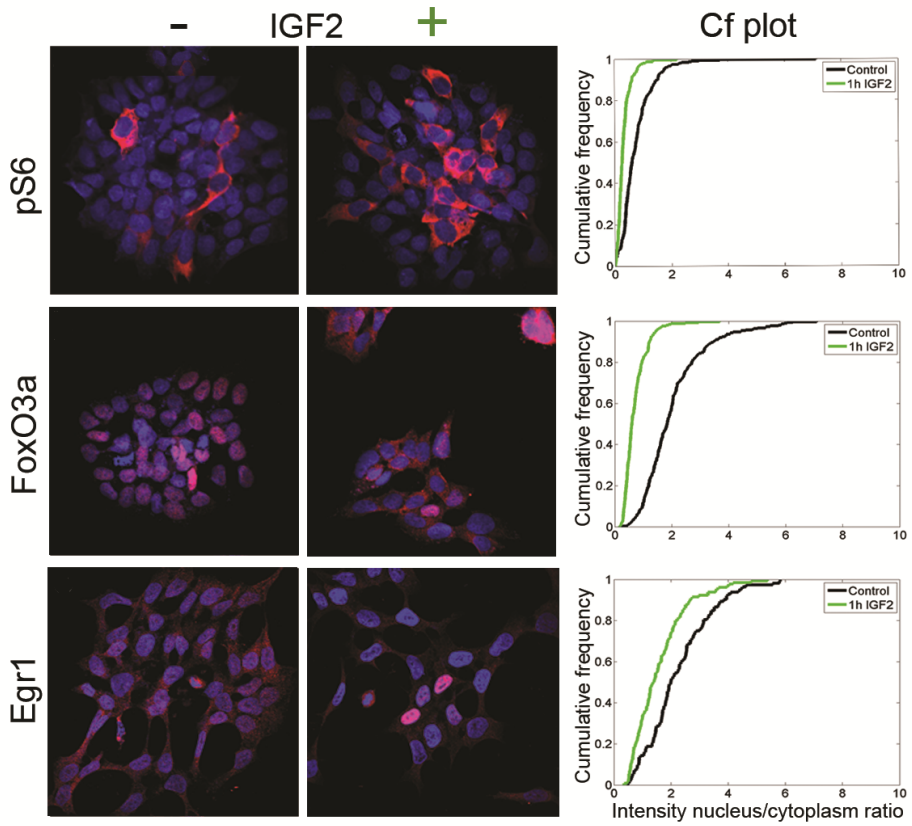


Figure 3-3. Responses of cell lines to IGF-2. SK-N-MC were incubated with (+) or without (-) IGF-2 for 1 hour following growth in serum free conditions. The activation of the IGF pathway through signalling biomarkers is illustrated by a cumulative frequency plots. Signalling pathway activity was quantified using image analysis with the markers (pS6, FoxO3a, Egr1) quantified in each cell compartment before and after treatment with IGF-2. An increase in expression intensity of ribosomal protein pS6 was shown in the cytoplasm. Furthermore the transcription factor FoxO3a translocates from the nucleus to the cytoplasm whereas Egr1, which is activated via the MEK/ERK pathway, translocates from the cytoplasm to the nucleus.

3.4.5 FoxO3a translocation in response to IGF-2 is heterogeneous in Ewing cell lines

In order to dissect the heterogeneity of response of the IGF pathway to the ligand IGF-2, the validated algorithm was applied to a panel of 10 Ewing sarcoma cell lines. FoxO3a translocates from the nulceus to the cytoplasm in all of the Ewing sarcoma cell lines analysed but to differing degrees. SK-N-MC and CHP-100 show particularly marked responses whereas RD-ES and RM82 demonstrate little change (Figure 3-4). FoxO3a, a member of the O subfamily of the forkhead transcription factors is a critical downstream molecule of the IGF-1/insulin signalling pathway (Figure 1-2). In response to IGF-1, IGF-2, or insulin, FoxO3a is phosphorylated by PI3K-Akt and excluded from the nucleus, which prevents its binding to the promoters of its target genes. Thus, this cytoplasmic retention impairs the transcriptional regulation function of FoxO3a (Calnan and Brunet 2008). This demonstrates the heterogeneity of responses of the PI3K-Akt axis to stimulation between and within different Ewing sarcoma cell lines.

3.4.6 pS6 increases in intensity when Ewing cell lines are exposed to IGF-2

STA-ET1 clearly shows an increase in pS6 on exposure of the cell line to IGF-2. This is similar to responses seen in all other lines, with the exception of RD-ES which does not show a response (Figure 3-4).

3.4.7 Egr1 translocates from 1 out 10 of Ewing cell lines on exposure to the ligand

Egr1, a read-out of the MAPK pathway translocates from the cytoplasm to the nucleus in SK-N-MC but not in other cell lines (Figure 3-4). Egr1 is regulated through the ERK pathway resulting in Egr1 transcription. Low Egr1 expression in tumour tissue has been observed in breast cancer, glioblastoma, and in other solid tumours as well as in immortalised cell lines (Liu, Yao et al. 1999, Baron, Adamson et al. 2006). This could be

an explanation for the overall lack of response to IGF-2 stimulation observed in cell lines tested.

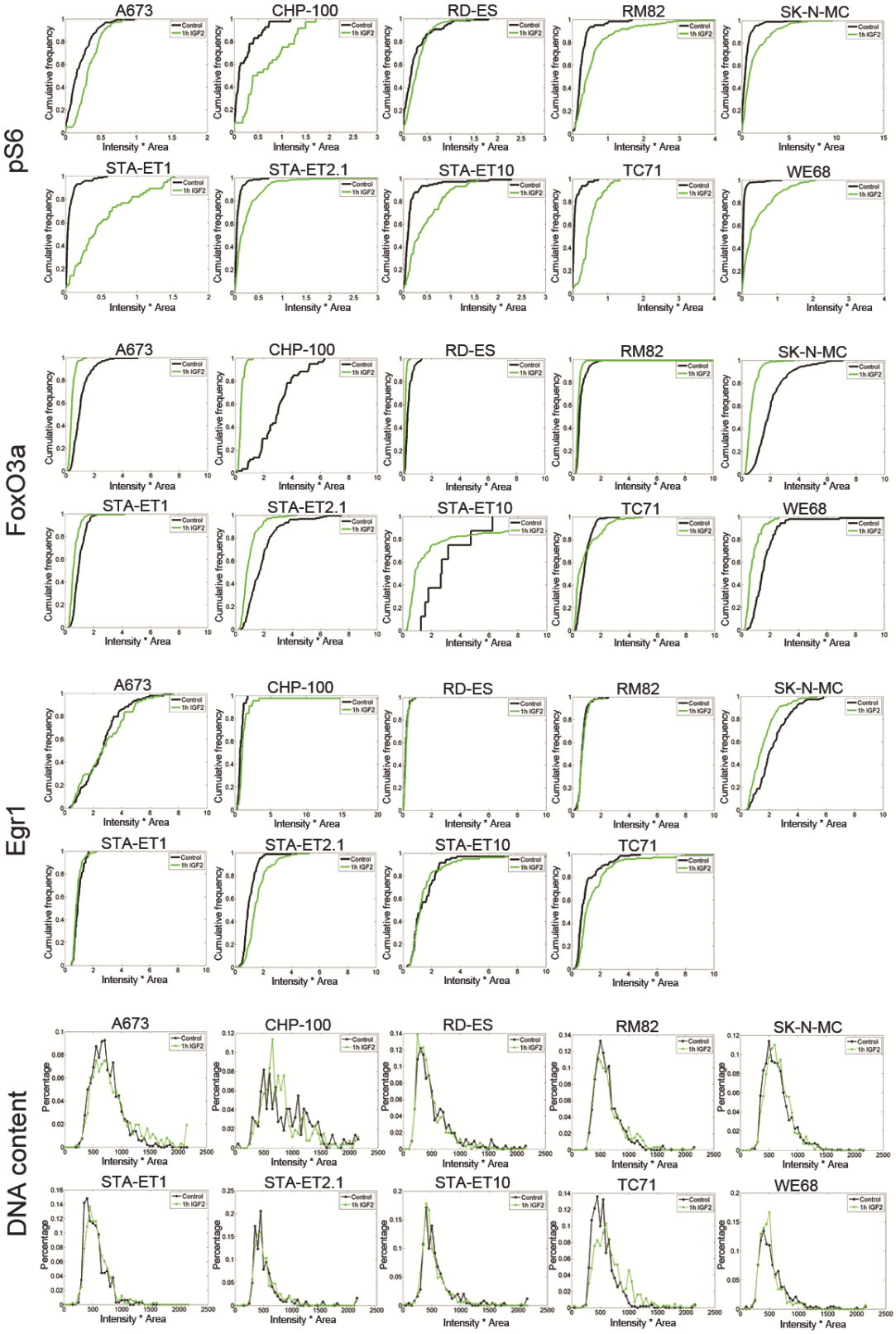


Figure 3-4. Signalling pathway activity was quantified by image analysis. Response of pS6, FoxO3a and Egr1 in cell lines was quantified before and after treatment with the ligand IGF-2. Each cell line responded with different degrees of heterogeneity. Total DNA intensity of both control and IGF-2 treated groups showed similarity within the cell lines. These data indicate the utility of the segmentation algorithm in the detection of biomarker heterogeneity.

3.4.8 Application of image segmentation algorithm to Ewing sarcoma cell cores

In order to mimic a more complex structure closer to that of Ewing sarcoma tissue, such as clumping or overlapping of cells, cell line cores were formed (FFPE) and the algorithm validation was carried out against these (Figure 3-5A+B) .

3.4.9 Unbiased quantification can be applied to Ewing sarcoma biopsies

The aim was to use the developed automated algorithm to analyse whether patient outcome could automatically be predicted by the algorithm and identify image features in Ewing sarcoma biopsy samples (EuroBoNet) which could distinguish between outcomes. Biopsy samples (118) assembled on a TMA (Figure 3-5C) were labelled with fluorescent antibodies against IGF pathway signalling proteins and the boundaries for nuclei and cells were identified from the DAPI and CD99 markers (fluorescence labelling and confocal microscopy performed by HBW and CB, development of algorithm SL and HY).

Again, image segmentation was validated using Hausdorff distance and Bland-Altman plots. The accuracy of the segmentation was similar in comparison to cells in culture and cores. The number of cells segmented per image was in the range of 50-500 depending on density and up to 4 images were taken from random sites for each patient and biomarker (Figure 3-5D+E). In total 476 multi-spectral confocal images were captured from the 118 patients resulting in 113,201 individual cells being analysed. Measurements of the marker intensities in single cells were obtained and used to create an overall distribution for each patient.

Although the development of the algorithm and analysis was carried out by colleagues (Yu and Li) for completeness a brief summary has been included. Using linked clinical outcome data for the TMAs (Table 3-2), marker distributions were analysed with respect to patient survival using random survival forests (RSF), a machine learning tool which

automatically generates predictions by combining features. The distribution of Ki67 being predictive of overall survival is suggested by existing research (Lopez-Guerrero, Machado et al. 2011) and this was confirmed by manual grading of images. It has been shown that Ki67 may be decreased by prolonged formalin fixation so technical factors have to be considered when interpreting data (Hitchman, Hodgkinson et al. 2011). Contrary to expectations the RSF suggested that cells with lower levels of CD99 in the cytoplasm were most discriminative, for reasons still to be determined (Figure 3-6).

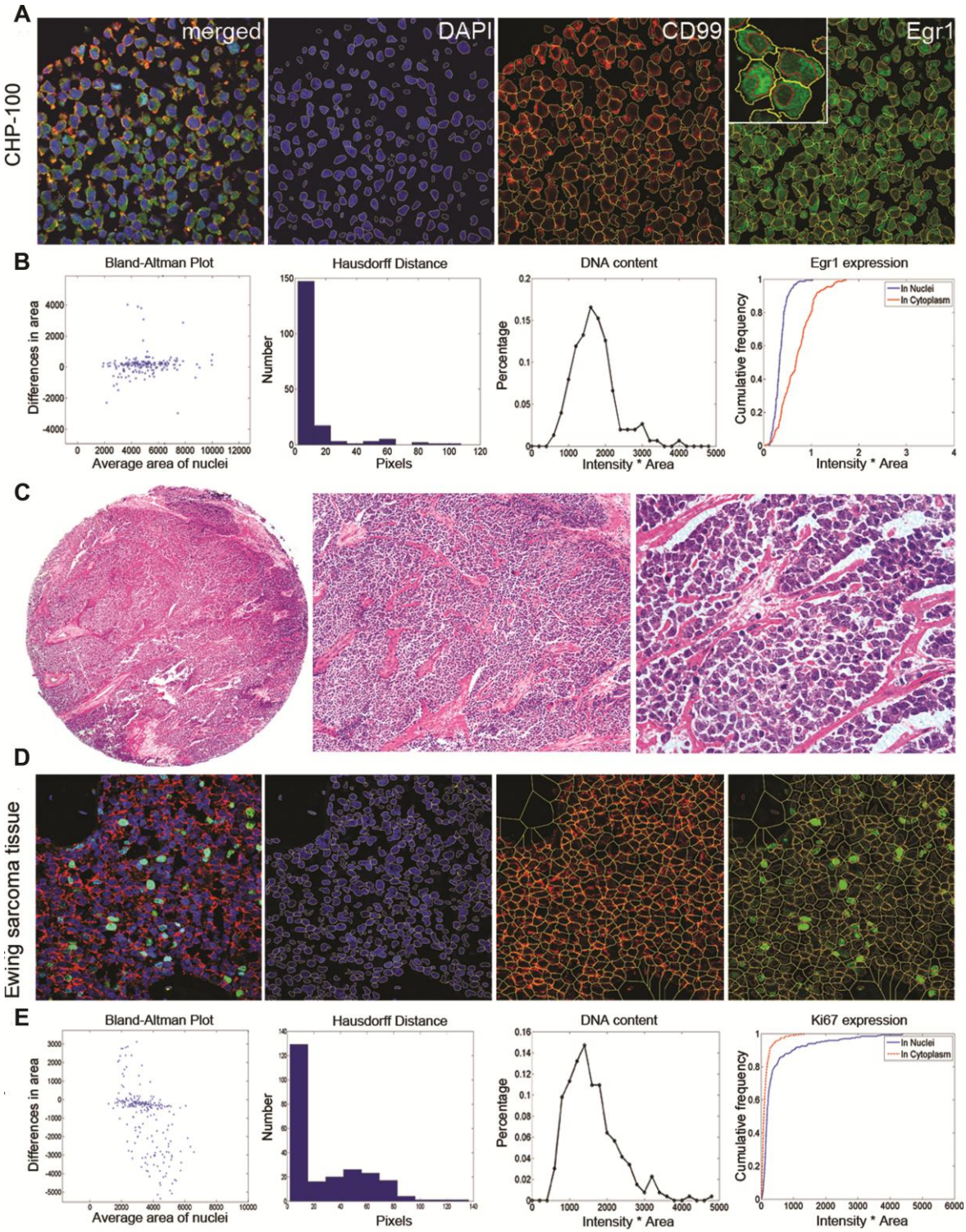


Figure 3-5. Confocal images of agar pellets of EWS-FLI1 positive Ewing sarcoma cell lines were used to optimise image segmentation. A - Multi-channel and single channel images (with segmentation lines) of CHP-100 in cores labelled with DAPI, CD99 and Egr1 biomarker indicating nucleus and cytoplasm localisation, respectively (see high magnification insert). **B** - >500 cells were manually segmented and compared to the image segmentation algorithm using Bland-Altman and Hausdorff distance. Also, example distributions are shown for nuclear DNA content and nuclear and cytoplasmic localisation of Egr1. **C** - Image segmentation was applied to tissue microarrays of Ewing sarcoma biopsies **D** - multi-channel confocal images captured for DAPI, CD99 and Ki67 proliferation marker. **E** - >500 cells were manually segmented and compared to the image segmentation algorithm using Bland-Altman and Hausdorff distance, with distributions for DNA and Ki67. Bars: 20 µm (a. and d.), and in c, 200, 100 and 50 µm, respectively.

Clinical features	Cohort a (n = 43)	Cohort b (n = 16)	Cohort c (n = 59)
Status (% alive)	70	33	62
Male: Female ratio	1.26:1	3:1	1.185:1
Mean age	19	19	18
Site (%, central: peripheral: extra-osseous)	39: 33: 28	19: 75: 6	31: 69: 0
Tumour volume (%, <200 ml: ≥200 ml: ND)	63: 26: 12	13: 25: 62	NA
Metastasis (Yes: No: ND)	98: 0: 2	19: 69: 12	34: 66
Translocation (%, EWS-FLI1: Non-FLI1*: ND)	74: 9: 16	31: 38: 31	88: 0: 12

* Non EWS-FLI1 = EWS-ERG; EWS-NFATC2 or EWSR1-re-arranged (no FLI or ERG partner).

Note: all patients treated in Europe with standard chemotherapeutic, radiotherapy and surgical trial protocol (EICESS92 / EE99 CESS81).

ND: data not available.

Table 3-3. Survival data from 118 patients from three separate European cohorts which correlate to biopsy samples analysed.

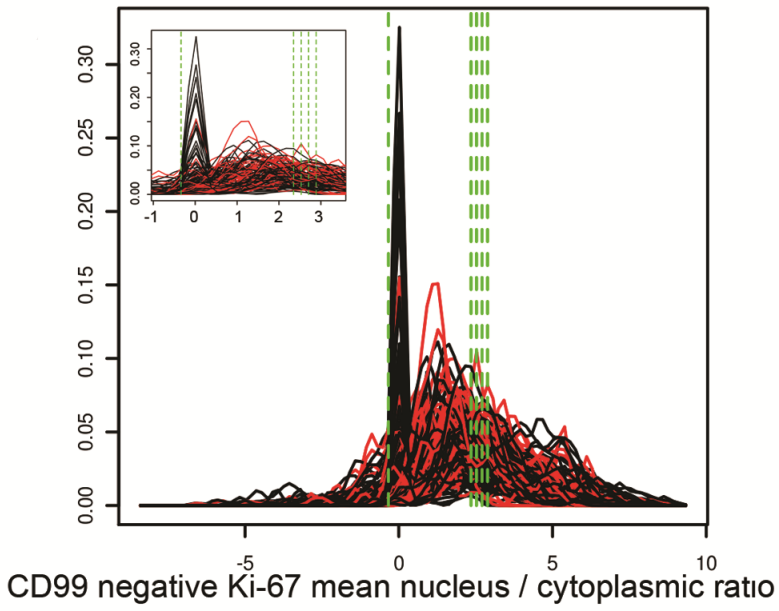


Figure 3-6. Random forest machine learning predicts a correlation between survival and cells which have low cytoplasmic labelling of CD99 and Ki67 positive cells. The black peak represents the image features of each patient predicted by random forest to correlate with overall survival (Analysis carried out by S Li).

3.5 Discussion

The principle outcome of this chapter was the observation, through the development of an automated method of unbiased quantification, that Ewing sarcoma cell lines are heterogeneous in their signalling response to IGF-2. When applied to tissue samples, image distribution features were analysed in relation to overall patient survival and a potential classifier observed between the proliferative marker Ki67 and a sub-population of cells with low cytoplasmic: nuclear ratio of CD99.

3.5.1 Development of a method of unbiased quantification confirms heterogeneity in Ewing sarcoma cell lines

Single cells can display varied behaviour even within a monoclonal population cultured under identical conditions. Multiple mechanisms exist for a particular cellular behaviour or activity which can vary between cells. The majority of experimental techniques to investigate heterogeneity have been carried out at a cellular population level which utilises statistical averages and does not consider individual cells and the different genetic mechanism which they can employ for the same cellular process (Pelkmans 2012).

Genetic and non-genetic variability can both be attributed to heterogeneity. The non-genetic sources are not fixed by heritable transmission and can be described as stochastic in nature, such as random fluctuations in transcription or translation. Yuan et al. described cell to cell variability in the PI3K pathway. Using flow cytometry they showed heterogeneity in PI3K activity in a breast cancer cell population. They proposed that heterogeneity of PI3K activity could be beneficial to normal tissues by restricting the activity of the pathway to a subset of cells, thereby protecting the population from an over activating pathway similar to that seen in cancers (Yuan, Wulf et al. 2011). When modelling acute responses to anticancer agents in drug sensitive cancer cell lines, Sharma et al. observed a population of reversibly drug tolerant cells. They found a subpopulation

of cells which transiently exhibit a distinct phenotype characterised by high IGF-1R signalling and KDM5A expression resulting in gefitinib resistance (Sharma, Lee et al. 2010).

High throughput image based technologies and computational image analysis have allowed large data sets to be constructed with measurements from multiple molecular and phenotypic states in large numbers of single cells (Boland and Murphy 1999, Carpenter 2009). Similarly, work in this chapter showed heterogeneity of cell line responses to treatment with IGF-2 within the IGF pathway. Using a method of unbiased quantification to analyse responses to the ligand, subtle changes in pathway activation were detected confirming not only heterogeneity but also the reliance of the IGF pathway to IGF-2.

The image segmentation algorithm successfully identified the boundaries of nuclei and cytoplasm of individual cells (Figure 3-2). Simultaneous fluorescent detection of phalloidin, DAPI and signalling biomarkers such as pS6, FoxO3a or Egr1, were imaged by multi-spectral confocal microscopy and validated relatively to three experts using Hausdorff (maximum discrepancy between boundaries) and Bland-Altman plots of segmented areas. Cumulative frequency plots revealed cell line specific effects of biomarker distributions within nucleus and cytoplasm of each cell, indicating there was significant heterogeneity between each cell's response within a given cell culture, and that the biomarker antibodies were also informative.

3.5.2 Heterogeneity of signalling responses between Ewing sarcoma cell lines

Analysis of data across a panel of Ewing sarcoma cell lines showed relatively constant expression of DAPI both between cell lines and following exposure of individual cell lines to IGF-2 indicating a similar DNA content between cell lines which was unaffected by ligand exposure (Figure 3-4). RD-ES overall appeared to show the least response to ligand

exposure where as the PI3K pathway was stimulated in all other cell lines analysed as demonstrated by the increased intensity of pS6 and the translocation of FoxO3a. Retrospectively to this initial course of experiments, RD-ES was not confirmed to be a Ewing sarcoma cell line which may explain the inconsistent result observed. The MAPK pathway was analysed via Egr1 which overall showed a lesser response to stimulation with IGF-2 however SK-N-MC showed clear response through both sides of the IGF pathway.

3.5.3 Application of validated algorithm to Ewing sarcoma tissue biopsies

Automated approaches for unbiased quantification have been developed, yet sometimes lack resolution at the level of individual cells (Camp, Chung et al. 2002). Machine learning algorithms such as random forests provide a platform where informative components in all sources of data can be identified and incorporated into a multi-parameter classifier (Chen, Wang et al. 2010). The work in this chapter has contributed to illustrating how high content image analysis of cell biomarkers in tissues can be developed at the cellular level with image segmentation and applied to patient outcome, in this case as a prognostic classifier. Using Ewing sarcoma biopsy material as an example of a tumour defined by a common somatic genetic abnormality, cohorts were enriched sharing a unified genetic basis. The results indicate that there is considerable heterogeneity between different Ewing sarcoma cell lines as well as between individual cells within a tumour biopsy sample.

3.5.4 A subpopulation of cells with high Ki67 expression are identified as a potential prognostic marker

Specifically it was shown that there was correlation between Ki67 expression and the development of metastases. Through collaboration an unbiased and completely automated approach demonstrated Ki67 as an informative prognostic marker in terms of patient survival and in a subset of the total cell populations which were relatively CD99 negative (Figure 3-6). This illustrates a finding which may have been overlooked using single

biomarker analysis however the biological basis of this still requires further experimental investigation.

As mentioned positive staining of Ki67 can be significantly altered by methods of sample preparation and fixation which could potentially alter outcomes. Hitchman et al. showed a significant decrease in Ki67 staining samples fixed for 24 and 48 hours (Hitchman, Hodgkinson et al. 2011). By applying strict image based quality control criteria in order to discard non-informative images, 62% of the sampled images had to be excluded, leaving only a total of 118 patients with any informative images (Table 3-3). This highlighted the potential limitation of this work, as is frequently the case when studying rare tumour types that the quality and quantity of patient samples was very much dependent on "pre analytical processing". To maximise the capabilities of an unbiased approach to machine based learning algorithms a standardised approach to tissue collecting and processing is required (Neumeister, Anagnostou et al. 2012).

This work which has been submitted for publication, involved the development of an assay using a novel method which should result in both the unbiased quantification of pathway responses and an assessment of the distribution of signalling pathway activation in Ewing tumours.

4 Characterisation of Ewing sarcoma cell lines and response to OSI-906, a dual kinase inhibitor

4.1 Introduction

Inhibition of IGF-1R signalling has been shown to increase the sensitivity of Ewing sarcoma cells to chemotherapy since IGF-1R signalling protects tumour cells from many insults, including chemotherapeutic agents, thus limiting the efficacy of such therapy. Combining IGF-1R with conventional therapy may have the advantage of lowering the effective dosage of radiotherapy and chemotherapy, minimizing side effects whilst maintaining efficacy (Benini, Manara et al. 2001, Beech, Perer et al. 2003, Manara, Perdichizzi et al. 2005).

As described the most recent trial evidence suggests variation in response to IGF-1R inhibitors despite clear evidence of IGF-1R involvement in Ewing sarcoma. One mechanism to account for this is upregulation of Insulin receptor (IR) signalling. This switch from IGF-1R to IR continues to maintain proliferation and survival which could lead to the lack of response to patients from IGF-1R inhibitors and supports the rationale for co-targeting both receptors (Garofalo, Manara et al. 2011).

4.1.1 OSI-906, dual kinase inhibitor

OSI-906, or linsitinib, (cis-3-[8-amino-1-(2-phenyl-quinolin-7-yl)-imidazo[1,5-a]pyrazin-3-yl]-1-methyl-cyclobutanol) is a dual kinase small molecule inhibitor which selectively inhibits both IGF-1R and IR. *In vitro* studies have shown that treatment of cell lines with OSI-906 enhances inhibition of the IRS1-Akt signalling pathway. In a panel of 32 tumour cell lines derived from 10 tumour types, Buck et al. demonstrated a significant increase in sensitivity to OSI-906 in those cell lines which exhibited the highest expression of genes on the IGF axis. These included cell lines derived from Ewing sarcoma (SK-ES, RD-ES

and A673) (Buck, Gokhale et al. 2010). Early trials are underway using OSI-906 alone or in combination with other chemotherapy agents in non small cell lung cancer (NSCLC), and adrenocortical carcinoma (NCT01186861, NCT00739453).

4.1.2 Cancer stem cells and heterogeneity in Ewing sarcoma

Recently cancer stem cells (CSC) have been identified in Ewing sarcoma and are believed to be a factor in accounting for discrepancies in survival of the disease (Suvà, Riggi et al. 2009). These cells have self-renewal capability, undergo asymmetric division and are resistant to standard chemotherapy agents, resulting in them being a key target for further investigation. Using an assay based on aldehyde dehydrogenase (ALDH) Ewing sarcoma presumed CSC have been isolated. They have been found to have enriched clonogenic and sphere forming activity, are able to reconstitute a heterogeneous population, are enriched for expression of stem cell genes and are resistant to chemotherapy agents (Ginestier, Hur et al. 2007, Huang, Hynes et al. 2009, Alison, Guppy et al. 2010, Awad, Yustein et al. 2010). Until recently the consensus was that CSCs could give rise to non-CSC but not vice versa resulting in a hierarchical cell-lineage structure. However studies with breast cancer cell lines have demonstrated that there can be bidirectional interconversion between CSC and non-CSC (Boman, Wicha et al. 2007, Gupta, Fillmore et al. 2011).

It is appreciated that tumour cell populations are heterogeneous in terms of their signalling and functional capabilities. Sharma et al. reported on a link between drug tolerance and heterogeneity within a cancer cell population (PC9, a NSCLC derived cell line) (Sharma, Lee et al. 2010). Here, a small subpopulation of cells was identified which could survive high concentration drug exposure and then resume proliferation in the presence of the drug reflecting phenotypic heterogeneity of the cell line (Sharma, Lee et al. 2010). In an *in vivo* setting intratumour heterogeneity has been described using multiregion sequencing to

characterise the tumour genetic landscape in patients with renal cell carcinomas (RCC). This highlights the variation of mutations across regions within an individual tumour and the underrepresentation of these from a single biopsy specimen. Via phylogenetic reconstruction it was revealed that branched evolutionary tumour growth occurred rather than a linear evolution (Gerlinger, Rowan et al. 2012). Similarly using single cell exome sequencing Xu et al. identified mutant genes and their frequencies in RCC demonstrating the presence of heterogeneity at a single cell level. This could potentially lead to a more detailed understanding of drug resistance and tumour relapse in genetically complex tumours (Xu, Hou et al. 2012).

CSCs often have significantly elevated aldehyde dehydrogenase (ALDH) activity (Cheung, Wan et al. 2007). In addition to responsibilities in cell signalling pathways, ALDHs play a role in the oxidation of toxic aldehydes during alcohol metabolism. This cellular function is likely crucial for CSC longevity and probably a key explanation for the reported resistance of CSCs to chemotherapies, especially those that generate toxic aldehyde intermediates (Keysar and Jimeno 2010). A substrate for ALDH1, Aldefluor has been used to separate CSCs in cell lines and tumour tissue (Moreb 2008). Aldefluor has been used successfully to detect elevated ALDH1 activity in stem and progenitor cells of Ewing sarcoma as well as other diseases such as prostate and breast cancer (Alison, Guppy et al. 2010, Awad, Yustein et al. 2010, Le Magnen, Bubendorf et al. 2013). Even though this method has been used to identify CSCs and has been validated for some cancers, it has not been employed as widely as techniques that identify CSC surface markers such as CD44 or CD133 (Keysar and Jimeno 2010).

4.1.3 ABC transporters and drug resistance

ABC transporter proteins have been implicated in the development of resistance in Ewing sarcoma treatment (Roundhill and Burchill 2013) with increased expression resulting in the removal of chemotherapeutic agents from the cell, reduced effectiveness of chemotherapeutics and decreased survival resulting in drug resistance (Burger, Foekens et al. 2003). From a population of Ewing sarcoma cells, Yang et al. isolated a side population with stem-like properties which decreased in the presence of a calcium channel blocker (Yang, Zhang et al. 2010). This led them to postulate that the resistant phenotype was based on the expression of ABC transporters as high expression of ABC proteins efflux lipophilic chemotherapeutic agents. Similarly Awad et al. observed higher expression of ABC transporters in those cells selected as being high in expression of ALDH, a potential marker of stemness (Awad, Yustein et al. 2010). They validated their findings by treating ALDH high and low cell groups with verapamil, a calcium channel blocker which blocks the activity of the ABC transporter proteins. This confirmed their theory as a decrease in viability of the ALDH high population in the presence of verapamil and doxorubicin was observed.

4.2 Chapter Aims

To further characterise a panel of Ewing sarcoma cell lines in order to model heterogeneity and resistance to an IGF-1R pathway inhibitor. This includes responsiveness of cell lines to stimulation with IGF-2 as measured by proliferation and apoptosis, the expression of IGF-1R and IR, the presence of CSC within cell lines, and the expression of ABC transporters.

Following this cell lines will be exposed to OSI-906 and functional heterogeneity of responses assessed through viability, proliferation, apoptosis, and cell cycle analysis.

4.3 Materials and Methods

4.3.1 Cell labelling with Aldefluor assay

Aldefluor contains the ALDH1 substrate BODIPY-aminoacetaldehyde (BAAA) which is converted by ALDH1 into the fluorescent product BODIPY-aminoacetate (BAA) as described in the product literature (Stem Cell Technologies).

Three cell lines SK-N-MC, CHP-100, and RD-ES were labelled with Aldefluor (Stem Cell Technologies) as per manufacturer's instructions. The aldefluor substrate BODIPY aminoacetaldehyde (BAAA) is taken up by live cells via passive diffusion where it is converted in the cytoplasm to a fluorescent molecule (BAA) under the action of ALDH. The fluorescent product accumulates in the cells due to the presence of ABC-transporter inhibitors in the assay buffer which prevents active efflux allowing cells with high and low ALDH activity to be isolated via flow cytometry. ALDH activity can be inhibited by the addition of DEAB (diethylaminobenzaldehyde) allowing the differentiation of those with high activity of ALDH. BAA is excited at 488nm and fluorescence detected by a standard 530/30 bandpass filter. Cells were sorted at The Weatherall Institute of Molecular Medicine.

4.3.2 qPCR of sorted aldefluor cells

RNA was extracted from cell groups grown in petri dishes (Qiagen RNeasy Plus Mini Kit). RT PCR (Invitrogen) and subsequent qPCR (Qiagen Rotagene 3000) were carried out and referenced to 3 housekeeping genes (see Chapter 2 for detailed methods). Data was analysed with Pfaffl formula.

4.3.3 Colony forming assay of cell lines

1ml of 0.6% agar (Sigma, A1296) prepared in complete media was added to each well of a 6 well plate and left at room temperature for 15 minutes to set. From the ALDH high, low

and unsorted cohorts, $3x10^4$ cells ml^{-1} in 0.3% agar were prepared and 1ml added to each well. Replicate wells for each sorted group were made. After 14 days cells were counted by eye with an inverted microscope at x4 magnification. 10 fields of view were counted and depth of field changed on 3 occasions for each well. Wells were seeded in replicate so this equated to 60 fields per group of sorted cells.

4.3.4 Preparation of OSI-906

OSI-906 was gifted by Astellas. Stock solution of 10mM was prepared with DMSO at room temperature and stored at -20°C. Repeated freeze thaw cycles were avoided.

The instructed maximum working concentration in cell based assays is 5µM. For dose response curves, OSI-906 was prepared from 10mM stock and diluted to a 10X solution in pre-warmed cell culture media containing 10% fetal calf serum and 5% DMSO.

4.3.5 Cell viability assay

To assess for cell viability the CellTiter 96® Aqueous One Solution Cell Proliferation Assay (Promega) was used following manufacturer's instructions. Cells were plated into 96 well plates, $1x10^4$ cells per well and left for 24 hours prior to incubation with OSI-906, 0-5µM (prepared as described above) for 72 hours.

The MTS Tetrazolium compound is bioreduced by cells into a coloured formazan product which is soluble in culture medium. The assay is performed by adding 20µl of MTS reagent to each well, incubating for 2 hours and recording absorbance at 490nm on a plate reader (SpectraMax). The quantity of formazan product is directly proportional to the number of living cells in culture.

4.3.6 SDS-PAGE electrophoresis and immunoblotting

Cells were grown in 10cm petri dishes until approximately 90% confluent. Media was removed and cells lysed with 1ml RIPA buffer (50mM Tris HCl pH8, 150 mM NaCl, 1%

NP-40, 0.5% sodium deoxycholate, 0.1% SDS) with protease and phosphastase inhibitors (Halt protease and phosphatase inhibitor cocktail, Thermo Scientific #78440). The lysate was spun at 13,000rpm at 4°C for 20 minutes. Protein levels were quantified using the CB-X assay (G-Biosciences, Cat no. 786-12X) as per manufacturer's instructions. The lysate was then mixed with 2x Laemlli sample buffer on ice and heated to 100°C for 5 minutes and then equal amounts of protein resolved by SDS-PAGE gel electrophoresis. Protein was transferred on to a PVDF membrane (Immobilon P, Millipore IPVH00010) and the membrane blocked with 5% BSA/0.1% TBST at room temperature for 1 hour. The membrane was then incubated with the primary antibody overnight with agitation at 4°C. Primary antibodies were prepared at 1:1,000 dilution unless otherwise stated.

Following incubation with the primary antibody the membrane was washed x3 in 5% BSA/0.1% TBST before incubation with a secondary goat anti-rabbit HPR conjugate (Dako P0448) or goat anti-mouse HPR conjugate (Dako P0447) 1:1,000 for 2 hours at room temperature. Again the membrane was washed x3 in 0.1% TBST and immunodetection performed using the Amersham ECL kit (RPN 2105) and Amersham Hyperfilm (28-9068-35) or Roche Lumifilm (11666657001) as per manufacturer's instructions.

4.3.7 EdU labelling

To assay proliferation cell lines were labelled with the thymidine analogue 5-ethynyl-2'-deoxyuridine (EdU). The Invitrogen Click-iT® EdU Alexa Fluor® 555 Imaging Kit (C10338) was used. EdU is incorporated in to DNA during active DNA synthesis. Detection is based on a click reaction, a copper catalyzed reaction between an azide (coupled to the Alexa Fluor® dye) and alkyne (found in the ethynyl moiety of EdU). This

click chemistry rather than antibody detection of the incorporated nucleotide does not require the DNA denaturation step needed with BrdU labelling.

Cells were seeded in to 6 well plates ($1x10^5$ cells per well). After 24 hours media was removed and cells were washed twice with PBS before being replaced by serum free media supplemented either with IGF-2 alone (dose range 0-100ng ml^{-1}), or 100ng ml^{-1} IGF-2 and OSI-906 (0, 0.1, 1μM). Incubation was for 24, 48, and 72 hours unless otherwise stated. Cells were labelled as per the manufacturer's instructions: a 2X working solution of EdU was prepared in complete media and incubated with cells at a final concentration of 10μM for 2 hours at 37°C. Cells were then trypsinised and fixed in 4% paraformaldehyde for 15 minutes at room temperature. Cells were washed twice in 3% BSA and incubated with TBS/Triton 0.5% for 20 minutes. They were washed twice more in 3% BSA and resuspended in 0.5ml of Click-iT® reaction cocktail and left to incubate for 30 minutes protected from light. The reaction cocktail was removed and cells washed prior to analysis by flow cytometry with excitation by a 488 laser and emission recorded with a PE band pass filter. $1x10^4$ live, single cells were recorded per time point and dose of OSI-906.

4.3.8 Measurement of apoptosis

Apoptosis was measured with a FAM FLICA™ Poly Caspase kit (ImmunoChemistry Technologies). The non-toxic FLICA™ FAM-VAD-FMK reagent permeates cells and irreversibly binds to activated caspases (caspase-1, -3, -4, -5, -6, -7, -8 and -9). Because the FLICA FAM-VAD-FMK reagent becomes covalently coupled to active caspases, it is retained within the cell, whereas any unbound FAM-VAD-FMK FLICA reagent diffuses out of the cell and is washed away. The remaining green fluorescent signal is a direct measure of the amount of caspase activity present in the cell at the time the reagent was

added. Cells that contain bound FLICA caspase detection reagent can be analyzed by flow cytometry. The carboxyfluorescein (FAM) FLICA reagent has an excitation range of 490 - 495 nm, and emission range of 515 - 525 nm. Samples can be counter-stained with Propidium Iodide (PI) to distinguish apoptosis from necrosis.

Cell lines were seeded in 6 well plates, $1x10^5$ cells per well. After 24 hours media was removed, wells were washed twice with PBS and replaced with serum free media supplemented with 100ng μl^{-1} of IGF-2. OSI-906 was added at a dose of 0, 0.1, and 1µM and incubated for 72 hours. Cells were stained following the manufacturer's protocol. In brief, cells were then trypsinised and resuspended in 290µl of media with 10µl of 30X FLICA reagent and incubated for 30-60 minutes at 37°C. They were then washed by adding 2ml 1X apoptosis wash buffer and centrifuged for 5 minutes. The supernatant was aspirated and cells were again resuspended in the apoptosis wash buffer and incubated for 10 minutes at 37°C to allow any unbound FLICA to diffuse out of the cells. They were then spun and resuspended in 600µl of buffer before the addition of 3µl of PI (prepared in kit) and a further incubation for 10 minutes prior to flow cytometry analysis ($2x10^4$ cells recorded per dose of OSI-906).

4.3.9 Cell cycle analysis

Cells were seeded at a density of $1x10^5$ cells per well in 6 well plates. After 24 hours they were exposed to 1µM OSI-906 or a DMSO control and incubated for 72 hours at 37°C. They were trypsinised, resuspended in 1ml of ice cold 4% paraformaldehyde, and left on ice for 30 minutes. They were washed twice with PBS and resuspended in 250µl PBS. 100µl of Propidium Iodide/ RNase mix (1mg ml^{-1} PI was mixed with 10µl of 100mg ml^{-1} RNase) was added and they were incubated for 30 minutes in the dark at room

temperature. They were analysed by flow cytometry. $2x10^4$ live, single cells were recorded per sample.

4.3.10 Flow cytometry analysis

To detect the effect of OSI-906 on proliferation, apoptosis, and cell cycle in cell lines samples were measured using flow cytometry on a Cyan (Beckman Coulter) cytometer and data analysed with FlowJo software.

4.4 Results

4.4.1 Ewing sarcoma cell lines vary in their expression of IR and IGF-1R genes

Expression of IR (both A and B isoforms) and IGF-1R was measured by qPCR in Ewing sarcoma cell lines (Figure 4-1). IGF-1R gene expression was measured by two separate assays, one using SYBR green reagent and the other with primers and probes designed using the Roche universal assay design webpage. This allowed for internal validation of findings and an assessment of the sensitivity of each assay. Results using SYBR green assay appeared to be marginally more sensitive than the primer/probe assay with similar patterns of expression being observed.

IR-A and IR-B expression was significantly elevated in SK-N-MC unlike IGF-1R expression which was low. STA-ET1 had high expression of IGF-1R in contrast with A673 and CHP-100 which have low expression. RD-ES is unique amongst the cell lines as it is the only one which expresses one IR isotype more highly than another (IR-B versus IR-A). All other cell lines appear to have consistency between IR-A and B expression.

4.4.2 Cell surface expression of IGF-1R and IR protein varies within cell lines

Surface expression of IGF-1R and IR was determined by flow cytometry. Cell lines were fixed and incubated with antibodies directed against IGF-1R, IR and an isotype control prior to incubation with a fluorescent secondary antibody.

STA-ET1 had significantly higher expression of IGF-1R compared with IR (Figure 4-2). This result is consistent with gene expression data analysed by qPCR (Figure 4-1). SK-N-MC had higher expression of IR compared with IGF-1R suggesting that there is correlation between the amount of surface receptor and expressed gene in the cell lines.

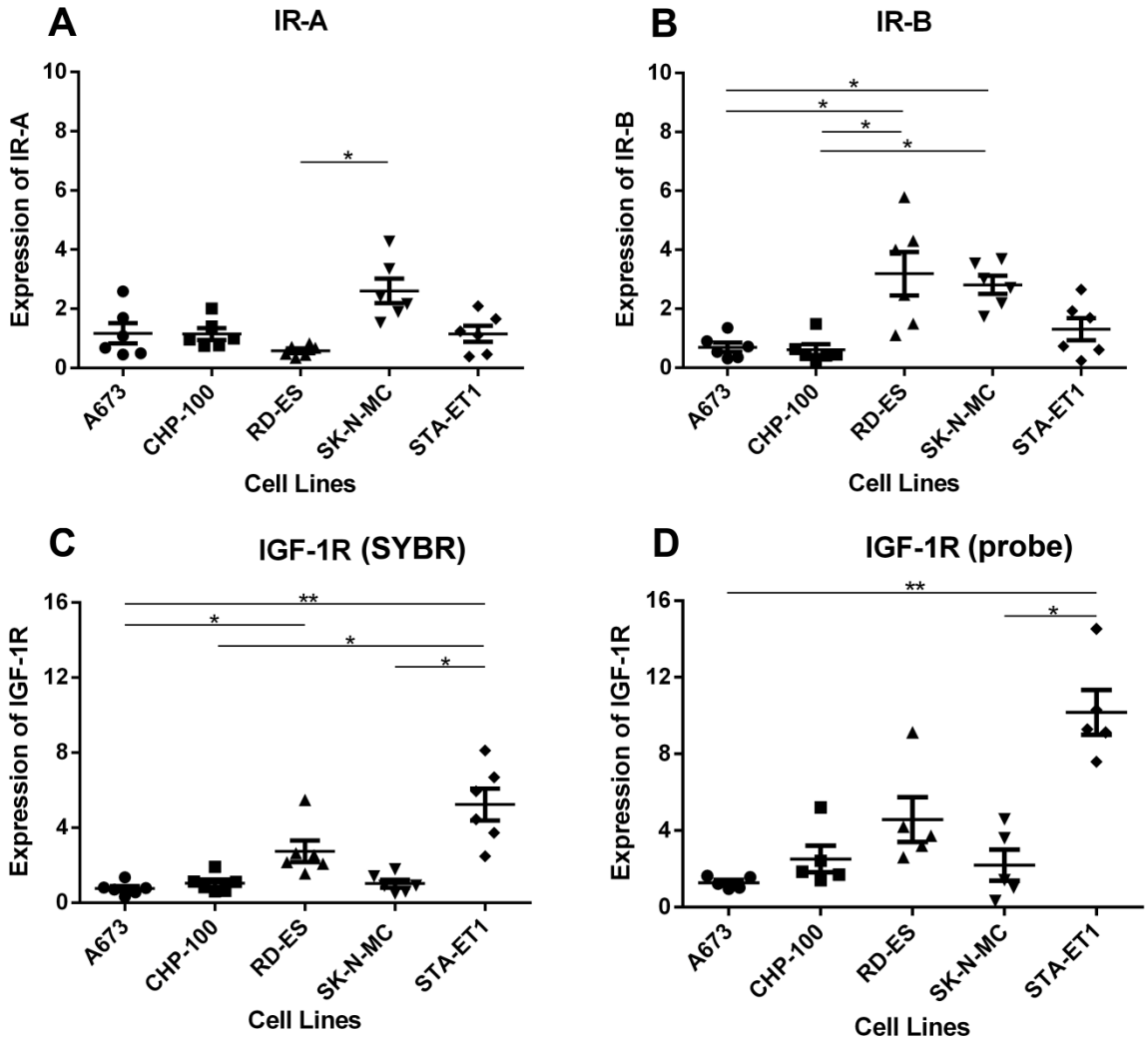


Figure 4-1. Ewing sarcoma cell lines vary in their expression of IR and IGF-1R genes. Expression of IR-A (**A**) and IR-B (**B**) were measured by qPCR. SK-N-MC showed higher expression of IR-A in comparison with RD-ES. SK-N-MC and RD-ES both had higher expression of IR-B isoform when compared with A673 and CHP-100. **C** – IGF-1R expression was measured with SYBR green assay. IGF-1R was more highly expressed in STA-ET1 compared with A673, CHP-100 and SK-N-MC (n=6). When validated against IGF-1R expression measured using primers designed via the Roche Universal Probe Library (**D**) STA-ET1 was confirmed to have increased expression in comparison with A673 and SK-N-MC but not with CHP-100 (n=5). Error lines represent ±SEM. Statistical comparison between cell lines was carried out using Kruskal Wallis test with Dunn's post test for multiple comparisons. * and ** represent $p<0.05$ and $p<0.01$ respectively.

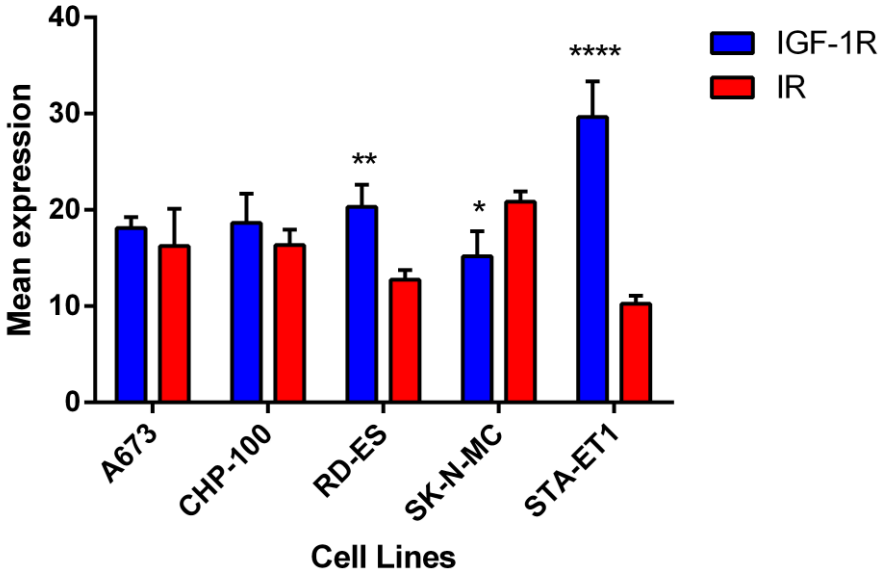


Figure 4-2. Expression of IGF-1R and IR in Ewing sarcoma cell lines measured by flow cytometry. Cell lines were labelled with antibodies directed against the cell surface receptors IGF-1R (blue) and IR (red). From a population of $2x10^4$ single, live cells, expression of both IGF-1R and IR was recorded. Statistical comparison was made between expression of both receptors. STA-ET1 had significantly greater expression of IGF-1R than IR where as SK-N-MC had higher expression of IR relative to IGF-1R. Statistical analysis used two way ANOVA with Sidek's test for multiple comparison. Results shown are an average of three separate experiments. Error bars represent SEM. (*, **, **** represent $p<0.05$, 0,1, and 0.0001 respectively).

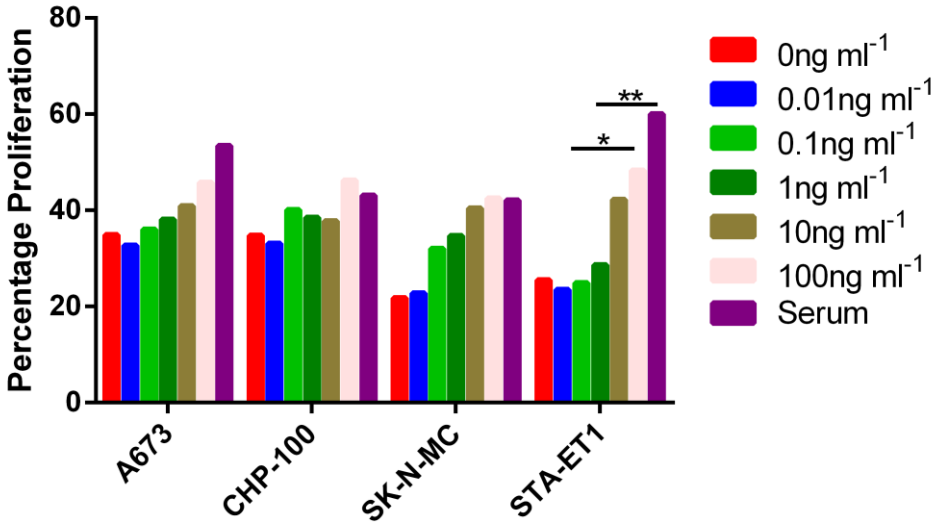


Figure 4-3. Proliferation in Ewing sarcoma cell lines increases in response to IGF-2 in a dose dependent manner. Cell lines were exposed to media supplemented with stated doses of IGF-2 or commercially purchased FCS. Proliferative response was measured at 72 hours via EdU assay. Each data point is a mean of three separate experiments. Comparison between IGF-2 doses was made. Each cell line shows an increase in proliferation with increasing doses of IGF-2. STA-ET1 showed the most marked effect with a significant difference observed between cells grown in 1ng ml^{-1} and 100ng ml^{-1}. Statistical comparison was made by one-way ANOVA with Tukey's post test to adjust for multiple comparisons. * and ** represent $p<0.05$, $p<0.01$ respectively, n=3. (For clarity of gating strategy applied reference **Figure 4-12**).

4.4.3 Proliferation of Ewing sarcoma cell lines increases in response to IGF-2

In order to characterise Ewing sarcoma cell lines further, response to IGF-2 was measured via EdU, an assay of proliferation. A series of doses of IGF-2 were added to cell lines as well as a complete serum to serve as a positive control (Figure 4-3). Cell lines were exposed for 72 hours before being analysed via flow cytometry. The gating strategy used was as in Figure 4-12. A mean of three separate experiments was used for comparison.

Each cell line showed an increase in percentage proliferation on increasing dose of IGF-2. The cells grown in serum had the highest levels of proliferation which allows for the assumption that the commercial foetal calf serum contains a higher concentration of IGF-2 than 100ng ml^{-1}. The least responsive cell line to the ligand was CHP-100 which did not demonstrate such a marked increase in proliferation unlike STA-ET1 which had a significant increase between 0.1ng ml^{-1} and 100ng ml^{-1} (Figure 4-3).

4.4.4 Ewing sarcoma cell lines have a subpopulation of cells with high expression of aldehyde dehydrogenase

Award et al. proposed the existence of a population of CSC within Ewing sarcoma cell lines by identifying those cells having high aldehyde dehyrogenase (ALDH) activity. Using the same assay reagent Aldefluor™ (Stem Cell Technologies) the aim was to determine the presence of cancer stem cells in 3 Ewing sarcoma cell lines through qPCR and a colony forming assay.

To determine whether Ewing sarcoma cell lines contain a high ALDH expressing stem cell-like population Aldefluor™ reagent was used to test ALDH activity in CHP-100, RD-ES, and SK-N-MC. Each cell line contained a population of cells with fluorescence which was inhibited by the ALDH inhibitor DEAB (Figure 4-4). There was a distribution of

activity across the population of cells and the most and least brightest were isloated and expanded in culture (Figure 4-5).

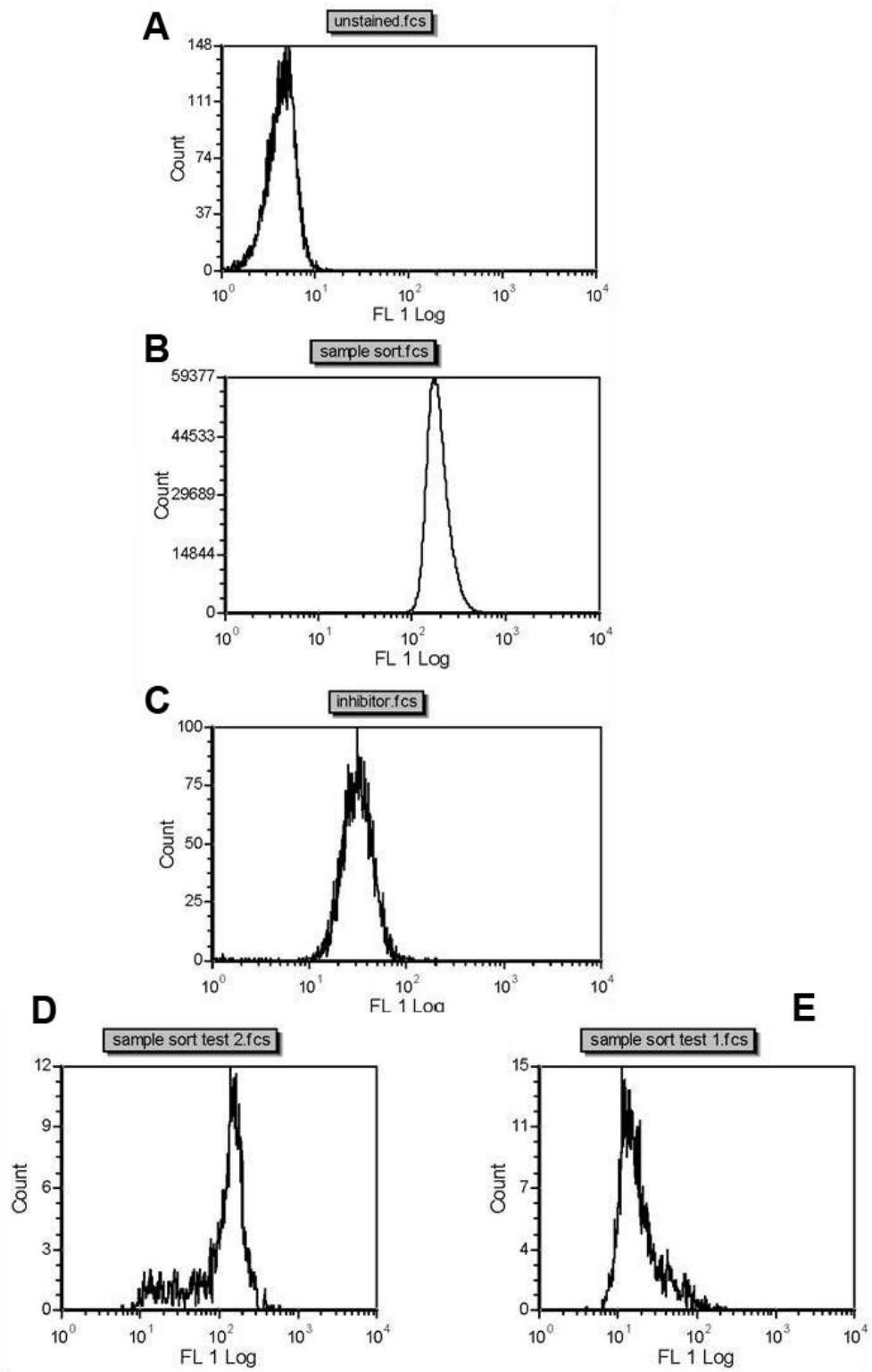


Figure 4-4. CHP-100 cells show ALDH expression which is inhibited by DEAB. A – Unstained CHP-100 cells. **B** – Aldefluor™ labelled cells show a fluorescent population **C** – which can be inhibited by DEAB. **D**, **E** – Post analysis of the high (**D**) and low (**E**) populations confirm that the gated regions were maintained throughout the sorting process.

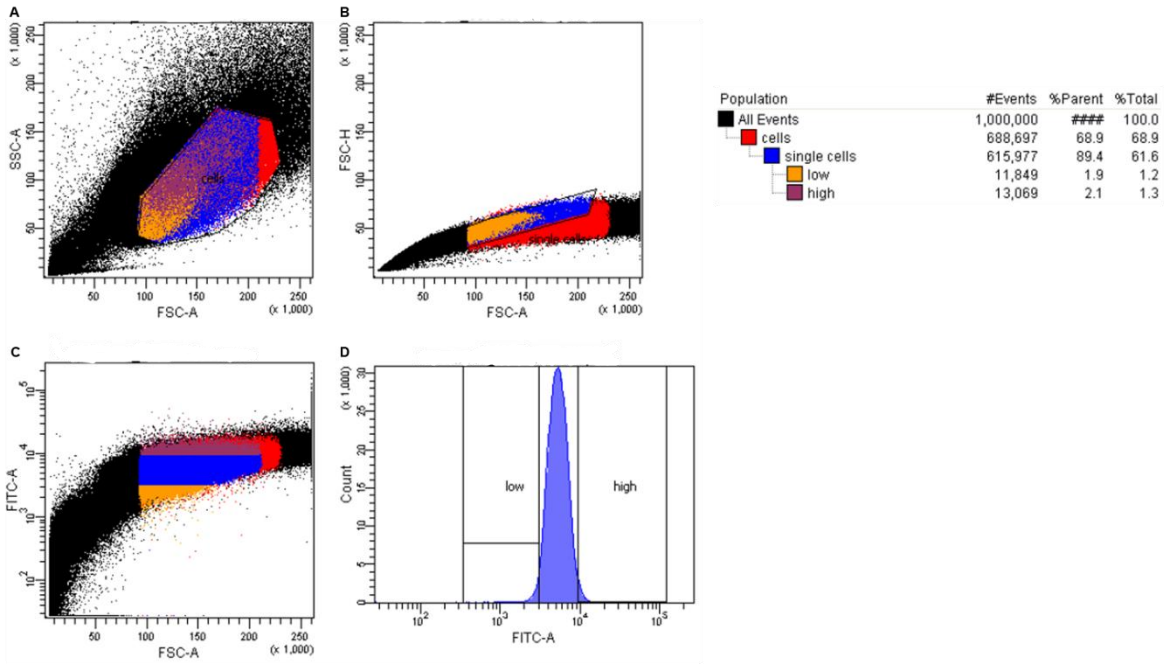


Figure 4-5. Illustration of cell population (CHP-100 in this example) sorted for ALDH, a marker of stemness. A - cell lines were labelled with Aldefluor™ assay and sorted with a flow cytometer at The Weatherall Institute of Molecular Medicine. **B** – from a population of $1x10^6$ cells viable, single cells were identified. **C** – Aldefluor™ expression in the cell population was detected by FITC. **D** – top 2% and bottom 2% of the single viable cells were gated. These populations (purple representing high, yellow representing low) were collected and expanded in culture for further experiments. These sorting experiments were performed a minimum of 3 times on each cell line.

4.4.5 Expression of stem cell genes is not related to ALDH expression in Ewing sarcoma cell lines

Subpopulations (ALDH high and ALDH low) of sorted Ewing sarcoma cell lines and the parent population were analysed for gene expression with qPCR referencing to three housekeeping genes (B2M, GAPDH, and HPRT) (Figure 4-6). It was predicted that the ALDH gene would be more highly expressed in the ALDH high groups in comparison with the ALDH low groups. Although not statistically significant, (possibly due to low numbers of samples tested), a trend towards higher expression of ALDH high compared with ALDH low sorted cells was observed in CHP-100, RD-ES, and SK-N-MC. This was expected as cell groups were analysed as promptly after flow cytometry sorting as possible. CD99 and EWS-FLI1 expression were not significantly altered between the cell groups indicating that cells in the low subpopulations continue to express the characteristic membrane marker of Ewing sarcoma. Interestingly, RD-ES had higher CD99 expression overall compared to CHP-100 and SK-N-MC. It was envisaged that the ALDH high groups of cells be enriched for expression of genes which are predicted to play key roles in stem cell biology such as the polycomb groups gene BMI-1 (Molofsky, Pardal et al. 2003), and the DNA binding domain-containing gene OCT-4 (Ponti, Costa et al. 2005). In contrast to previous work (Awad, Yustein et al. 2010) no significant difference was noted between the sorted groups. It is likely that low sample numbers have not allowed a conclusive result to be gauged however it could indicate that ALDH may not be identifying stem cell populations in these cell lines. To validate whether this is the case comparison with alternative markers of stem cell such as CD133 could be made.

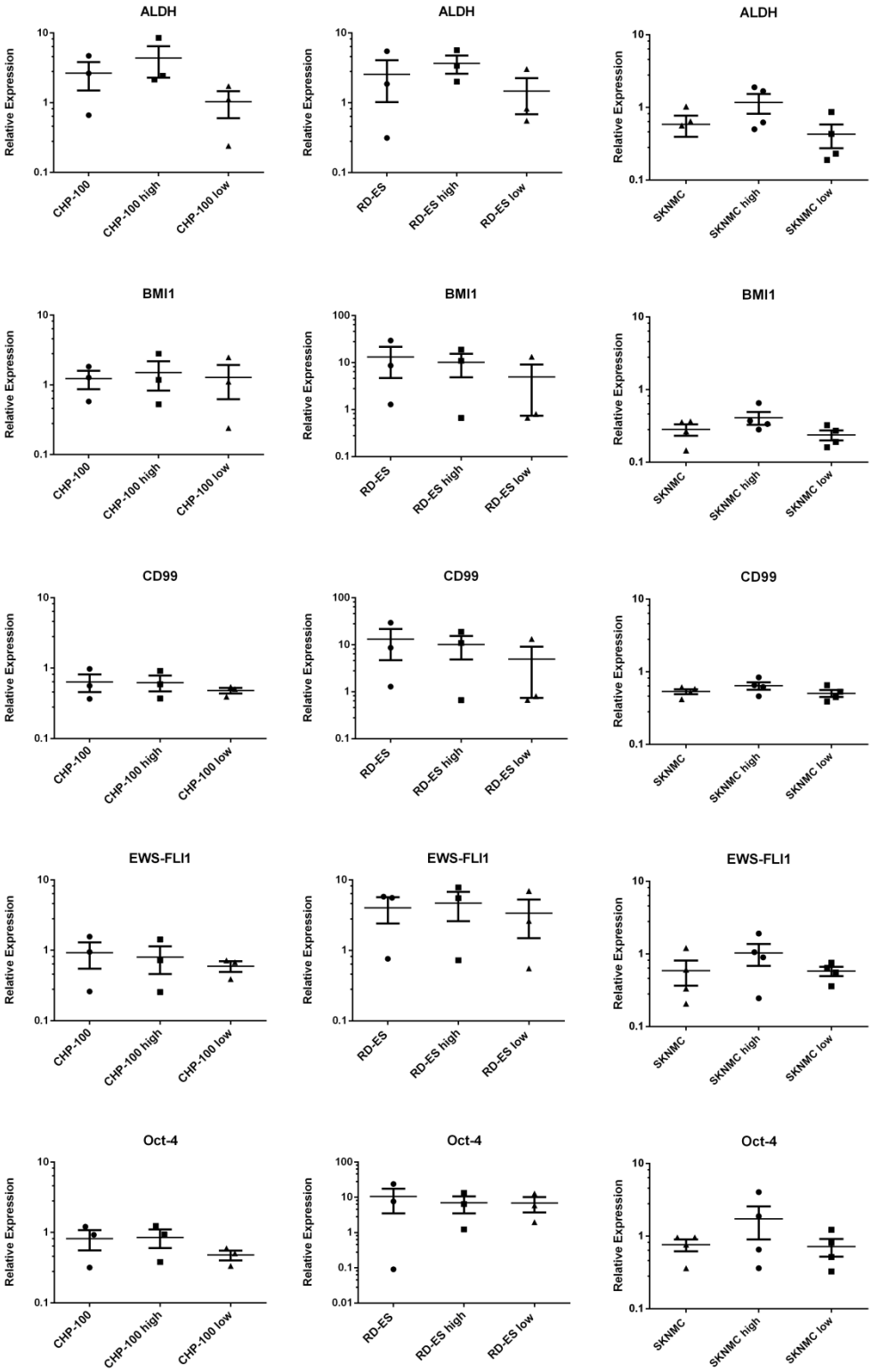


Figure 4-6. ALDH high cell populations do not increased expression of stem cell genes. Ewing sarcoma cell lines, expanded from an ALDH sorted population (ALDH high ALDH low, and parent population), were analysed via qPCR for expression of ALDH, BMI1, CD99, EWS-FLI1 and OCT-4 genes. Although not significant each cell line appeared to have higher expression of ALDH in the high subgroup compared with the ALDH low subgroups. CD99 and EWS-FI1 are uniformly expressed between subgroups although overall RD-ES has higher expression of CD99. Stem cell genes BMI1 and OCT-4 are not significantly varied between ALDH high and low populations. (n=3). Comparison was made between ALDH sorted groups for each with Kruskal-Wallis test using Dunn's post test to adjust for multiple comparisons. No statistical significance was observed. Error bars represent ±SEM.

4.4.6 Colony formation is increased in the ALDH high fraction of Ewing sarcoma cells

Cells were seeded into agar for colony formation and then grown for 2 weeks and analysed (Figure 4-7). CHP-100 had the highest overall number of colonies and SK-N-MC the least. There was an increase in colony formation in CHP-100 ALDH high group compared with the ALDH low group ($p<0.001$). RD-ES had significantly less growth in the high ($p<0.001$) and low groups ($p<0.01$) compared with the unsorted cells and both groups had similar colony growth to each other. SK-N-MC had lower overall colony numbers than the other 2 cell lines and showed a tendency for increased colony number in the ALDH low group compared with the ALDH high group ($p<0.0001$). This was counter to the belief that the more positive ALDH cells would show greater tumour initiating activity which is characteristic of cancer stem cells.

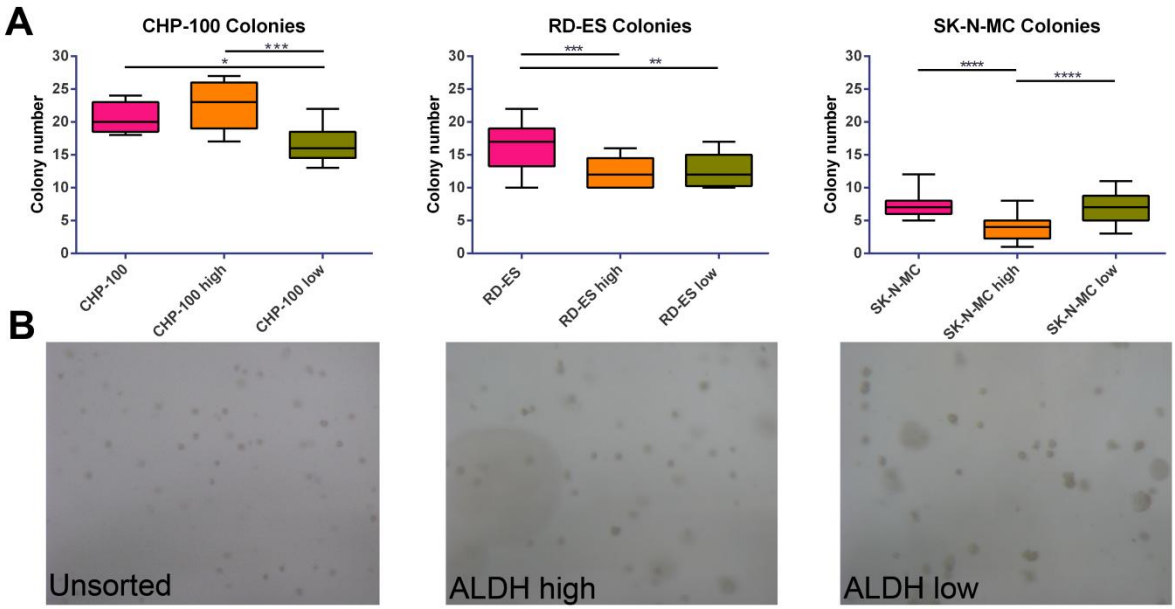


Figure 4-7. ALDH sorted cells show variation in colony forming potential. A – unsorted, and ALDH high and low cells were seeded in to agar and grown in 6 well plates for 2 weeks. Colonies were counted by eye at x4 magnification. Box and whisker plots show median, maximum and minimum values. Representative images of two experiments are shown. Statistical comparison between groups was made by one-way ANOVA with Tukey's post test to adjust for multiple comparisons. *, **, ***, **** represent $p<0.05$, $p<0.01$, $p<0.001$, $p<0.0001$ respectively. B – Representative microscopy images of CHP-100 cells, unsorted, ALDH high group, and ALDH low group at x4 magnification. For each depth of view, 10 fields of view were counted. Three depths of view were recorded. Only colonies in focus were included.

4.4.7 RD-ES and STA-ET1 express ABC transporter genes most highly

ABC (ATP-binding cassette) transporters have the capacity to export cytotoxic drugs there by potentially contributing to resistance (Doyle and Ross 2003). To investigate the abundance of ABC transporters related to multi-drug resistance, real-time RT-PCR assay was used to determine the relative mRNA expression of ABC transporters in Ewing sarcoma cell lines (Figure 4-8). Four major drug transporters (ABCA2, ABCB1, ABCC1, and ABCG2) were analysed.

The most striking observation was the high expression of ABC transporter genes ABCB1 and ABCG2 in RD-ES. The ABCB subfamily of ABC transporters have been shown to confer the strongest resistance to the widest variety of chemotherapeutic drugs (Szakács, Paterson et al. 2006). ABCG2, which is overexpressed in several cell lines selected for anticancer drug resistance, is a high-capacity transporter with wide substrate specificity. Transported substrates include cytotoxic drugs, toxins and carcinogens found in food products and importantly, tyrosine kinase inhibitors (Ozvegy-Laczka, Cserepes et al. 2005).

STA-ET1 showed the highest expression of ABCA2 in comparison with other cell lines whilst SK-N-MC and RD-ES the highest ABCC1 expression. ABCC1 has been shown to be expressed in a wide range of tissues, clinical tumours and cancer cell lines (Szakács, Annereau et al. 2004). This experiment not only confirms expression of ABC transporters in Ewing sarcoma cell lines which could contribute to drug resistance, but also shows variation in the expression of different subgroups between cell lines.

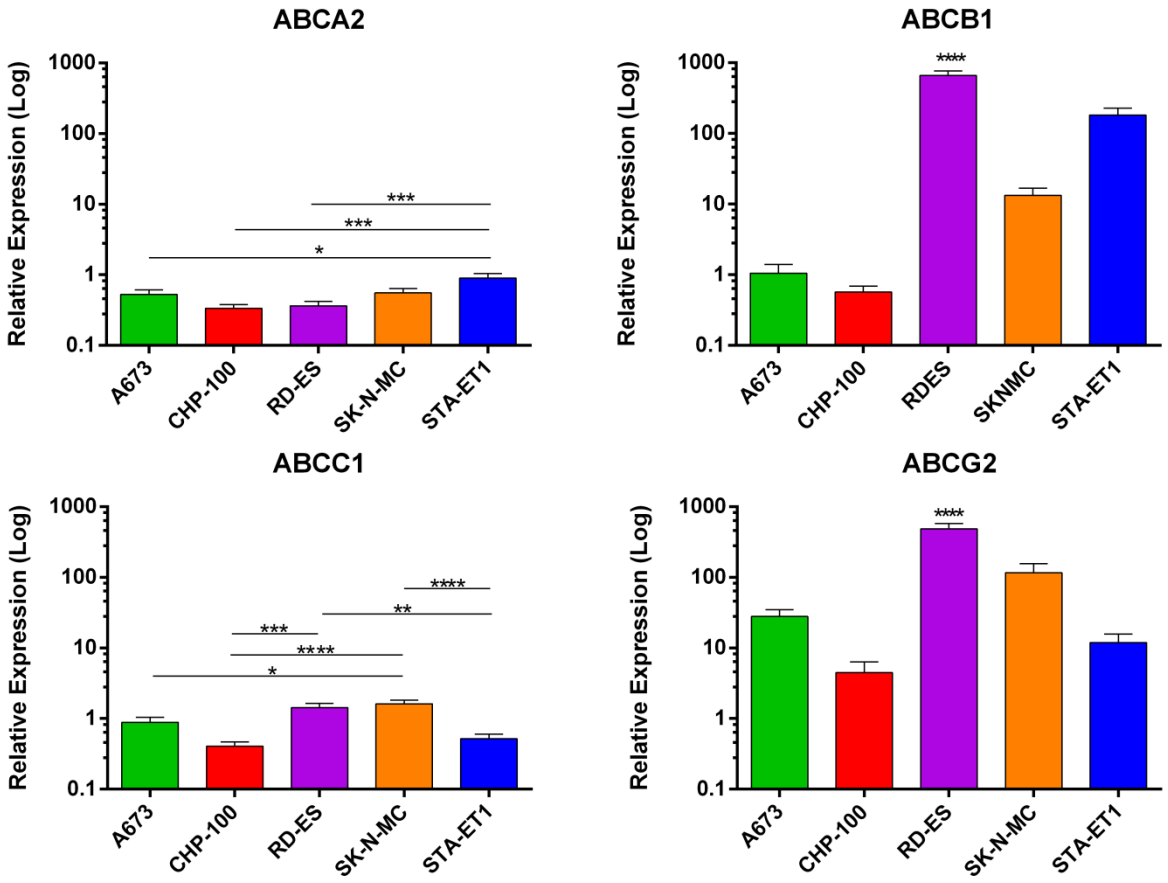


Figure 4-8. ABC transporter genes have varied expression in Ewing sarcoma cell lines. RD-ES has greater expression overall than the other cell lines. Gene expression of 4 ABC transporters, ABCA2, ABCB1, ABCC1, and ABCG2 were measured by qPCR (n=5). Expression was referenced to 3 housekeeping genes and calculated by the Pfaffl method. RD-ES was significantly elevated in comparison to all other cell lines in ABCB1 and ABCG2 ($p<0.0001$). Comparison between cell lines was made using one-way ANOVA with Tukey's post test. *, **, ***, **** indicate $p<0.05$, $p<0.01$, $p<0.001$, $p<0.0001$ respectively. Error bars represent SEM.

4.4.8 Ewing sarcoma cell lines confer overall sensitivity to OSI-906

Ewing sarcoma cell lines were exposed to OSI-906 for 72 hours and IC_{50} measured by MTS assay (Figure 4-9). A673 and CHP-100 were the most resistant cell lines with average IC_{50s} of 0.44μM and 0.56μM respectively. STA-ET1 and RM-82 were the most sensitive cell lines each with an IC_{50} of 0.07μM.

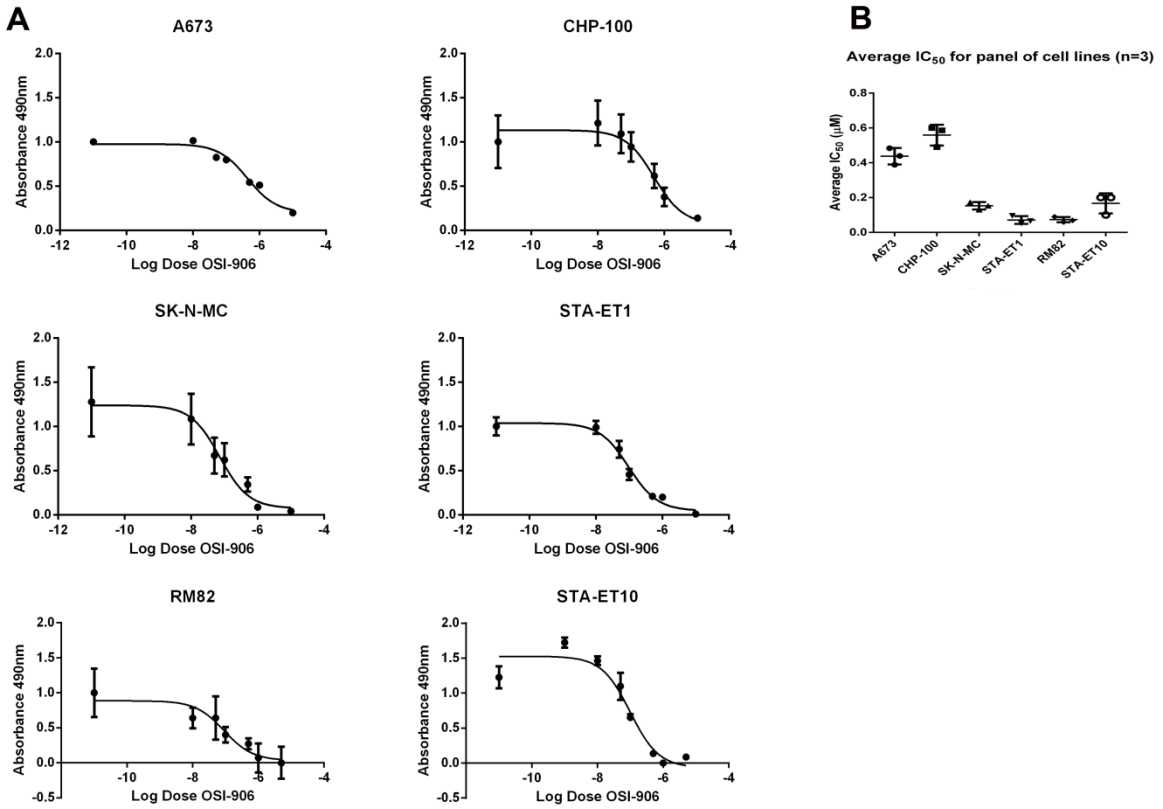


Figure 4-9. Ewing sarcoma cell lines respond to treatment with OSI-906. A – a panel of 6 cell lines was treated with OSI-906 for 72 hours and a dose response measured by MTS assay. Representative graphs are shown for each cell line. **B** – average IC_{50} for replicates of 3 experiments are shown. Error bars in B represent mean values ±SEM.

4.4.9 OSI-906 inhibits IGF stimulated IGF-1R phosphorylation and downstream pathways in Ewing sarcoma cell

Cell lines were treated with or without OSI-906 for 2 hours and analysed for target protein content by Western blot. OSI-906 reduced phosphoIGF-1R/IR in each of the four Ewing sarcoma cell lines tested (Figure 4-10). Additionally downstream proteins of the IGF-1 pathway were found to be inhibited confirming the effect. Complete inhibition of phospho-AKT and partial inhibition of phospho-MAPK (Figure 4-11) in CHP-100 and SK-N-MC were observed by Western blot analysis.

4.4.10 Proliferation of Ewing sarcoma cell lines is decreased by OSI-906

Proliferation of cell lines treated with OSI-906 was recorded by EdU assay. All four cell lines were analysed over 3 separate experiments. The gating strategy used was to identify single cells with forward and side scatter, then limit them to only individual cells, and subsequently measure proliferation with EdU as a percentage of the total population (Figure 4-12). Cell lines were analysed on three separate occasions and inter-experimental variation was observed. Although no combined analysis could be performed because of this, each experiment was analysed separately using Mann-Whitney statistical test and no significant difference was seen between groups. The suggestion by observing the data is that OSI-906 does indeed decrease proliferation in cell lines in a dose responsive manner. In addition the affect appears to be most marked at the 24 - 48 hour time points (Figure 4-13).

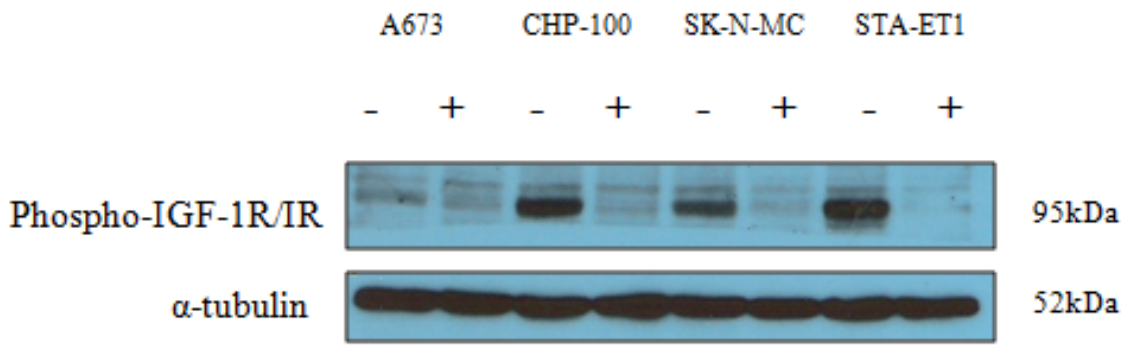


Figure 4-10. PhosphoIGF-1R/IR is inhibited by OSI-906. Cell lines were exposed to OSI-906 for 2 hours prior to cell lysis. Evaluation by Western blot shows inhibition of phosphoIGF-1R/IR with exposure to the drug (+). The expected molecular weight was 95kDa. α-tubulin was used as a loading control (molecular weight 52kDa).

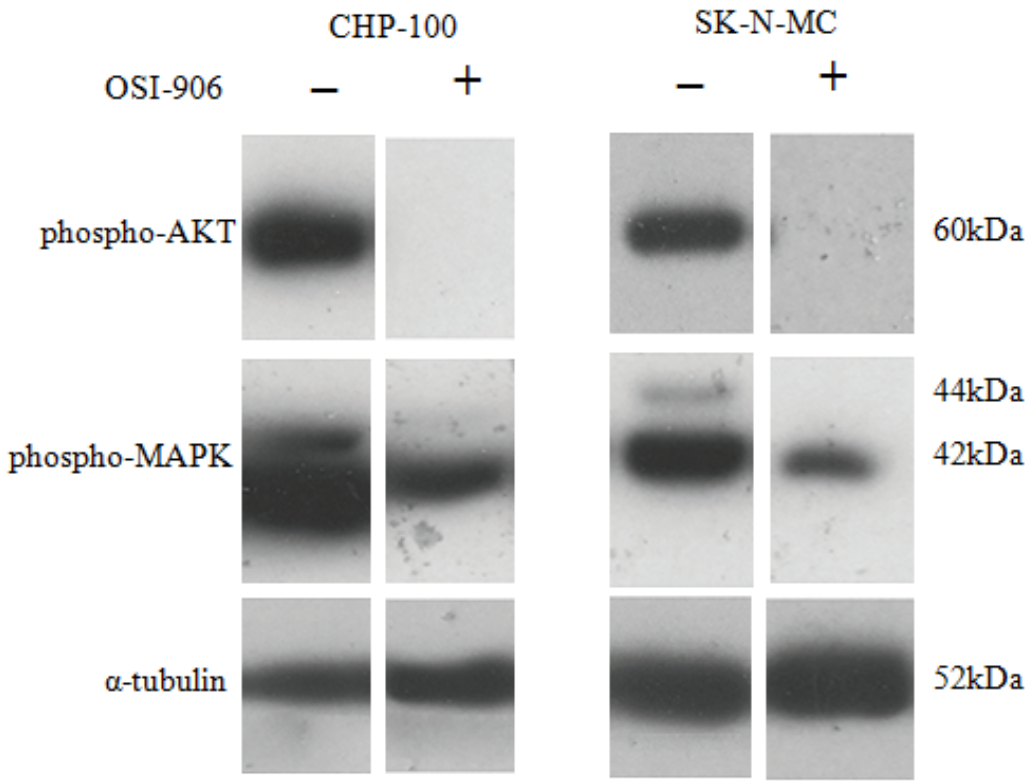


Figure 4-11. Treatment with OSI-906 results in blockade of phosphoMAPK and AKT. CHP-100 and SK-N-MC were treated with and without OSI-906 resulting in a complete inhibition of phospho-AKT in both cell lines. PhosphoMAPK which exists as 2 bands is decreased but not completely inhibited by OSI-906 treatment. α-tubulin was used as a loading control. (Western blot performed by D. Barnes).

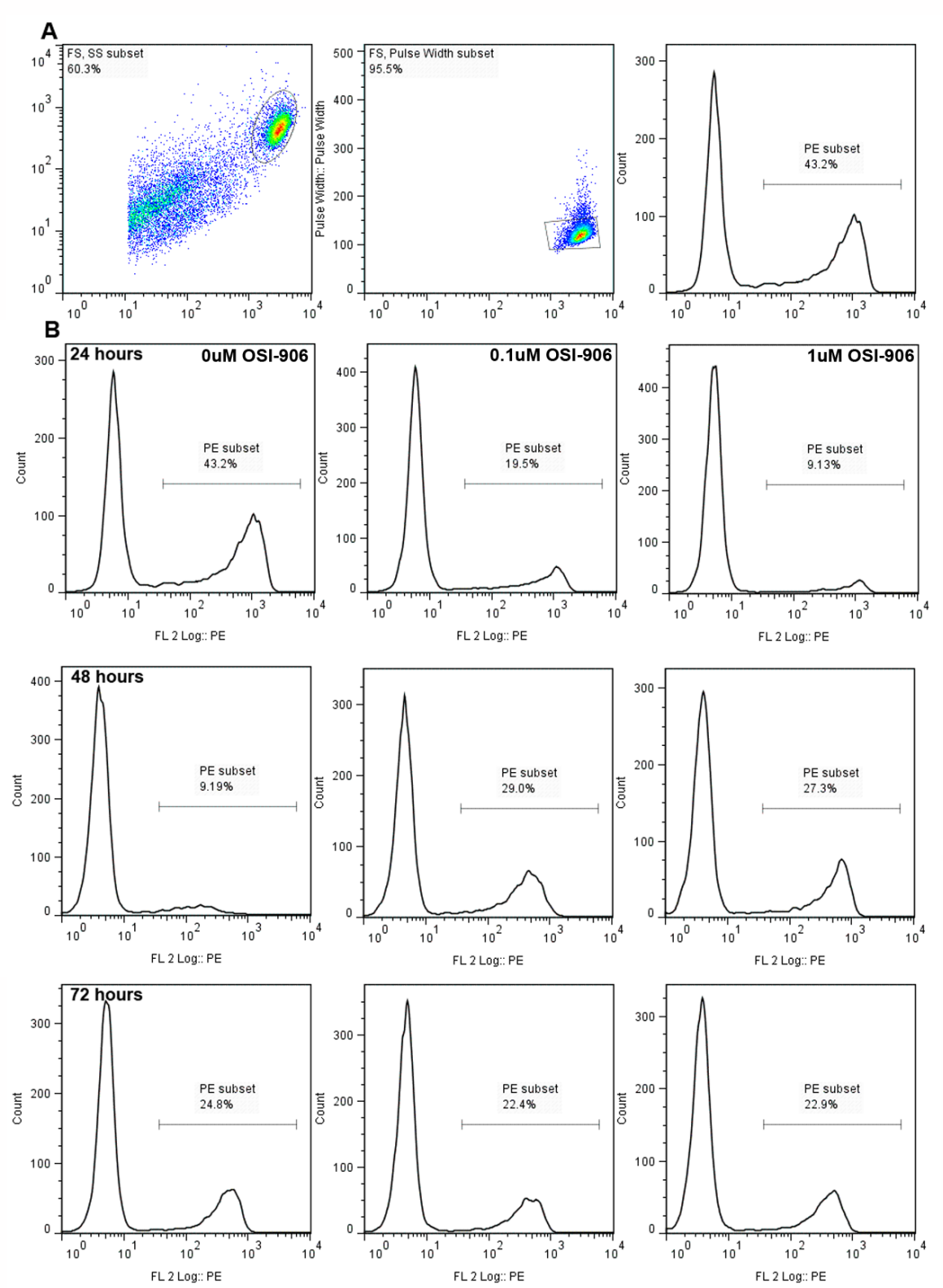


Figure 4-12. OSI-906 decreases proliferation of Ewing sarcoma cell lines. A – gating strategy illustrated. Live cells were initially gated (left box) before exclusion of doublets (middle box) and proliferating cells calculated (right box). **B** – Cell line A673 was treated with for 24, 48, and 72 hours with three doses of OSI-906 (0-1μM) and proliferation assessed by EdU assay using gating strategy as in **A**. (n=3 for each cell line).

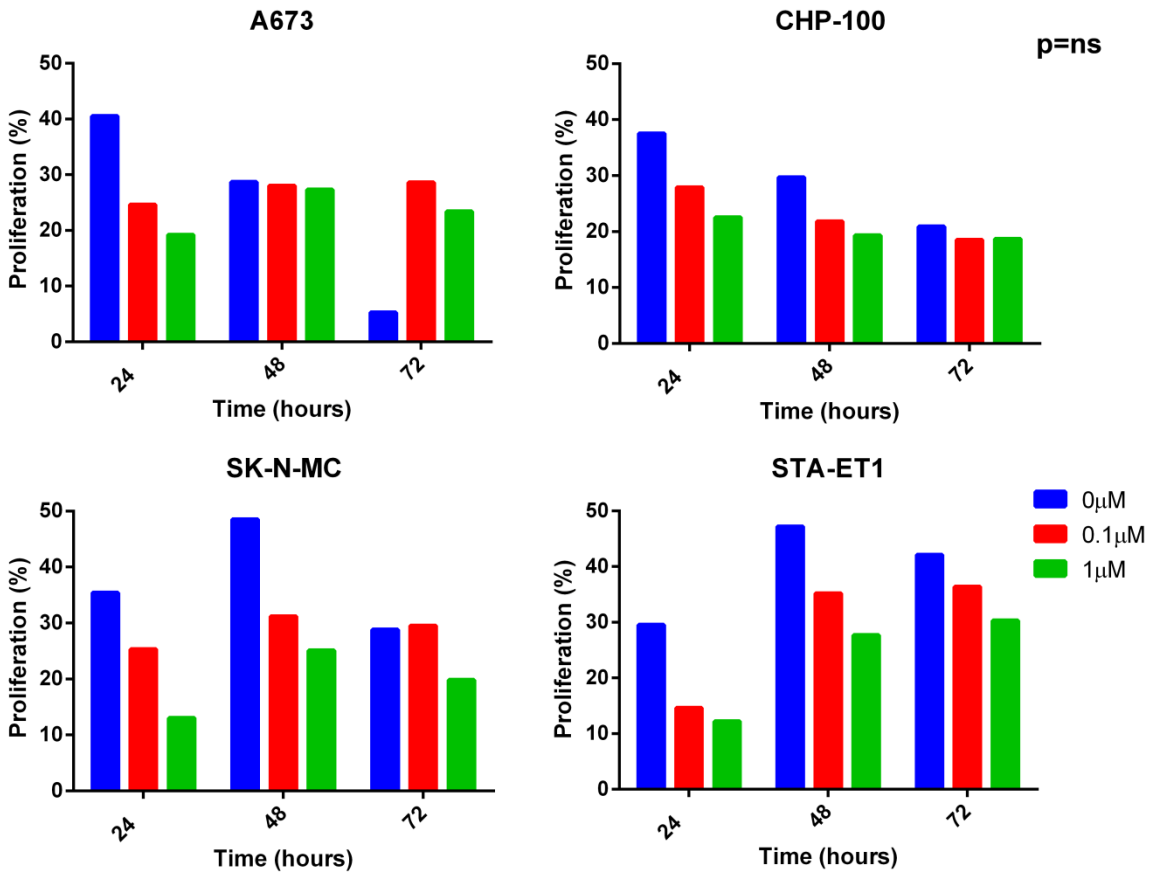


Figure 4-13. Proliferation of Ewing sarcoma cell lines is inhibited by OSI-906. Representative experimental graphs of each cell line show a decrease in proliferation at increasing doses of OSI-906 at indicated time points. They were analysed by Mann Whitney statistical test which was not significant (p=ns). The experiment was repeated three times for each cell line.

4.4.11 OSI-906 induces apoptosis in A673, CHP-100 and SK-N-MC

Cell lines were exposed to OSI-906 for 72 hours and stages of apoptosis assessed using FAM-FLICA™ assay with a PI counterstain via flow cytometry. No exclusion gating was applied to the analysis in order that data from necrotic cells were included, however quadrants were allocated based on instrument controls (Figure 4-14).

Viable cells were recorded as those within the bottom left quadrant (Q4). A difference in viability between cell lines was noted without OSI-906 exposure with the viable population of CHP-100 and STA-ET1 cell lines being approximately 80% at 72 hours in comparison with A673 and SK-N-MC which was 40% (Figure 4-15). For analysis early apoptotic cells, late apoptotic cells, and necrotic cells were all grouped as non-viable (quadrants 1-3). Despite a significant difference not being recorded, A673 and CHP-100 show a dose dependent increase in non-viable cells and decrease in viable cells at 72 hours with SK-N-MC demonstrating a similar effect albeit less marked. STA-ET1 was constant in percentage of viable cells irrelevant of OSI-906 dose. This is somewhat surprising as MTS assay suggested that IC_{50} for STA-ET1 was 0.07µM following 72 hours exposure so it was predicted that an apoptotic response would be observed with doses of 0.1 and 1µM of OSI-906.

4.4.12 Cell cycle is not altered by OSI-906

Cell lines were incubated for 72 hours with or without OSI-906 (1µM) and the effect on cell cycle was analysed by flow cytometry using PI (Figure 4-16). Automated gating of cell cycle was performed by Watson pragmatic model using the FlowJo software. This showed that although not significant, CHP-100 and SK-N-MC both had an increase in cells in the sub G1 phase of the cell cycle on exposure to OSI-906. The decrease in the proportion of cells dividing with exposure to the drug suggests that OSI-906 is exerting an antiproliferative effect which correlates with previous data.

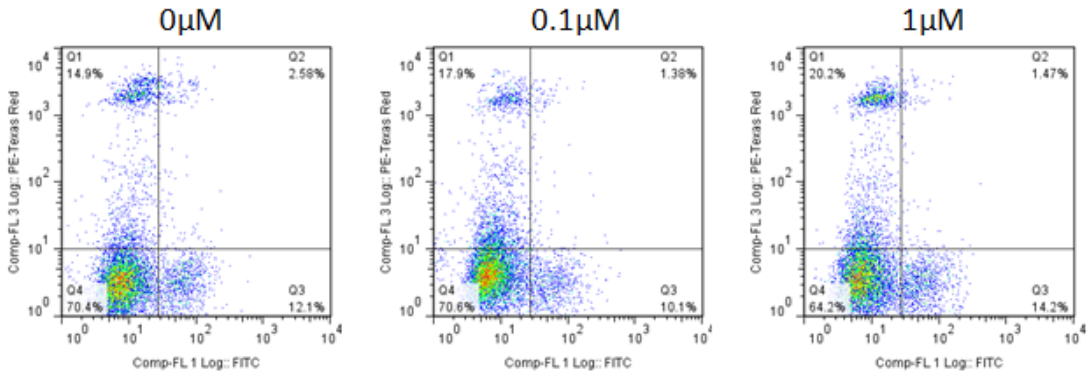


Figure 4-14. Representation of apoptosis analysis by FAM-FLICA™ assay. A673 was exposed to doses of OSI-906 (0, 0.1, and 1µM) for 72 hours and assessed for apoptosis by flow cytometry. Plots show FITC (FAM-FLICA™) on the x-axis and PI on the y-axis. Quadrants were established using PI instrument controls. Q1 (top left) shows necrotic cells, Q2 (top right) late apoptotic, Q3 (bottom right) early apoptotic and Q4 (bottom left), viable cells. In this example, the percentage of viable cells (Q4) decreases with increasing dose of OSI-906 and the early apoptotic increases.

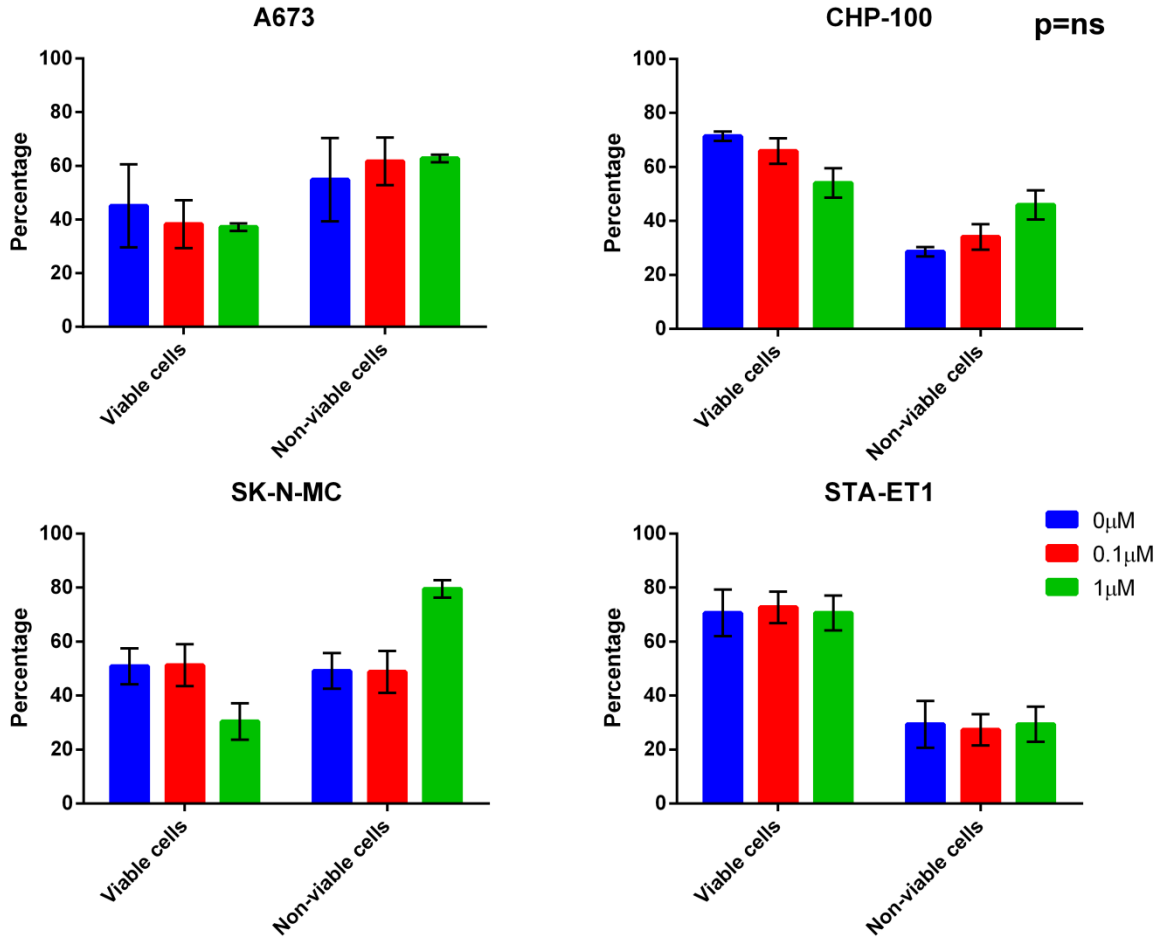


Figure 4-15. Apoptosis was shown in cell lines in response to OSI-906. Cell lines exposed to OSI-906 (0-1µM) were measured for apoptosis using FAM-FLICA™ assay. Comparison between viable (Q4) and non-viable cells (data combined from Q1-Q3) were made at different OSI-906 doses. Data was analysed using Mann Whitney. No significant differences were observed. Errors bars represent ±SEM (n=2).

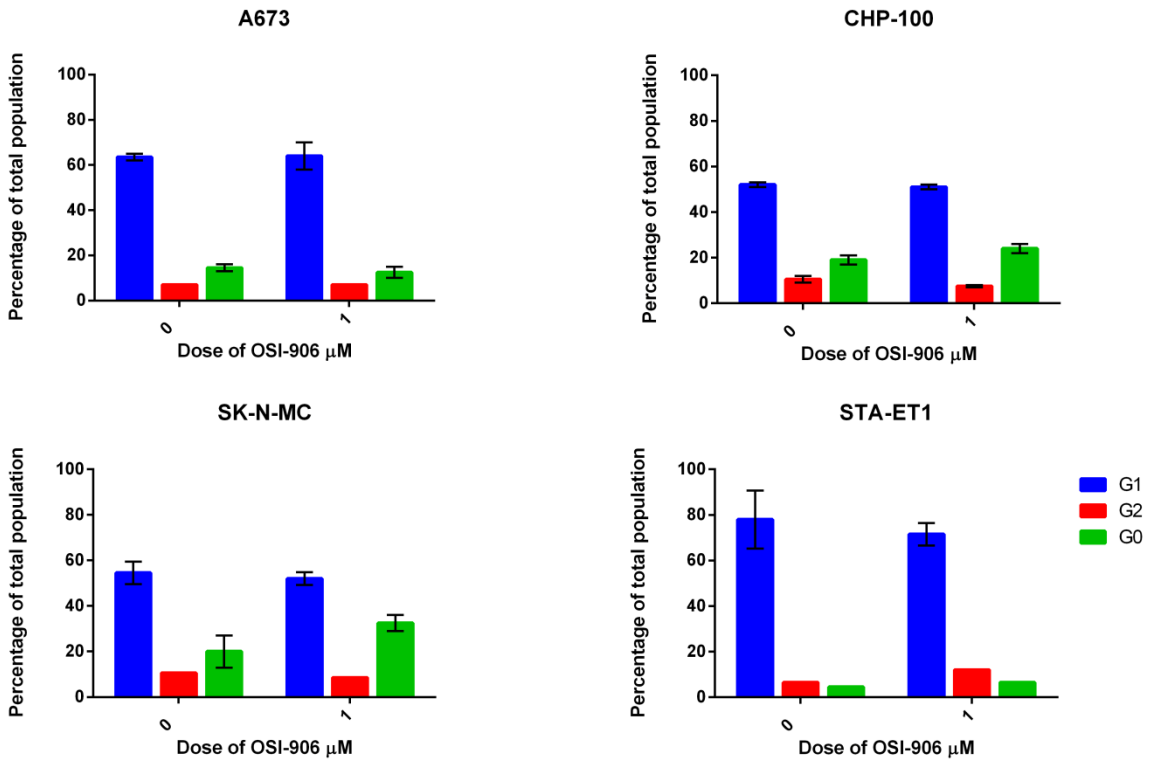


Figure 4-16. The effect of OSI-906 on cell cycle. Cell lines were exposed to a vehicle only control or to 1μM OSI-906 for 72 hours and cell cycle was measured by flow cytometry with PI stain. 2 x10^4 live, single cells were analysed per cell line. Data was gated by Watson pragmatic mathematical software which was built in to the Flowjo programme. Each population is expressed as percentage of gated cells (mean of two independent experiments). Error bars are representative of ±SEM.

4.5 Discussion

This work and that of the previous chapter has illustrated that identical cells within the same cell population have variation in their expression of certain proteins which may result in non uniform responses to anti cancer agents such as OSI-906. Population heterogeneity can be due to genetic and non genetic variability. Non genetic sources of variation can be stochastic in nature and may fluctuate in translation or be regulated through feedback mechanisms so that variety is maintained. The work described above suggests that Ewing sarcoma cell lines are heterogeneous in their response to stimulation with IGF-2.

4.5.1 Ewing sarcoma cell lines differentially express IGF-1R and IR

Human IR is encoded by a large single gene comprising 22 exons and the protein expressed as two different isoforms that differ at the carboxyl terminus of the α-subunits by 12 amino acids (Moller, Yokota et al. 1989). The presence (IR–B, or IR exon 11+) or absence (IR-A, or exon 11-) of these residues alters the functional properties of the isoform. IR–B is a classical IR that regulates glucose uptake. In contrast, IR-A has potent mitogenic and anti-apoptotic functions and plays a key role in cell proliferation (Denley, Bonython et al. 2004). Ewing sarcoma cell lines have been shown to be varied in their expression levels of IGF-1R and IR with STA-ET1 showing high expression of IGF-1R and SK-N-MC high expression of IR-A. Similarity of cell line proliferation must be assumed for comparison of expression levels between cell lines to occur. Later experiments using EdU, a thymidine substitute incorporated into the newly synthesized DNA of replicating cells (during the S phase of the cell cycle) confirm similar proliferation rates between cell lines at 24 hours between 30-40% (Figure 4-13). Cell line gene expression of IR and IGF-1R was found to be comparable to protein expression measured by flow cytometry.

4.5.2 OSI-906 is inhibitory to Ewing sarcoma cell lines

The role of IGF-IR in the initiation of Ewing sarcoma (Toretsky, Kalebic et al. 1997), *in vitro* and *in vivo* effects of blocking IGF-IR (Scotlandi, Benini et al. 1998, Benini, Manara et al. 2001) and the expression of signalling components in patients with Ewing sarcoma (Prieur, Tirode et al. 2004). As mentioned previously, inhibition of IGF-1R results in upregulation of IR resulting in the rationale for dual kinase inhibition of both receptors. All six cell lines tested demonstrate a dose response to OSI-906 (IC_{50} 0.07-0.56μM) all be it with a range of almost 10 times between the most sensitive (STA-ET1, RM-82) and the most resistant (A673 and CHP-100) cell lines. Interestingly both STA-ET1 which has high expression of IGF-1R, and SK-N-MC which has high expression of IR-A are both relatively sensitive to the effects of OSI-906 in comparison with A673 and CHP-100 which have lower expression of the receptors. This suggests that OSI-906 is reliant on the presence of IGF-1R and IR and was confirmed via Western blot analysis where a decrease in AKT and MAPK were observed. Proliferation of cell lines sequentially decrease with time and drug dose, and apoptosis appeared to increase in a dose dependent manner in all but STA-ET1.

4.5.3 ALDH and Ewing sarcoma stem cells

In the absence of an inducible *in vitro* or *in vivo* model of transformation in Ewing sarcoma, multipotent mesenchymal stromal cells (MSC) have emerged the most likely candidate cell of origin and a potential cellular platform to which EWS-FLI1 mediated transformation can be more thoroughly characterized and understood (Riggi, Cironi et al. 2005). Many cancer stem cell markers have been identified and applied to Ewing sarcoma cell lines in order to isolate potential stem cell populations including ALDH, CD133, CD166, CD105, CD90 and CD73 (Awad, Yustein et al. 2010, Amaral, Manara et al. 2014). In this work, a commercially available ALDH based assay, previously reported as a

marker of stem cells, resulted in data that was less convincing than that previously published as comparable observations were not reported (Awad, Yustein et al. 2010). Despite successful application of the assay, gene expression, albeit in a fairly small dataset, was varied between cell lines without convincing evidence of stemness. Colony formation between cell groups was also varied leading to the conclusion that a more robust assay is needed to confidently identify potential stem cells and that there is not conclusive evidence suggesting distinct populations are present based on ALDH. In order to validate results, or indeed use as an alternative, other stem cell markers could be used such as CD133. Cancer stem cell subpopulations positive for CD133 have been shown to more highly express genes implicated in stem cell maintenance and nuclear reprogramming including OCT4 and NANOG in Ewing sarcoma cells (Suvà, Riggi et al. 2009, Riggi, Suvà et al. 2010).

Using a drug based assay as an alternative method, could allow subpopulations of cells which are tolerant to chemotherapy to be fractioned and investigated in more detail. Work later in this thesis develops upon such methods as a mechanism to identify resistant cell populations to OSI-906. A further limitation of this assay was the need to let the isolated subpopulations of cells recover and proliferate following flow cytometry sorting in order to have the quantity required experimentation. Although experiments were performed as swiftly as possible following cell sorting, the initial fraction of cells may therefore lose purity prior to their use.

4.5.4 Expression of ABC transporters in Ewing sarcoma

Expression of ABC transporter genes was varied between subtype and cell lines (Figure 4-8). High expression of ABCB1 which has been implicated in drug resistance in Ewing sarcoma cell lines was found to be elevated in RD-ES, SK-N-MC, and STA-ET1 (Scotlandi, Perdichizzi et al. 2002, Okada, Tanaka et al. 2006) however they have not been

found to be significant predictors of prognosis (Riley, Burchill et al. 2003, Scotlandi, Remondini et al. 2009).

Cause of drug resistance to tyrosine kinase inhibitors are multiple with the most common reported being point mutations within the kinase domain impeding inhibitor access to the ATP-binding loop and/or activation loop of the kinase (Shukla, Chen et al. 2012). In addition to kinase mutations, resistance due to the expression of ABC drug transporters has been linked to constitutive and acquired drug resistance to tyrosine kinase inhibitors by being substrates or modulators of ABCC and ABCG2 although to date, no studies have been reported in Ewing sarcoma (Assef, Rubio et al. 2009).

Further work could therefore aim to investigate effects of ABC transporters and OSI-906 in Ewing sarcoma. Cell lines could be exposed to verapamil, a calcium channel blocker which acts to inhibit ABC transporters and effect assessed. One would postulate that cells high in expression of ABC transporters such as STA-ET1 would have greater viability than those with lower expression such as CHP-100. In addition, in an isolated cancer stem cell population expression of ABC transporters could be compared to parent populations to identify if there is evidence to support findings made by Awad et al. that ALDH high subpopulations of Ewing sarcoma cell lines have higher expression of ABC transporters than ALDH low populations (Awad, Yustein et al. 2010).

5 Genome wide analysis of Ewing sarcoma cell lines

5.1 Introduction

5.1.1 Clinical application of NGS

Within cancer care there are several clinical needs which can be met by NGS. These are the identification of single nucleotide changes or point mutations, alterations in copy number, and changes in expression levels of genes. To endeavour to make NGS more economic to the health care industry, whole exome sequencing which captures coding regions only, rather than whole genome sequencing offers a more realistic choice. In addition, the development of targeted cancer panels by some biotechnology companies offers sequencing over a panel of common cancer related genes, typically 50 or more, which reduces costs further.

Single nucleotide changes can lead to activation of oncogenes or inhibition of tumour suppressor genes which may influence therapeutic choices. For example, 40-60% of melanoma patients have mutation of BRAF (Davies, Bignell et al. 2002). Of these, 90% have a mutation which substitutes glutamic acid for valine at codon 600, V600E (Curtin, Fridlyand et al. 2005). Studies using a RAF inhibitor PLX4032 (vemurafenib) have shown that malignant cells can be targeted in a mutant BRAF selective manner (Joseph, Pratilas et al. 2010). A randomized Phase 3 clinical trial indicated that patients with V600E mutation had a response rate of 48% when treated with a BRAF inhibitor vemurafenib (Chapman, Hauschild et al. 2011). This is an instance where single gene testing has a clinical application, however coverage of the entire genome would give comprehensive information for defining the pathways and mutations which drive pathogenesis.

Paired DNA from patients' normal tissue (usually blood) can be used to identify germline mutations allowing germline and somatic variants to be differentiated. In addition, matched samples, before and after a treatment, can be used to identify resistance mechanisms at a genomic level. Although biopsy samples will have some degree of contamination from genetically normal tissue, this can be minimised by using microdissection or radiologically guided sample collection in collaboration with pathology colleagues.

As discussed, NGS has shown that cancers do not comprise a single dominant clone. Intratumour heterogeneity has been described in an *in vivo* setting using multiregion sequencing to characterise the tumour genetic landscape in patients with renal cell carcinomas (RCC). This emphasised that there are a range of mutations across regions within an individual tumour and that these are under-represented in a single biopsy specimen. Phylogenetic reconstruction revealed that branched evolutionary tumour growth occurred rather than linear evolution (Gerlinger, Rowan et al. 2012). Similarly, using single cell exome sequencing, Xu et al. identified mutant genes and their frequencies in RCC, highlighting the presence of heterogeneity at a single cell level. These studies suggest that a more detailed understanding of drug resistance and tumour relapse in genetically complex tumours can be sought using NGS technologies (Xu, Hou et al. 2012).

Copy number variations (CNVs) are common in cancer and recurrent alterations have been seen in many cancer types (Baudis 2007, Beroukhim, Mermel et al. 2010). CNVs (gains, or losses, of whole genes and/or chromosomal regions) can increase or decrease the levels of important coding and noncoding RNA transcripts. Focal CNVs have been shown to contain cancer causing genes which may influence therapeutic approaches in patients (Eder, Sui et al. 2005, Weir, Woo et al. 2007). Mackintosh et al. recognised CNVs in 67 Ewing sarcoma samples via comparative genomic hybridisation (CGH). These included

chromosome 8 gain, 12p gain, and most frequently 1q gain which was present in 31% of patients. With increasing proportions of genome altered there was a decrease in survival and 1q gain alone was the copy number alteration associated with the most significant detrimental effect (Mackintosh, Ordóñez et al. 2012).

CNVs can be identified using DNA microarrays using comparative genomic hybridization (CGH). CGH was first developed as a method for comparing the copy number of differentially labelled test and normal reference DNAs using fluorescence *in situ* hybridization (FISH) (Kallioniemi, Visakorpi et al. 1996). By measuring the fluorescence ratio along the length of each chromosome, regions of loss and gain were measured relative to a test sample (the reference DNA being assumed to be diploid in copy number). Improvements in the resolution of CGH were possible due to the human genome project which allowed for the development of libraries of clones which could be accurately mapped to the human genome and spotted robotically onto glass slides (Cheung, Nowak et al. 2001). DNA from the sample to be tested is labelled with a coloured fluorophore and a reference DNA sample is labelled with an alternatively coloured fluorophore. Equal quantities of the two DNA samples are mixed and cohybridized to a DNA microarray of several thousand evenly spaced cloned DNA fragments or oligonucleotides. After hybridization, digital imaging systems are used to capture and quantify the ratio of relative fluorescence intensities of each of the hybridized fluorophores. This is proportional to the copy number of DNA sequences in the test and reference genomes meaning that, if equal, there is normal copy number and if altered, there is a loss or gain of DNA at that specific region (Bejjani and Shaffer 2006, Shinawi and Cheung 2008).

The addition of single nucleotide polymorphism (SNP) measurements to CGH microarrays enables the detection of copy-neutral loss of heterozygosity (LOH) events and allelic imbalances.

5.1.2 RNA-sequencing

In Ewing sarcoma it is well established that there is the presence of a balanced reciprocal chromosomal translocation, most commonly EWS-FLI1. Gene fusions, resulting from chromosomal rearrangements are common in sarcomas, leukaemias and lymphomas, however, there is growing evidence that they could have prognostic and predictive use in solid tumours too. Recent evidence has suggested that in a small subset of patients (2-7%) with non small cell lung cancer there is an oncogenic fusion gene consisting of EML4 and anaplastic lymphoma kinase (ALK) which renders these patients susceptible to treatment with crizotinib, an inhibitor of ALK tyrosine kinase (Kwak, Bang et al. 2010). In addition the fact that translocations are unique to tumour cells makes them an obvious clinical target and much work has therefore focussed on targeting EWS-FLI1 in Ewing sarcoma (Boro, Prêtre et al. 2012, Sengupta, Rahman et al. 2013).

Aside from EWS-FLI1, further genomic rearrangements may be present in Ewing sarcoma which could influence prognosis (Mackintosh, Ordonez et al. 2012). Within cancers "driver aberrations", which may modulate the behaviour of oncogenes, tumour suppressor genes and those involved in DNA stability may exist alongside "passenger" aberrations which do not contribute to cancer pathophysiology (Vogelstein and Kinzler 2004). Stephens et al. investigated 24 breast cancers via paired-end sequencing and identified a total of 2,166 somatic rearrangements with the majority being intra-chromosomal highlighting the high level of rearrangements present in their cohort. Novel fusion genes were identified but none were found to be expressed indicating that these were most likely passenger aberrations (Stephens, McBride et al. 2009).

RNA sequencing (RNA-seq) can be used to identify chimeric transcripts, alternative splicing within genes, point mutations and, taken simultaneously, infer overall gene expression. Using paired-end reads and RNA-seq has proved to be an effective means of

denoting exon structure and as the sequences are obtained from transcribed genes, potential "driver" mutations are more likely to be identified (Morin, Bainbridge et al. 2008, Mortazavi, Williams et al. 2008, Sultan, Schulz et al. 2008). Paired-end short-read sequencing of RNA alleviates the reliance of the read to traverse the fusion junction and provides increased coverage by sequencing from the ends of a transcribed fragment, allowing for easier mapping of the end product (Maher, Palanisamy et al. 2009).

5.2 Chapter Aims

Massively parallel sequencing strategies enable genuinely genome-wide screening to be carried out for point mutations, copy number changes and rearrangements using a single platform. Here, such technology is employed to systematically detect and characterise genomic rearrangements in a panel of 8 Ewing sarcoma cell lines. In collaboration with Oxford Gene Technology (OGT), extracted cell line nucleic acids underwent NGS (RNA-seq, whole exome sequencing) and aCGH/SNP array in order to classify translocations, identify point mutations, and copy number variation. Functional experimentation followed to further validate results.

5.3 Methods

5.3.1 Preparation of samples for RNA-seq , whole exome sequencing, and CNV

Validated Ewing sarcoma cell lines were obtained from the EuroBoNet consortium as used in earlier experiments (Ottaviano, Schaefer et al. 2010).

NGS requirements were followed. For DNA, 3-5µg was eluted in TE buffer (10mM Tris, 0.5mM EDTA). RNase treatment step (the addition of 4µl of RNase A (100mg ml^{-1})) was performed as described in the QiAamp DNA mini kit (Qiagen, 51304). Nanodrop readings of 260/280 ratio >1.8 and 260/230 ratio >1.5 were required to confirm the quality of the DNA.

RNA (1-10µg) was eluted in 30µl of ultrapure water. Throughout extraction strict RNase free techniques were used with preparation of surfaces and equipment with RNaseAway (Ambion) and the use of RNase free plasticware and RNase free water. Samples were frozen at -80°C and transported on dry ice.

5.3.2 NGS Analysis

Data from whole exome analysis was generated following library preparation (Figure 5-1), enrichment (Figure 5-2), and Ilumina platform sequencing. Sequence reads were analysed by OGT via their bioinformatic pipeline with regular quality control steps through the process (Figure 5-3, Table 5-1). Initial raw read data is aligned against organism specific reference sequence, generated transcripts are assembled via Bowtie (Langmead, Trapnell et al. 2009) and BLAT (Kent 2002), quantified, and data ultimately provided as a report within a web-based interface. Their laboratory information management system (LIMS) has been validated on high-throughput genomic studies, including the Wellcome Trust aCGH population study of >20,000 samples and certified to the ISO9001:2008 and ISO27001:2005 international standards for quality and information security management set by the British Standards Institute.

Using Ewing sarcoma cell line RNA, OGT carried out RNA-seq. The samples were prepared from extracted RNA using the Illumina Tru-Seq protocol which involved selection of poly-A RNA, conversion into cDNA before amplification and sequencing (Figure 5-4). The Illumina HiSeq platform was used to sequence the samples to an overall depth of 40 million paired end reads. Fusions were identified by an analysis pipeline which used Bowtie and BLAT alignment tools to map paired end reads to the hg19 reference genome (Figure 5-5).

CNV was measured using the Agilent human genome CGH and SNP microarray (4 x 180k). This is a dual colour array containing 60-mer oligonucleotide CGH and SNP probes synthesised using Agilent's inkjet SurePrint technology. It allows for simultaneous detection of copy number changes and copy neutral aberrations, such as LOH and uniparental disomy (UPD), on the same array.

The data was analysed using OGT's CytoSure™ Interpret Software which employs circular binary segmentation to translate intensity measurements from aCGH data into copy number aiming to reduce noise in the data (Olshen, Venkatraman et al. 2004).

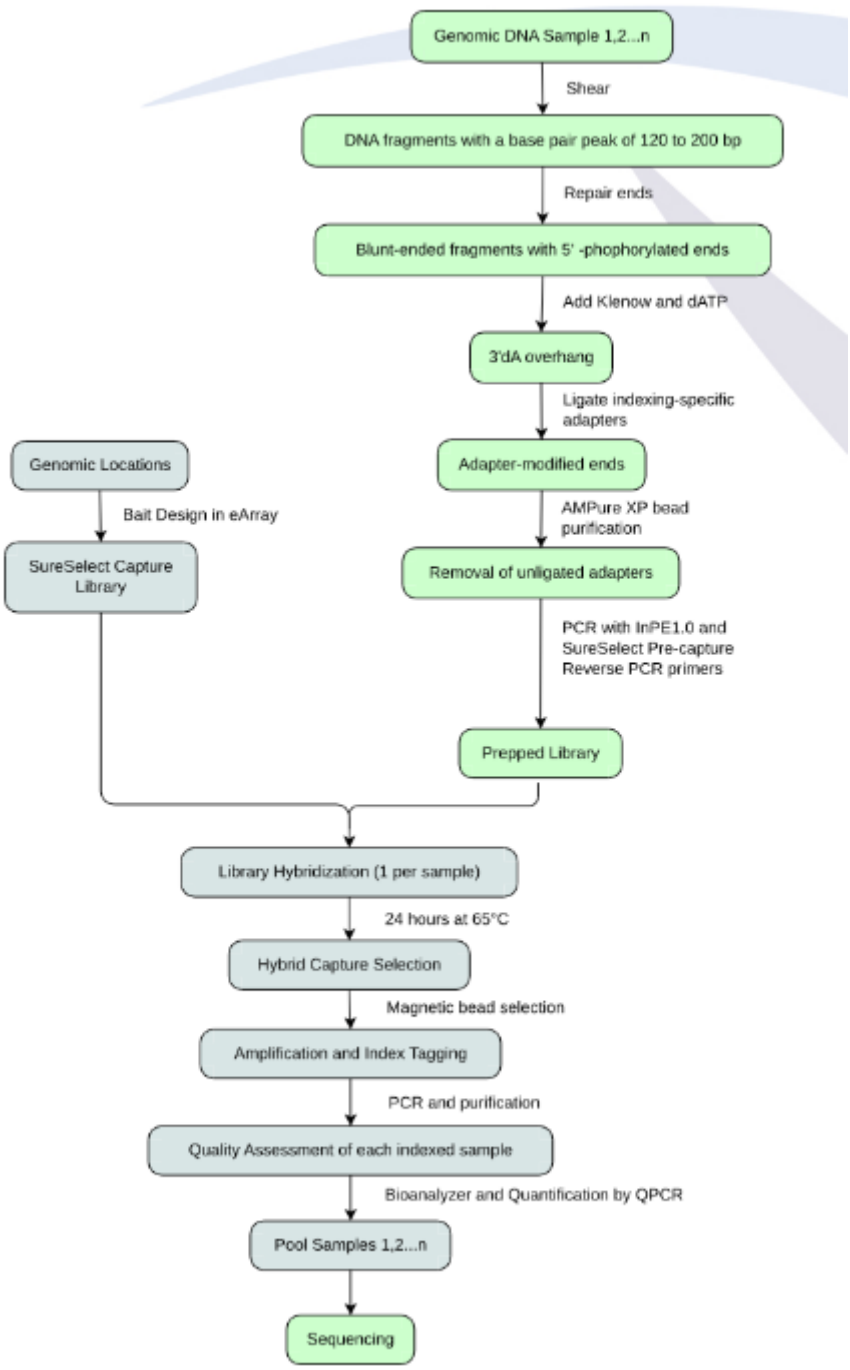


Figure 5-1. Workflow of enrichment and library preparation for whole exome sequencing. Library preparation was performed prior to hybridisation (**Figure 5-2**). The concentration of each library was determined using Agilent's qPCR NGS library quantification kit and samples pooled prior to sequencing each with a final concentration of 10nM. Sequencing was performed on the Illumina HiSeq2000 platform using TruSeq v3 chemistry. (Workflow diagram prepared by OGT).

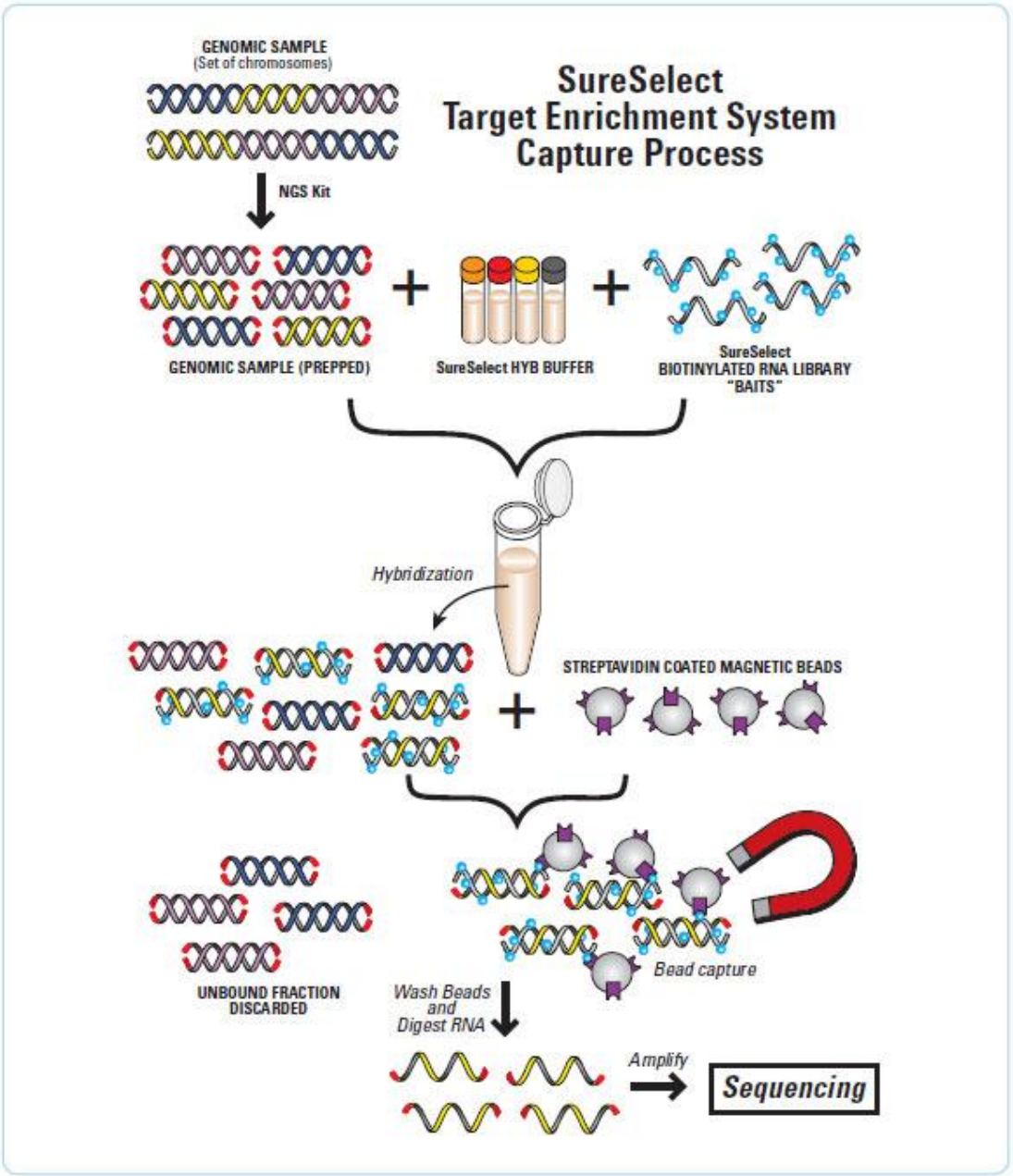


Figure 5-2. Preparation of DNA for whole exome sequencing with SureSelect Target Enrichment. From gDNA, a shearing step was performed to produce small fragments, and a library prepared with sequencer specific adaptors and indexes (**Figure 5-1**). Then the sample was hybridized for 24 hours with biotinylated 120mer RNA library baits and target regions selected using magnetic streptavidin beads. Samples were then amplified and loaded on to the sequencer.

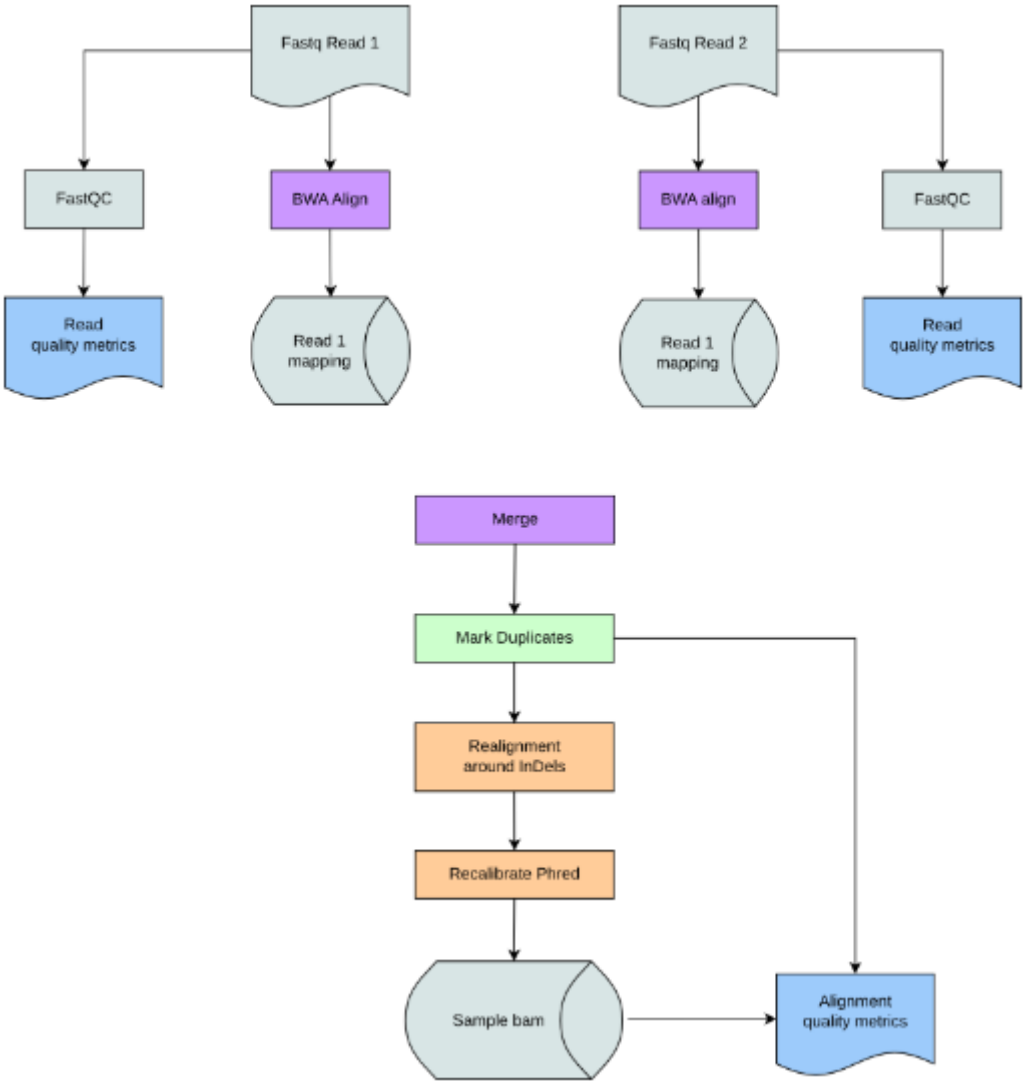


Figure 5-3. Illustration of mapping and alignment of whole exome sequencing. Read files (Fastq) were generated from the sequencing platform and mapped to their location in the most recent build of the human genome (hg19/b37) using Burrows-Wheeler alignment. Duplicate reads which were likely to be the result of PCR bias were removed as they can introduce false positive identification of SNPs. Where potential insertions and deletions were identified local realignment was carried out to reduce false-positive SNP calls and accurately determine indel length. Phred scores were then recalibrated and SNP and indel variants called. Variants were then annotated with gene and gene function data from Ensembl.

	A673	CHP-100	RD-ES	SK-N-MC	STA-ET1
Mapped Probes	110873/134741	110873/134741	110873/134741	110873/134741	110873/134741
DLR Spread	0.1347	0.1461	0.1354	0.1496	0.1385
Red Signal Intensity	1,706.39	1,789.55	1,681.83	1,671.18	1,773.67
Green Signal Intensity	928.305	1,045.65	1,082.77	912.49	1,146.58
Red Background Noise	7.9003	7.8218	7.0696	7.8033	7.291
Green Background Noise	5.0789	5.1263	4.5333	4.7793	5.153
Red Signal-to-Noise Ratio	215.99	228.789	237.895	214.163	243.268
Green Signal-to-Noise Ratio	182.777	203.977	238.845	190.925	222.507

Table 5-1. Quality control metrics for CNV by CGH/SNP arrays. Cell lines were analysed using OGT's customised array to detect CNV. Each cell line was assessed for derivative log ratio spread (DLR spread). This is a measurement of probe to probe-noise level. Samples with high values of DLR tend to have poor signal to noise properties and accurate CNV detection can be difficult. OGT (based on Agilent thresholds) consider ratios of <0.2 to be classified as excellent and <0.3 satisfactory. Signal intensity levels of >500, background noise levels <10 and background to noise ratio >85 are considered to be excellent.

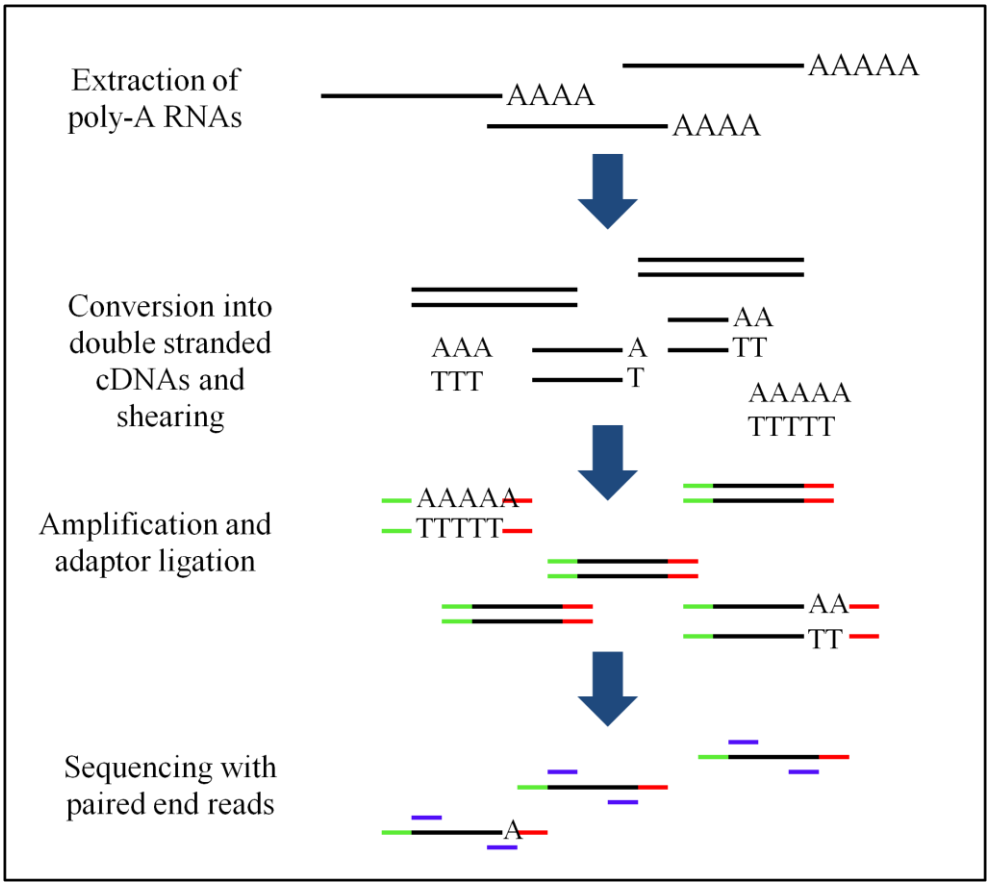


Figure 5-4. Preparation of samples for RNA-seq. Library preparation starts 100ng-1µg of total RNA which is poly-A selected with magnetic beads. Once converted in to double stranded cDNA and sheared, the samples undergo adaptor ligation and amplification prior to sequencing by paired end reads.

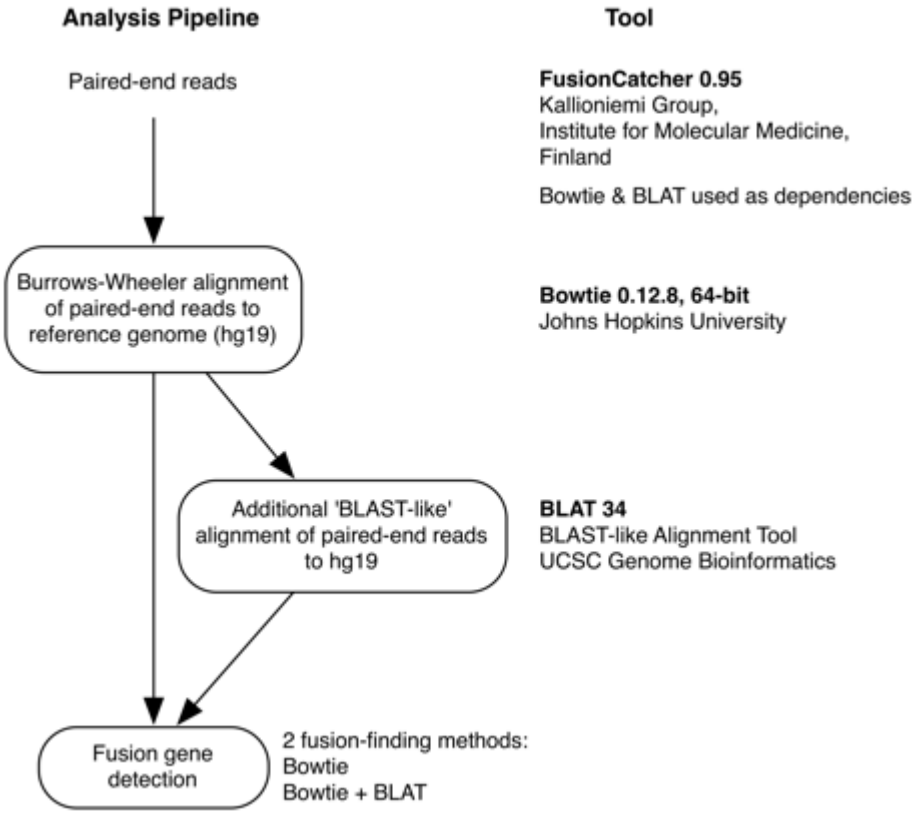


Figure 5-5. RNA-seq analysis pipeline. Paired-end sequencing reads were aligned to reference genome hg19 via Burrows-Wheeler and BLAT alignment tool in order to identify fusion genes.

5.3.3 Primer design for expression of RP11-680G10.1-GSE1 translocation

In order to measure expression of the RP11-680G10.1-GSE fusion gene demonstrated by RNA-Seq (Table 5-2, Table 5-3, Table 5-4, Table 5-5), qPCR of cell lines was carried out to ascertain expression levels. Initially, a panel of cell lines (6 Ewing sarcoma, 4 Osteosarcoma) were screened for expression of GSE1 gene via qPCR (methods previously described) with primers designed using the Roche Universal Probe Library.

Further sets of primers were designed specifically to the fusion protein. Reverse primers were designed separately to identify translocations involving Exon 2 and Exon 3 as identified by sequencing.

5.3.4 Etoposide

Etoposide (Sigma, E1383) was prepared as a 50mM stock in dimethyl sulphoxide (DMSO) and stored at -20°C as per manufacturer's instructions.

Cell lines were seeded at $1x10^4$ cells per well in 96 well plates and left for 24 hours. Etoposide was diluted from stock solution in RPMI media to desired concentrations (50, 10, 1, 0.5, 0.1, 0µM) and added to cells. Plates were incubated at 37°C for 72 hours following which dose response was measured by MTS assay as previously described.

5.3.5 Cisplatin

Cisplatin (Sigma, P4394) was prepared as a stock in sterile water and stored at -20°C until required. In a similar format to etoposide, cells were seeded into 96 well plates and doses between 0-50µM of cisplatin were added to cells and incubated for 72 hours. Response was measured by MTS.

5.3.6 Olaparib

Olaparib (AZD-2281) (LKT Labs, O4402) is a poly ADP ribose polymerase (PARP) inhibitor developed by KuDOS pharmaceuticals (Menear, Adcock et al. 2008). It was prepared as a 6mM stock in DMSO and stored at -20°C until needed.

Cell lines were seeded at $1x10^4$ cells per well in 96 well plates and left for 24 hours. Olaparib was diluted from stock solution in DMSO (100, 10, 5, 1, 0.1, 0µM) and added to cells. After 72 hours exposure cells were analysed via MTS assay.

5.3.7 Retinoic Acid

Retinoic Acid (Sigma, R2625) was dissolved in DMSO and stored in the dark at -20°C until needed. Doses between 0-100µM were added to cells seeded in 96 well plates and the plates analysed via MTS following 72 hours incubation.

5.3.8 Imatinib

Imatinib (Cell Signaling #9084) was reconstituted with DMSO to a stock solution and stored at -20°C. Previous literature suggested that Ewing sarcoma cell lines required a dose of 10-12µM in order to inhibit 50% of growth (Merchant, Woo et al. 2002). Doses from 0-50µM were added to cells and incubated for 72 hours prior to being analysed.

5.4 Results

5.4.1 NGS of a panel of Ewing sarcoma cell lines

DNA and RNA from six Ewing sarcoma cell lines was sequenced by OGT and data supplied for analysis. In summary each cell line underwent; RNA-seq for identification of chromosomal rearrangement, aCGH/ SNP array for copy number variation, and whole exome sequencing for mutational analysis. Circos plots (generated using http://www.circos.ca/) demonstrate heterogeneity between these cell lines and the intricacy and variety of their individual genomic make up (Krzywinski, Schein et al. 2009) (Figure 5-6). Conventional karyotypes were not carried out as the CGH/SNP array used for detection of genomic copy number variation does so at a higher resolution (Shinawi and Cheung 2008). Similarly to previously reported, A673 had a complex translocation, t(11;22;13) (Martínez-Ramírez, Rodríguez-Perales et al. 2003). There was the specific EWS-FLI1 translocation of Ewing sarcoma, although this was located on a derivative chromosome 13 with a complex translocation between chromosomes 13, 11, and 22. Both STA-ET10 and RM-82 had atypical translocations as expected. Overall most genomic variation was observed in SK-N-MC which had considerable copy number gains and losses as well as translocations. More detailed discussion of specific findings is discussed further in following pages.

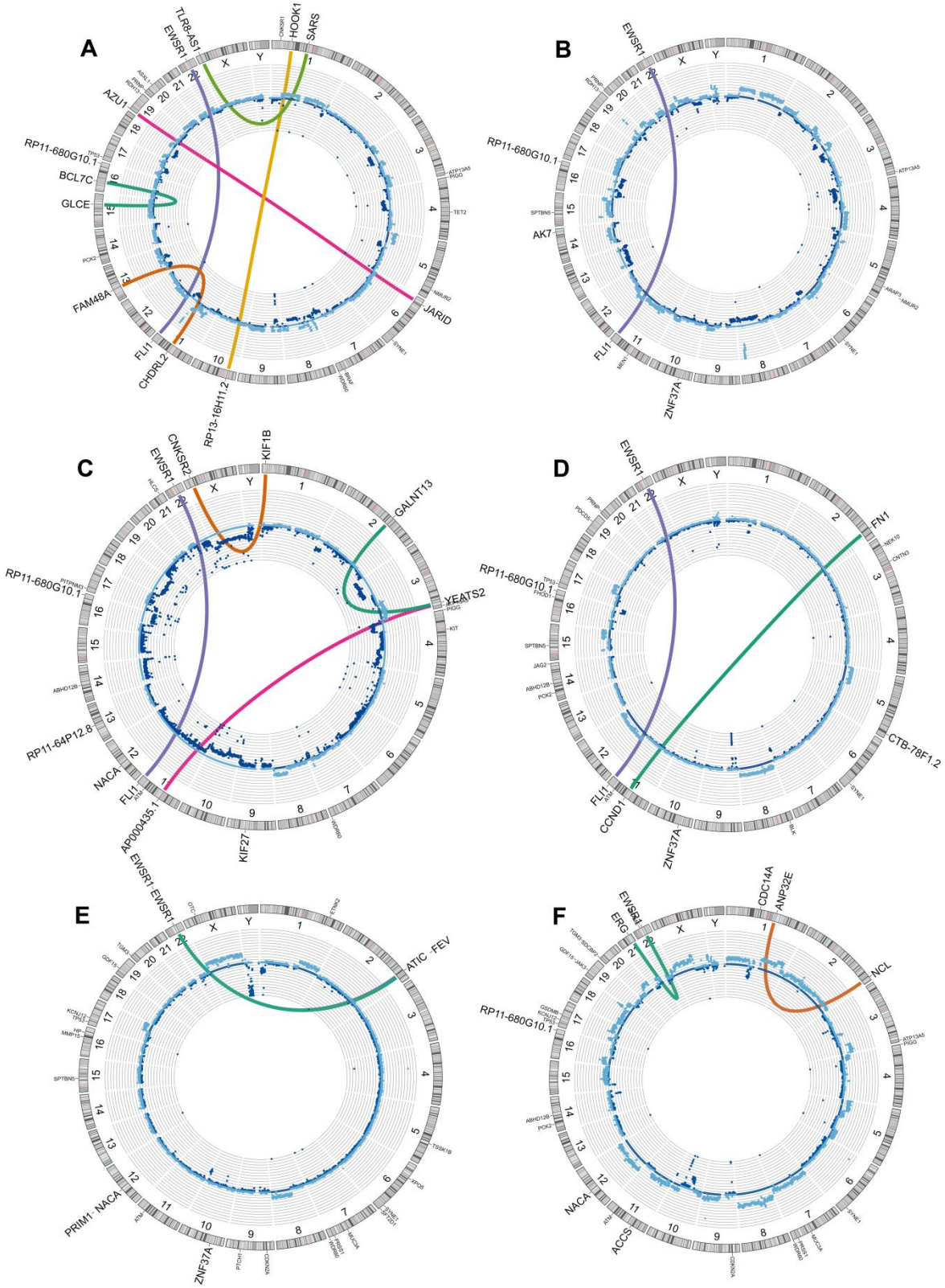


Figure 5-6. Circos plots of somatic modifications in Ewing sarcoma cell lines A673 (A), CHP-100 (B), SK-N-MC (C), STA-ET1 (D), STA-ET10 (E) and RM-82 (F). Individual chromosomes are depicted on the outer circle followed by concentric tracks for point mutation which are COSMIC annotated, copy number gains and losses shown in blue, and chromosomal rearrangement data relative to mapping position in the genome in bold coloured lines. Characteristic EWS-FLI1 translocation is illustrated in purple.

5.4.2 RNA-seq of panel of Ewing sarcoma cell lines identifies translocations

Ewing sarcoma is characterised by the presence of a chromosomal translocation which results in a chimeric transcript encoding the N-terminal trans-activating of EWS and the DNA-binding domain of ETS transcription factor (Delattre, Zucman et al. 1992). Assessment of chromosomal abnormality in a panel of presumed Ewing sarcoma cell lines was performed via RNA-Seq. Findings were referenced against characterisation performed as part of the EuroBoNet collaboration (Ottaviano, Schaefer et al. 2010). For each cell line data are presented as tables with 5' and 3' fusion partners described and the chromosomal position of the fusion (Table 5-2, Table 5-3, Table 5-4, Table 5-5). Sequencing read depths for the cell lines were $4x10^7$ paired end reads.

A673

5' Fusion partner	3' Fusion partner	Fusion point for 5' fusion partner	Fusion point for 3' fusion partner	Structural change	Exon
GLCE	BCL7C	15:69453096:+	16:30863643:-	Translocation	
FAM48A	CHRDL2	13:37633696:-	11:74408342:-	Translocation	
EWSR1	FLI1	22:29683123:+	11:128675261:+	Translocation	
RP11-680G10.1	GSE1	16:85391249:+	16:85667520:+	Deletion	e2
FAM48A	CHRDL2	13:37633617:-	11:74408342:-	Translocation	
JARID2	AZU1	6:15246815:+	19:828230:+	Translocation	
TR8-AS1	SARS	X:12926335:-	1:109766600:+	Translocation	
EWSR1	FLI1	22:29683123:+	11:128677075:+	Translocation	
RP11-680G10.1	GSE1	16:85391249:+	16:85682158:+	Deletion	e3
EWSR1	FLI1	22:29683123:+	11:128675261:+	Translocation	
FAM48A	CHRDL2	13:37633696:-	11:74408342:-	Translocation	
JARID2	AZU1	6:15246815:+	19:828230:+	Translocation	
FAM48A	CHRDL2	13:37633617:-	11:74408342:-	Translocation	
RP11-680G10.1	GSE1	16:85391249:+	16:85667520:+	Deletion	e2
RP13-16H11.2	HOOK1	10:26957336:-	1:60324100:+	Translocation	
RP11-680G10.1	GSE1	16:85391249:+	16:85682158:+	Deletion	e3
FLI1	EWSR1	11:128651918:+	22:29688126:+	Translocation	

CHP-100

5' Fusion partner	3' Fusion partner	Fusion point for 5' fusion partner	Fusion point for 3' fusion partner	Structural change	Exon
EWSR1	FLI1	22:29683123:+	11:12861853:+	Translocation	
RP11-680G10.1	GSE1	16:85391249:+	16:85682158:+	Deletion	e3
ZNF37BP	ZNF37A	10:43047025:-	10:38384672:+	Deletion	
EWSR1	FLI1	22:29683123:+	11:12861853:+	Translocation	
RP11-680G10.1	GSE1	16:85391249:+	16:85682158:+	Deletion	e3
AK7	PAPOLA	14:96949556:+	14:96986392:+	Deletion	

Table 5-2. RNA from cell lines A673 (top) and CHP-100 (bottom) were sequenced by Illumina NGS and fusion genes identified. The characteristic EWS-FLI1 translocation between chromosomes 11 and 22 was observed along with the reciprocal arrangement of the two partner (FLI1- EWSR1). The different exon position of GSE1 involved in the RP11-68010.1-GSE1 translocation is indicated (right hand column).

SK-N-MC

5' Fusion partner	3' Fusion partner	Fusion point for 5' fusion partner	Fusion point for 3' fusion partner	Structural change	Exon
EWSR1	FLI1	22:29683123:+	11:128675261:+	Translocation	
YEATS2	GALNT13	3:183415781:+	2:154996850:+	Translocation	
KIF1B	CNKSR2	1:10322028:+	X:21515905:+	Translocation	
RP11-680G10.1	GSE1	16:85391249:+	16:85682158:+	Deletion	e3
RP11-680G10.1	GSE1	16:85391249:+	16:85667520:+	Deletion	e2
YEATS2	GALNT13	3:183415781:+	2:155098543:+	Translocation	
PRIM1	NACA	12:57127931:-	12:57108471:-	Deletion	
KIF27	RP11-213G2.3	9:86523367:-	9:88452674:+	Deletion	
EWSR1	FLI1	22:29684775:+	11:128675261:+	Translocation	
HNRNPA1L2	RP11-64P12.8	13:53191817:+	13:52760958:-	Deletion	
YEATS2	GALNT13	3:183415781:+	2:154996850:+	Translocation	
EWSR1	FLI1	22:29683123:+	11:128675261:+	Translocation	
KIF1B	CNKSR2	1:10322028:+	X:21515905:+	Translocation	
RP11-680G10.1	GSE1	16:85391249:+	16:85682158:+	Deletion	e3
RP11-680G10.1	GSE1	16:85391249:+	16:85667520:+	Deletion	e2
EWSR1	FLI1	22:29684775:+	11:128675261:+	Translocation	
PRIM1	NACA	12:57127931:-	12:57108471:-	Deletion	
YEATS2	GALNT13	3:183415998:+	2:154996850:+	Translocation	
EIF4A2	AP000435.1	3:186504017:+	11:58010186:-	Translocation	
YEATS2	GALNT13	3:183415781:+	2:155098543:+	Translocation	

STA-ET1

5' Fusion partner	3' Fusion partner	Fusion point for 5' fusion partner	Fusion point for 3' fusion partner	Structural change	Exon
EWSR1	FLI1	22:29683123:+	11:128675261:+	Translocation	
CTB-78F1.2	TENM2	5:167148412:+	5:167302991:+	Deletion	
RP11-680G10.1	GSE1	16:85391249:+	16:85667520:+	Deletion	e2
ZNF37BP	ZNF37A	10:43047025:-	10:38384672:+	Deletion	
RP11-680G10.1	GSE1	16:85391249:+	16:85682158:+	Deletion	e3
EWSR1	FLI1	22:29683123:+	11:128675261:+	Translocation	
EWSR1	FLI1	22:29683123:+	11:128657318:+	Translocation	
FLI1	EWSR1	11:128651918:+	22:29684595:+	Translocation	
RP11-680G10.1	GSE1	16:85391249:+	16:85682158:+	Deletion	e3
RP11-680G10.1	GSE1	16:85391249:+	16:85667520:+	Deletion	e2
CCND1	FN1	11:69467598:+	2:216241788:-	Translocation	

Table 5-3. RNA-seq to a read depth of $4x10^7$ paired end reads confirms the presence of EWS-FLI1 translocation in SK-N-MC and STA-ET1. The presence of additional fusion genes were identified including a deletion on chromosome 16 resulting in the fusion of RP11-680G10.1 and GSE1.

RD-ES

5' Fusion partner	3' Fusion partner	Fusion point for 5' fusion partner	Fusion point for 5' fusion partner	Structural change
PAFAH1B2	FOXR1	11:117023244:+	11:118849492:+	Deletion
SIK3	C11orf92	11:116968859:-	11:111169391:-	Deletion
DIAPH2	HEBP1	X:96396793:+	12:13128413:-	Translocation
PAFAH1B2	FOXR1	11:117015134:+	11:118849492:+	Deletion
SNED1	FARP2	2:241938467:+	2:242401938:+	Deletion
DPYSL3	FMNL2	5:146889041:-	2:153471365:+	Translocation
SLC29A1	HSP90AB1	6:44200165:+	6:44216367:+	Deletion
UBASH3B	IL10RA	11:122526918:+	11:117859097:+	Deletion
RP11-680G10.1	GSE1	16:85391249:+	16:85682158:+	Deletion
PRIM1	NACA	12:57127931:-	12:57108471:-	Deletion
ZNF37BP	ZNF37A	10:43047025:-	10:38384672:+	Deletion
PAFAH1B2	FOXR1	11:117023244:+	11:118849492:+	Deletion
PAFAH1B2	FOXR1	11:117015134:+	11:118849492:+	Deletion
SNED1	FARP2	2:241938467:+	2:242401938:+	Deletion
SIK3	C11orf92	11:116968859:-	11:111169391:-	Deletion
UBASH3B	IL10RA	11:122526918:+	11:117859097:+	Deletion
DPYSL3	FMNL2	5:146889041:-	2:153471365:+	Translocation
SLC29A1	HSP90AB1	6:44200165:+	6:44216367:+	Deletion
RP11-680G10.1	GSE1	16:85391249:+	16:85682158:+	Deletion
EXOC2	MET	6:693019:-	7:116395409:+	Translocation
PRIM1	NACA	12:57127931:-	12:57108471:-	Deletion
BRIX1	RP11-119N19.1	5:34923339:+	8:52348725:+	Translocation

Table 5-4. RNA-seq did not demonstrate the presence of the expected EWS-FLI1 translocation in RD-ES. Sequencing failed to confirm the cell line as one of Ewing sarcoma. Alternative translocations were observed which may be oncogenic. These included a deletion on chromosome 11 between PAFAH1B2 and FOXR1.

RM-82

5' Fusion partner	3' Fusion partner	Fusion point for 5' fusion partner	Fusion point for 3' fusion partner	Structural change
EWSR1	ERG	22:29683123:+	21:39764366:-	Translocation
PRIM1	NACA	12:57127931:-	12:57108471:-	Deletion
EWSR1	ERG	22:29683123:+	21:39764366:-	Translocation
NCL	ANP32E	2:232326295:-	1:150199041:-	
PRIM1	NACA	12:57127931:-	12:57108471:-	Deletion
RP11-680G10.1	GSE1	16:85391249:+	16:85667520:+	Translocation
NCL	ANP32E	2:232326304:-	1:150199041:-	
RP11-680G10.1	GSE1	16:85391249:+	16:85682158:+	Translocation
NCL	ANP32E	2:232326288:-	1:150199041:-	
ACCS	EXT2	11:44104861:+	11:44129233:+	
CDC14A	AKNAD1	1:100905554:+	1:109359799:-	
NCL	ANP32E	2:232326300:-	1:150199035:-	

STA-ET10

5' Fusion partner	3' Fusion partner	Fusion point for 5' fusion partner	Fusion point for 3' fusion partner	Structural change
EWSR1	FEV	22:29688158:+	2:219849027:-	Translocation
ZNF37BP	ZNF37A	10:43047438:-	10:38384466:+	
EWSR1	FEV	22:29688158:+	2:219849027:-	Translocation
PRIM1	NACA	12:57127931:-	12:57108471:-	Deletion
ATIC	EWSR1	2:216214412:+	22:29688477:+	Translocation
ATIC	EWSR1	2:216213972:+	22:29692229:+	Translocation

Table 5-5. RM-82 and STA-ET10 are confirmed to express atypical translocations of EWSR1-ERG and EWSR1-FEV respectively. STA-ET10 is the only cell line which does not express the RP11-680G10.1-GSE1 deletion seen in the other cell lines.

5.4.2.1 EWS-FLI1 and other translocations detected by RNA-seq of A673, CHP-100, SK-N-MC and STA-ET1

RNA-seq confirmed the presence of EWS-FLI1 translocation in A673, CHP-100, SK-N-MC, and STA-ET1 (Table 5-2, Table 5-3). The other common aberration was a deletion on chromosome 16 resulting in the fusion of RP11-680G10.1 and GSE1 identified in all cell lines except STA-ET10. This is a novel observation. CHP-100 had a translocation between PAPOLA-AK7 (Table 5-2). This has previously been reported by Maher et al. in breast cancer cell lines however Asmann et al. in a publication describing a novel bioinformatics pipeline, did not find evidence to support this fusion (Maher, Palanisamy et al. 2009). They related this to the small distance of 65kb between PAPOLA and AK7 which was below their default setting of 100kb as the minimum distance between two fusion partner genes if both are located on the same chromosome (Asmann, Hossain et al. 2011). A number of other translocations were detected for example, SK-N-MC had a translocation between CNKSR2 (connector enhancer of kinase suppressor of ras2) on the X chromosome and KIF1B (kinesin-like protein) on chromosome 1 (Table 5-3).

RD-ES, along with all other cell lines, was from the characterised cell bank established by EuroBoNet. Surprisingly this cell line did not harbour the expected EWS-FLI1 translocation which had been reported in previous literature (Ottaviano, Schaefer et al. 2010, Huang, Angelo et al. 2011) (Table 5-4). A deletion on chromosome 11 resulting in the fusion of PAFAH1B2 and the transcription factor FOXR1 was identified which has been reported in neuroblastoma and in the osteosarcoma cell line HOS. It is thought that the deletion results in overexpression of FOXR1 leading to oncogenic activation (Santo, Ebus et al. 2012). Similar to the previous cell lines tested, a deletion was observed on chromosome 16 resulting in the fusion of RP11-680GA0.1 and GSE1. This translocation had not been identified in previous sequencing carried out by OGT for other institutions

and was therefore unlikely to be a consequence of contamination of the pipeline. The consistency of this translocation within cell lines tested has yet to be fully explained.

As RNA-seq failed to confirm the characteristic pathognomnic translocation of Ewing sarcoma in RD-ES, this cell line was excluded from further analysis and experimentation as genomic characterisation was not centred on an ETS based fusion gene.

5.4.2.2 Atypical translocation of Ewing sarcoma in RM-82 and STA-ET10

Although the majority, 85%, of Ewing sarcoma tumour specimens harbour the 4(11'22)(q24;q12) chromosomal abnormality, a proportion carry an alternative translocation. EWS can fuse to other ETS family transcription factors including ERG, ETV1, ETV4, and FEV1 which all likely mimic EWS-FLI1 (Sorensen, Lessnick et al. 1994, Peter, Couturier et al. 1997). RM-82 was confirmed to have an atypical translocation between chromosome 21 and 22 resulting in the fusion of EWS and ERG. Similarly STA-ET10 had an atypical translocation resulting in the fusion of EWS and FEV1 (Table 5-5). In addition a further translocation between EWS and ATIC was also identified which has not been reported previously. ATIC encodes 5-aminimidazole-4-carboxaminde ribonucleotide formyltransferase/IMP cyclohydrolase, a bifunctional enzyme which catalyzes the penultimate and final steps of the purine nucleotide synthesis pathway and is ubiquitously expressed (Sugita, Aya et al. 1997). ATIC is believed to act as a strong promoter in the ATIC-ALK fusion gene, a known variant ALK gene fusion in anaplastic large cell lymphoma (Colleoni, Bridge et al. 2000).

5.4.2.3 Deletion in chromosome 10 resulting in ZNF37BP-ZNF37A fusion gene

A deletion of chromosome 10 was recognised in CHP-100, STA-ET1, and STA-ET10 (Table 5-2, Table 5-3, Table 5-5) resulting in the fusion of zinc finger 37 binding protein (ZNF37BP) with zinc finger 37A (ZNF37A) both of which have no reported function. The

pericentromeric region of chromosome 10, where ZNF37A and ZNF37BP are located, is reported to not uncommonly have intrachromosomal duplications which can result in microdeletions (Guy, Hearn et al. 2003).

5.4.2.4 PRIM1-NACA fusion gene is identified in SK-N-MC, RM-82 and STA-ET10

Not previously described in Ewing sarcoma cell lines, a deletion in chromosome 12 resulting in the fusion of PRIM1, a DNA primase required for discontinuous DNA replication, and NACA (Cloutier, Hamel et al. 1997), involved in myogenic differentiation was reported in three cell lines (Yotov and St-Arnaud 1996) (Table 5-3, Table 5-5). The PRIM1-NACA fusion has previously been described though RNA-seq in a chronic myeloid leukaemia cell line (Levin, Berger et al. 2009) although no function has yet been proposed.

5.4.3 Novel translocations and fusion protein identified in Ewing sarcoma cell lines

RNA-seq identified a deletion on chromosome 16 between a pseudogene, RP11-680G10.1 (Exon 1) and genetic suppressor element 1 (GSE1) (KIAA0182) (Exons 2 or 3). Given that the deletion was present in all of the Ewing cell lines except STA-ET10, change in expression of GSE1 was proposed (Table 5-2, Table 5-3, Table 5-5).

Gudkov et al. first identified GSE1 in a mammalian gene cloning strategy, as a cDNA that could induce resistance to DNA-damaging drugs such as etoposide (Gudkov, Kazarov et al. 1994). KIAA0182, first sequenced by Nagase et al. in 1996 as part of an effort to identify the coding sequences of 40 unidentified genes, encodes a putative genetic suppressor element 1 protein, (GSE1) which may exhibit RNA-binding activity (Nagase, Seki et al. 1996). However, there is little literature about the function of the gene. A study by Landi et al. found mutation of the KIAA0182 gene to be significantly associated with the risk of developing colorectal cancer (Landi, Gemignani et al. 2012).

Three separate qPCR assays were designed; primers designed to the GSE1 gene, and those designed to the gene fusion (both exons 2 and 3) (Figure 5-7). Expression of GSE1 was found to vary across the panel of cell lines, including 4 Osteosarcoma lines, with RM-82 appearing to have the highest expression in the gene alone. STA-ET10, known to not have the deletion, did not have markedly different expression relative to the other cell lines. Data suggests that the presence of the deletion does not alter the expression of GSE1.

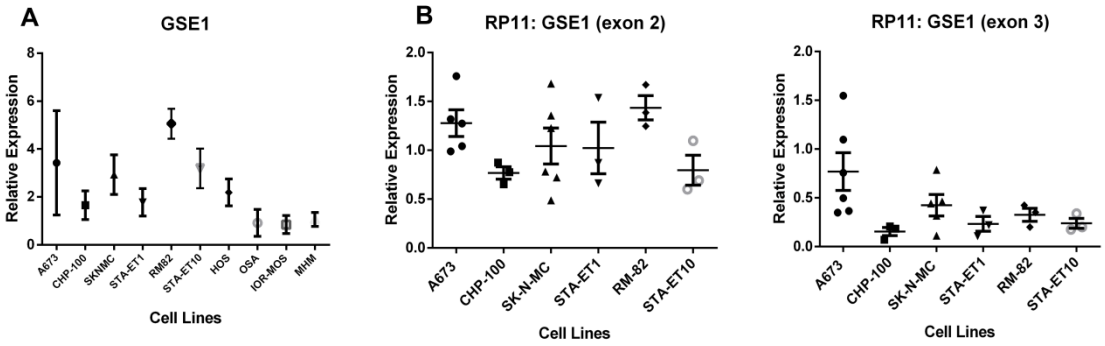


Figure 5-7. The novel fusion of RP11-GSE1 does not result in increased expression of GSE1. A – Expression of the wild type GSE1 gene was measured in a panel of Ewing and Osteosarcoma cell lines. Expression levels were not consistently altered in those lines known to have the translocation of RP11-680G10.1-GSE1 which included all cell lines except STA-ET10. **B** - Primers designed to span the fusion gene (fusion point for 3' end on exons 2 or 3) also demonstrated no clear elevation of expression in comparison with STA-ET10 which was known not to have the translocation (n=3).

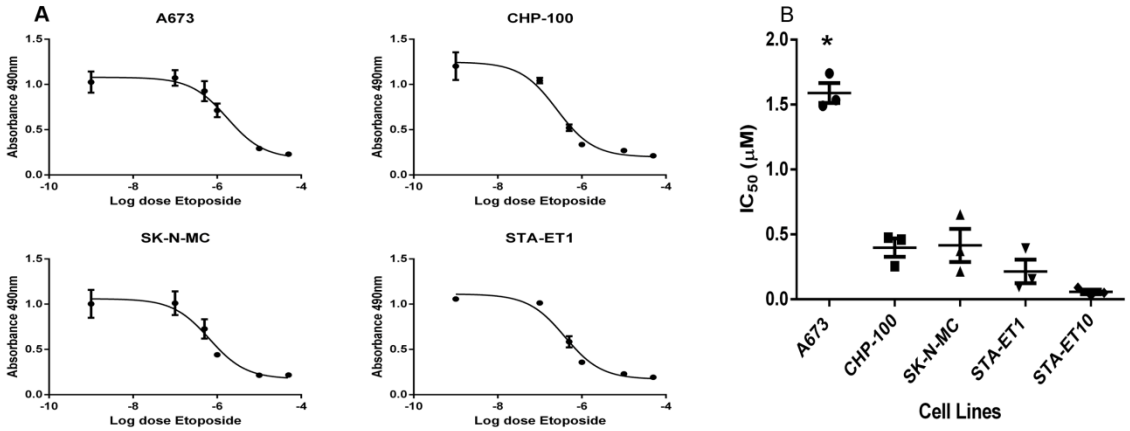


Figure 5-8. A673 is resistant to etoposide in comparison to other Ewing sarcoma lines. Cell lines were exposed to etoposide for 72 hours and dose response measured by MTS. **A** – representative dose response curves to etoposide for each cell line tested (n=3). **B** – IC_{50} from 3 separate experiments. Statistical comparison was made between individual cell lines (multiple t test) showing a statistical difference in sensitivity of A673 with the remaining cell lines ($p<0.05$). Gudkov et al. suggested GSE1 could induce resistance to etoposide. Due to the uniformity of expression of GSE1, resistance to etoposide by A673 could not be related to the RP11-680G10.1-GSE1 fusion gene in this panel. Error bars represent mean values ±SEM.

5.4.4 A673 demonstrates relative resistance to etoposide

Etoposide, a type 2 topoisomerase inhibitor, is routinely used in the chemotherapeutic management of Ewing sarcoma (Juergens, Weston et al. 2006, Ladenstein, Pötschger et al. 2010). In a panel of cell lines A673 was found to have an IC_{50} significantly higher (1.6μM) ($p<0.05$), indicating less sensitivity than other lines (for example in SK-N-MC 0.4μM) (Figure 5-8). Due to the uniformity of expression of GSE1, this finding could not be affiliated to the RP11-680G10.1-GSE1 fusion gene.

5.4.5 CHP-100 has a gain of 1q

Previous research has suggested a gain of 1q in approximately 30% of tumour samples as tested by aCGH and associated with poor survival in patients (Mackintosh, Ordóñez et al. 2012). 1q gain was assessed in 4 cell lines (Figure 5-9). SK-N-MC and STA-ET1 were found to have normal copy number. A673 had a gain of part of 1q and a loss of one region, and CHP-100 had a gain in copy number (4 copies) of the entire region. The presence of 1q gain results in overexpression of CDT2, a 1q-located candidate gene encoding a protein involved in cell cycle control through regulating entry in to the S phase of the cell cycle. Overexpression of CDT2 is believed to lead to deregulation of cell cycle and increased proliferation potentially resulting in worse outcome for patients with this subtype (Mackintosh, Ordonez et al. 2012).

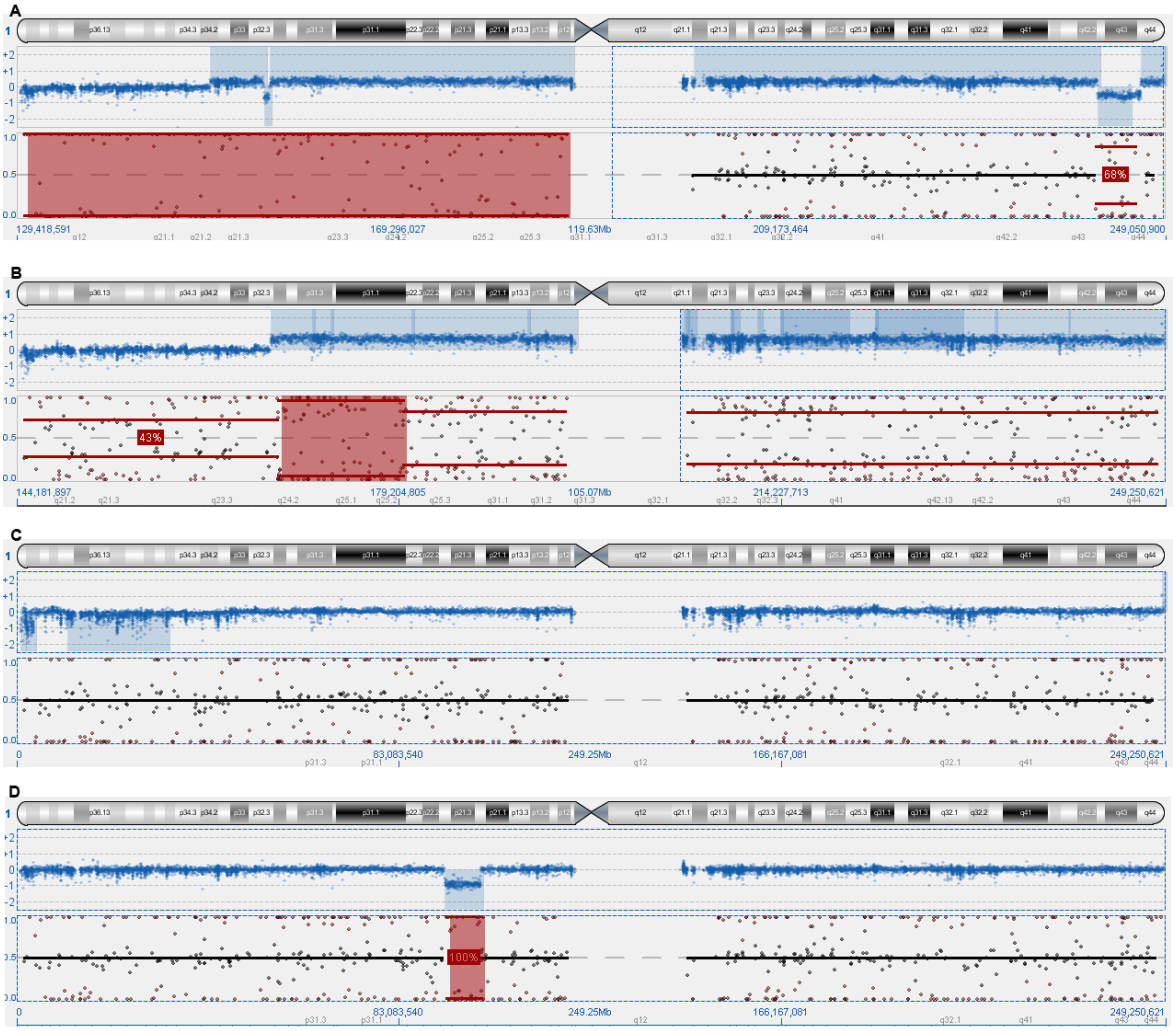


Figure 5-9. CHP 100 has gained copies of 1q. Cell line data was assessed for copy number variation in 1q using an Agilent aCGH/SNP array and displayed using CytoSure™ software. A673 (**A**) had a gain in the majority of the chromatid but a loss in one area. CHP-100 (**B**) had a gain in copy number of 1q which is shown by the blue highlighted region. SK-N-MC (**C**) and STA-ET1 (**D**) were both heterozygous for 1q.

5.4.6 Copy number of CDKN2A is decreased in cell lines

Analysis via aCGH confirmed loss of CDKN2A ($p16^{Ink4A}$) in A673 and STA-ET1 with mean log ratios of -1.029 and -2.338 respectively (Figure 5-10). This is consistent with array aCGH data published by Ottaviano et al. who also confirmed a loss of CDKN2A along with normal copy number of the gene in SK-N-MC. CHP-100 was found to have a normal copy number of CDKN2A which was inconsistent with previously published data which suggests a loss of copy number (Ottaviano, Schaefer et al. 2010). The reason for difference in results is unclear. The detection method used for the by Ottaviano et al. was by multiplex ligation-dependent probe amplification (MLPA) showing hemizygous deletion, immunohistochemistry which showed moderate staining, and aCGH where a loss was observed. Other than technical error, it may be that CHP-100 cells in culture have through selection, regained the deletion over time resulting in normal copy number.

5.4.7 c-Myc is over-expressed in CHP-100

There was an increase in copy number of c-Myc in each cell line consistent with evidence that EWS-FLI1 fusion up-regulates c-Myc (Dauphinot, De Oliveira et al. 2001), the most marked increase being in CHP-100 which has a c-Myc gain of 9 copies (Figure 5-11).

Related genes such CDK4, involved in cell cycle progression, show variation between cell lines. Id2 is homozygous for all cell lines except SK-N-MC which only has one copy. Interestingly CHP-100, which has the highest gain of c-Myc, has normal expression of CDK4, Id2, and MDM2, an inhibitor of p53.

5.4.8 p53 mutations are present in CHP-100, SK-N-MC and STA-ET1

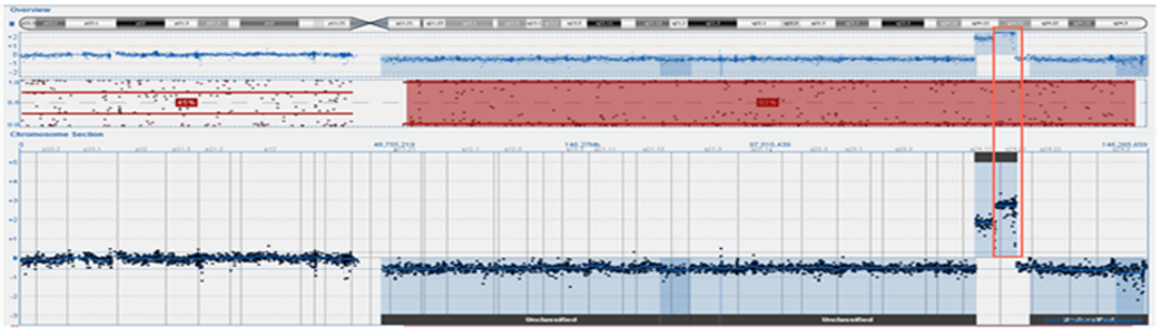
p53, a tumour suppressor gene acting as a transcription factor, causes cell cycle arrest and apoptosis when activated. In normal cells its levels are kept low by murine double minute 2 (MDM2), forming a negative feedback with p53 to maintain appropriate cellular levels.

Approximately 50% of cancers have p53 mutations and 17% have MDM2 gene amplifications (Momand, Jung et al. 1998, Levine and Oren 2009). In this panel of cell lines whole exome sequencing showed that all lines except A673 have a mutation of p53. CHP-100 has an indel and SK-N-MC a substitution both of which are not COSMIC annotated. STA-ET1 has a substitution of cysteine to guanine, reported previously in an ovarian tumour (Concin, Hofstetter et al. 2005) (Figure 5-11).



Figure 5-10. CDKN2A is lost in 3 Ewing sarcoma cell lines. A – Illustration of Cytosure Interpret Software of chromosome 9 in A673 showing loss of copy of CDKN2A. **B** – Similarly loss is seen in STA-ET1. SK-N-MC had normal copy number (data not shown). **C** – CHP-100 had normal copy number of CDKN2A.

A



B

Cell Line	c-Myc	CDK4	Id2	MDM2	p53 mutation
A673	Gain (3)	Gain (3)	Normal	Normal	Negative
CHP-100	Gain (9)	Normal	Normal	Normal	Serious indel
SK-N-MC	Gain (3)	Loss (1)	Loss (1)	Loss (1)	C>G subsitution
STA-ET1	Gain (3)	Gain (3)	Normal	Gain (3)	C>G substitution

Figure 5-11. c-Myc is over-expressed in a panel of cell lines. Via the CytoSure Interpret Analysis, gain in copy number is seen in cell lines. **A** – Illustration of chromosome 8 in CHP-100 showing gain in c-Myc relative to baseline (red rectangle). **B** – mean log ratio of cell lines indicating gains in each and that CHP-100 has 9 copies of the gene. Other members of related cell cycle pathway were also analysed and despite the large gain in CHP-100, related pathway genes are normally expressed. SK-N-MC however shows heterozygosity for CDK4, Id2 and MDM2. p53 mutational status from whole exome sequencing is also shown highlighting the mutations present in each cell line except A673.

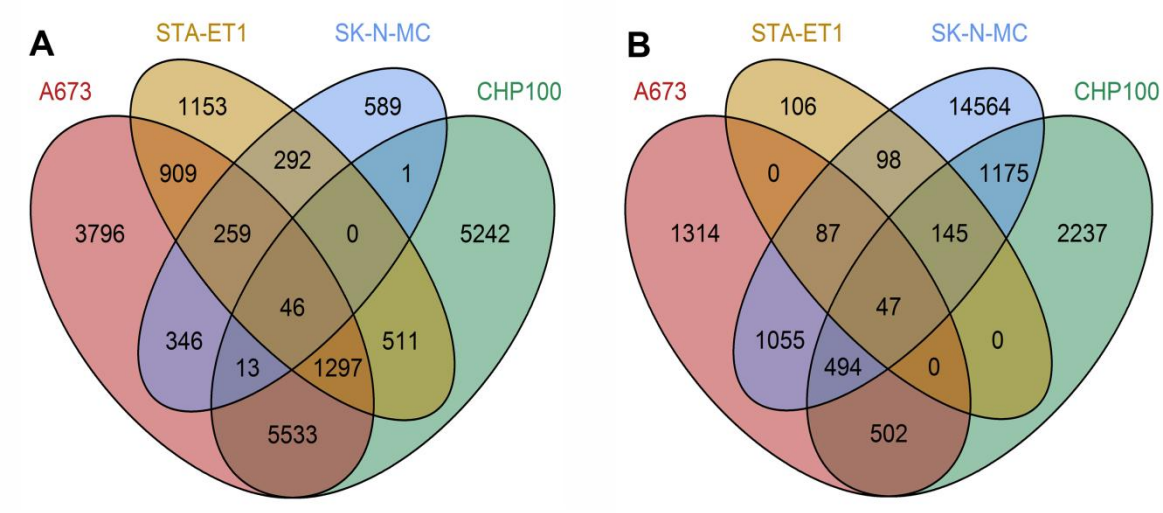


Figure 5-12. Cell lines have gains and losses in copy number. Copy number variation analysis by Cytosure™ Interpret Software confirmed gains (**A**) and losses (**B**) in panel of 4 Ewing sarcoma cell lines (A673, CHP-100, SK-N-MC, STA-ET1). **A** – Gains are shown in all cell lines, with all lines having gains in common except between CHP-100, SK-N-MC and STA-ET1. **B** – Similarly losses are seen in all cell lines with STA-ET1 having the least overall.

Losses - chromomsome 9

IFNAS	SLC24A2
IFNA20P	AL512635.1
KHLH9	MLLT3
IFNA6	AL163193.1
IFNA13	KIAA1797
IFNA2	MIR491
IFNA11P	PTPLAD2
IFNA12P	IFNNP1
IFNA8	IFNB1
IFNWP2	IFNWP4
IFNA1	IFNW1
IFNWP19	IFNA21
MIR3JHG	IFNWP15
IFNE	IFNA4
MIR3J	IFNWP9
KHSRPP1	IFNA7
AL355679.1	IFNA10
MTAP	IFNWP18
C9orf53	IFNA16
CDKN2A	IFNA17
CDKN2B-AS	IFNWP5
CDKN2B	IFNA14
UBA52P6	IFNA22P
DMRTA1	

Gains - chromosome 8

DERL1	ARF1P3
WDR67	TMEM65
RNY4P5	TRMT12
HMGB1P19	RNF139
FAM83A	TATDN1
C8orf76	NDUFB9
ZHX1-C8ORF76	MTSS1
UBA52P5	ZNF572
ZHX1	SQLE
TRNAF14P	KIAA0196
ATAD2	NSMCE2
MIR548D1	AC084083.1
DUPT2	TRIB1
IMPDH1P6	AC090573.1
WDYHV1	FAM84B
FBXO32	POU5F1B
AC090193.1	MYC
CTD-2552K11.2	PVT1
KLHL38	MIR1204
ANXA13	AC103705.1
FAM91A1	TMEM75
FER1L6	MIR1205
FER1L6-AS1	MIR1207

Figure 5-13. Gains and losses shared by A673, CHP-100, SK-N-MC and STA-ET1. Genes commonly lost between cell lines (left hand side) or gained (right hand side) were all found on chromosomes 9 and 8 respectively. The gains were all identified in the region of 8q24 around the MYC locus.

5.4.9 Common 46 genes gained and 47 genes lost across panel of cell lines

Venn diagrams show an overview of genes lost and gained in cell lines as measured by Cytosure™ Interpret Software (Figure 5-12, Figure 5-13). CHP-100 has the most unique gains (5,242 total) and SK-N-MC the least (589). Interestingly only 1 of those gains is common between these two cell lines suggesting the high levels of heterogeneity present. Most gene losses are reported in SK-N-MC (14,564) and the least in STA-ET1 (106).

When focusing on the common gains in chromosome 8 (8q24), several genes related to c-Myc have a gain in copy number in all the cell lines (Figure 5-11, Figure 5-13). These include PVT-1, an oncogene which is a c-Myc target (Carramusa, Contino et al. 2007) and known to be upregulated in breast and ovarian cancer (Haverty, Hon et al. 2009, Sircoulomb, Bekhouche et al. 2010), ATAD2, a co-factor of c-Myc which is believed to stimulate its transcriptional activity (Ciró, Prosperini et al. 2009), and miRs 1204, 1205 and 1207 which are produced by PVT-1 (Barsotti, Beckerman et al. 2012).

Common losses are all on chromosome 9 and are, for the most part, interferons (Figure 5-13). CDKN2A and CDKN2B contribute to cell cycle control and act as tumour suppressors. CDKN2A loss has been reported in Ewing sarcoma cell lines as well as other malignancies such as pancreatic carcinomas and oesophageal cancers (Schutte, Hruban et al. 1997, Ottaviano, Schaefer et al. 2010, Gu, Pfeiffer et al. 2013).

5.4.10 Specific gene mutations reported on whole exome sequencing and RNA-seq

Cell lines underwent whole exome sequencing by OGT allowing for identification of mutations. This was carried out using the Illumina HiSeq platform. A minimum of 82.06% of the on target regions were covered to a depth of x20 (Table 5-6). Variations in reads between reference genome and cell lines were around $41x10^3$- $50x10^3$. Of these $8x10^3$ - $10x10^3$ were identified as being in non-synonymous coding regions and predicted to have

consequences (Table 5-7). Several commonly mutated genes were analysed for mutational status and functional experiments performed (Table 5-8, Figure 5-14, Figure 5-15, Figure 5-16, Figure 5-17).

	A673	CHP-100	RD-ES	SK-N-MC	STA-ET1
Estimated Library Size (excl. duplicates)	232,370,513	325,818,872	295,443,661	363,596,108	345,948,403
% Reads Aligned	98.41%	98.63%	98.52%	98.54%	98.62%
% High Quality Aligned Bases (>=Q20)	95.64%	95.66%	95.58%	95.66%	95.69%
Number of Paired Reads	20,716,154	26,394,438	25,443,267	21,494,444	28,410,222
% Target Bases with Zero Coverage	0.33%	0.26%	0.29%	0.32%	0.25%
% Target Bases with 2x Coverage	99.48%	99.59%	99.55%	99.47%	99.62%
% Target Bases with 10x Coverage	94.46%	96.28%	95.89%	94.63%	97.07%
% Target Bases with 20x Coverage	82.06%	87.50%	86.62%	82.75%	90.05%
% Target Bases with 30x Coverage	67.69%	76.28%	75.07%	68.92%	80.39%

Table 5-6. Quality control metrics for whole exome sequencing. Whole exome sequencing was carried out on 5 samples, using the Illumina HiSeq platform. A minimum of 82.06% of the on-target regions were covered to a depth of at least 20x. A total of 24.21 gigabases of sequence data were read and aligned at high quality. 217,218 variations from the reference genome were identified. Across the samples, 45,301 variations indicative of serious consequences in coding sequences were found.

All Genotypes					
	A673	CHP-100	RD-ES	SKNMC	STA-ET1
Number of Variations	41,337	42,869	41,091	42,018	49,903
Variations Overlapping Genes	41,050	42,577	40,781	41,737	49,557
Variations Overlapping Transcripts	41,050	42,577	40,781	41,737	49,557
Variations Overlapping Regulatory Regions	8,511	8,815	8,488	8,647	10,031
Variations Overlapping Protein Domains	27,573	28,499	27,562	28,046	33,205
Intergenic Variations	287	292	310	281	346
Variations With Predicted Serious Consequences	8,957	9,446	9,038	9,248	10,752
Variations With Other Predicted Consequences	38,836	40,279	38,599	39,441	46,921
Non-Synonymous Coding Variations with Consequences	8,580	9,052	8,665	8,855	10,149

Table 5-7. All variants identified by whole exome sequencing. Whole exome sequencing was carried out by OGT on 5 cell lines. The variations between each cell line and reference genome were between $41x10^3$- $50x10^3$. Variations within non-synonymous coding regions were between 8,488 – 10,031.

5.4.10.1 BRCA1 mutations are present in Ewing sarcoma cell lines

BRCA mutations are associated with risk of developing breast, ovarian and prostate cancers (Stratton, Gayther et al. 1997, Peto, Collins et al. 1999, Edwards, Kote-Jarai et al. 2003). Cells which carry the heterozygous loss of function BRCA mutations can lose the remaining wild-type allele resulting in deficient homologous recombination DNA repair causing genetic aberrations which may drive malignancy (Farmer, McCabe et al. 2005). This results in the emergence of a tumour which carries a DNA repair defect which is not present in non-malignant cells.

The poly (adenosine diphosphate [ADP]-ribose) polymerases (PARPs) are a large family of enzymes which are involved in single strand DNA repair through base excisions (Dantzer, de La Rubia et al. 2000). In tumour cells with deficient homologous recombination repair of DNA, PARP inhibitors such as olaparib, lead to the accumulation of DNA with unrepaired single strand breaks which are likely to cause the accumulation of DNA with double strand breaks and collapsed replication forks in tumour cells with defective BRCA function (McCabe, Turner et al. 2006).

Recently, comprehensive genomic and drug sensitivity analysis resulted in the identification of BRCA1/2 mutations in cancer cell lines which included both ovarian and Ewing sarcoma (Garnett, Edelman et al. 2012).

Whole exome sequencing of A673, CHP-100, SK-N-MC and STA-ET1 revealed missense mutations of BRCA1 in SK-N-MC and STA-ET1 (substitution of T to C) (Table 5-8). These, although not recorded within the COSMIC database, are indicated to have a deleterious and therefore possible or probable effect on the gene. This would imply that they are not germline mutations but this cannot be assured with total certainty as germline DNA is not available for analysis. A673 and CHP-100 were not found to have BRCA1 mutations.

5.4.10.2 Cell lines show variation in response to cisplatin

Cisplatin (*cis*-diamminedichloroplatinum(II)) binds to and causes crosslinking of DNA resulting in DNA damage which, when unable to be repaired, results in apoptosis of the cell. In breast and ovarian cancer patients who have a BRCA1 mutation, cisplatin has been shown to be effective due to defects in homologous recombination DNA repair (Byrski, Dent et al. 2012).

In view of this, one prediction was that cell lines SK-N-MC and STA-ET1, both known to have a mutation of BRCA1, would be sensitive to the effects of cisplatin treatment. This was confirmed as SK-N-MC was significantly more sensitive to the drug than CHP-100 ($p<0.05$) (Figure 5-14). STA-ET1 did not have a statistically different sensitivity. Moreover copy number analysis of CHP-100 also showed gain of copy number (x3) of non-mutated BRCA1 which might explain its resistance to treatment with cisplatin.

5.4.10.3 SK-N-MC and STA-ET1 show sensitivity to treatment with olaparib

A673, CHP-100, SK-N-MC and STA-ET1 were next exposed to the PARP inhibitor, olaparib (LKT Laboratories) for 72 hours. It was anticipated that they would be more sensitive to olaparib due to the synthetic lethality with BRCA loss of function which may occur (Ashworth 2008). Although not statistically significant there was a trend towards SK-N-MC and STA-ET1 being more sensitive to treatment with the drug than A673 and CHP-100 which lack the BRCA1 mutation (Figure 5-15). However these data do not show significant cisplatin or olaparib sensitivity in Ewing sarcoma cell lines with associated BRCA mutations.

A

Gene location	Base change	Gene	Consequence	cDNA position	CDS position	Protein position	Amino Acid	Codon	Outcome	Effect
17:41246481	T/C	ENSG00000012048	Non Synonymous	1228	1067	356	Q/R	cAg/cGg	Deleterious	Possibly damaging
17:41246481	T/C	ENSG00000012048	Non Synonymous	1260	1067	356	Q/R	cAg/cGg	Deleterious	Probably damaging
17:41246481	T/C	ENSG00000012048	Non Synonymous	1102	989	330	Q/R	cAg/cGg	Deleterious	Probably damaging
17:41246481	T/C	ENSG00000012048	Non Synonymous	427	179	60	Q/R	cAg/cGg	Deleterious	Possibly damaging
17:41246481	T/C	ENSG00000012048	Non Synonymous	1261	1067	356	Q/R	cAg/cGg	Deleterious	Possibly damaging
17:41246481	T/C	ENSG00000012048	Non Synonymous	1186	1067	356	Q/R	cAg/cGg	Deleterious	Possibly damaging
17:41246481	T/C	ENSG00000012048	Non Synonymous	664	665	222	Q/R	cAg/cGg	Deleterious	Possibly damaging
17:41246481	T/C	ENSG00000012048	Non Synonymous	1207	179	60	Q/R	cAg/cGg	Deleterious	Possibly damaging
17:41246481	T/C	ENSG00000012048	Non Synonymous	1299	1067	356	Q/R	cAg/cGg	Deleterious	Possibly damaging
17:41246481	T/C	ENSG00000012048	Non Synonymous	1158	926	309	Q/R	cAg/cGg	Deleterious	Possibly damaging
17:41246481	T/C	ENSG00000012048	Non Synonymous	1299	1067	356	Q/R	cAg/cGg	Deleterious	Possibly damaging
17:41246481	T/C	ENSG00000012048	Non Synonymous	1299	1067	356	Q/R	cAg/cGg	Deleterious	Possibly damaging

B

Gene location	Base change	Gene	Consequence	cDNA position	CDS position	Protein position	Amino Acid	Codon	Outcome	Effect
17:41246481	T/C	ENSG00000012048	Non Synonymous	1228	1067	356	Q/R	cAg/cGg	Deleterious	Possibly damaging
17:41246481	T/C	ENSG00000012048	Non Synonymous	1260	1067	356	Q/R	cAg/cGg	Deleterious	Probably damaging
17:41246481	T/C	ENSG00000012048	Non Synonymous	1102	989	330	Q/R	cAg/cGg	Deleterious	Probably damaging
17:41246481	T/C	ENSG00000012048	Non Synonymous	427	179	60	Q/R	cAg/cGg	Deleterious	Possibly damaging
17:41246481	T/C	ENSG00000012048	Non Synonymous	1261	1067	356	Q/R	cAg/cGg	Deleterious	Possibly damaging
17:41246481	T/C	ENSG00000012048	Non Synonymous	1186	1067	356	Q/R	cAg/cGg	Deleterious	Possibly damaging
17:41246481	T/C	ENSG00000012048	Non Synonymous	664	665	222	Q/R	cAg/cGg	Deleterious	Possibly damaging
17:41246481	T/C	ENSG00000012048	Non Synonymous	1207	179	60	Q/R	cAg/cGg	Deleterious	Possibly damaging
17:41246481	T/C	ENSG00000012048	Non Synonymous	1299	1067	356	Q/R	cAg/cGg	Deleterious	Possibly damaging
17:41246481	T/C	ENSG00000012048	Non Synonymous	1158	926	309	Q/R	cAg/cGg	Deleterious	Possibly damaging
17:41246481	T/C	ENSG00000012048	Non Synonymous	1299	1067	356	Q/R	cAg/cGg	Deleterious	Possibly damaging
17:41246481	T/C	ENSG00000012048	Non Synonymous	1299	1067	356	Q/R	cAg/cGg	Deleterious	Possibly damaging

Table 5-8. SK-N-MC and STA-ET1 both harbour potentially harmful mutations of BRCA1. A search of whole exome sequencing data was performed to identify potential serious mutations in BRCA1. Benign mutations or those reported to be synonymous were excluded. The resultant mutations are listed above. **A** – SK-N-MC has a substitution of a T for a C resulting in an amino acid change from glutamine to arginine. This is deleterious and potentially damaging although not reported in the COSMIC database. **B** – STA-ET1 appears to have a similar substitution of base which also causes an amino acid change, from glutamine to arginine. The position of base substitution is limited to 5 common coding sequence (CDS) positions in the 2 cell lines.

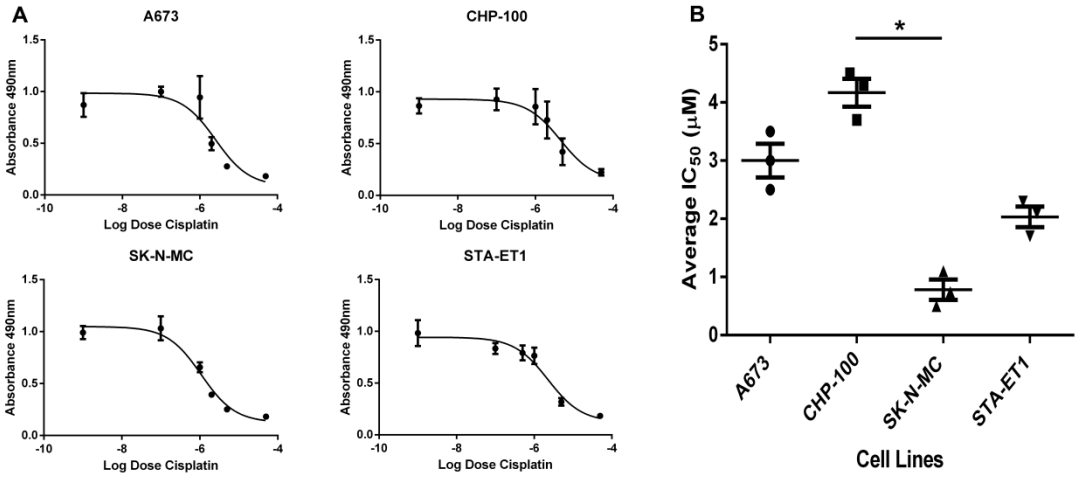


Figure 5-14. SK-N-MC and STA-ET1 demonstrated sensitivity to cisplatin. Cell lines were treated for 72 hours with cisplatin and analysed via MTS. **A** – representative dose (0-50μM) response curves for each cell line. **B** – average IC_{50} (μM) for each cell line (n=3). Comparison between the cell lines was made by the Kruskal-Wallis test with Dunn's post test to adjust for multiple comparisons. CHP-100 is significantly less sensitive to cisplatin than SK-N-MC. The error bars represent mean values ±SEM. * indicates $p<0.05$.

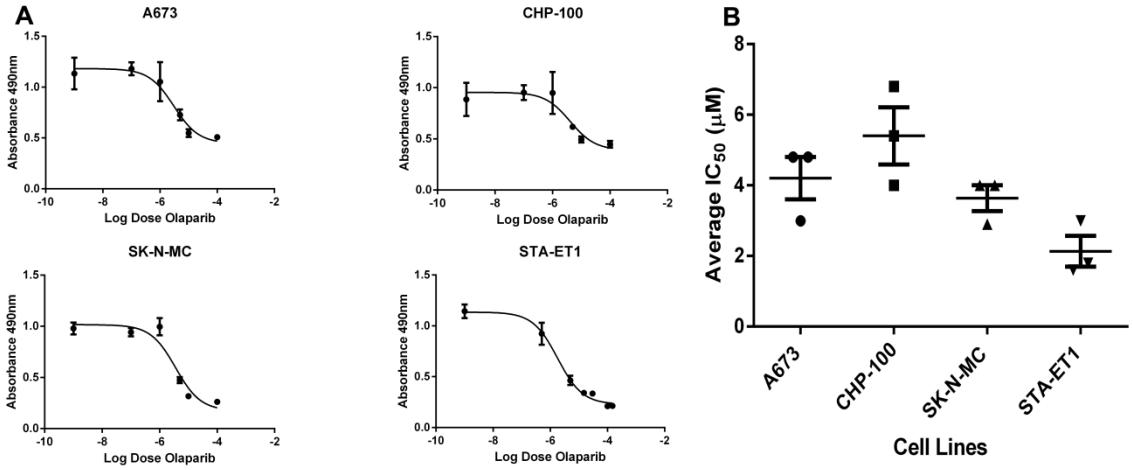


Figure 5-15. STA-ET1 shows increased sensitivity to the PARP inhibitor olaparib. Cell lines were treated with olaparib (0-100μM) for 72 hours and measured by MTS. **A** – Representative dose response curves from cell lines A673, CHP-100, SK-N-MC, STA-ET1 following 72 hours exposure to olaparib. **B** – average IC_{50} for each cell line (n=3). Comparison was made between cell lines with Kruskal-Wallis test but significance was not observed. Error bars indicate mean values ±SEM.

5.4.10.4 Ewing sarcoma cell lines are resistant to treatment with retinoic acid

Whole exome sequencing confirmed the presence of a homozygous mutation in retinol dehydrogenase 13 (all trans/9-cis) (RDH13) in A673 and CHP-100. This mutation, which is referenced on the COSMIC database (COSM51056) involves the substitution of a base resulting in a change of amino acid from asparagine to lysine. RDH13, a mitrochondrial enzyme distributed throughout the body (including skeletal muscle), is important in retinoic acid synthesis converting retinol to retinal (Belyaeva, Korkina et al. 2008). All trans retinoic acid, used as a treatment in acute promyelocytic leukaemia, is believed to induce differentiation and arrest proliferation (Tallman, Andersen et al. 2002). In the panel of cell lines tested with exogenous addition of all trans retinoic acid, no clear distinction was made between those cell lines known to have a mutation of RDH13 (A673 and CHP-100) and SK-N-MC and STA-ET1 which don't (Figure 5-16). Previous research has described a similar result in CHP-100 cells treated with retinoic acid, however when combined with 8-chlorocyclic-AMP a synergistic effect was observed and growth arrest and apoptosis reported (Srivastava, Srivastava et al. 1998).

5.4.10.5 Cell lines are resistant to effects of imatinib

Sequencing highlighted the presence of a substitution (A to C) resulting in an activating KIT M541L mutation (COSM28026) within exon 10 associated with sensitivity to imatinib in SK-N-MC (Gonçalves, Monges et al. 2006, Krüger, Emig et al. 2006, Saini, Jha et al. 2012). Cell lines were treated with imatinib and dose response analysed via MTS assay (Figure 5-17). None of the four cell lines showed a dose dependent response and this was confirmed on replicate experiments. SK-N-MC which had a KIT M541L mutation, observed in the general population, appeared to be unaffected by the presence of imatinib. M541L is in the transmembrane domain of KIT and doesn't cause activation of the receptor unlike W557 and K558 found in GISTs which are located in the juxtamembrane

region causing the receptor to dimerize, autophosphorylate and activate signalling in the absence of the ligand. Imitanib targets autophosphorylation of KIT which may explain why no response was seen in these experiments.

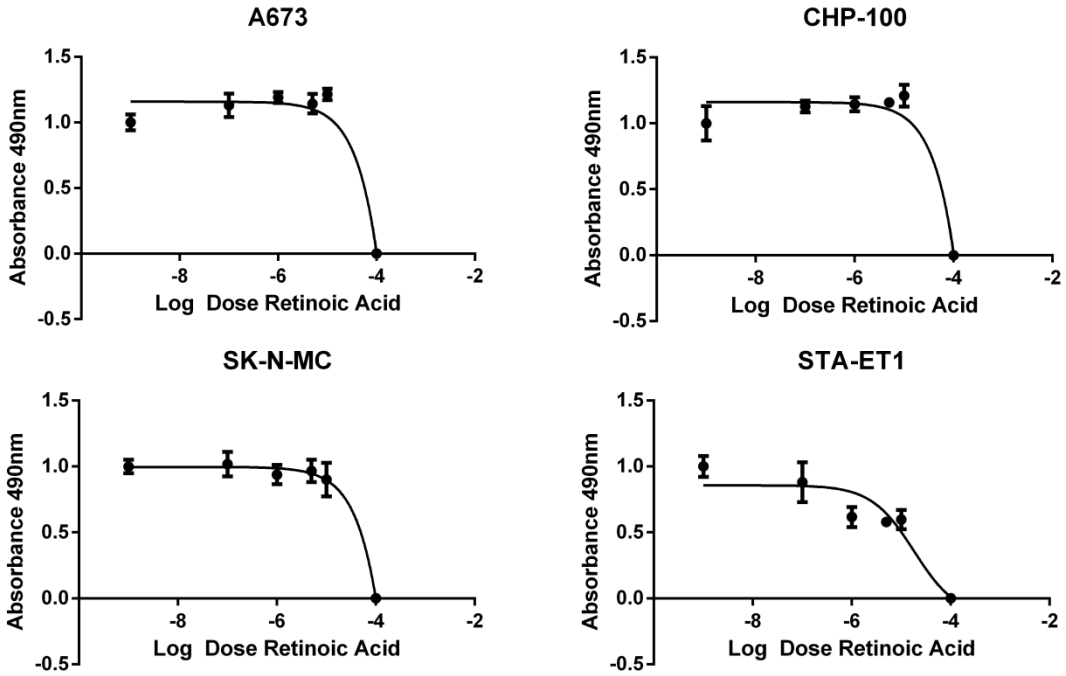


Figure 5-16. Ewing sarcoma cell lines appear to be resistant to exposure to retinoic acid. Cell lines were treated with retinoic acid for 72 hours before being analysed by MTS assay. A673 and CHP-100, both known to have a non-synonymous mutation of RDH13, appear to be resistant to the effects of retinoic acid except at the highest doses (100µM). SK-N-MC also shows resistance to treatment where as STA-ET1 is more responsive at doses above 10µM (n=3).

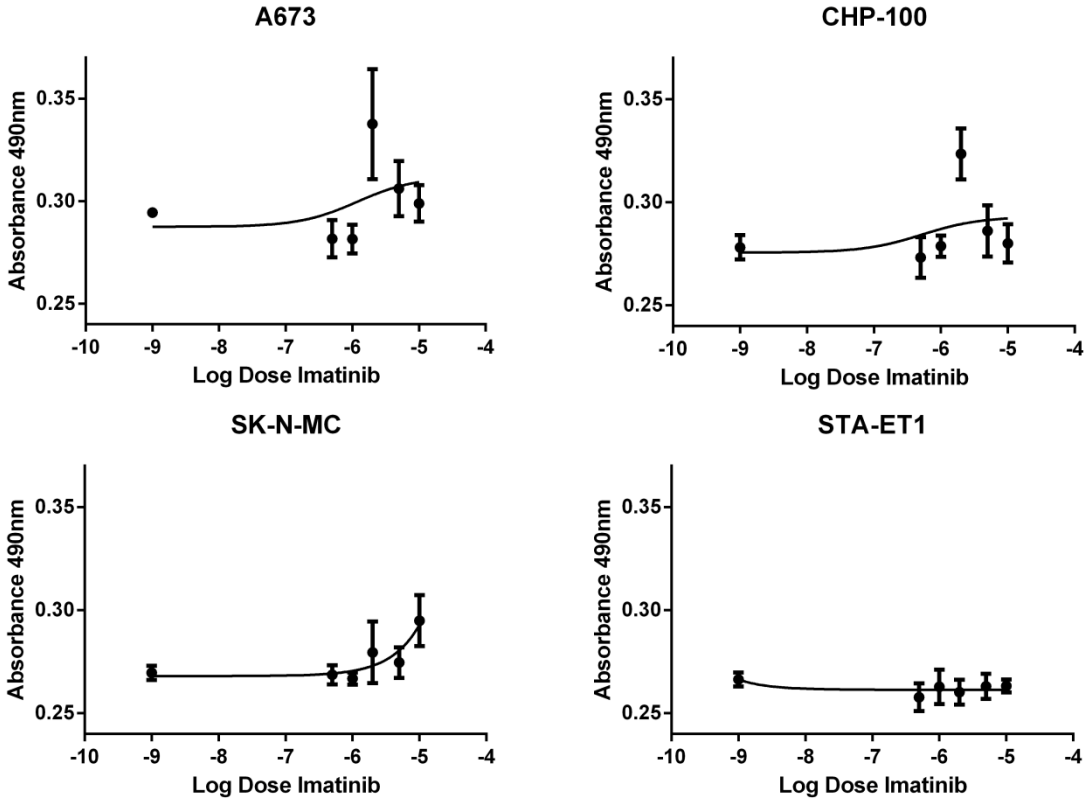


Figure 5-17. Ewing sarcoma cell lines are resistant to the effect of imatinib. Cell lines A673, CHP-100, SK-N-MC, STA-ET1 were exposed to imatinib (0-50μM) for 72 hours and viability measured by MTS. No dose response was seen and SK-N-MC, which has a KIT mutation, showed no variation in response in comparison with other cell lines. Representative graphs shown (n=3).

5.5 Discussion

The principle result of this chapter was the characterisation of whole genome abnormalities using RNA-seq, whole exome sequencing, and to provide detailed and complete genomic analysis of a panel of Ewing sarcoma cell lines. Based on the genomic findings, rationalised drug treatments were performed using common place chemotherapeutics with relatively little evidence of specific sensitivity or resistance associated with mutations identified. Notably, the presence of a chromosomal deletion was identified (RP11680G10.1-GSE1) and the characteristic EWS-ETS translocation confirmed in each cell line by RNA-seq with novel mutations were identified through whole exome sequencing and the spectrum of copy number alterations observed via aCGH.

5.5.1 Use of NGS in genomic analysis of Ewing sarcoma cell lines

Personalized therapy by identification and targeting of tumour-specific molecular abnormalities is rapidly becoming an important component in the management of cancer patients. Consequently, algorithms for tumour diagnosis necessitate not only morphological and immunophenotypic assessment but also molecular mutational profiling (Kanagal-Shamanna, Portier et al. 2013). Through NGS analysis in collaboration with OGT, this work has demonstrated that beyond the EWS-FLI1 translocation there appears significant genomic heterogeneity within Ewing sarcoma cell lines meaning that at least in cell lines NGS may influence therapeutic decisions. A limitation to this work was the lack of the germline DNA available for sequencing so the relevance of some findings cannot be confirmed.

5.5.2 RD-ES was not confirmed as a Ewing sarcoma cell line

Although obtained from the EuroBoNet cell bank in parallel with other Ewing sarcoma cell lines, RD-ES, which is reported to have initiated from an osseous primary Ewing

sarcoma of the humerus in a 19 year old male (ATCC, HTB-166™), did not have the expected documented genomic footprint when NGS was carried out. Most importantly the presence of the EWS-FLI1 translocation was absent and the suggestion that it was a neuroblastoma or osteosarcoma cell line was made from RNA-seq data. This was a surprise and has meant that previous experiments in this thesis have to be considered in a different light to the one originally anticipated. No osteosarcoma or neuroblastoma cell lines have been grown in our laboratory during the period of this research so it is unclear where this anomaly occurred.

5.5.3 RNA-seq reveals presence of RP11680G10.1-GSE1 fusion protein generated by intergenic deletion

RNA-seq demonstrated the presence of this novel deletion on chromosome 16 which has not been previously described. Predictions were that the expression of GSE1 may increase under the control of a new promoter (RP11680G10.1). qPCR data suggests that GSE1 expression is relatively consistent across the cell lines in comparison with STA-ET10 which was not found to have the fusion protein (Figure 5-7). It is presently unclear whether this finding is a novel result, an artefact of the NGS process, or has been acquired by cell lines grown in culture. Clarity on this will be provided as RNA-seq of Ewing sarcoma tumour tissue takes place.

It is well known that tumour cell lines can exhibit genomic drift, which, in combination with different growth conditions in different laboratories, may result in significant divergence between cell lines (Hughes, Marshall et al. 2007). Since genomic instability is probably the driving force behind generation of some fusion transcripts, it is plausible that the cells with the greatest genomic instability will also have the greatest number of fusion transcripts. Although cell lines were obtained from a centralised source, their duration in culture and passage number may have influenced the results which were detected. It is

therefore possible that many of the fusion transcripts which have been identified by this work and in others, may have arisen after isolation of the cell lines and may not reflect the fusion transcript profile that was obtained in the primary tumour from which the cells were initially isolated. If this hypothesis is correct, it would be expected that fewer fusion transcripts would be seen in primary tumour samples and via biopsies from the previously described EuroSarc LINES trial, allowing this theory to be validated in primary material from Ewing sarcoma tumours.

5.5.4 Etoposide sensitivity varies between cell lines

Etoposide is used as part of the recognised VDC-IE (vincristine, doxorubicin, and cyclophosphamide, alternating with ifosfamide and etoposide) and VIDE (EuroEwing 99) protocol for the treatment of Ewing sarcoma. As described resistance of A673 to treatment with the drug could not be related to the presence of a deletion on chromosome 16 so an alternative explanation was sought (Figure 5-8). Iida et al. recently published on the potential involvement of mir125b in resistance to chemotherapeutics in Ewing sarcoma cell lines (Iida, Fukushi et al. 2013). In this panel of cell lines, no mutation or copy number variation was identified for mir125b which could be attributed to A673 resistance so at present no actionable difference has been identified.

5.5.5 CDKN2A has a loss of copy number in most cell lines

The CDKN2A gene is a tumour suppressor that encodes the CDK4/6 inhibitor $p16^{ink4a}$. In all but one cell line tested (CHP-100) a loss of CDKN2A was observed resulting in a loss of the p16 gene. This is consistent with previous literature which describes a deletion in 62% of Ewing sarcoma cell lines screened (Mackintosh, Ordóñez et al. 2012). Particularly, loss or epigenetic silencing of CDKN2A is very common in cell lines, suggesting that the process of culture selects against the expression of $p16^{ink4a}$ (Witkiewicz, Knudsen et al. 2011). Approximately 10–15% of all primary Ewing tumours exhibit either homozygous

or hemizygous deletion of the CDKN2A gene and some analysis suggests a poor correlation with overall survival (Huang, Illei et al. 2005, Brownhill, Taylor et al. 2007, Mackintosh, Ordóñez et al. 2012).

The loss of $p16^{ink4a}$ has been suggested to facilitate aberrant cell cycle progression by relieving an important aspect of control (CDK4/6 inhibition) over G1/S progression through the retinoblastoma pathway (Witkiewicz, Knudsen et al. 2011). In the Ewing cell lines there is a gain in copy number (3 copies) of CDK4 in A673 and STA-ET1 which in the absence of CDKN2A could lead to further disruption of the cell cycle in these lines.

5.5.6 Ewing sarcoma cell lines are sensitive to PARP inhibitors

Through a large screen of cancer cell lines and 130 drugs (a total of 48,178 drug-cell line combinations recording cell viability) Garnett et al. recognised the potential role PARP inhibitors such as olaparib may have in Ewing sarcoma (Garnett, Edelman et al. 2012). They record the average IC_{50} as 4.7μM which is comparable with the results obtained from this study and relate their results to the presence of the transcriptional activity of the EWS-FLI1 translocation resulting in PARP sensitivity. Interestingly they did not observe BRCA1 mutations or evidence to indicate that DNA damage response is defective in Ewing sarcoma which conflicts with this work as SK-N-MC and STA-ET1 were both identified as having potentially serious BRCA1 mutations (Table 5-8).

5.5.7 Identification of potentially actionable mutations

Through RNA-seq a translocation between kinesin family member 1B (KIF1B) and connector enhancer of kinase suppressor of Ras 2 (CNKSR2) was identified which has not previously been identified in literature. In addition whole exome sequencing confirmed COSMIC annotated mutations in connector enhancer of kinase suppressor of Ras1 (CNKSR1) in A673. As it is known that the IGF pathway is an oncogenic driver in Ewing

sarcoma, the relationship between CNKSR and Ewing sarcoma cell lines will be interrogated in the following chapter and correlated with IGF pathway sensitivity.

6 Actionable target in Ewing sarcoma

6.1 Introduction

The previous chapter highlighted the presence of a chromosomal translocation in SK-N-MC which was recognised by RNA-seq. This novel translocation between kinesin family membrane 1B (KIF1B) and connector enhancer of kinase suppressor of Ras 2 (CNKSR2) has not previously been described in literature. Whole exome sequencing confirmed the presence of a mutation in connector enhancer of kinase suppressor of Ras 1 (CNKSR1) in A673. In view of the dependence of Ewing sarcoma on the insulin like growth factor pathway, further investigation of CNKSR was warranted as possible modifiers of the pathway.

6.2 Connector enhancer of kinase (CNK) suppressor of Ras

Kinase suppressor of Ras (KSR) is required for efficient signal transmission within the RAS/MAPK cascade. Therrien et al. through a screen of modifiers of KSR in *Drosophila melanogaster*, recognised a novel gene, connector enhancer of KSR (CNK), which functioned upstream or in parallel to RAF in the RAS pathway. They recognised that the protein which CNK encodes contains several protein–protein interaction domains, implying that it acts as a scaffold bringing together signalling molecules in receptor tyrosine kinase pathways by interactions with Raf (Therrien, Wong et al. 1998).

Members of the CNK family act as protein scaffolds regulating the selection of a signal input and determining the choice of downstream target. They enable Raf activation and have important function in the regulation of the Raf-MEK-ERK pathway by facilitating phosphorylation and activation of MEK by Raf and in turn activation of ERK by MEK (Dhillon and Kolch 2002). In more detail activation of a tyrosine kinase receptor triggers receptor dimerization and activation resulting in the recruitment of guanine nucleotide

exchange factors (GEFs) to the cell membrane which activate Ras small GTPases (H-Ras, N-Ras, K-Ras) (McCubrey, Steelman et al. 2007). Ras proteins function as a GDP/GTP-regulated switch, being active in the GTP-bound form and inactive in the GDP-bound form (Rajalingam, Schreck et al. 2007). GEFs promote formation of Ras-GTP by catalyzing the replacement of GDP with GTP, whereas GTPase-activating proteins (GAPs) stimulate GTP hydrolysis to GDP. Once activated Ras binds to a spectrum of downstream effector targets, including Raf, resulting in Raf serine/threonine kinases (A-Raf, B-Raf, and C-Raf) being recruited to the cell membrane and activated in a complex series of events including association with scaffolding proteins (McCubrey, Steelman et al. 2007). Raf proteins directly activate MEK1 and MEK2 through phosphorylation resulting in ERK translocation to the nucleus and the activation of transcription factors such as EGR1 by phosphorylation, thus altering the expression of specific genes. Moreover CNK1 has been shown to promote insulin signalling in cells. Knock down of CNK1 neither alters phosphorylation of the Insulin receptor (IR) nor the Insulin like growth factor-1 receptor (IGF-1R) however it does reduce phosphorylation of IRS1 and AKT along with downstream S6 (Lim, Zhou et al. 2010). Furthermore in CNK1 depleted cells, insulin mediated membrane recruitment of IRS1 (which initiates signalling through the PI3K pathway) is decreased. Lim et al. believe that the CNK1 scaffold facilitates insulin induced recruitment of cytohesins (Arf guanine nucleotide exchange factors) to the plasma membrane which generate a PIP_2 rich microenvironment required for IRS1/AKT signalling (Lim, Zhou et al. 2010). This has been enforced by Hafner et al. who described insulin resistance in the presence of a cytohesin inhibitor, SechinH3, in mice (Hafner, Schmitz et al. 2006) (Figure 6-1).

All three CNK family members, CNK1, CNK2A or Maguin-1 and the spliced form CNK2B/Maguin-2, (present in mammals) contain an α motif (SAM), a conserved region in

CNK domain and a PSD-985/DLG-1/ZO-1 (PDZ) domain (Yao, Hata et al. 1999) (Figure 6-2, Figure 6-3).

6.2.1 CNK2

The human neuron-specific isoform CNK2, which is almost exclusively found in neuronal tissues, contributes to nerve growth factor induced sustained activation of ERK. Bumeister et al. showed that with siRNA knockdown of CNK2, there was suppression of neurite outgrowth in phaeochromocytoma cells suggesting a role in neural differentiation (Bumeister, Rosse et al. 2004).

6.2.2 CNK1

Unlike CNK2, CNK1 is widely expressed primarily in epithelial tissues and has been observed to be cytosolic until stimulated whence it is recruited to the plasma membrane (Ziogas, Moelling et al. 2005). CNK1 binds to preactivated (by Ras) Raf-1 and activated Src forming a trimeric complex which results in Src-dependent tyrosine phosphorylation and activation of Raf-1. Knockdown of CNK1 results in VEGF dependent ERK stimulation, a pathway which is known to involve Src as an activator of Raf-1 suggesting that it is CNK1 which allows cross talk between Src and Raf-1 resulting in full activation (Alavi, Hood et al. 2003, Ziogas, Moelling et al. 2005).

CNK1, localised to the plasma membrane (ie activated) has been identified in invasive breast cancer compared with breast epithelial tissue suggesting that it promotes oncogenic signalling through AKT in breast cancer tumours (Fritz, Varga et al. 2010).

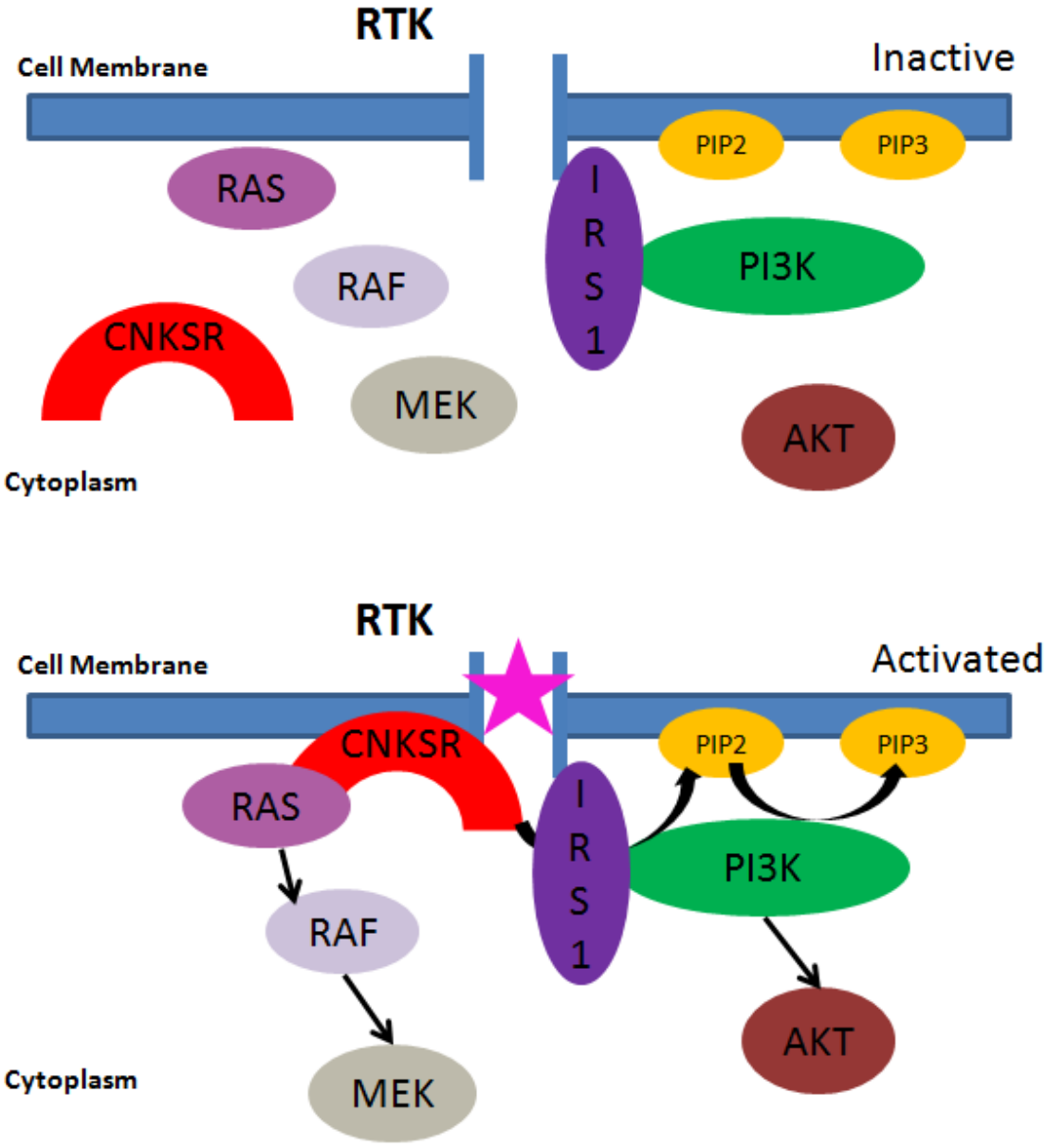


Figure 6-1. Schematic representation of CNK pathway. In the absence of RTH signals (top panel) CNK is cytosolic and maintains RAF in an inhibited state. Upon RTH activation (pink star denotes ligand binding) CNK moves to the membrane where it results in RAS activation leading to activity through RAF and MEK. In addition CNK helps activation of PIP2 through membrane recruitment of cytohesins (not shown). This results in activation of PI3K.

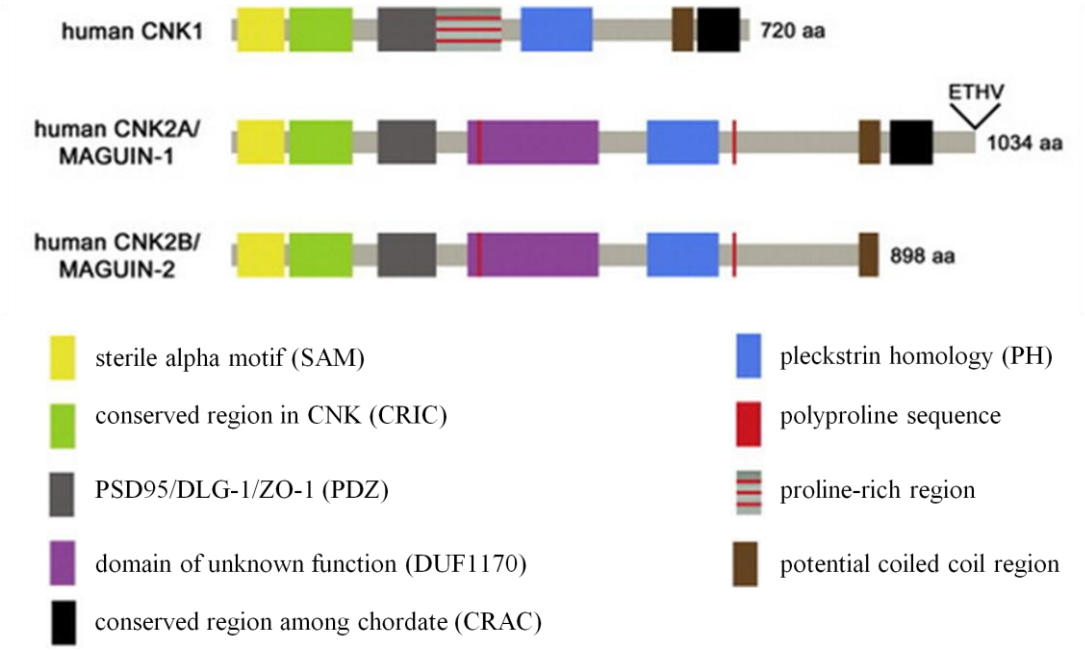


Figure 6-2. Schematic depiction of CNK proteins. CNK1 is found primarily in epithelial tissue, whereas CNK2A and the alternatively spliced CNK2B are found in neuronal tissues. The N-terminal part of CNK harbours a sterile alpha motif (SAM), a conserved region (CRIC) and a PSD95/DLG-1/ZO-1 (PDZ) domain. The C-terminal end of CNK consists of a pleckstrin homology (PH) domain and polyproline sequences. CNK1 has a unique proline-rich region which spans around 90 amino acids instead of a polyproline sequence. CNK2A and CNK2B contain an additional domain with unknown function (DUF1170). The conserved region among chordates (CRAC) domain interacts with coiled- coil motifs and associates with cytohesins. Numbers to the right indicate protein length in amino acids. Images based on illustration drawn by Fritz et al. (Fritz, Varga et al. 2010).

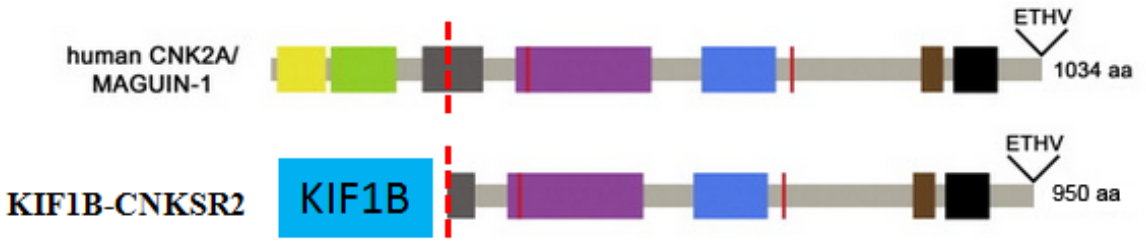


Figure 6-3. Schematic of KIF1B-CNKSR2 fusion protein as a result of the translocation identified in SK-N-MC. The PDZ domain in CNK2A protein (depicted above) has a break point at amino acid 228 (shown by red dashed line). This results in the loss of the SAM and CRIC domains (yellow and green boxes respectively). KIF1B, which has a role in transporting synaptic vesicles has a break point at amino acid 143 where it forms a fusion protein with CNKSR2.

6.3 Chapter Aims

As described above the CNK scaffolds are intimately linked to IR/IGF-1R signalling and downstream pathway activation in cancer cells. Ewing sarcoma is considered to have constitutively activated mitogen-activated protein kinase (MAPK) and phosphatidylinositol-3-kinase (PI3-K) signalling pathways (Benini, Manara et al. 2004). It could be predicted to be sensitive to alterations within, or allied to these pathways. As described previously RNA-seq identified a novel potentially active fusion protein which was in frame, between KIF1B and CNKSR2 in SK-N-MC. In addition, whole exome sequencing highlighted a non synonymous mutation of CNKSR1 in A673 which is reported in the COSMIC database. The aim of this chapter is to examine expression of CNK1 and 2 in a panel of Ewing sarcoma cell lines, to assess for the presence of a chromosomal translocation in patient samples and to ascertain whether they could be potentially actionable targets.

6.4 Methods

6.4.1 qPCR expression of CNKSR2 and CNKSR1

qPCR primers were designed firstly across the KIF1B-CNKSR2 fusion protein using Geneous and secondly for wild type CNKSR2 and CNKSR1 (with Roche Universal Probe Library Assay design centre) as previously described. cDNA template was used from 3 separate RNA extractions and RT-PCR. Standard curves were formulated.

6.4.2 RNA extraction and RT-PCR from FFPE fixed Ewing sarcoma patient tumours

Using TMAs obtained from EuroBoNet, 2-5mm diameter discs of individual patient's paraffin embedded tissue were lifted from slides using a separate sterile needle for each patient and placed in an eppendorf tube. RNA extraction was carried out using the Qiagen RNeasy FFPE kit with an initial xylene de-paraffinization step. The RNeasy FFPE Kit uses special lysis and incubation conditions to reverse formaldehyde modification of RNA. The lysis buffer releases RNA from FFPE tissue samples, preventing further RNA degradation. RNA extracted was measured by Nanodrop. Samples with an amount of RNA less than 2ng μl^{-1} were excluded and converted to cDNA (protocol as described previously). Following RT-PCR all samples were corrected to 2ng μl^{-1} and expression of CNKSR2 fusion protein analysed as described above.

Due to the low quantity of cDNA present C_q values were corrected to the lowest value and referenced against C_q values for STA-ET1 (as a negative control) and SK-N-MC (as a positive control) which were corrected to the same concentration and analysed alongside the patient samples.

6.4.3 siRNA knockdown CNKSR2

Initially a pilot experiment was performed to assess for efficiency of siRNA knockdown of CNKSR2 (FlexiTube siRNA Qiagen 1027417) and to ascertain an approximate time

course. A673, CHP-100, SK-N-MC and STA-ET1 were seeded in to 6 well plates at $1x10^5$ cells per ml in complete media (RPMI 1640, 10% FCS, 1% PS) and grown to 75-80% confluence. For each cell line wells were prepared for a non-transfected control, transfection of scrambled siRNA (Mission® SiRNA Universal Negative Control SIC001), and siRNA CNKSR2. When desired numbers of cells were obtained media was changed to RPMI containing 10% FCS.

Using Lipofectamine™ 2000, siRNA was transfected in to cells as per manufacturer's published protocol. In brief, 94pmol siRNA was diluted in 235µl Opti-Mem® and mixed gently. In parallel 4.7µl Lipofectamine™ 2000 was diluted in 235µl Opti-Mem® and left to incubate for 5 minutes. After incubation diluted siRNA and diluted Lipofectamine™ 2000 were combined and incubated for 20 minutes prior to addition of the total volume to each well. Cells were incubated for 24 and 48 hours before RNA extraction and RT-PCR performed as described previously.

6.4.4 Knockdown of CHP-100 and SK-N-MC with siRNA CNKSR2 and OSI-906 treatment

Once knockdown was confirmed as per the methods described above, two cell lines, CHP-100 and SK-N-MC were seeded in to 96 well plates ($1x10^4$ cells per well) and left for 24 hours in RPMI with 10% FCS (200µl per well). siRNA was prepared as per above with appropriate reduction in volume proportional to lesser surface area of wells. 4 hours post transfection, OSI-906 was added (dose range 0-10µM). After 72 hours plates were analysed via MTS assay.

6.4.5 Immunofluorescence of CNKSR1 and CNKSR2 on exposure to OSI-906

A modified version of the protocol described in Chapter 2 was used to immunolabel cells for CNKSR1 and CNKSR2 proteins. Cell lines were seeded on coverslips in 24 well plates at a density of $4x10^4$ cells per well in a volume of 500µl media and left for 24 hours to

adhere to the coverslip. Wells were then exposed to OSI-906 (1μM) or vehicle only control for 2 hours. Fixation was carried out with 4% paraformaldehyde in PBS and following permeabilisation and blocking, coverslips were incubated overnight with primary antibodies; CNKSR2 (rabbit polyclonal) (Sigma HPA001502) or CNKSR1 (rabbit polyclonal) (Sigma HPA030847) (1:100 dilution). The next day coverslips were washed and incubated for 2 hours with Alexa Fluor® 594 goat-anti-rabbit secondary antibody (1:300 dilution) followed by Phalloidin Alexa 488 and DAPI to define actin cytoskeleton and nucleus respectively. Coverslips were mounted with Prolong Gold Antifade and confocal images captured.

6.5 Results

6.5.1 Expression of CNKSR2 is elevated in cell line SK-N-MC

RNA-seq data confirmed the presence of a translocation between chromosome 1 and the X chromosome between KIF1B and CNKSR2. To validate expression of CNKSR2, qPCR was performed with primers designed to cross the fusion gene. Data showed a significant increase in expression of CNKSR2 in SK-N-MC, the cell line harbouring the translocation in comparison to the other lines. The qPCR product was clearly evident on an agarose gel (expected size 193bp) (Figure 6-4).

Expression of wild type CNKSR2 was also significantly elevated in SK-N-MC in comparison with all the other cell lines except for RM-82 (Figure 6-5). RM-82 lacks a fusion gene involving CNKSR2 and does not have a mutation of CNKSR2.

6.5.2 Expression of KIF1B-CNKSR2 fusion gene in samples from 62 patients, taken from 3 European cohorts

RNA was extracted from FFPE TMAs from Dusseldorf (25), Leiden (22), and Valencia (15) and expression of fusion gene KIF1B-CNKSR2 was measured via qPCR. STA-ET1, known to not contain the fusion gene and SK-N-MC known from RNA-seq to harbour the fusion were used as negative and positive controls respectively. Patient 16 from the Dusseldorf cohort appears to show the highest expression of the fusion protein. Although this was equivalent to expression levels seen in the cell line STA-ET1 (negative control) and not as high as expression in SK-N-MC (positive for the fusion) it warranted further investigation (Figure 6-6). Sanger sequencing confirmed the presence of the KIF1B-CNKSR2 fusion in the patient sample (Figure 6-7).

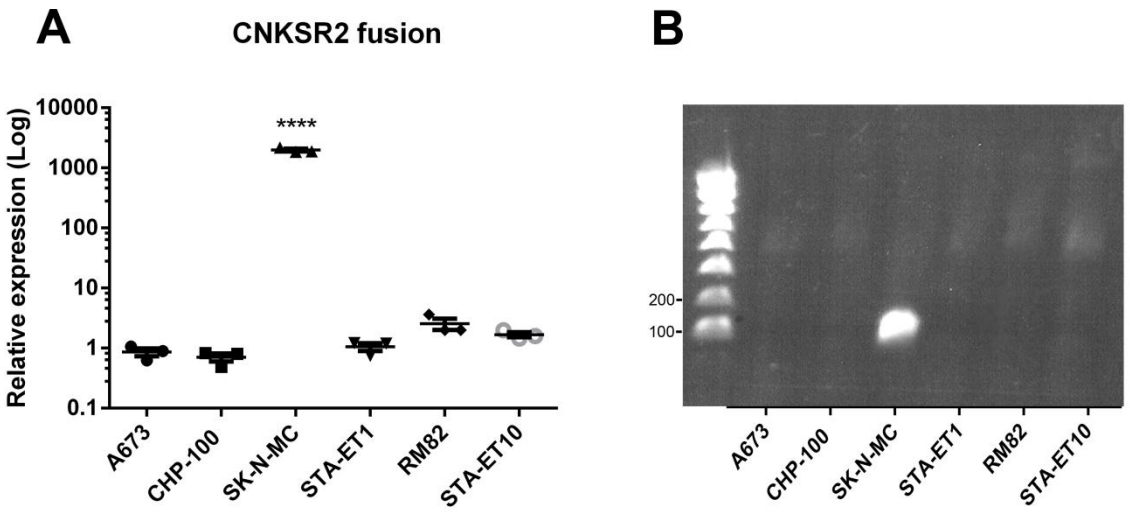


Figure 6-4. Expression of CNKSR2 is elevated in SK-N-MC which harbours a translocation of KIF1B-CNKSR2. **A -** Primers designed across the fusion of KIF1B and CNKSR2 confirmed translocation specific elevation of expression of CNKSR2 in cell line SK-N-MC. **B** – qPCR product of **A** run on 1% agarose gel confirms the absence of the KIF1B-CNKSR2 translocation in cell lines except SK-N-MC. Expected product size 193bp. Statistical comparison between cell lines was performed using one-way ANOVA with Tukey's post test. **** represents $p < 0.0001$. Error bars indicate ±SEM.

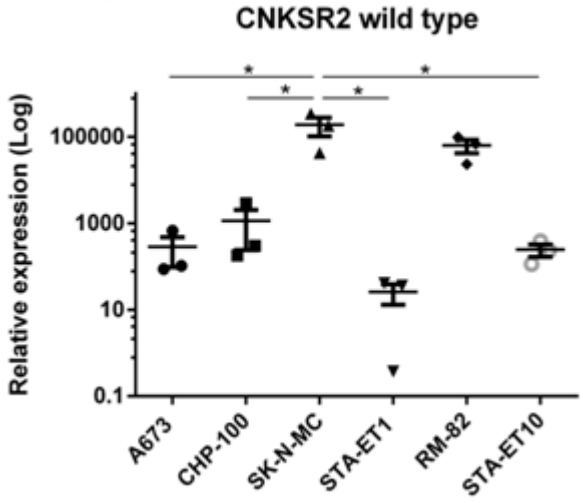


Figure 6-5. CNKSR2 gene expression is elevated in SK-N-MC . Wild type CNKSR2 expression was significantly elevated in SK-N-MC when compared to other cell lines except RM-82. Statistical comparison between cell lines was performed by one-way ANOVA with Tukey's post test to adjust for multiple comparisons. * represents $p<0.05$. Error bars indicate ±SEM.

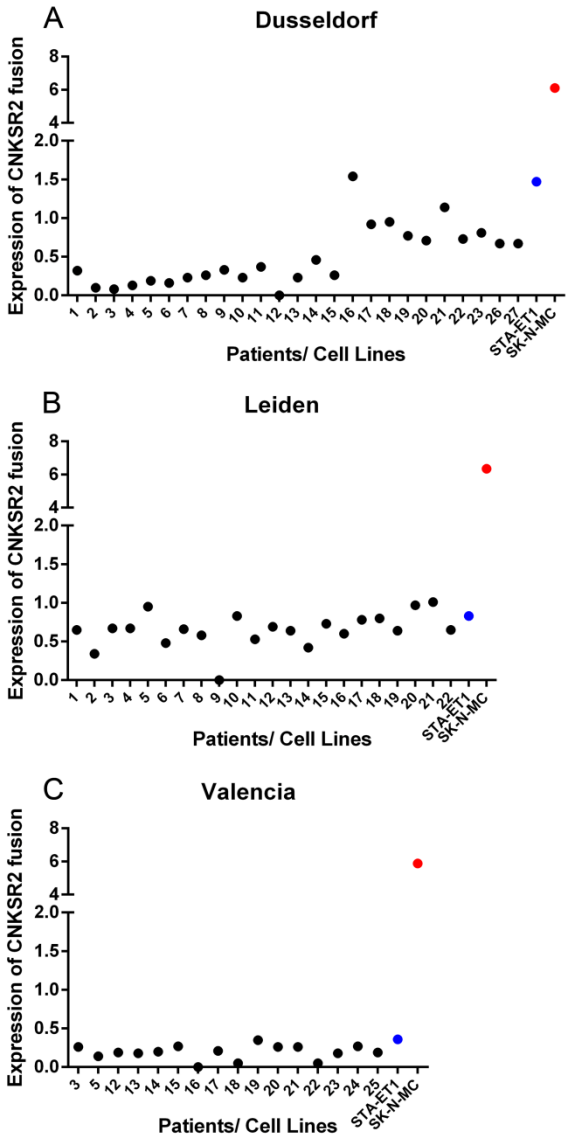


Figure 6-6. Expression of KIF1B-CNKSR2 fusion gene is analysed in patient sample from three European centres. RNA was extracted from FFPE embedded TMAs and RT-PCR performed. Expression of CNKSR2 was measured using primers designed to span the KIF1B-CNKSR2 fusion. 25 samples from Dusseldorf, 22 from Leiden, and 15 from Valencia were corrected to 2ng μl^{-1} and expression measured. STA-ET1 (blue dot) and SK-N-MC (red dot) were used to indicate negative and positive expression based on previous cell line experiments.

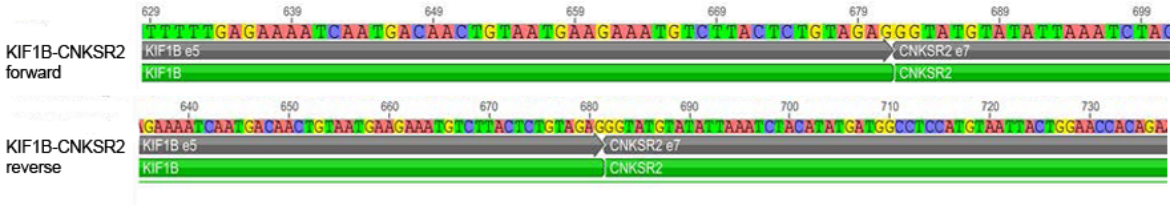


Figure 6-7. Sanger sequencing confirms the presence of the KIF1B-CNKSR2 translocation in a patient sample. DNA of sample 16 from the Dusseldorf cohort was sent for Sanger sequencing which confirmed the presence of the fusion gene between exon 5 of KIF1B and exon 7 of CNKSR2.

6.5.3 Calculation of siRNA knockdown using qPCR analysis

In the RNAi knockdown experiment expression of the siRNA–treated CNKSR2 (Gene ID 22866) target gene (TAR) was normalized to the non-targeted GAPDH reference gene (REF) expression levels within the same sample to determine ΔC_q (Step 1). This served to correct for non-treatment related variation. The C_q was exponentially transformed to ΔC_q expression (Step 2) and then normalised to the expression of CNKSR2 (TAR) from a separate well treated with non-targeting siRNA to find $\Delta\Delta C_q$ expression (Step 3). This accounted for any effects associated with the experimental procedure and was expressed as the ratio of the ΔC_q expression to the non-targeted ΔC_q expression.

Percent knockdown (KD) was calculated by subtracting the normalized $\Delta\Delta C_q$ expression and multiplying by 100 (Step 4). Table 6-1 illustrates the method of calculating KD in SKNMC cells exposed to siRNA targeted against CNKSR2 for 24 hours. Here 94.9% knockdown was illustrated.

6.5.4 siRNA knockdown of CNKSR2 was optimal at 24 hours

Percentage KD was similarly measured for all cell lines at two time points (24 and 48 hours) with the most effective KD occurring at 24 hours. STA-ET1 is resistant to siRNA knockdown at the conditions tested so was excluded from further experiments. SK-N-MC has 94.9% knockdown at 24 hours which is reduced to 36.9% at 48 hours. Similarly A673 (87.1% to 17.1%) and CHP-100 (91.5% vs 4.1%) showed a more notable knockdown at 24 versus 48 hours.

A

	Given Values		Step 1	Step 2	Step 3	Step 4
	$C_{q(REF)}$	$C_{q(TAR)}$	$C_{q(TAR)-(REF)}$	ΔC_q Expression	$\Delta\Delta C_q$	% KD
Non –targeting Control	14.32	20.32	6	0.015625	1	-
TAR_{CNKSR2}	13.03	23.32	10.29	0.000799	0.05	94.9

B

	% Knockdown in cell lines			
	A673	CHP-100	SK-N-MC	STA-ET1
24 Hours	87.1	91.5	94.9	n/a
48 Hours	17.1	4.1	36.3	2.73

Table 6-1. siRNA knockdown of CNKSR2 is most abundant at 24 hours. Cell lines A673, CHP-100, SK-N-MC and STA-ET1 were treated with siRNA to CNKSR2 and a scrambled control for 24 and 48 hours. RNA was extracted and analysed by qPCR against a housekeeping gene, GAPDH. **A** – breakdown of $\Delta\Delta C_q$ analysis of knockdown **B** – C_q values analysed as per A and percentage knockdown calculated relative to non –targeting control.

6.5.5 Sensitivity of SK-N-MC to OSI-906 is reduced with siRNA knockdown of CNKSR2

CNKSR2 functions in nerve growth factor induced sustained stimulation of ERK leading to neuronal differentiation (Bumeister, Rosse et al. 2004). Here, experiments showed that siRNA directed against CNK2 caused a 4.5 fold decrease in the IC_{50} of OSI-906 rendering the cells even more sensitive to the effects of the drug.

6.5.6 Knockdown of CHP-100 infers increased resistance to OSI-906

Whole exome and RNA-seq have shown that CHP-100 has the wild type CNKSR2 gene. Under normal conditions it would be expected that CNKSR interacts with Raf kinases, functioning as a scaffold for the Raf-MAPK cascade promoting proliferation and differentiation and to supply PIP_2 which is a substrate of PI3K (Fritz, Varga et al. 2010) (Figure 6-1). In the presence of OSI-906, a dual kinase inhibitor of the IGF-1R and IR receptor, it has been confirmed through earlier work in this thesis that cells show a decrease in proliferation, increase in apoptosis and decrease in viability in a dose dependent manner. When CNKSR2 is inhibited, the IC_{50} of CHP-100 in response to OSI-906 increases, implying that the cells become more resistant to the effects of OSI-906 and that CNKSR2 modifies this sensitivity (Figure 6-8). The hypothesis is that in knocked down cells, there is a decrease in the activity of the scaffold protein CNKSR, resulting in less PIP_2 activation which is required for normal PI3K signalling. OSI-906, which inhibits IGF-1R and IR, is rendered less effective as cells are not reliant on usual signalling pathways initiated by activation of IGF-1R or IR.

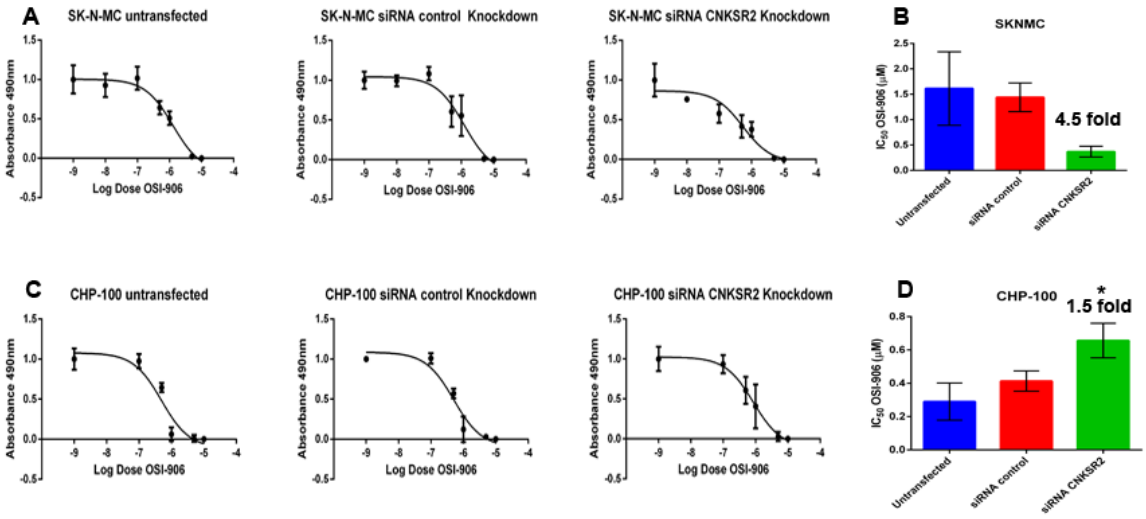


Figure 6-8. Knockdown of CNKSR2 confers 4.5 fold increase in sensitivity to OSI-906 in SK-N-MC and a decrease of 1.5 fold in CHP-100. SK-N-MC and CHP-100, transfected with siRNA CNKSR2, were exposed for 72 hours to OSI-906 and analysed by MTS assay. **A** and **B** – SK-N-MC showed an increase in sensitivity to OSI-906 with a 4.5 fold reduction in IC_{50}. **C** and **D** – CHP-100 showed an significant increase in IC_{50} on exposure to OSI-906 of 1.5 times the basal level suggesting increased resistance to the drug. Representative graphs (**A** and **C**) of MTS analysis are shown with untransfected, siRNA control transfection, and siRNA CNKSR2 knockdown plotted. Bar charts (**B** and **D**) illustrating fold change in IC_{50} from data shown. Fold change calculated as an average from three separate experiments. Statistical comparison was made by two-way ANOVA. (* represents $p<0.05$). Error bars ±SEM.

6.5.7 CNKSR1 is elevated in A673, CHP-100, and RM-82

Expression of CNKSR1 was quantified in cell lines. Through whole exome sequencing it was known that A673 has a COSMIC annotated mutation of CNKSR1. A673 has a substitution resulting in an amino acid change from Histidine to Asparagine (COSM30503). No mutations of CNKSR1 were found to be present in CHP-100 or RM-82. Review of copy number variation did not show a gain in copies of CNKSR1 (chromosome 1) so elevated expression may be related to an associated pathway yet to be identified (Figure 6-9).

6.5.8 CNKSR1 localises to the cytoplasm and CNKSR2 to the nucleus shown by immunofluorescence

CNK1 is localised in the cytoplasm until activated when it is recruited to the plasma membrane (Lim, Zhou et al. 2010). Cell lines were assessed for base levels of CNKSR1 by immunofluorescence and confocal microscopy. Cytoplasmic expression was observed in each cell line. Conversely, CNKSR2 appeared to be located to the nucleus in its distribution (Figure 6-10, Figure 6-11).

Comparison of nuclear to cytoplasmic ratio was made in cell lines with and without treatment with OSI-906 (Figure 6-12). No significant difference in localisation of CNKSR1 or CNKSR2 was found on exposure to OSI-906. A673, which is known to have a mutation of CNKSR1 did not show a change in localisation on exposure to OSI-906. This was a similar result to CHP-100, SK-N-MC and STA-ET1 all of which are CNKSR1 wild type. SK-N-MC which harbours the KIF1B-CNKSR2 translocation previously shown to have increased expression of CNKSR2 (Figure 6-4, Figure 6-5) did not show a change in cellular localisation of CNKSR2 on exposure to OSI-906. Although not significant, STA-ET1 appeared to have more nuclear localisation of CNKSR2 on exposure to OSI-906. This would correlate with a hypothesis that inhibition of IGF-1R/IR by OSI-906 does

prevent activity at the tyrosine kinase receptor and hence CNKSR2 is not recruited to the cell surface. A converse observation was made in A673 with cells appearing to have more cytoplasmic expression of CNKSR2 on exposure to OSI-906.

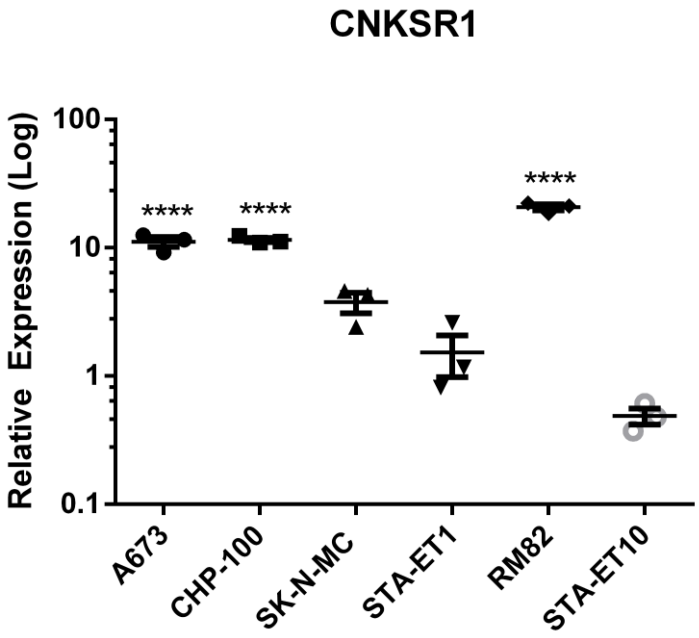


Figure 6-9. CNKSR1 expression is elevated in A673, CHP-100 and RM-82. qPCR was used to measure expression of CNKSR1 in Ewing sarcoma cell lines. All were referenced to two housekeeping genes (GAPDH and HPRT). A significant increase in expression of A673, CHP-100 and RM-82 was observed. A673 has a non-synonymous mutation of CNKSR1 found on whole exome sequencing (**** represents p<00001). Statistical comparison between cell lines was made using one-way ANOVA and Tukey's post test analysis for multiple comparisons. Error bars represent ±SEM. Three experimental replicates were performed.

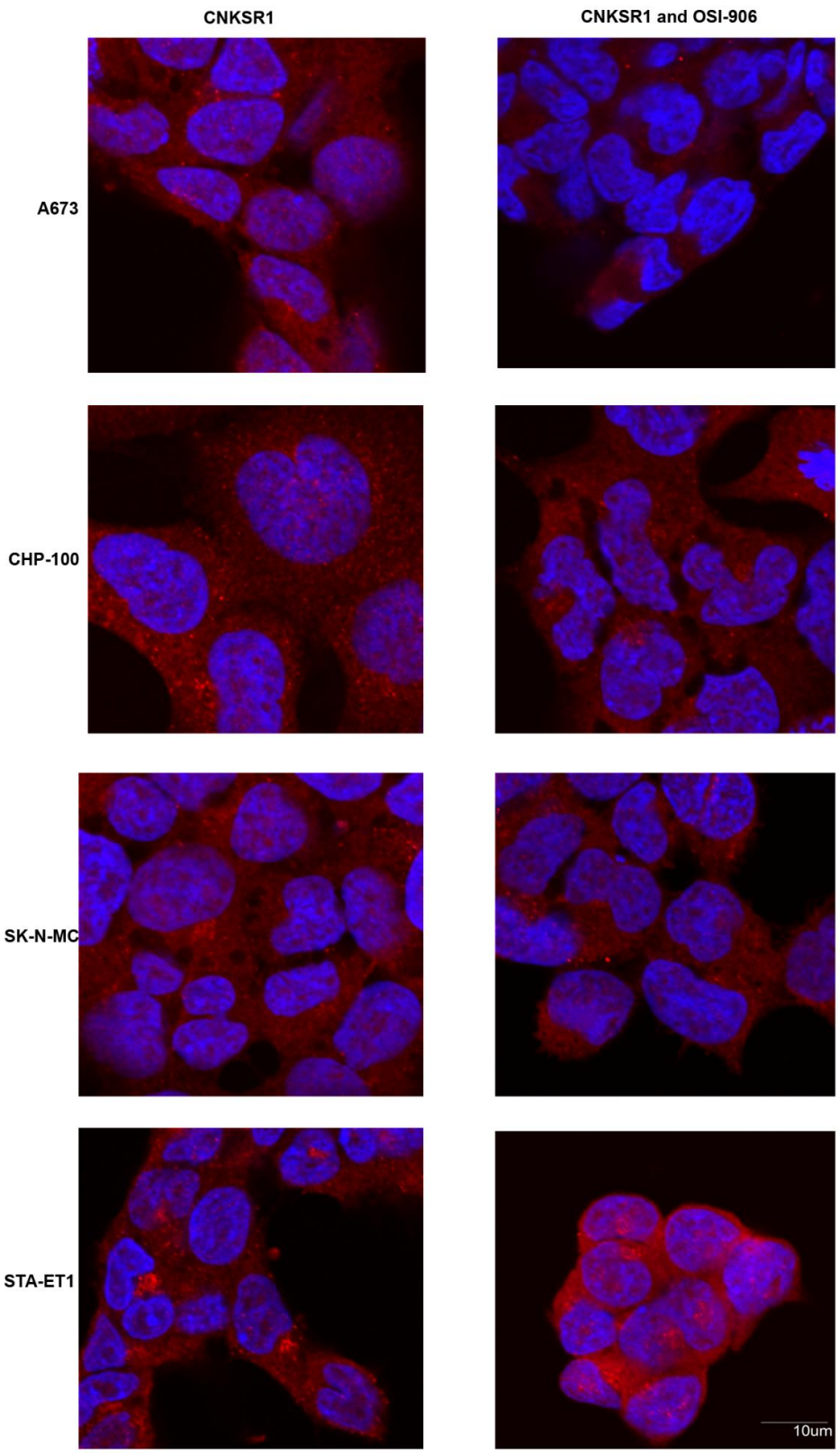


Figure 6-10. Representative confocal microscopy images showing cytoplasmic CNKSR1 with and without treatment with OSI-906 in Ewing sarcoma cell lines. Left column, CNKSR1 staining of cell lines (red) and DAPI the nuclei (blue). Right column shows response to 1 hour treatment with OSI-906.

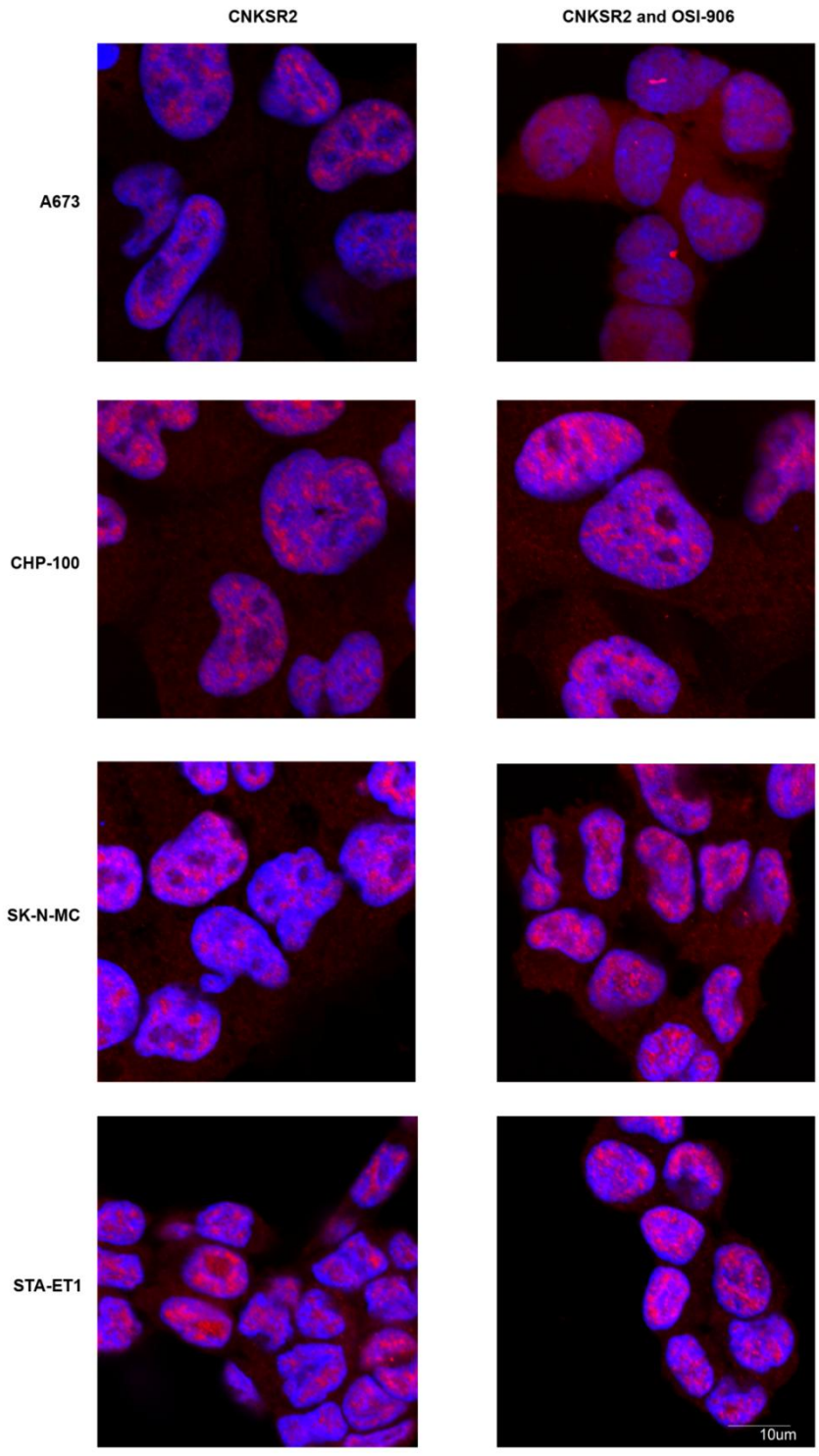


Figure 6-11. CNKSR2 shows nuclear localisation in Ewing sarcoma cell lines. Cell lines were labelled with CNKSR2 (red) and DAPI (blue) and imaged using confocal microscopy. Untreated cells (left column) showed nuclear localisation of CNKSR2. When treated with OSI-906, A673 and SK-N-MC appear to have an increase in cytoplasmic localisation.

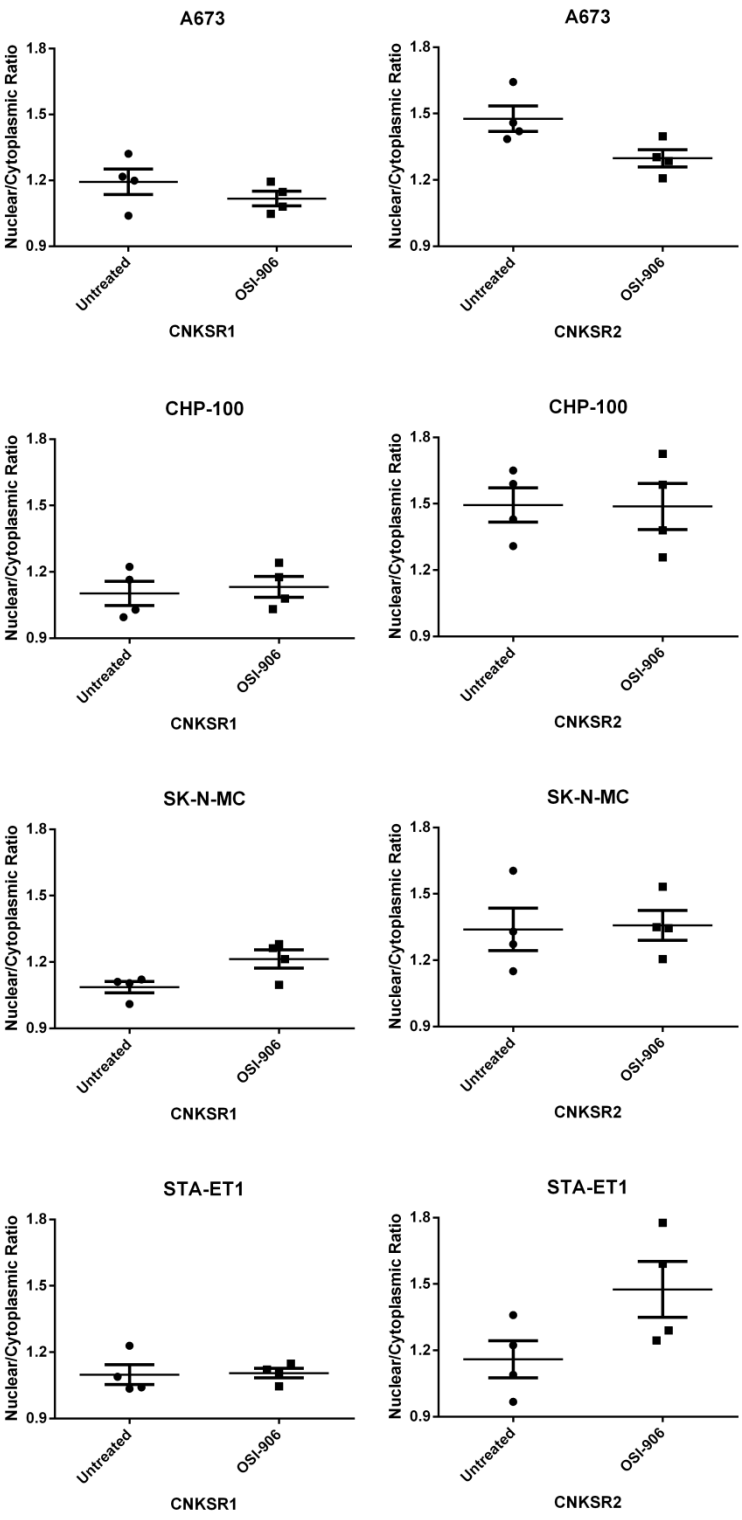


Figure 6-12. Cellular localisation of CNKSR1 and CNKSR2 in response to OSI-906 in Ewing sarcoma cell lines. Using confocal software (FV10-ASW 3.0 viewer) nuclear to cytoplasmic ratio was calculated in 4 Ewing sarcoma cell lines. Three separate measurements of nuclear and corresponding cytoplasmic localisation of CNKSR1 and CNKSR2 were taken for each group of treated and OSI-906 exposed cells. No significant difference was noted (Mann-Whitney statistical test) in localisation however STA-ET1 appears to have more nuclear expression of CNKSR2 on OSI-906 exposure compared with untreated cells. Error bars represent ±SEM.

6.6 Discussion

In this chapter the role of CNK in Ewing sarcoma cell lines is further explored. RNA-Seq and whole exome sequencing highlighted this family of genes which could be considered as potential actionable targets in Ewing sarcoma in view of their emerging intrinsic involvement in the IGF pathway.

6.6.1 CNKSR1 is expressed in Ewing sarcoma cell lines

Although the primary focus of the chapter has been on the effects of CNKSR2 in cell lines CNKSR1 expression has also been recognised to be elevated in A673, CHP-100, and RM-82. A673 is known to have a non-synonymous mutation of the gene but CHP-100 and RM-82 have no mutation noted on whole exome sequencing data. In agreement with other published research the localisation of CNKSR1 appears to be cytoplasmic (Lim, Zhou et al. 2010). CNK1 has been shown to accumulate at the cell functioning as a scaffold for cytohesins, moderating changes in the plasma membrane lipid environment and resulting in activation of the PI3K/AKT cascade (Lim, Zhou et al. 2010). Further experimentation is required to assess the effect of IGF-2 activation of the cell lines to confirm whether localisation changes to the plasma membrane is as expected in its role as a scaffold involved in insulin pathway signalling via AKT (Fritz, Varga et al. 2010).

6.6.2 CNKSR2 may act as a lineage survival factor in SK-N-MC

Scaffold proteins play important roles in MAPK signalling cascade by interacting with MAPK pathway components to form functional signalling molecules that control the specificity of signal transduction. CNKSR2 acts similarly to CNKSR1 mediating PI3K pathway as well as the RAF-MEK-ERK (Liu, Channavajhala et al. 2009).

Earlier experiments have shown that SK-N-MC contains a translocation, KIF1B-CNKSR2, which it is assumed results in elevated expression of CNKSR2. Inhibition of the fusion

gene and endogenous CNKSR2 gene through siRNA knockdown showed an increased sensitivity to OSI-906. This could suggest a dominant negative effect of the fusion gene resulting in relative resistance of SK-N-MC to OSI-906 and that the dependency of the cell line is reliant on an activated form of the gene for maintenance of the growth phenotype. Smolen et al. showed that in gastric cancer cell lines, which have an amplification of MET (a receptor tyrosine kinase), there is constitutive activation of the receptor, driving proliferative and survival signals. On inhibition with a specific tyrosine kinase inhibitor, extensive apoptosis was observed which was not seen in cell lines with unaltered copy number (Smolen, Sordella et al. 2006).

From 62 patients, RNA was extracted from TMAs and expression of KIF1B-CNKSR2 measured by qPCR. Only one of the samples tested from three European centres appeared to potentially express the translocation identified in SK-N-MC. This result was verified by Sanger sequencing and presence of the fusion gene was confirmed. Although this implies that the translocation is present in a human cohort, further clarification of this is required to confirm the result simply wasn't one of experimental contamination. Nevertheless, the high expression of CNKSR2 in SK-N-MC could be useful for unravelling the function of CNK in the future.

Although too early to confirm with this work alone, in this cell line it could be hypothesised that lineage-survival is evoked by CNKSR2 explaining the increase in sensitivity.

CNKSR2 is reported to be found primarily in neuronal tissues (Lanigan, Liu et al. 2003) and this work has confirmed its presence in Ewing sarcoma cell lines. This is not entirely a surprise as although it is believed that Ewing sarcoma is derived from mesenchymal cells, it has been shown to have some evidence of neuronal differentiation due to expression of neuronal markers (Lizard-Nacol, Lizard et al. 1989). CHP-100, which is wildtype for

CNKSR2, demonstrates an increase in resistance to treatment with OSI-906. This could be due to a decrease in PIP_2 production as previously described resulting in less PI3K/MAPK pathway activation, or it may be that the cell line switches reliance for survival onto another, as yet unidentified pathway.

6.6.3 Summary

Although too early to confirm with this work alone, CNKSR1 and CNKSR2 could have an important and previously unidentified role in Ewing sarcoma. Further work to elicit the dependency of Ewing sarcoma cell lines on CNK would be to "knock in" CNKSR2 following knockdown to see if the phenotype can be rescued. With OSI-906 (Linsitinib) in the upcoming clinical trial, the access to whole exome sequencing, and the ability to perform further mechanistic studies on patient samples, it will possible to further exploit the role of CNKSRs through an integrated genomics approach.

7 Use of N-ethyl-N-nitrosourea (ENU) mutagenesis to identify potential mechanisms of resistance to OSI-906

7.1 Introduction

Resistance to a tyrosine kinase inhibitor (TKI) can occur via direct mutation of the target. In those with chronic myeloid leukaemia (CML) point mutations within the kinase domain of BCR-ABL impair imatinib binding and are found in 50-90% of patients following imatinib treatment (Gorre, Mohammed et al. 2001, Shah, Nicoll et al. 2002). In CML, this has prompted the development of novel ATP-competitive small molecule tyrosine kinase inhibitors with activity against the observed mutants (Shah, Tran et al. 2004, Weisberg, Manley et al. 2005). Similarly, gastro-intestinal stromal tumours (GISTs) treated with imatinib which selectively blocks the activation of c-Kit, present as a gain of function mutation in up to 90% of GISTs, can also develop an acquired secondary c-Kit mutation resulting in imatinib resistance (Hirota, Isozaki et al. 1998, Antonescu, Besmer et al. 2005).

Sharma et al. identified a more complex mechanism which conferred stable resistance to cancer drugs and the presence of a metastable drug tolerant state involving reversible drug tolerant cells (Sharma, Lee et al. 2010). They exposed PC9, a lung adenocarcinoma cell line with an activating epidermal growth factor receptor (EGFR) mutation to erlotinib, an EGFR inhibitor. They analysed gene expression profiles of the parent cell line and of drug tolerant persisters (cells which survived drug treatment) and expanded persisters (drug tolerant cells which re-grew in the presence of erlotinib). A highly non random distribution of differentially expressed genes along chromosomes was observed which showed chromatin alterations in the drug tolerant persister population. The KDM5A gene, which encodes for histone demethylase, was elevated in expression in both the drug tolerant and expanded persisters. This appeared to be critical for acquiring the resistance phenotype as

knockdown of KDM5A reduced the generation of drug tolerant and expanded persisters from the parent cell lines. In addition, treatment with an inhibitor of histone deacetylases resulted in rapid death of the drug tolerant and expanded persisters but not of the parental cell line. They then went on to combine erlotinib with an IGF-1R inhibitor (AEW541) which prevented the re-emergence of drug tolerant expanding persisters presumed to be via reduction in KDM5A expression thereby linking the inhibition of histone deacetylase to reversible drug resistance. Ultimately their work showed that reversible drug tolerance appears to be have dynamic heterogeneity within a cancer cell population which can be established following the clonal expansion of single drug-sensitive cells and suggest that IGF-1R enables populations to maintain viability despite high drug exposure.

Screens have also been performed to look at resistance mechanisms which occur following IGF-1R inhibition. Pavlicek et al. used a combination of *in vitro* screens and extensive molecular profiling to attempt to identify biomarkers of sensitivity and resistance to figitumumab, an monoclonal antibody inhibitor of IGF-1R in a panel of 93 cancer cell lines (Pavlicek, Lira et al. 2013). They recorded correlations between copy number variation and figitumumab sensitivity revealing that components of the IGF pathway, including IRS2 (insulin receptor substrate 2) and IGFBP5 (insulin-like growth factor-binding protein 5), played a role in determining the sensitivity of cell lines to the drug. To identify potential resistance mechanisms to OSI-906, Pitts et al. performed gene array and pathway enrichment analysis along with shRNA knockdown of highly ranked genes in colorectal cell lines found to be most and least sensitive to OSI-906. This revealed that the RAS/RAF/MAPK signalling pathway was one of the top enriched pathways in the colorectal cancer cell lines which were resistant to OSI-906 (Pitts, Tan et al. 2010).

Although it is hoped that treatment with OSI-906 in the LINES trial is successful in some patients, it is likely that resistance to therapy may occur over time in others. Thus the

objective is to identify modifiers of the response to OSI-906 in order to evaluate potential resistance and sensitivity variants. In anticipation of this, *in vitro* work has commenced developing an ENU mutagenesis screen to identify potential mutations which confer drug resistance allowing for a rational approach to resistance mechanisms.

7.1.1 Methods to generate resistant mutations

Using random chemical mutagenesis as a screen for resistance requires the generation of point mutations whereby nucleotides are substituted, inserted or deleted at a rate which is not detrimental to a cell's protein function or viability. Methods used for generating point mutations include chemical mutagens (usually alkylating agents or azides) (Bradeen, Eide et al. 2006), PCR methods (DNA shuffling or error-prone PCR) (Cadwell and Joyce 1992) or through the use of mutator strains (such as *E.coli* XL1-red) (Muteeb and Sen 2010).

Two main methods have been used *in vitro* to generate resistant mutation profiles. The first of these, saturation mutagenesis, aims to generate all mutations at a specific site, or narrow region of a gene. Azam et al. applied this to CML and randomly mutagenized the *BCR-ABL* plasmid by propagation in a bacterial strain. They then transduced BaF3 cells and grew them in the presence of imatinib. Colonies formed from cells carrying *BCR-ABL* cDNAs which expressed drug-resistant variants and genomic DNA isolated and sequenced to identify mutants (Azam, Latek et al. 2003). The disadvantage with this method was that only the BCR-ABL mutations are recovered so there is limited information of alternative resistance mechanisms which may be active. Alternatively, Von Bubnoff et al. isolated resistant clones from BaF3-p185$^{BCR-ABL}$ cells grown in the presence of imatinib in a cell based screen. This allowed for BCR-ABL dependent and independent mechanisms of resistance to be identified but at the cost of being relatively low yield with 3.9 colonies per 10^6 cells (von Bubnoff, Veach et al. 2005). Using an ethyl-N-nitrosourea mutagenesis screen, Bradeen et al. expanded upon earlier methods and exposed BaF3-

$p210^{BCR\text{-}ABL}$ cells to ENU and grew them in the presence of imatinib. This was advantageous as it allowed for an accelerated process and did not limit dependent or independent mechanisms of resistance (Bradeen, Eide et al. 2006).

Activating gene rearrangements of anaplastic lymphoma kinase (ALK) have been identified as driver mutations in non-small-cell lung cancer (NSCLC) and inflammatory myofibroblastic tumours (Morris, Kirstein et al. 1994, Soda, Choi et al. 2007, Webb, Slavish et al. 2009). Treatment of tumours with targeted inhibitors which express oncogenic kinases commonly leads to acquired resistance due to point mutations in the kinase domain. Zhang et al. utilised an ENU mutagenesis screen to identify potential resistance mechanisms to crizotinib, a dual MET/ALK inhibitor in NSCLC cell lines (Zhang, Wang et al. 2011). They identified mutations in 16 residues structurally clustered into five regions around the kinase active site which conferred varying degrees of resistance. The screen predicted the L1196M, C1156Y, and F1174L mutations, previously identified in crizotinib-resistant patients and all of which are implicated in binding of crizotinib (Choi, Soda et al. 2010, Katayama, Khan et al. 2011). Although the identification of mutations resulting in resistance to crizotinib allows for additional guidance in study design and offers help to the development of future generations of drugs in order that ALK-based mechanisms of resistance be overcome, the disadvantage of such screens is that they do not allow for alternative resistance mechanisms such as gene amplification or upregulation of parallel signalling pathways to be explored. By combining the outputs of mutagenesis screens with next generation sequencing, alternative resistant mechanisms may be pursued.

7.1.2 N-ethyl-N-nitrosourea (ENU)

ENU, a chemical mutagen, is a direct-acting ethylator and is mutagenic to human cells. It acts primarily through its alkylating moiety by transferring its ethyl group to nitrogen or

oxygen sites found on deoxyribonucleotides. The action of ENU on DNA results, for the most part, in a nucleotide substitution. Most commonly (in 70-85% of cases) these are an A-T or T-A transversion or A-T to G-C transition. Following translation into proteins these substitutions result in approximately 70% non-synonymous changes of which around 65% are missense mutations (Takahasi, Sakuraba et al. 2007).

Strong bias of ENU towards specific base substitutions may be a limiting factor as some genes will be mutated more frequently than others due to their nucleotide composition.

7.2 Chapter Aims

The initial aim was to establish a methodology for performing a rapid cell-based mutagenesis screen using ENU in Ewing sarcoma cell lines. This required optimisation of mutagenesis by ENU and a means by which clones resistant to treatment with OSI-906 could be identified. Ewing cell lines were transfected with a fluorescent construct so that clonal growth could be identified in a quantitative manner, if present. Then colonies resistant to OSI-906 were re-challenged with the drug and if still viable, expanded further for DNA extraction and whole exome sequencing. The outcome of the work was to identify the resistance mutation profile of OSI-906 in Ewing sarcoma cell lines and, in particular to look for common mutations between different clones sequenced.

7.3 Methods

7.3.1 Transformation of competent cells with pRetroQ-mCherry-N1 Vector

Competent cells (JM109) in a volume of 250µl were thawed on ice. pRetroQ-mCherry-N1 Vector (Clontech, 632568) was purchased at a concentration of 500ng μl^{-1}. 50ng of pRetroQ-mCherry-N1 Vector was added per 10µl of cells and left for 30 minutes on ice. Heat shock was carried out in a water bath set to 42°C for 45 seconds after which the vial of cells was placed immediately on ice and left for 2 minutes. They were then added to 1ml of Luria-Bertani (LB) buffer and left for 1 hour in a shaking incubator (300rpm) at 37°C after which they were plated-out (agar plates with ampicillin 100µg ml^{-1}) and left overnight at 37°C.

An individual colony was selected and placed in 10ml of LB buffer containing 100µg ml^{-1} of ampicillin and left in a shaking incubator at 37°C for 6 hours before transferring into a large sterile conical flask containing 250ml of LB media supplemented with ampicillin and left shaking overnight at 37°C (300rpm).

The following day, using the protocol (Qiagen 12663, QIAfilter Plasmid Maxi Kit), DNA was eluted and quality and quantity was measured by nanodrop. The DNA was stored at 20°C until required.

7.3.2 Puromycin dose for antibiotic selection of transfected cells

Ewing sarcoma cells were seeded at $1x10^5$ cells per well in a 6 well plate and left for 24 hours to adhere. A range of puromycin doses was added (0-5µg ml^{-1}) to each cell line and incubated for 48 hours. Cell viability was measured by counting cells using trypan blue and a Neubauer cell counter.

7.3.3 Retroviral Transduction of Ewing sarcoma cell lines with pRetroQ-mCherry-N1 Vector

Phoenix cells were plated out ($1x10^6$ cells per 10cm petri dish) in complete medium and left overnight to adhere. The following day medium was replaced with fresh (10ml) and the cells were left for 2 hours before the addition of 25µM chloroquine to each plate for 15 minutes. Meanwhile, a mix of pRetroQ-mCherry-N1 Vector and the transfection reagent PEI was prepared. 500µl of serum free media was mixed with 10µg of DNA (previously prepared pRetroQ-mCherry-N1 Vector). Then to each preparation (one needed per petri dish of phoenix cells) 40µl of PEI stock solution was added (1mg ml^{-1}), they were mixed, and left to incubate for 10 minutes at room temperature to allow complexes to form. These were then added to petri dishes and left to incubate for 9 hours.

The following day, Ewing cell lines to be transduced with retrovirus were prepared with $1x10^6$ cells seeded per petri dish. A further 24 hours later, media from phoenix cell petri dishes was removed and placed in a 15ml falcon tube with the addition of 6µg ml^{-1} polybrene. This was then exchanged with the media on the target cells (Ewing cell lines) and incubated for 48 hours before changing to whole media containing the antibiotic selection reagent (puromycin) at a previously determined dose (1µg ml^{-1}).

Medium containing fresh puromycin was changed every 2-3 days until pRetroQ-mCherry-N1 Vector transduced Ewing sarcoma cells and could be expanded. Cells continued to be grown in culture in the presence of puromycin 1µg ml^{-1} throughout the time course of the experiment.

7.3.4 Preparation of ENU

ENU (Sigma N3385) was prepared as per manufacturer's instructions in DMSO to render a 400mM stock. Aliquots were frozen at -80°C until required. When applied to cells, serial dilutions were made in DMSO to the required dose.

7.3.5 Establishing optimal ENU dose

A preliminary experiment to establish the dose of ENU which would induce mutations but cause minimal toxicity to the cells was performed. Three cell lines, A673, CHP-100 and STA-ET1 were seeded at a concentration of $1x10^4$ cells per well into 96 well plates. After 24 hours to allow for adherence, cells were treated with doses of ENU (0, 0.2, 0.4, 1, 2, 4mM) and measured after 24 hours by MTS assay.

7.3.6 Mutagenesis screen for SK-N-MC and STA-ET1

The first attempt at this experiment was unsuccessful so modifications were made which resulted in the growth of clones which were resistant to OSI-906. Initially SK-N-MC and STA-ETC (both transduced with pRetroQ-mCherry-N1) were single cell seeded in 96 well glass-bottomed plates (SensoPlate™, VWR, 82050-792) (5 plates per cell line). These were left for 24 hours for cells to adhere and ENU added at equivalent 1mM concentration per well. This remained for 24 hours prior to the well being aspirated, washed x2 with PBS, and 200µl of fresh cell culture media (RPMI1640, 10% FCS, 1%P/S) added containing the equivalent of 1µM OSI-906. The media containing OSI-906 was changed every 72 hours for 21 days. No colonies were identified in any wells.

It was assumed that the failure of the initial screen was due to treating cells individually in the first instance thus reducing the chances of clone formation because of the combined insults of ENU mutagenesis and then OSI-906 applied to each cell. Therefore in the follow on experiment a bulk approach was taken to the ENU mutagenesis and exposure to OSI-906 prior to the transfer of individual cells into 96 well plates.

In more detail, pRetroQ-mCherry-N1 transduced SK-N-MC and STA-ET1 were plated in 10cm petri dishes $1x10^6$ cells and left to adhere for 24 hours. ENU was added at a dose of 0.5 mM or 1mM and incubated for a further 24 hours. At this point the media containing ENU was removed and the petri dishes were washed x2 with PBS before the addition of

complete media containing 1µM OSI-906. Petri dishes were incubated for 72 hours before the remaining cells were trypsinised, resuspended, and pipetted, using a multichannel pipette, into 200µl of complete media containing 1µM OSI-906 at the equivalent concentration of 1 cell per well (5 cells per ml). This was achieved by calculating the number of cells per ml using a Neubauer-improved cell counter and diluting appropriately with complete media. 5 plates were seeded per dose of ENU, per cell line. Plates were left for 21 days and then assessed for clonal growth. Although the cell lines were transduced with pRetroQ-mCherry-N1 retrovirus, this reporter was not used for assessment of cell growth as the plate reader was not sensitive enough to detect the fluorescence of the small, compact clones which formed (Figure 7-5).

7.3.7 Mutagenesis screen for A673 and CHP-100

In order to take resistant cell lines and confer sensitivity to OSI-906 a similar, reciprocal experiment was attempted. Cell lines A673 and CHP-100, which had previously been shown to be more resistant to the effects of OSI-906, were exposed to 1µM OSI-906 in complete media for 72 hours in a 10cm petri dish. Media was then exchanged and the remaining cells, assumed to be resistant to the effects of the drug, were exposed to 1mM ENU for 24 hours. Individual cells were seeded in 96 well plates in a volume of 200µl of complete media (5 plates per cell line). They were left until clones were identified.

The principle informing this experimental design was that when individual clones were identified, they would be split into two corresponding 96 well plates to generate “twins” of the clone. Twin 1 would be re-exposed to OSI-906 and twin 2, derived from the same initial clone as twin 1, would be used as comparison. If twin 1 remained viable in the presence of OSI-906 this would not be a hit as the cell remains resistant to the effects of the drug. However if twin 1 did not remain viable then this would be considered a hit and

twin 2 would be available to grow up for DNA extraction and NGS sequencing to analyse mutations altering sensitivity to the drug.

Unfortunately, although this experiment was repeated no clones could be evolved from any of the single cells seeded in each well. This was somewhat surprising as cells had been assessed for ENU toxicity as previously described, and were being seeded in complete medium not containing OSI-906. The reason behind the failing of this experiment has yet to be established (Figure 7-7).

7.3.8 Resistance Screen

Wells were inspected, under an inverted microscope, for signs of cell growth and colour change of media at 21 days. Clones were classified as being a clearly defined cluster of cells which could be seen at x4 magnification accompanied by a change in the colour of the media due to acidification by cellular metabolites. Clones were transferred to a 24 well plate and expanded in the presence of OSI-906 for a further 72 hours before being prepared for NGS with DNA extraction as described in Chapter 5.

7.4 Results

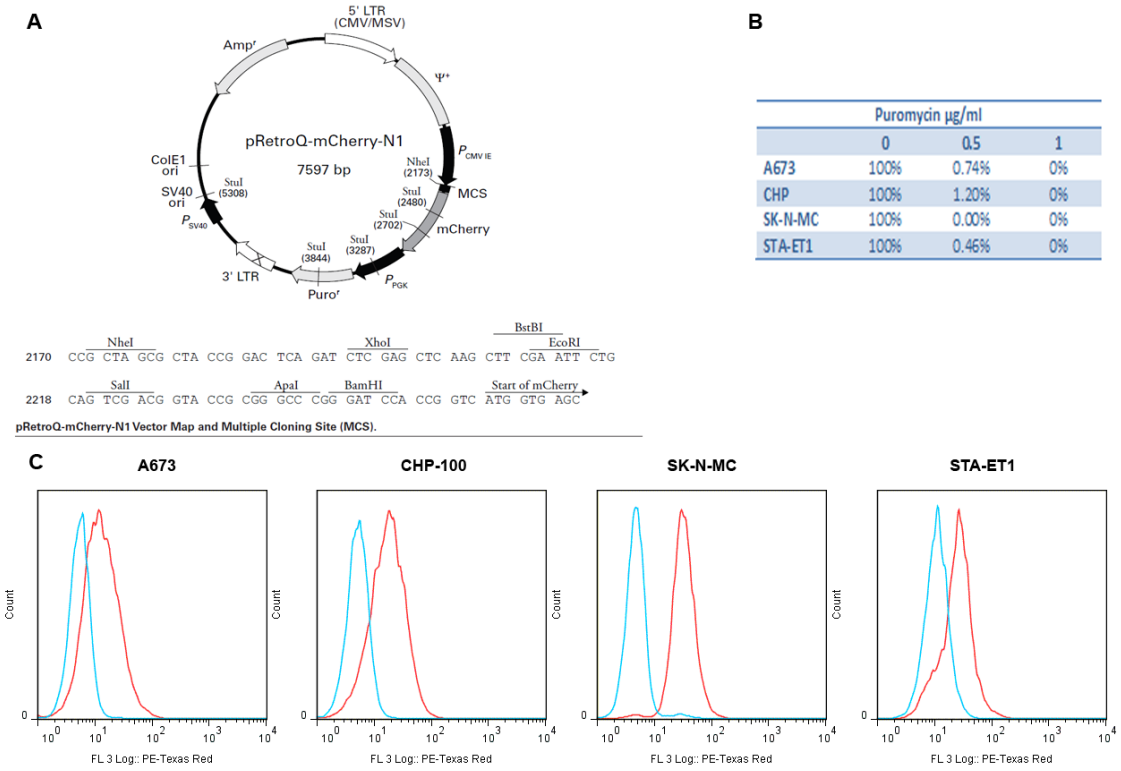
7.4.1 Determination of the optimal dose of puromycin for selection of pRetroQ-mCherry-N1 Vector transduced Ewing cell lines

The optimal dose of puromycin for selecting Ewing sarcoma cell lines transduced with pRetroQ-mCherry-N1 retrovirus was determined by exposing non-transduced cells to the drug for 48 hours. From literature, it was expected that the dose required would be between 1-5µg ml^{-1} (www.puromycin.com, (Cironi, Riggi et al. 2008)). Assessment was made by cell counting and results normalised to vehicle only control. Each cell line was found to be sensitive to puromycin at 0.5ug ml^{-1} with no viable cells noted at 1µg ml^{-1}.

In order that only pRetroQ-mCherry-N1 vector positive Ewing cells were selected, a dose of 1µg ml^{-1} puromycin was chosen to ensure that all non-transduced cells were killed.

7.4.2 Transduction of Ewing sarcoma cell lines with pRetroQ-mCherry-N1 was confirmed by flow cytometry

In order to ensure that cell lines were successfully transduced, flow cytometry analysis was performed. pRetroQ-mCherry-N1 is excited at 587nm and emits at 610nm. Transduction was confirmed when the fluorescent signal for a cell was greater than the autofluorescence of non-transduced control cells of the same cell line.



Puromycin µg/ml			
	0	0.5	1
A673	100%	0.74%	0%
CHP	100%	1.20%	0%
SK-N-MC	100%	0.00%	0%
STA-ET1	100%	0.46%	0%

NheI XhoI BstBI EcoRI
2170 CCG CTA GCG CTA CCG GAC TCA GAT CTC GAG CTC AAG CTT CGA ATT CTG
SalI ApaI BamHI Start of mCherry
2218 CAG TCG ACG GTA CCG CGG GCC CGG GAT CCA CCG GTC ATG GTG AGC

pRetroQ-mCherry-N1 Vector Map and Multiple Cloning Site (MCS).

Figure 7-1. Ewing sarcoma cell lines were transduced with pRetroQ-mCherry-N1 retrovirus followed by puromycin selection. A - Competent cells were transformed with a commercial fluorescent vector, pRetroQ-mCherry-N1. The vector has an ampicillin resistance gene, Amp^r and puromycin resistance gene, $Puro^r$ which were required for selection. **B** - 48 hour exposure to puromycin (doses 2-4µg ml^{-1} data not shown) indicated that the optimal dose for ensuring only transformed Ewing sarcoma cells were selected was 1µg ml^{-1}. **C** – Flow cytometry confirmed transduction of pRetroQ-mCherry-N1 in A673, CHP-100, SK-N-MC, STA-ET1. Data was obtained on a CyAN™ Flow Cytometer using a 488nm laser for excitation at 587nm and emission at 610nm using the FL3 bandpass filter. Each measurement was representative of 10,000 live, single cells. Blue lines represent untransduced control, Red lines pRetroQ-mCherry-N1 transduced Ewing sarcoma cell line.

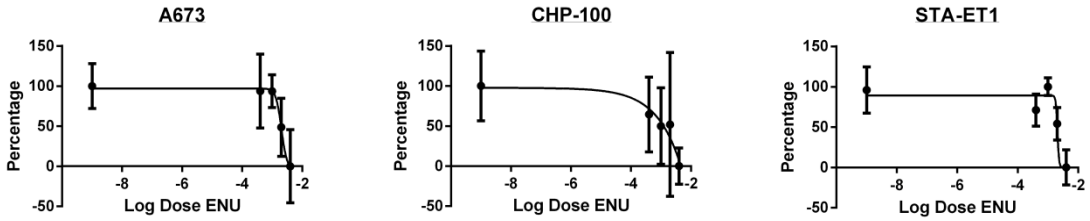


Figure 7-2. ENU kill curves for Ewing sarcoma cell lines. A673, CHP-100, STA-ET1 were exposed to a series of ENU doses between 0-2mM. After 24 hours, dose response was measured via MTS assay. A maximum dose of 1mM was chosen for the mutagenesis screen.

7.4.3 The optimal dose of ENU for the mutagenesis screen was determined to be 1mM

Cell lines A673, CHP-100, STA-ET1 were exposed to ENU for 24 hours and viability measured by MTS assay. The aim was to select a dose which would result in multiple mutations without being unduly detrimental to cell viability. Hence the dose which would kill only 15% of cells, retaining 85% as viable (the IC_{85}) was determined for the cell lines. The maximum dose selected to achieve this was 1mM.

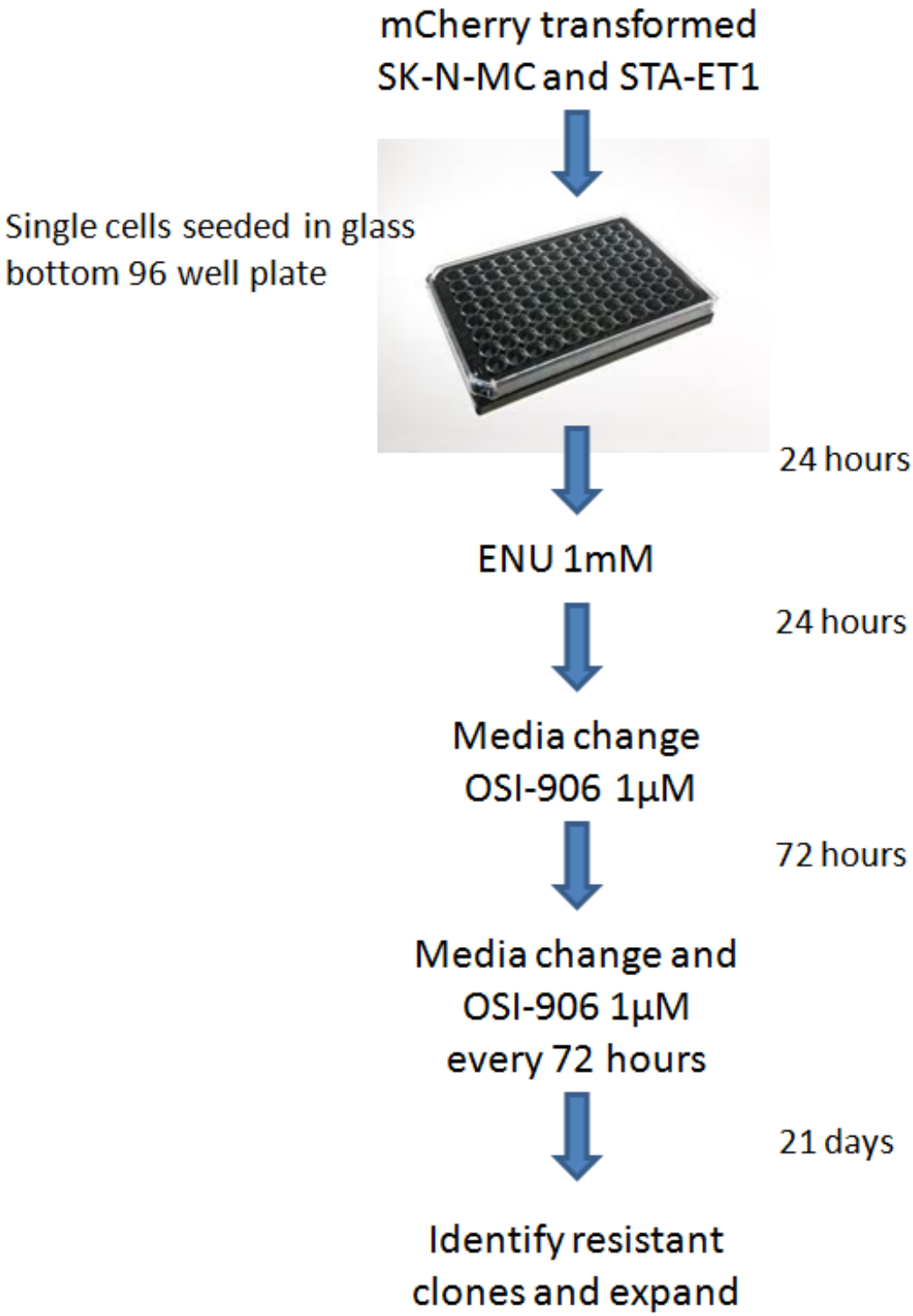


Figure 7-3. Initial strategy for formation of resistant clones using ENU mutagenesis. Cell lines SK-N-MC and STA-ET1 transduced with mCherry were seeded as individual cells in glass bottomed, black, 96 well plates and left for 24 hours to adhere. ENU was added (1mM) and after 24 hours exposure, media was changed and OSI-906 1µM was added. This remained on the cells, being changed every 72 hours for 3 weeks.

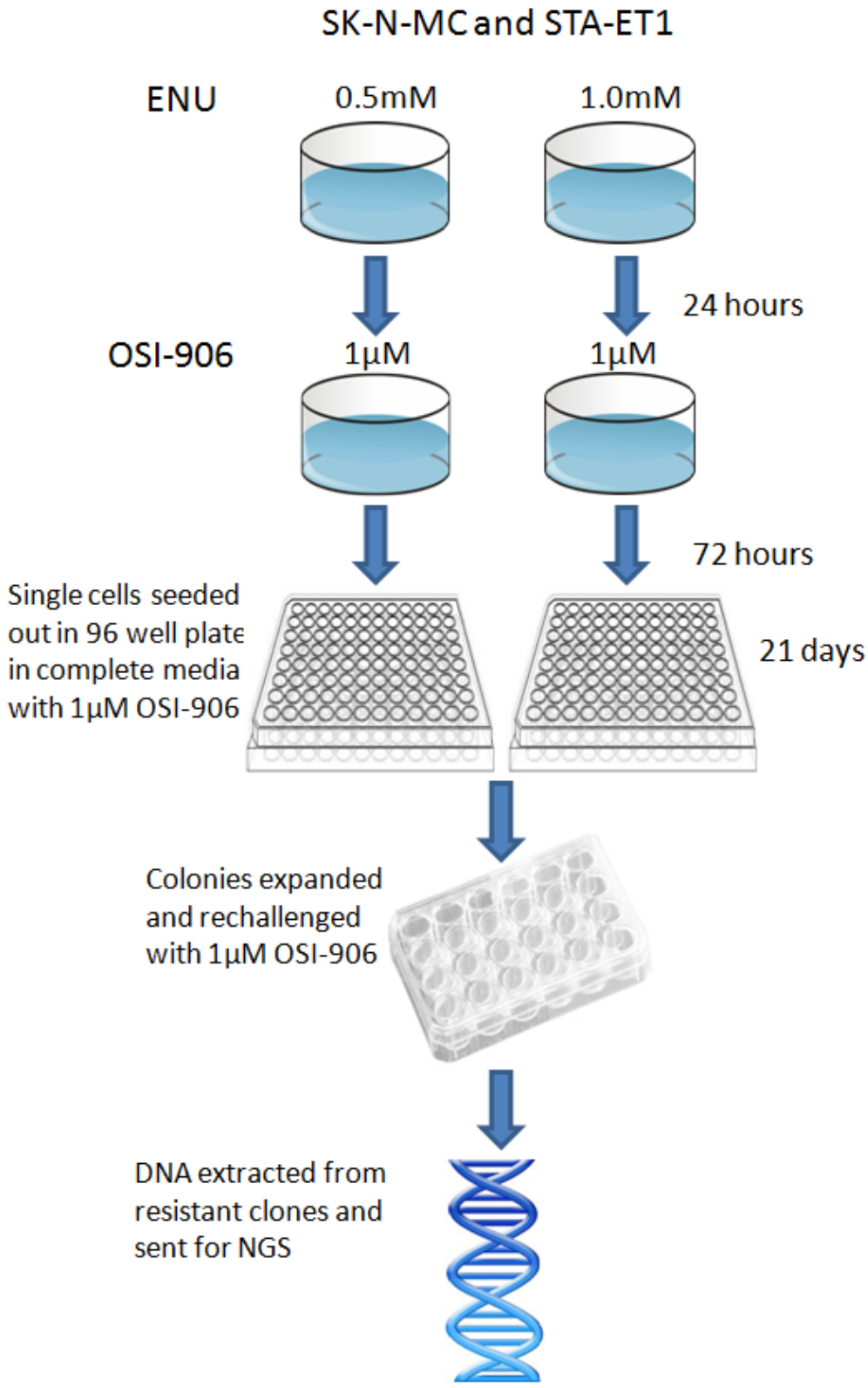


Figure 7-4. Amended method for ENU mutagenesis to generate resistant clones for cell lines SK-N-MC and STA-ET1. Cells were grown in 10cm petri dishes and allowed to adhere for 24 hours before the addition of either 0.5mM or 1mM of ENU. 24 hours later media was replaced with an equal volume containing 1µM OSI-906 and left for 72 hours. Cells were trypsinised and individual cells were seeded in complete media containing 1µM OSI-906 in 96 well plates (5 per cell line per dose of ENU). These were left at 37°C for 21 days at which point resistant clones were identified and expanded in 24 well plates with media containing 1µM OSI-906. Following this rechallenge to OSI-906, DNA was extracted from remaining clones and sent for NGS sequencing.

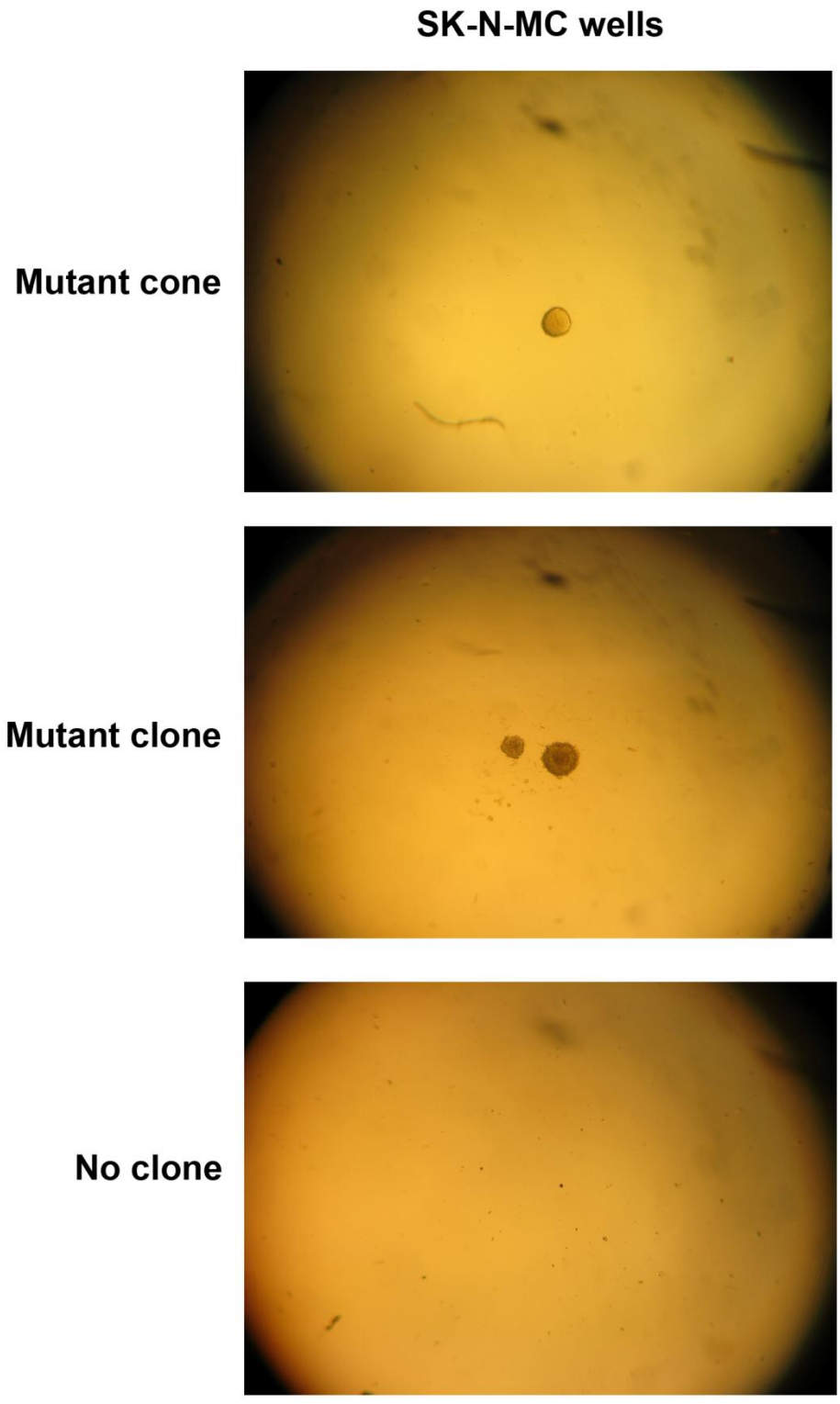


Figure 7-5. Mutant clones viewed under an inverted light microscope at x4 magnification following 3 weeks growth. SK-N-MC cells (shown as a representative example) were exposed to ENU for 24 hours. Following this they were incubated for 72 hours with OSI-906 1µM before being seeded into 96 well plates in a volume of 200µl complete media containing OSI-906 at the equivalent concentration of 1 cell per well. After 21 days mutant clones were identified. The top and middle images clearly show clones present in the well in comparison with the bottom image where no clones are seen.

A

SK-N-MC

Plate	0.5mM ENU 1µM OSI-906	1mM ENU 1µM OSI-906
A	6	13
B	8	14
C	3	41
D	0	24
E	0	6

B

STA-ET1

Plate	0.5mM ENU 1µM OSI-906	1mM ENU 1µM OSI-906
A	15	36
B	23	38
C	41	14
D	21	10
E	19	18

Figure 7-6. Resistant clones are generated in the ENU mutagenesis screen. Clones were identified by a change in the colour of the media in the well and a defined collection of cells visible at x4 magnification. **A** – SK-N-MC generated more resistant clones with 1mM ENU (right column) compared with 0.5mM. **B** – In comparison STA-ET1 has a less marked difference in clone generation between the 2 ENU doses.

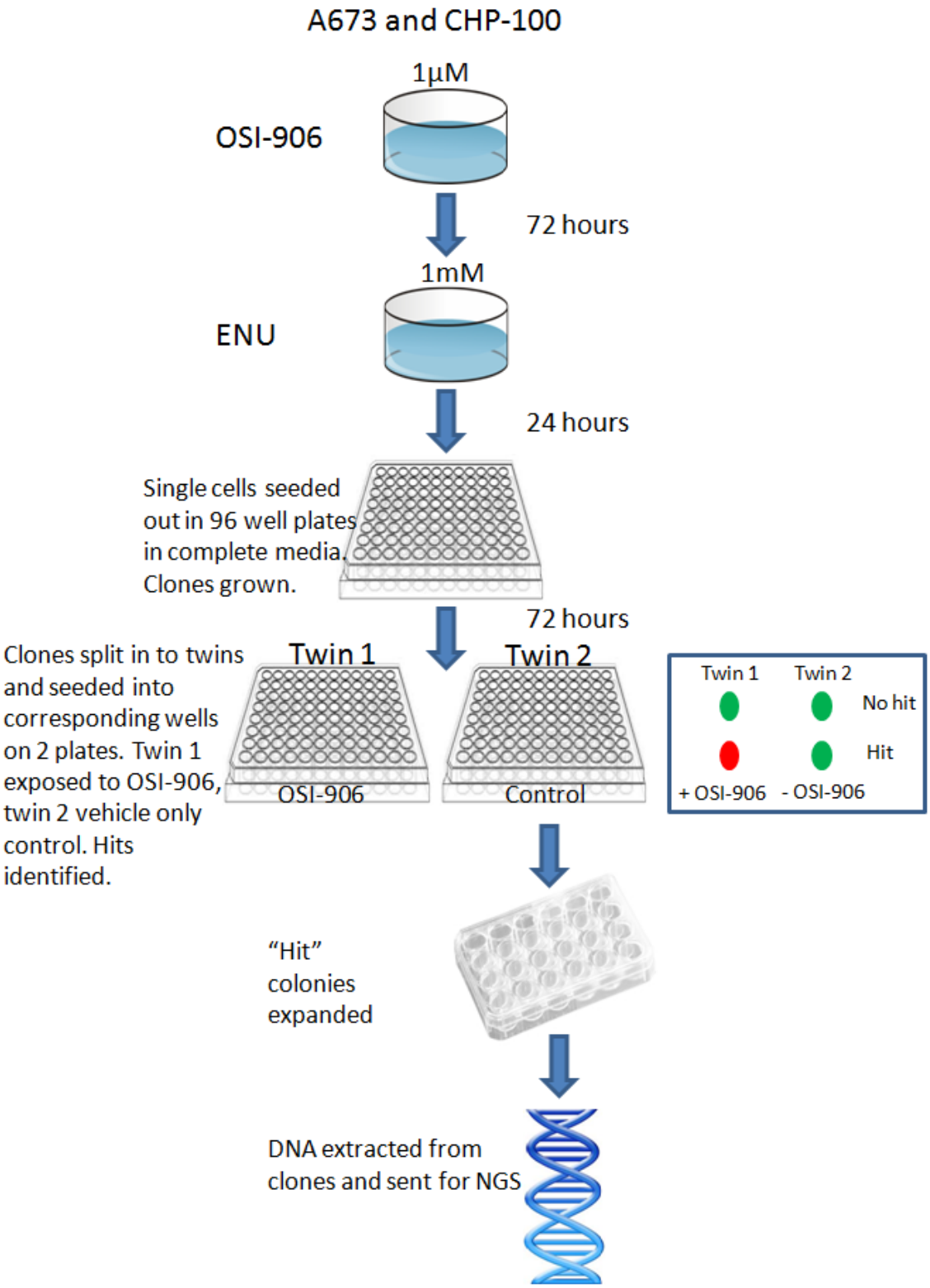


Figure 7-7. Principle of ENU mutagenesis used to re-sensitise resistant cell lines A673 and CHP-100 to OSI-906. Cells were grown in 10cm petri dishes and allowed to adhere for 24 hours before the addition of 1µM OSI-906 . After 72 hours media was changed and 1mM ENU added for 24 hours. Cells were trypsinised and individual cells were seeded in complete media in 96 well plates (5 per cell line per dose of ENU). These were left at 37°C until clones were identified. Clones were then spit in to wells in 2 corresponding 96 well plate. To twin 1, OSI-906 1µM was added and to twin 2 a vehicle control. After 72 hours hits were recorded. A hit was considered if twin 1 was no longer viable following OSI-906 exposure. The corresponding twin 2 cells were expanded and DNA extracted for NGS sequencing.

7.5 Discussion

This chapter describes the methodology used to develop a mutagenesis screen for identifying potential mechanisms of resistance in Ewing sarcoma cell lines. SK-N-MC and STA-ET1, both characterised previously as being sensitive to the effects of OSI-906 (with IC_{50s} of 0.15μM and 0.07μM respectively), were used to ascertain whether, following ENU mutagenesis, clones resistant to OSI-906 could be established. This would allow for the identification of point mutations which could render cell lines no longer responsive to the effect of the drug. The ENU approach is random and can be validated against sequencing data which is already available for each cell line. The other advantages are that it is relatively rapid to perform in comparison with sublethal screens but most importantly by starting with single cells, homogeneous clonal populations should be obtained.

Although NGS data from mutant clones is not yet available, it is hoped that mutations will be present which account for resistance to OSI-906. It is predicted that mutations conferring resistance may prevent binding of OSI-906 due to a mutation in the binding pockets of either IGF-1R or IR. In anaplastic large cell lymphoma cell lines, Zhang et al. conducted a mutagenesis screen with ENU to identify potential resistance mechanisms to crizotinib, a MET/ALK inhibitor. They identified 16 amino acid exchanges which were clustered in to 5 regions around the kinase active site and conferred resistance (Zhang, Wang et al. 2011).

The limitation of this method is that mutation focused screens such as these, do not probe alternative resistance mechanisms such as gene amplification resulting in upregulation of parallel signalling pathways. However, with the commencement of LINES, where mutations are identified in resistant clones in this cell line data, their potential presence and relevance can be assessed in patients enrolled in the trial before and after exposure to OSI-906. From a practical point of view it is a disadvantage that the technique requires the

researcher to work with ENU, a potent mutagen, and that a relative large number of single cells fail to develop in to clones following seeding in to 96 well plates. In addition, should the technique be used in the future, it would be beneficial to develop further a quantitative method of analysing colony growth which was the intention on commencing this series of experiments with the transfection of the fluorescent vector.

8 Discussion and future work

Intratumour heterogeneity is a formidable challenge that must be addressed in the development of personalised medicine and biomarker development. Single-cell variation heterogeneity leads to a distribution which can either be normal, skewed, or multimodal presenting a dilemma for biological research, especially for cancer research. While most molecular biological dogma is based on experimental measures conducted at the cellular population level that utilise statistical averages, single cells produce a high level of variability that does not equate to the average cell.

8.1.1 The potential importance of genetic heterogeneity in Ewing sarcoma

In order to have impact on Ewing sarcoma tumours, drugs need to target driver mutations which activate oncogenic pathways and inactivate tumour suppressors (Vogelstein and Kinzler 2004). Driver mutations are those which are advantageous to the cells survival allowing the cell lineage to populate the tumour, where as passenger mutations are either neutral or deleterious mutations that persist because they are genetically linked to driver mutations but do not appear to confer a selective fitness advantage to the cell (Sprouffske, Merlo et al. 2012). Driver mutations are central to current understanding of the genetic basis of human cancer, however both driver and passenger mutations are likely to have implications for cancer therapeutics as they may emerge as dominant populations after the selective pressure of therapy.

Driver mutations promote tumours and hence targeting them specifically is used in many tumour types such as the V600E mutation of BRAF in melanoma and BCR-ABL mutations in CML (Shah, Nicoll et al. 2002, Chapman, Hauschild et al. 2011). However intra-tumour heterogeneity in driver mutations has been implicated in therapeutic resistance mechanisms (Lovly and Shaw 2014). For example in CML, resistance to imatinib may arise because of amplification of BCR-ABL, overexpression of the

multidrug-resistant P-glycoprotein (MDR-1), and the emergence of mutations in the ABL-kinase domain as well as the development of BCR-ABL independent pathways of signal transduction (Milojkovic and Apperley 2009).

The relatively rapid proliferation rate and the increased mutation rates commonly seen in cancers (mainly due to genomic instability) allow for substantial genetic diversification of populations of tumour cells. Resistance to BRAF inhibitors in melanoma may be due to the presence of BRAF splice variants, bypass signalling including increased IGF-1R phosphorylation, BRAF amplification or the presence of concurrent MEK and RAS mutations (Lovly and Shaw 2014).

The emergence of resistance to drugs represents a critical issue. The theme if this thesis has been to identify heterogeneity within a panel of Ewing sarcoma cell lines and potential mechanisms which may account for resistance and sensitivity to OSI-906 and variation in its tumour efficacy. Next generation sequencing data confirmed the presence of the EWS-FLI1 translocation, of which effects on IGF signalling are well reported, and also highlighted common gains in copy number of genes such as c-MYC. Although no one common mutation was identified between cell lines, potentially harmful mutations of specific genes were validated through functional experiments. For example the treatment of cell lines with cisplatin showed that SK-N-MC, which had a non-synonymous mutation of BRCA1, was more sensitive to the effects of the drug than other cell lines potentially due to defects in homologous recombination (Byrski, Dent et al. 2012).

As resistance to IGF-1R inhibitors has been reported clinically, it should be assumed that OSI-906 will ultimately follow a similar path. To address this *in vitro*, mutagenesis screens carried out as part of this work may highlight acquired mutations or suggest pathways, or mechanisms through which resistance has been acquired. This will be validated through biopsy samples taken as part of the LINES trial of linsitinib (OSI-906) in relapsed Ewing

sarcoma and ultimately could lead to a change in drug combinations and/or dosing regimes.

Although undoubtedly important and a primary focus of this thesis, genetic events alone may not explain the heterogeneity underlying the biological characteristics of cancers. Stochastic heterogeneity illustrates how cellular phenotypes are not static, with individual cells within populations having substantial cell-to-cell variability caused by non-genetic mechanisms which may be altered in cancers and affect phenotypic diversity. Epigenetic alterations, consisting mainly of DNA methylation alterations and histone modification alterations, are often observed in cancers that are associated with chronic inflammation and frequently associated with tumour aggressiveness and poor patient outcome (Kanai 2010). As an example of this Sharma et al. linked therapy resistance with a distinct epigenetic change which occurred via chromatin modification and resulted in a reversible phenotypic switch (Sharma, Lee et al. 2010). This phenotypic state persisted for multiple cell generations and could therefore potentially serve as a substrate for selection.

8.1.2 IGF signalling pathway heterogeneity and its effect on responses in Ewing sarcoma cell lines

One problem facing the treatment of Ewing sarcoma is that the IGF pathway and other pathways are heterogeneous in their nature. Previous literature has reported that there is a potentially broad role of IGF-1R signalling in drug tolerance and its activation has been linked to drug resistance in cell culture settings (Buck, Eyzaguirre et al. 2008, Eckstein, Servan et al. 2009). Biomarker assays to initially select patients more likely to respond to IGF pathway inhibition remain unavailable, and drug development programmes have been curtailed as a result (Juergens, Daw et al. 2011, Pappo, Patel et al. 2011).

There is therefore a need for a validated, automated, unbiased method of measuring relevant image features which may confirm the extent of variation and heterogeneity in

pathway activation within the same and similarly genotyped tumours. By developing a quantitative multi-fluorescence based assay in Ewing sarcoma cell lines using confocal microscopy and high content image analysis the distribution of signalling pathway activation can be illustrated prior to application in biopsy samples. To do this, through collaboration, a reliable and robust computer algorithm which was both sensitive and specific was developed and thoroughly validated. Ewing sarcoma cell lines, in the presence of the ligand IGF-2 were found to be heterogeneous in their downstream signalling response. This confirmed that despite Ewing sarcoma being characterised by the presence of a chromosomal translocation between the EWS gene and one of several members of ETS genes and its association with the IGF pathway, cell lines are varied in their response to the ligand. Interestingly RD-ES, which was subsequently identified as not being a Ewing sarcoma cell line, did not show evidence of a response to stimulation with IGF-2 relative to other cell lines. In retrospect this could be attributed to less reliance on the IGF pathway for activation. Touched on in this initial chapter was also the application of the developed algorithm to Ewing sarcoma biopsy samples with linked clinical data, trying, through a semi-automated and unbiased manner to identify image features which correlate with outcome. Somewhat surprisingly it was found that subpopulations of cells which had low staining of CD99 but high staining of Ki67 were predictive of worse outcome. The reasoning behind this has yet to be established but further datasets will be assayed through the upcoming LINES trial.

8.1.3 Next generation sequencing has a role in the future understanding of Ewing sarcoma

Genetic and epigenetic changes which arise during oncogenic transformation and tumour progression alter and diversify cellular phenotypes resulting in a major obstacle to the understanding and clinical management of cancers. This work has generated models which

may be linked to potential resistance mechanisms and which can be validated in data from the clinical trial. Not only where translocations identified in Ewing sarcoma cell lines using RNA-seq, but copy number variations and mutational analysis was carried out providing a comprehensive assessment of the genomic make up of the cell lines. Alongside previously reported translocations, novel translocations such as RP11-GSE1 were identified through RNA-seq of which the clinical relevance has yet to be fully understood. Copy number variations analysed by SNP/array CGH were observed in all cell lines with SK-N-MC having marked losses and gains. Common gains on chromosome 8 around the MYC locus were observed between each of the cell lines tested and common losses identified on chromosome 9. CHP-100 had a gain of 1q which has previously been described in Ewing sarcoma (Mackintosh, Ordonez et al. 2012). In addition whole exome sequencing identified specific mutations of genes within cell lines for example, a BRCA mutation in SK-N-MC and STA-ET1, and an activating KIT mutation in SK-N-MC.

Interestingly genomic analysis indicated that the protein signalling scaffolds CNKSR1 and CNKSR2, which have previously been linked to IGF pathway signalling, may be implicated in Ewing sarcoma cell lines and therefore a potential actionable target. Functional assays were carried out and confirmed that such proteins could be intrinsically linked to the IGF pathway in Ewing sarcoma cell lines and will be validated through the upcoming trial.

Although sequencing technologies have been applied to cell lines only in this work, literature has highlighted the presence of intra-tumour heterogeneity in tumours such as breast cancer (Navin and Hicks 2010). Here, the existence of subclones were demonstrated derived from a common clonal progenitor but were shown to vary between samples taken from different regions of a primary tumour. Interestingly no correlation between tumour grade and immunohistochemical staining was observed illustrating the advantages of

sequencing technologies and in the context of this thesis, the importance of multiple biopsy sampling in future trial patients.

8.1.4 Drug resistance in Ewing sarcoma

The relatively rapid acquisition of resistance to drugs remains a key obstacle to successful treatment of Ewing sarcoma (Pappo, Patel et al. 2011). Methods to understand drug resistance across many cancers have revealed a variety of mechanisms present including drug efflux, acquisition of receptor mutations, and engagement of alternative survival pathways (Redmond, Wilson et al. 2008). These mechanisms are believed to reflect the existence of rare, stochastic, resistance conferring genetic alterations within a tumour cell population which are selected during drug treatment. In addition non mutational mechanisms of drug resistance can occur such as the presence of cancer stem cells. As mentioned, epigenetic mechanisms have also been implicated suggesting that gaining resistance to drugs does not necessarily need to be a stable genetic alteration.

Therapeutic resistance involves genetic alterations that can lead to lack of response and subsequent relapse in many different ways. Mutations which prevent the binding of a drug to its target for example resistance to imatinib in mutant forms of BCR-ABL, have been implicated in relapse of CML (Azam, Latek et al. 2003). Additionally mutations may activate signalling pathways or activate alternative pro-survival signalling pathways (Smolen, Sordella et al. 2006).

Further characterisation of cell lines to treatment with OSI-906 highlighted differences in response to the drug with A673 and CHP-100 being more resistant to its effects than other cell lines. This was somewhat surprising as referencing earlier imaging data, both A673 and CHP-100 appeared to show a marked response in pS6 and FoxO3a when stimulated by IGF-2. In addition Western blot analysis clearly shows a decrease in phospho-IGF-1R/IR on exposure to OSI-906 in both cell lines. This may indicate that Ewing sarcoma differs

between cells due to epigenetic or protein phosphoryation differences. By giving a drug to the patient and repeating a biopsy in a clinical trial, it will become clear whether it is new resistant clones which appear, or whether resistance is due to the same resistant clones with different stochastic/epigenetic qualities. Additionally, resistance could be due to upregulation of associated signalling pathways which have yet to be established.

ABC transporters may also have an emerging role in drug resistance as they have been implicated in resistance to imatinib and other tyrosine kinase inhibitors (Shukla, Chen et al. 2012) however at present no clear role has been identified in Ewing sarcoma.

Selective pressures exerted by drug therapy may lead to the expansion of resistant clones that either existed before the onset of treatment or that formed as a result of new mutations which were gained during the treatment (Burrell, McGranahan et al. 2013). Sequencing studies have allowed for analyse of the effect of therapy on tumour evolution and genomic instability. For example, the analysis of pairs of primary and relapsed tumour cells from eight patients with AML found relapse-specific mutations and an increase in base transversions after chemotherapy highlighting how treatment itself may initiate exogenous instability (Ding, Ley et al. 2012). Similarly through integrative genomic analyses of human tumours Solomon et al. identified inactivation of STAG2, a gene encoding a subunit of the cohesion complex leading to chromatid cohesion defects and aneuploidy and therefore chromosomal instability, a hallmark of cancer (Solomon, Kim et al. 2011). This level of heterogeneity provides challenges when treating patients in the clinic.

Through characterising a panel of Ewing sarcoma cell lines and carrying out genome wide analysis a comprehensive approach has been taken in an *in vitro* setting. Although not presently available, sequencing of clones resistant to OSI-906 through an ENU mutagenesis screen may provide further insight in to potential resistance mechanisms present and potential candidates validated in the LINES trial.

8.1.5 Testing resistance at a single cell level

In order to effectively identify mutations responsible for resistance in Ewing sarcoma, this needs to be carried out at a single cell level. Work in this thesis has attempted to ascertain causative mutations by taking a clonal cell line, exposing it to OSI-906, and establishing resistant clones which were interrogated next generation sequencing. This method of a mutagenesis screening appears to be a novel technique in Ewing sarcoma cell lines. High throughput cancer cell line screening strategies are used not only to identify drug sensitivity patterns, but also potential therapeutic targets in cancer research (Potratz, Saunders et al. 2010, Garnett, Edelman et al. 2012). Potratz et al. used high throughput RNA interference, a method of post transcriptional silencing of genes by double stranded DNA, to identify single siRNA kinase targets for Ewing sarcoma cells. They identified seventeen specific siRNAs (corresponding to sixteen genes) that led to a reduction in growth and proliferation in Ewing sarcoma cells. In particular they identified 2 genes, STK10 and TNK2 to be important in survival and a potential therapeutic target for future drug development (Potratz, Saunders et al. 2010).

In order to identify potential inhibitors of EWS-FLI1, the chromosomal translocation commonly associated with Ewing sarcoma, Grohar et al. evaluated more than 50 000 compounds for inhibition of EWS-FLI1 activity in Ewing sarcoma cells. Via a cell-based luciferase reporter screen using the EWS-FLI1 downstream target NR0B1 promoter they identified mithramycin as a potential inhibitor of EWS-FLI1 activity (Grohar, Woldemichael et al. 2011). Similarly, Garnett et al. performed a large scale screen of cancer cell lines, incorporating detailed genomic and gene expression analysis to identify, in a systematic manner, drug-sensitivity biomarkers. Specifically they found that Ewing sarcoma cell lines harbouring the EWS-FLI1 translocation were sensitive to olaparib, a PARP inhibitor. Interestingly, work in this thesis did not entirely validate their findings.

Although sensitivity of cell lines to olaparib was comparable, similar BRCA mutations identified in this work were not reported in their data. The inconsistency of findings could be due to cell line contamination or mislabelling, the development of the mutation within culture, or the sensitivity of techniques used for mutational analysis resulting in a false negative or positive outcome.

The advantage of such screens is that cell lines of rare cancer phenotypes such as Ewing sarcoma can be analysed relatively rapidly providing comprehensive and robust genomic data. Work such as that carried out in this thesis and by others has illustrated the complex network of biological factors which could contribute to the sensitivity of cell lines to cancer drugs. This highlights the challenge of identifying preselected patient populations for targeted therapies as well as the opportunities to improve existing therapies.

The disadvantages of such screens are that cell lines grown in two dimensional culture may not be representative of the complexity of the tumour environment and therefore experimental models which better mimic this may improve understanding of drug sensitivities. Additionally the availability of matched germline DNA is very often unavailable from long term immortalised cell lines. However cell models will allow for initial landscaping of drug sensitivity patterns to be explored across a broad set of different cancer types and genomic backgrounds.

8.1.6 Summary

The work within this thesis has illustrated that ultimately, personalising cancer treatment in Ewing sarcoma must most likely be based on detailed genomic and molecular characterisation of tumour samples. Through IGF pathway signalling, next generation sequencing and drug resistance screens, the scale of heterogeneity within Ewing sarcoma cell lines has been illustrated. Accordingly, approaches that provide global assessment of the catalogue of somatic genetic and epigenetic aberrations and tumour microenvironment-

based biomarkers are clearly important for accurately selecting targeted therapies for individual patients.

Ultimately the goal in Ewing sarcoma and in cancer therapy in general, is to devise an individually tailored treatment which targets growth promoting pathways and circumvents drug resistance.

9 Appendix

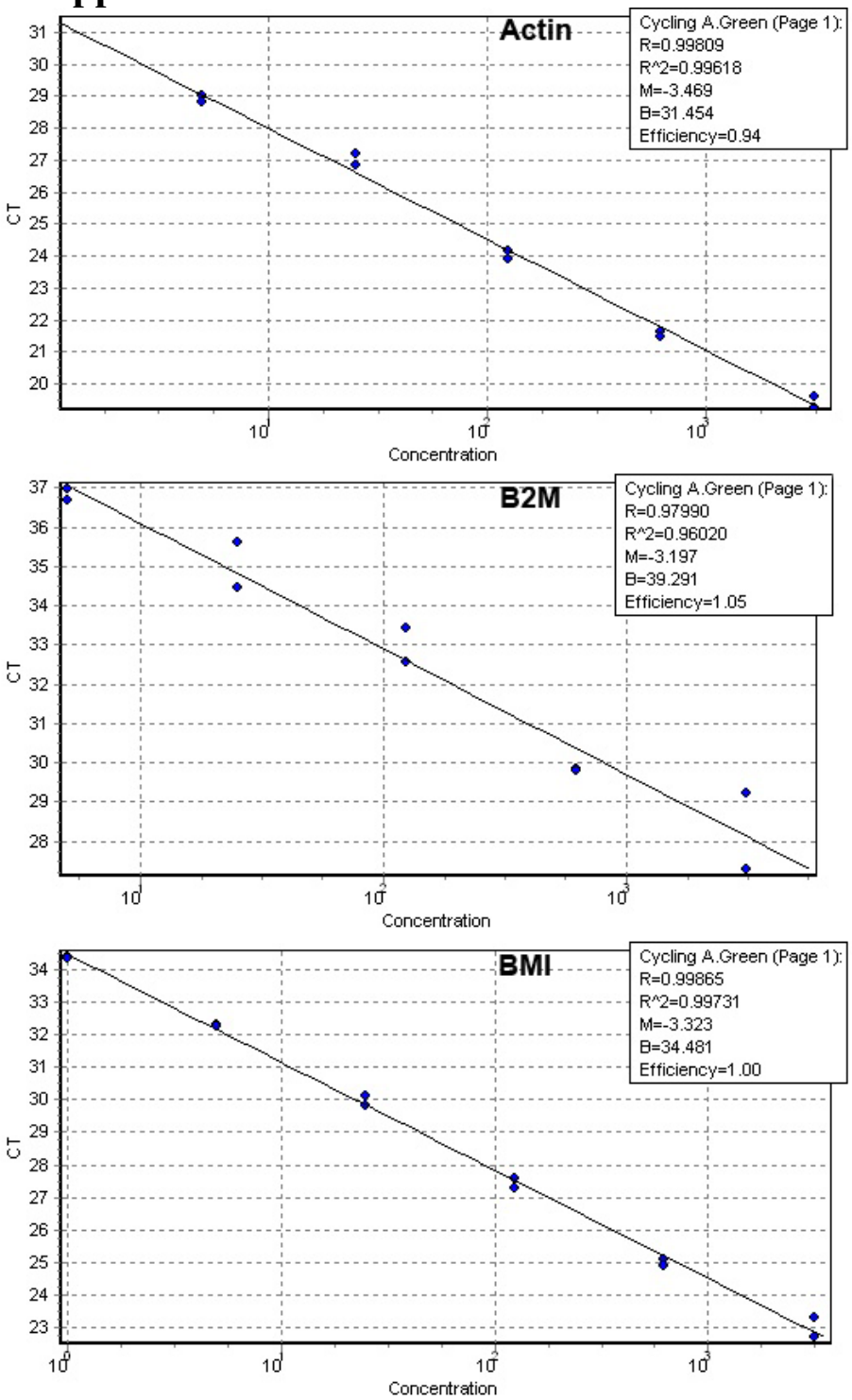


Figure 9-1. Standard curves for Actin, B2M and BMI1 genes.

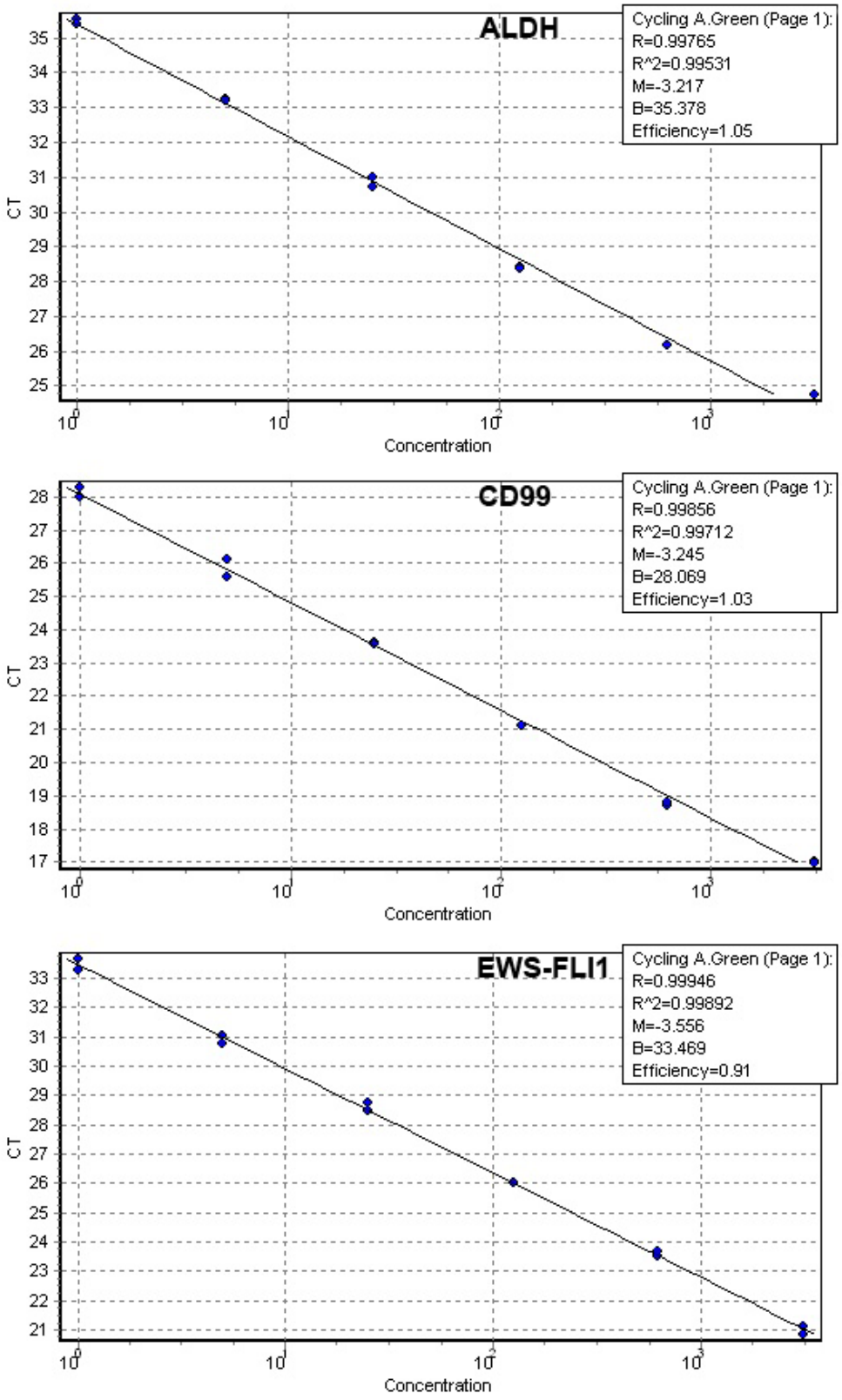


Figure 9-2. Standard curve for ALDH, CD99 and EWS-FLI1 primer/probes. For each qPCR experiment carried out in this thesis, an equivalent standard curve was calculated.

10 References

(EBCTCG), E. B. C. T. C. G. (2005). "Effects of chemotherapy and hormonal therapy for early breast cancer on recurrence and 15-year survival: an overview of the randomised trials." Lancet **365**(9472): 1687-1717.

Alavi, A., J. D. Hood, R. Frausto, D. G. Stupack and D. A. Cheresh (2003). "Role of Raf in vascular protection from distinct apoptotic stimuli." Science **301**(5629): 94-96.

Alilou, M., V. Kovalev and V. Taimouri (2013). "Segmentation of cell nuclei in heterogeneous microscopy images: A reshapable templates approach." Comput Med Imaging Graph.

Alison, M. R., N. J. Guppy, S. M. Lim and L. J. Nicholson (2010). "Finding cancer stem cells: are aldehyde dehydrogenases fit for purpose?" J Pathol **222**(4): 335-344.

Amaral, A. T., M. C. Manara, D. Berghuis, J. L. Ordóñez, M. Biscuola, M. A. Lopez-García, D. Osuna, E. Lucarelli, F. Alviano, A. Lankester, K. Scotlandi and E. de Álava (2014). "Characterization of human mesenchymal stem cells from ewing sarcoma patients. Pathogenetic implications." PLoS One **9**(2): e85814.

Amos, W. and J. White (2003). "How the confocal laser scanning microscope entered biological research." Biol Cell **95**(6): 335-342.

Antonescu, C. R., P. Besmer, T. Guo, K. Arkun, G. Hom, B. Koryotowski, M. A. Leversha, P. D. Jeffrey, D. Desantis, S. Singer, M. F. Brennan, R. G. Maki and R. P. DeMatteo (2005). "Acquired resistance to imatinib in gastrointestinal stromal tumor occurs through secondary gene mutation." Clin Cancer Res **11**(11): 4182-4190.

Ashworth, A. (2008). "A synthetic lethal therapeutic approach: poly(ADP) ribose polymerase inhibitors for the treatment of cancers deficient in DNA double-strand break repair." J Clin Oncol **26**(22): 3785-3790.

Asmann, Y. W., A. Hossain, B. M. Necela, S. Middha, K. R. Kalari, Z. Sun, H. S. Chai, D. W. Williamson, D. Radisky, G. P. Schroth, J. P. Kocher, E. A. Perez and E. A. Thompson (2011). "A novel bioinformatics pipeline for identification and characterization of fusion transcripts in breast cancer and normal cell lines." Nucleic Acids Res **39**(15): e100.

Assef, Y., F. Rubio, G. Coló, S. del Mónaco, M. A. Costas and B. A. Kotsias (2009). "Imatinib resistance in multidrug-resistant K562 human leukemic cells." Leuk Res **33**(5): 710-716.

Aurias, A., C. Rimbaut, D. Buffe, J. Dubousset and A. Mazabraud (1983). "[Translocation of chromosome 22 in Ewing's sarcoma]." C R Seances Acad Sci III **296**(23): 1105-1107.

Awad, O., J. T. Yustein, P. Shah, N. Gul, V. Katuri, A. O'Neill, Y. Kong, M. L. Brown, J. A. Toretsky and D. M. Loeb (2010). "High ALDH activity identifies chemotherapy-resistant Ewing's sarcoma stem cells that retain sensitivity to EWS-FLI1 inhibition." PLoS One **5**(11): e13943.

Azam, M., R. R. Latek and G. Q. Daley (2003). "Mechanisms of autoinhibition and STI-571/imatinib resistance revealed by mutagenesis of BCR-ABL." Cell **112**(6): 831-843.

Baker, A. F., T. Dragovich, N. T. Ihle, R. Williams, C. Fenoglio-Preiser and G. Powis (2005). "Stability of phosphoprotein as a biological marker of tumor signaling." Clin Cancer Res **11**(12): 4338-4340.

Balamuth, N. and R. Womer (2010). "Ewing's sarcoma." Lancet Oncol **11**(2): 184-192.

Baldini, E. H., G. D. Demetri, C. D. Fletcher, J. Foran, K. C. Marcus and S. Singer (1999). "Adults with Ewing's sarcoma/primitive neuroectodermal tumor: adverse effect of older age and primary extraosseous disease on outcome." Ann Surg **230**(1): 79-86.

Ban, J., G. Jug, P. Mestdagh, R. Schwentner, M. Kauer, D. N. Aryee, K. L. Schaefer, F. Nakatani, K. Scotlandi, M. Reiter, D. Strunk, F. Speleman, J. Vandesompele and H. Kovar (2011). "Hsa-mir-145 is the top EWS-FLI1-repressed microRNA involved in a positive feedback loop in Ewing's sarcoma." Oncogene **30**(18): 2173-2180.

Baron, V., E. D. Adamson, A. Calogero, G. Ragona and D. Mercola (2006). "The transcription factor Egr1 is a direct regulator of multiple tumor suppressors including TGFbeta1, PTEN, p53, and fibronectin." Cancer Gene Ther **13**(2): 115-124.

Barsotti, A. M., R. Beckerman, O. Laptenko, K. Huppi, N. J. Caplen and C. Prives (2012). "p53-Dependent induction of PVT1 and miR-1204." J Biol Chem **287**(4): 2509-2519.

Baudis, M. (2007). "Genomic imbalances in 5918 malignant epithelial tumors: an explorative meta-analysis of chromosomal CGH data." BMC Cancer **7**: 226.

Beech, D. J., E. Perer, J. Helms, A. Gratzer and N. Deng (2003). "Insulin-like growth factor-I receptor activation blocks doxorubicin cytotoxicity in sarcoma cells." Oncol Rep **10**(1): 181-184.

Bejjani, B. A. and L. G. Shaffer (2006). "Application of array-based comparative genomic hybridization to clinical diagnostics." J Mol Diagn **8**(5): 528-533.

Belyaeva, O. V., O. V. Korkina, A. V. Stetsenko and N. Y. Kedishvili (2008). "Human retinol dehydrogenase 13 (RDH13) is a mitochondrial short-chain dehydrogenase/reductase with a retinaldehyde reductase activity." FEBS J **275**(1): 138-147.

Benini, S., M. C. Manara, N. Baldini, V. Cerisano, Massimo Serra, M. Mercuri, P. L. Lollini, P. Nanni, P. Picci and K. Scotlandi (2001). "Inhibition of insulin-like growth factor I receptor increases the antitumor activity of doxorubicin and vincristine against Ewing's sarcoma cells." Clin Cancer Res **7**(6): 1790-1797.

Benini, S., M. C. Manara, V. Cerisano, S. Perdichizzi, R. Strammiello, M. Serra, P. Picci and K. Scotlandi (2004). "Contribution of MEK/MAPK and PI3-K signaling pathway to the malignant behavior of Ewing's sarcoma cells: therapeutic prospects." Int J Cancer **108**(3): 358-366.

Beroukhim, R., C. H. Mermel, D. Porter, G. Wei, S. Raychaudhuri, J. Donovan, J. Barretina, J. S. Boehm, J. Dobson, M. Urashima, K. T. Mc Henry, R. M. Pinchback, A. H. Ligon, Y. J. Cho, L. Haery, H. Greulich, M. Reich, W. Winckler, M. S. Lawrence, B. A. Weir, K. E. Tanaka, D. Y. Chiang, A. J. Bass, A. Loo, C. Hoffman, J. Prensner, T. Liefeld, Q. Gao, D. Yecies, S. Signoretti, E. Maher, F. J. Kaye, H. Sasaki, J. E. Tepper, J. A. Fletcher, J. Tabernero, J. Baselga, M. S. Tsao, F. Demichelis, M. A. Rubin, P. A. Janne, M. J. Daly, C. Nucera, R. L. Levine, B. L. Ebert, S. Gabriel, A. K. Rustgi, C. R. Antonescu, M. Ladanyi, A. Letai, L. A. Garraway, M. Loda, D. G. Beer, L. D. True, A. Okamoto, S. L. Pomeroy, S. Singer, T. R. Golub, E. S. Lander, G. Getz, W. R. Sellers and M. Meyerson (2010). "The landscape of somatic copy-number alteration across human cancers." Nature **463**(7283): 899-905.

Boland, M. V. and R. F. Murphy (1999). "Automated analysis of patterns in fluorescence-microscope images." Trends Cell Biol **9**(5): 201-202.

Boman, B. M., M. S. Wicha, J. Z. Fields and O. A. Runquist (2007). "Symmetric division of cancer stem cells--a key mechanism in tumor growth that should be targeted in future therapeutic approaches." Clin Pharmacol Ther **81**(6): 893-898.

Boro, A., K. Prêtre, F. Rechfeld, V. Thalhammer, S. Oesch, M. Wachtel, B. W. Schäfer and F. K. Niggli (2012). "Small-molecule screen identifies modulators of EWS/FLI1 target gene expression and cell survival in Ewing's sarcoma." Int J Cancer **131**(9): 2153-2164.

Bovée, J. and P. Hogendoorn (2010). "Molecular pathology of sarcomas: concepts and clinical implications." Virchows Arch **456**(2): 193-199.

Bradeen, H. A., C. A. Eide, T. O'Hare, K. J. Johnson, S. G. Willis, F. Y. Lee, B. J. Druker and M. W. Deininger (2006). "Comparison of imatinib mesylate, dasatinib (BMS-354825), and nilotinib (AMN107) in an N-ethyl-N-nitrosourea (ENU)-based mutagenesis screen: high efficacy of drug combinations." Blood **108**(7): 2332-2338.

Braunreiter, C., J. Hancock, C. Coffin, K. Boucher and S. Lessnick (2006). "Expression of EWS-ETS fusions in NIH3T3 cells reveals significant differences to Ewing's sarcoma." Cell Cycle **5**(23): 2753-2759.

Brognard, J. and T. Hunter (2011). "Protein kinase signaling networks in cancer." Curr Opin Genet Dev **21**(1): 4-11.

Brownhill, S. C., C. Taylor and S. A. Burchill (2007). "Chromosome 9p21 gene copy number and prognostic significance of p16 in ESFT." Br J Cancer **96**(12): 1914-1923.

Buck, E., A. Eyzaguirre, M. Rosenfeld-Franklin, S. Thomson, M. Mulvihill, S. Barr, E. Brown, M. O'Connor, Y. Yao, J. Pachter, M. Miglarese, D. Epstein, K. K. Iwata, J. D. Haley, N. W. Gibson and Q. S. Ji (2008). "Feedback mechanisms promote cooperativity for small molecule inhibitors of epidermal and insulin-like growth factor receptors." Cancer Res **68**(20): 8322-8332.

Buck, E., P. C. Gokhale, S. Koujak, E. Brown, A. Eyzaguirre, N. Tao, M. Rosenfeld-Franklin, L. Lerner, M. I. Chiu, R. Wild, D. Epstein, J. A. Pachter and M. R. Miglarese (2010). "Compensatory insulin receptor (IR) activation on inhibition of insulin-like growth factor-1 receptor (IGF-1R): rationale for cotargeting IGF-1R and IR in cancer." Mol Cancer Ther **9**(10): 2652-2664.

Bumeister, R., C. Rosse, A. Anselmo, J. Camonis and M. A. White (2004). "CNK2 couples NGF signal propagation to multiple regulatory cascades driving cell differentiation." Curr Biol **14**(5): 439-445.

Burger, H., J. A. Foekens, M. P. Look, M. E. Meijer-van Gelder, J. G. Klijn, E. A. Wiemer, G. Stoter and K. Nooter (2003). "RNA expression of breast cancer resistance protein, lung resistance-related protein, multidrug resistance-associated proteins 1 and 2, and multidrug resistance gene 1 in breast cancer: correlation with chemotherapeutic response." Clin Cancer Res **9**(2): 827-836.

Burrell, R. A., N. McGranahan, J. Bartek and C. Swanton (2013). "The causes and consequences of genetic heterogeneity in cancer evolution." Nature **501**(7467): 338-345.

Byrski, T., R. Dent, P. Blecharz, M. Foszczynska-Kloda, J. Gronwald, T. Huzarski, C. Cybulski, E. Marczyk, R. Chrzan, A. Eisen, J. Lubinski and S. A. Narod (2012). "Results of a phase II open-label, non-randomized trial of cisplatin chemotherapy in patients with BRCA1-positive metastatic breast cancer." Breast Cancer Res **14**(4): R110.

Cadwell, R. C. and G. F. Joyce (1992). "Randomization of genes by PCR mutagenesis." PCR Methods Appl **2**(1): 28-33.

Calnan, D. R. and A. Brunet (2008). "The FoxO code." Oncogene **27**(16): 2276-2288.

Camp, R. L., G. G. Chung and D. L. Rimm (2002). "Automated subcellular localization and quantification of protein expression in tissue microarrays." Nat Med **8**(11): 1323-1327.

Camp, R. L., G. G. Chung and D. L. Rimm (2002). "Automated subcellular localization and quantification of protein expression in tissue microarrays." Nat Med **8**(11): 1323-1327.

Carboni, J. M., M. Wittman, Z. Yang, F. Lee, A. Greer, W. Hurlburt, S. Hillerman, C. Cao, G. H. Cantor, J. Dell-John, C. Chen, L. Discenza, K. Menard, A. Li, G. Trainor, D. Vyas, R. Kramer, R. M. Attar and M. M. Gottardis (2009). "BMS-754807, a small molecule inhibitor of insulin-like growth factor-1R/IR." Mol Cancer Ther **8**(12): 3341-3349.

Carpenter, A. E. (2009). "Extracting rich information from images." Methods Mol Biol **486**: 193-211.

Carramusa, L., F. Contino, A. Ferro, L. Minafra, G. Perconti, A. Giallongo and S. Feo (2007). "The PVT-1 oncogene is a Myc protein target that is overexpressed in transformed cells." J Cell Physiol **213**(2): 511-518.

Carvajal, R. and P. Meyers (2005). "Ewing's sarcoma and primitive neuroectodermal family of tumors." Hematol Oncol Clin North Am **19**(3): 501-525, vi-vii.

Chansky, H. A., F. Barahmand-Pour, Q. Mei, W. Kahn-Farooqi, A. Zielinska-Kwiatkowska, M. Blackburn, K. Chansky, E. U. Conrad, J. D. Bruckner, T. K. Greenlee and L. Yang (2004). "Targeting of EWS/FLI-1 by RNA interference attenuates the tumor phenotype of Ewing's sarcoma cells in vitro." J Orthop Res **22**(4): 910-917.

Chapman, P. B., A. Hauschild, C. Robert, J. B. Haanen, P. Ascierto, J. Larkin, R. Dummer, C. Garbe, A. Testori, M. Maio, D. Hogg, P. Lorigan, C. Lebbe, T. Jouary, D. Schadendorf, A. Ribas, S. J. O'Day, J. A. Sosman, J. M. Kirkwood, A. M. Eggermont, B. Dreno, K. Nolop, J. Li, B. Nelson, J. Hou, R. J. Lee, K. T. Flaherty, G. A. McArthur and B.-S. Group (2011). "Improved survival with vemurafenib in melanoma with BRAF V600E mutation." N Engl J Med **364**(26): 2507-2516.

Chen, X., L. Wang and H. Ishwaran (2010). "An Integrative Pathway-based Clinical-genomic Model for Cancer Survival Prediction." Stat Probab Lett **80**(17-18): 1313-1319.

Cheung, A. M., T. S. Wan, J. C. Leung, L. Y. Chan, H. Huang, Y. L. Kwong, R. Liang and A. Y. Leung (2007). "Aldehyde dehydrogenase activity in leukemic blasts defines a subgroup of acute myeloid leukemia with adverse prognosis and superior NOD/SCID engrafting potential." Leukemia **21**(7): 1423-1430.

Cheung, V. G., N. Nowak, W. Jang, I. R. Kirsch, S. Zhao, X. N. Chen, T. S. Furey, U. J. Kim, W. L. Kuo, M. Olivier, J. Conroy, A. Kasprzyk, H. Massa, R. Yonescu, S. Sait, C. Thoreen, A. Snijders, E. Lemyre, J. A. Bailey, A. Bruzel, W. D. Burrill, S. M. Clegg, S. Collins, P. Dhami, C. Friedman, C. S. Han, S. Herrick, J. Lee, A. H. Ligon, S. Lowry, M. Morley, S. Narasimhan, K. Osoegawa, Z. Peng, I. Plajzer-Frick, B. J. Quade, D. Scott, K. Sirotkin, A. A. Thorpe, J. W. Gray, J. Hudson, D. Pinkel, T. Ried, L. Rowen, G. L. Shen-Ong, R. L. Strausberg, E. Birney, D. F. Callen, J. F. Cheng, D. R. Cox, N. A. Doggett, N. P. Carter, E. E. Eichler, D. Haussler, J. R. Korenberg, C. C. Morton, D. Albertson, G. Schuler, P. J. de Jong, B. J. Trask and B. R. Consortium (2001). "Integration of cytogenetic landmarks into the draft sequence of the human genome." Nature **409**(6822): 953-958.

Choi, Y. L., M. Soda, Y. Yamashita, T. Ueno, J. Takashima, T. Nakajima, Y. Yatabe, K. Takeuchi, T. Hamada, H. Haruta, Y. Ishikawa, H. Kimura, T. Mitsudomi, Y. Tanio, H. Mano and A. L. C. S.

Group (2010). "EML4-ALK mutations in lung cancer that confer resistance to ALK inhibitors." N Engl J Med **363**(18): 1734-1739.

Cironi, L., N. Riggi, P. Provero, N. Wolf, M. L. Suvà, D. Suvà, V. Kindler and I. Stamenkovic (2008). "IGF1 is a common target gene of Ewing's sarcoma fusion proteins in mesenchymal progenitor cells." PLoS One **3**(7): e2634.

Ciró, M., E. Prosperini, M. Quarto, U. Grazini, J. Walfridsson, F. McBlane, P. Nucifero, G. Pacchiana, M. Capra, J. Christensen and K. Helin (2009). "ATAD2 is a novel cofactor for MYC, overexpressed and amplified in aggressive tumors." Cancer Res **69**(21): 8491-8498.

Claxton, N., T. Fellers and M. Davidson Laser Scanning Confocal Microscopy. Optical Microscopy**:** 1-37.

Cloutier, S., H. Hamel, M. Champagne and W. V. Yotov (1997). "Mapping of the human DNA primase 1 (PRIM1) to chromosome 12q13." Genomics **43**(3): 398-401.

Colleoni, G. W., J. A. Bridge, B. Garicochea, J. Liu, D. A. Filippa and M. Ladanyi (2000). "ATIC-ALK: A novel variant ALK gene fusion in anaplastic large cell lymphoma resulting from the recurrent cryptic chromosomal inversion, inv(2)(p23q35)." Am J Pathol **156**(3): 781-789.

Concin, N., G. Hofstetter, A. Berger, A. Gehmacher, D. Reimer, R. Watrowski, D. Tong, E. Schuster, L. Hefler, K. Heim, E. Mueller-Holzner, C. Marth, U. M. Moll, A. G. Zeimet and R. Zeillinger (2005). "Clinical relevance of dominant-negative p73 isoforms for responsiveness to chemotherapy and survival in ovarian cancer: evidence for a crucial p53-p73 cross-talk in vivo." Clin Cancer Res **11**(23): 8372-8383.

Cotterill, S., S. Ahrens, M. Paulussen, H. Jürgens, P. Voûte, H. Gadner and A. Craft (2000). "Prognostic factors in Ewing's tumor of bone: analysis of 975 patients from the European Intergroup Cooperative Ewing's Sarcoma Study Group." J Clin Oncol **18**(17): 3108-3114.

Curtin, J. A., J. Fridlyand, T. Kageshita, H. N. Patel, K. J. Busam, H. Kutzner, K. H. Cho, S. Aiba, E. B. Bröcker, P. E. LeBoit, D. Pinkel and B. C. Bastian (2005). "Distinct sets of genetic alterations in melanoma." N Engl J Med **353**(20): 2135-2147.

Dantzer, F., G. de La Rubia, J. Ménissier-De Murcia, Z. Hostomsky, G. de Murcia and V. Schreiber (2000). "Base excision repair is impaired in mammalian cells lacking Poly(ADP-ribose) polymerase-1." Biochemistry **39**(25): 7559-7569.

Dauphinot, L., C. De Oliveira, T. Melot, N. Sevenet, V. Thomas, B. E. Weissman and O. Delattre (2001). "Analysis of the expression of cell cycle regulators in Ewing cell lines: EWS-FLI-1 modulates p57KIP2and c-Myc expression." Oncogene **20**(25): 3258-3265.

Davies, H., G. R. Bignell, C. Cox, P. Stephens, S. Edkins, S. Clegg, J. Teague, H. Woffendin, M. J. Garnett, W. Bottomley, N. Davis, E. Dicks, R. Ewing, Y. Floyd, K. Gray, S. Hall, R. Hawes, J. Hughes, V. Kosmidou, A. Menzies, C. Mould, A. Parker, C. Stevens, S. Watt, S. Hooper, R. Wilson, H. Jayatilake, B. A. Gusterson, C. Cooper, J. Shipley, D. Hargrave, K. Pritchard-Jones, N. Maitland, G. Chenevix-Trench, G. J. Riggins, D. D. Bigner, G. Palmieri, A. Cossu, A. Flanagan, A. Nicholson, J. W. Ho, S. Y. Leung, S. T. Yuen, B. L. Weber, H. F. Seigler, T. L. Darrow, H. Paterson, R. Marais, C. J. Marshall, R. Wooster, M. R. Stratton and P. A. Futreal (2002). "Mutations of the BRAF gene in human cancer." Nature **417**(6892): 949-954.

de Alava, E., C. R. Antonescu, A. Panizo, D. Leung, P. A. Meyers, A. G. Huvos, F. J. Pardo-Mindan, J. H. Healey and M. Ladanyi (2000). "Prognostic impact of P53 status in Ewing sarcoma." Cancer **89**(4): 783-792.

de Alava, E., A. Kawai, J. Healey, I. Fligman, P. Meyers, A. Huvos, W. Gerald, S. Jhanwar, P. Argani, C. Antonescu, F. Pardo-Mindan, J. Ginsberg, R. Womer, E. Lawlor, J. Wunder, I. Andrulis, P. Sorensen, F. Barr and M. Ladanyi (1998). "EWS-FLI1 fusion transcript structure is an independent determinant of prognosis in Ewing's sarcoma." J Clin Oncol **16**(4): 1248-1255.

Delattre, O., J. Zucman, B. Plougastel, C. Desmaze, T. Melot, M. Peter, H. Kovar, I. Joubert, P. de Jong and G. Rouleau (1992). "Gene fusion with an ETS DNA-binding domain caused by chromosome translocation in human tumours." Nature **359**(6391): 162-165.

Denley, A., E. R. Bonython, G. W. Booker, L. J. Cosgrove, B. E. Forbes, C. W. Ward and J. C. Wallace (2004). "Structural determinants for high-affinity binding of insulin-like growth factor II to insulin receptor (IR)-A, the exon 11 minus isoform of the IR." Mol Endocrinol **18**(10): 2502-2512.

Dhillon, A. S. and W. Kolch (2002). "Untying the regulation of the Raf-1 kinase." Arch Biochem Biophys **404**(1): 3-9.

Di Cataldo, S., E. Ficarra, A. Acquaviva and E. Macii (2009). Achieving the way for automated segmentation of nuclei in cancer tissue images through morphology-based approach: A quantitative evalution. Computerized Medical Imaging and Graphics.

Ding, L., T. J. Ley, D. E. Larson, C. A. Miller, D. C. Koboldt, J. S. Welch, J. K. Ritchey, M. A. Young, T. Lamprecht, M. D. McLellan, J. F. McMichael, J. W. Wallis, C. Lu, D. Shen, C. C. Harris, D. J. Dooling, R. S. Fulton, L. L. Fulton, K. Chen, H. Schmidt, J. Kalicki-Veizer, V. J. Magrini, L. Cook, S. D. McGrath, T. L. Vickery, M. C. Wendl, S. Heath, M. A. Watson, D. C. Link, M. H. Tomasson, W. D. Shannon, J. E. Payton, S. Kulkarni, P. Westervelt, M. J. Walter, T. A. Graubert, E. R. Mardis, R. K. Wilson and J. F. DiPersio (2012). "Clonal evolution in relapsed acute myeloid leukaemia revealed by whole-genome sequencing." Nature **481**(7382): 506-510.

Doyle, L. and D. D. Ross (2003). "Multidrug resistance mediated by the breast cancer resistance protein BCRP (ABCG2)." Oncogene **22**(47): 7340-7358.

DuBois, S. G., M. D. Krailo, S. L. Lessnick, R. Smith, Z. Chen, N. Marina, H. E. Grier, K. Stegmaier and C. s. O. Group (2009). "Phase II study of intermediate-dose cytarabine in patients with relapsed or refractory Ewing sarcoma: a report from the Children's Oncology Group." Pediatr Blood Cancer **52**(3): 324-327.

Durai, R., W. Yang, S. Gupta, A. Seifalian and M. Winslet (2005). "The role of the insulin-like growth factor system in colorectal cancer: review of current knowledge." Int J Colorectal Dis **20**(3): 203-220.

Eckstein, N., K. Servan, B. Hildebrandt, A. Pölitz, G. von Jonquières, S. Wolf-Kümmeth, I. Napierski, A. Hamacher, M. U. Kassack, J. Budczies, M. Beier, M. Dietel, B. Royer-Pokora, C. Denkert and H. D. Royer (2009). "Hyperactivation of the insulin-like growth factor receptor I signaling pathway is an essential event for cisplatin resistance of ovarian cancer cells." Cancer Res **69**(7): 2996-3003.

Eder, A. M., X. Sui, D. G. Rosen, L. K. Nolden, K. W. Cheng, J. P. Lahad, M. Kango-Singh, K. H. Lu, C. L. Warneke, E. N. Atkinson, I. Bedrosian, K. Keyomarsi, W. L. Kuo, J. W. Gray, J. C. Yin, J. Liu, G. Halder and G. B. Mills (2005). "Atypical PKCiota contributes to poor prognosis through loss of apical-basal polarity and cyclin E overexpression in ovarian cancer." Proc Natl Acad Sci U S A **102**(35): 12519-12524.

Edwards, S. M., Z. Kote-Jarai, J. Meitz, R. Hamoudi, Q. Hope, P. Osin, R. Jackson, C. Southgate, R. Singh, A. Falconer, D. P. Dearnaley, A. Ardern-Jones, A. Murkin, A. Dowe, J. Kelly, S.

Williams, R. Oram, M. Stevens, D. M. Teare, B. A. Ponder, S. A. Gayther, D. F. Easton, R. A. Eeles, C. R. U. B. P. G. U. F. P. C. S. Collaborators and B. A. o. U. S. S. o. Oncology (2003). "Two percent of men with early-onset prostate cancer harbor germline mutations in the BRCA2 gene." Am J Hum Genet **72**(1): 1-12.

Ewing, B. and P. Green (1998). "Base-calling of automated sequencer traces using phred. II. Error probabilities." Genome Res **8**(3): 186-194.

Eyre, R., R. Feltbower, E. Mubwandarikwa, H. Jenkinson, S. Parkes, J. Birch, T. Eden, P. James, P. McKinney, M. Pearce and R. McNally (2009). "Incidence and survival of childhood bone cancer in northern England and the West Midlands, 1981-2002." Br J Cancer **100**(1): 188-193.

Farmer, H., N. McCabe, C. J. Lord, A. N. Tutt, D. A. Johnson, T. B. Richardson, M. Santarosa, K. J. Dillon, I. Hickson, C. Knights, N. M. Martin, S. P. Jackson, G. C. Smith and A. Ashworth (2005). "Targeting the DNA repair defect in BRCA mutant cells as a therapeutic strategy." Nature **434**(7035): 917-921.

Fletcher, B., Hogendoorn, Mertens (2013). WHO Classification of Tumours of Soft Tissue and Bone, WHO Press.

Forbes, S. A., G. Bhamra, S. Bamford, E. Dawson, C. Kok, J. Clements, A. Menzies, J. W. Teague, P. A. Futreal and M. R. Stratton (2008). "The Catalogue of Somatic Mutations in Cancer (COSMIC)." Curr Protoc Hum Genet **Chapter 10**: Unit 10.11.

Frasca, F., G. Pandini, P. Scalia, L. Sciacca, R. Mineo, A. Costantino, I. D. Goldfine, A. Belfiore and R. Vigneri (1999). "Insulin receptor isoform A, a newly recognized, high-affinity insulin-like growth factor II receptor in fetal and cancer cells." Mol Cell Biol **19**(5): 3278-3288.

Friedenberger, M., M. Bode, A. Krusche and W. Schubert (2007). "Fluorescence detection of protein clusters in individual cells and tissue sections by using toponome imaging system: sample preparation and measuring procedures." Nat Protoc **2**(9): 2285-2294.

Fritz, R. D., Z. Varga and G. Radziwill (2010). "CNK1 is a novel Akt interaction partner that promotes cell proliferation through the Akt-FoxO signalling axis." Oncogene **29**(24): 3575-3582.

García-Aragoncillo, E., J. Carrillo, E. Lalli, N. Agra, G. Gómez-López, A. Pestaña and J. Alonso (2008). "DAX1, a direct target of EWS/FLI1 oncoprotein, is a principal regulator of cell-cycle progression in Ewing's tumor cells." Oncogene **27**(46): 6034-6043.

Garnett, M. J., E. J. Edelman, S. J. Heidorn, C. D. Greenman, A. Dastur, K. W. Lau, P. Greninger, I. R. Thompson, X. Luo, J. Soares, Q. Liu, F. Iorio, D. Surdez, L. Chen, R. J. Milano, G. R. Bignell, A. T. Tam, H. Davies, J. A. Stevenson, S. Barthorpe, S. R. Lutz, F. Kogera, K. Lawrence, A. McLaren-Douglas, X. Mitropoulos, T. Mironenko, H. Thi, L. Richardson, W. Zhou, F. Jewitt, T. Zhang, P. O'Brien, J. L. Boisvert, S. Price, W. Hur, W. Yang, X. Deng, A. Butler, H. G. Choi, J. W. Chang, J. Baselga, I. Stamenkovic, J. A. Engelman, S. V. Sharma, O. Delattre, J. Saez-Rodriguez, N. S. Gray, J. Settleman, P. A. Futreal, D. A. Haber, M. R. Stratton, S. Ramaswamy, U. McDermott and C. H. Benes (2012). "Systematic identification of genomic markers of drug sensitivity in cancer cells." Nature **483**(7391): 570-575.

Garofalo, C., M. C. Manara, G. Nicoletti, M. T. Marino, P. L. Lollini, A. Astolfi, G. Pandini, J. A. López-Guerrero, K. L. Schaefer, A. Belfiore, P. Picci and K. Scotlandi (2011). "Efficacy of and resistance to anti-IGF-1R therapies in Ewing's sarcoma is dependent on insulin receptor signaling." Oncogene **30**(24): 2730-2740.

Garofalo, C., C. Mancarella, A. Grilli, M. C. Manara, A. Astolfi, M. T. Marino, A. Conte, S. Sigismund, A. Carè, A. Belfiore, P. Picci and K. Scotlandi (2012). "Identification of common and distinctive mechanisms of resistance to different anti-IGF-IR agents in Ewing's sarcoma." Mol Endocrinol **26**(9): 1603-1616.

Gelin, C., F. Aubrit, A. Phalipon, B. Raynal, S. Cole, M. Kaczorek and A. Bernard (1989). "The E2 antigen, a 32 kd glycoprotein involved in T-cell adhesion processes, is the MIC2 gene product." EMBO J **8**(11): 3253-3259.

Gerlinger, M., A. J. Rowan, S. Horswell, J. Larkin, D. Endesfelder, E. Gronroos, P. Martinez, N. Matthews, A. Stewart, P. Tarpey, I. Varela, B. Phillimore, S. Begum, N. Q. McDonald, A. Butler, D. Jones, K. Raine, C. Latimer, C. R. Santos, M. Nohadani, A. C. Eklund, B. Spencer-Dene, G. Clark, L. Pickering, G. Stamp, M. Gore, Z. Szallasi, J. Downward, P. A. Futreal and C. Swanton (2012). "Intratumor heterogeneity and branched evolution revealed by multiregion sequencing." N Engl J Med **366**(10): 883-892.

Gerlinger, M., A. J. Rowan, S. Horswell, J. Larkin, D. Endesfelder, E. Gronroos, P. Martinez, N. Matthews, A. Stewart, P. Tarpey, I. Varela, B. Phillimore, S. Begum, N. Q. McDonald, A. Butler, D. Jones, K. Raine, C. Latimer, C. R. Santos, M. Nohadani, A. C. Eklund, B. Spencer-Dene, G. Clark, L. Pickering, G. Stamp, M. Gore, Z. Szallasi, J. Downward, P. A. Futreal and C. Swanton (2012). "Intratumor heterogeneity and branched evolution revealed by multiregion sequencing." N Engl J Med **366**(10): 883-892.

Ginestier, C., M. H. Hur, E. Charafe-Jauffret, F. Monville, J. Dutcher, M. Brown, J. Jacquemier, P. Viens, C. G. Kleer, S. Liu, A. Schott, D. Hayes, D. Birnbaum, M. S. Wicha and G. Dontu (2007). "ALDH1 is a marker of normal and malignant human mammary stem cells and a predictor of poor clinical outcome." Cell Stem Cell **1**(5): 555-567.

Ginty, F., S. Adak, A. Can, M. Gerdes, M. Larsen, H. Cline, R. Filkins, Z. Pang, Q. Li and M. C. Montalto (2008). "The relative distribution of membranous and cytoplasmic met is a prognostic indicator in stage I and II colon cancer." Clin Cancer Res **14**(12): 3814-3822.

Gonçalves, A., G. Monges, Y. Yang, F. Palmerini, P. Dubreuil, T. Noguchi, J. Jacquemier, D. Di Stefano, J. R. Delpero, H. Sobol and F. Bertucci (2006). "Response of a KIT-positive extra-abdominal fibromatosis to imatinib mesylate and KIT genetic analysis." J Natl Cancer Inst **98**(8): 562-563.

Gore, M. E. and J. M. Larkin (2011). "Challenges and opportunities for converting renal cell carcinoma into a chronic disease with targeted therapies." Br J Cancer **104**(3): 399-406.

Gorre, M. E., M. Mohammed, K. Ellwood, N. Hsu, R. Paquette, P. N. Rao and C. L. Sawyers (2001). "Clinical resistance to STI-571 cancer therapy caused by BCR-ABL gene mutation or amplification." Science **293**(5531): 876-880.

Greaves, M. and C. C. Maley (2012). "Clonal evolution in cancer." Nature **481**(7381): 306-313.

Grier, H. (1997). "The Ewing family of tumors. Ewing's sarcoma and primitive neuroectodermal tumors." Pediatr Clin North Am **44**(4): 991-1004.

Grohar, P. J., G. M. Woldemichael, L. B. Griffin, A. Mendoza, Q. R. Chen, C. Yeung, D. G. Currier, S. Davis, C. Khanna, J. Khan, J. B. McMahon and L. J. Helman (2011). "Identification of an inhibitor of the EWS-FLI1 oncogenic transcription factor by high-throughput screening." J Natl Cancer Inst **103**(12): 962-978.

Gu, F., R. M. Pfeiffer, S. Bhattacharjee, S. S. Han, P. R. Taylor, S. Berndt, H. Yang, A. J. Sigurdson, J. Toro, L. Mirabello, M. H. Greene, N. D. Freedman, C. C. Abnet, S. M. Dawsey, N. Hu, Y. L. Qiao, T. Ding, A. V. Brenner, M. Garcia-Closas, R. Hayes, L. A. Brinton, J. Lissowska, N. Wentzensen, C. Kratz, L. E. Moore, R. G. Ziegler, W. H. Chow, S. A. Savage, L. Burdette, M. Yeager, S. J. Chanock, N. Chatterjee, M. A. Tucker, A. M. Goldstein and X. R. Yang (2013). "Common genetic variants in the 9p21 region and their associations with multiple tumours." Br J Cancer **108**(6): 1378-1386.

Gudkov, A. V., A. R. Kazarov, R. Thimmapaya, S. A. Axenovich, I. A. Mazo and I. B. Roninson (1994). "Cloning mammalian genes by expression selection of genetic suppressor elements: association of kinesin with drug resistance and cell immortalization." Proc Natl Acad Sci U S A **91**(9): 3744-3748.

Gupta, P. B., C. M. Fillmore, G. Jiang, S. D. Shapira, K. Tao, C. Kuperwasser and E. S. Lander (2011). "Stochastic state transitions give rise to phenotypic equilibrium in populations of cancer cells." Cell **146**(4): 633-644.

Gurcan, M. N., L. E. Boucheron, A. Can, A. Madabhushi, N. M. Rajpoot and B. Yener (2009). "Histopathological image analysis: a review." IEEE Rev Biomed Eng **2**: 147-171.

Guy, J., T. Hearn, M. Crosier, J. Mudge, L. Viggiano, D. Koczan, H. J. Thiesen, J. A. Bailey, J. E. Horvath, E. E. Eichler, M. E. Earthrowl, P. Deloukas, L. French, J. Rogers, D. Bentley and M. S. Jackson (2003). "Genomic sequence and transcriptional profile of the boundary between pericentromeric satellites and genes on human chromosome arm 10p." Genome Res **13**(2): 159-172.

Hafner, M., A. Schmitz, I. Grüne, S. G. Srivatsan, B. Paul, W. Kolanus, T. Quast, E. Kremmer, I. Bauer and M. Famulok (2006). "Inhibition of cytohesins by SecinH3 leads to hepatic insulin resistance." Nature **444**(7121): 941-944.

Hanahan, D. and R. A. Weinberg (2011). "Hallmarks of cancer: the next generation." Cell **144**(5): 646-674.

Hankinson, S., W. Willett, G. Colditz, D. Hunter, D. Michaud, B. Deroo, B. Rosner, F. Speizer and M. Pollak (1998). "Circulating concentrations of insulin-like growth factor-I and risk of breast cancer." Lancet **351**(9113): 1393-1396.

Haverty, P. M., L. S. Hon, J. S. Kaminker, J. Chant and Z. Zhang (2009). "High-resolution analysis of copy number alterations and associated expression changes in ovarian tumors." BMC Med Genomics **2**: 21.

Hennessy, B. T., D. L. Smith, P. T. Ram, Y. Lu and G. B. Mills (2005). "Exploiting the PI3K/AKT pathway for cancer drug discovery." Nat Rev Drug Discov **4**(12): 988-1004.

Hirota, S., K. Isozaki, Y. Moriyama, K. Hashimoto, T. Nishida, S. Ishiguro, K. Kawano, M. Hanada, A. Kurata, M. Takeda, G. Muhammad Tunio, Y. Matsuzawa, Y. Kanakura, Y. Shinomura and Y. Kitamura (1998). "Gain-of-function mutations of c-kit in human gastrointestinal stromal tumors." Science **279**(5350): 577-580.

Hitchman, E., C. Hodgkinson, D. Roberts, G. Ashton, Z. Yunus, R. Byers, T. Ward, C. Womack and C. Dive (2011). "Effect of prolonged formalin fixation on immunohistochemical staining for the proliferation marker Ki67." Histopathology **59**(6): 1261-1263.

Hou, Y., L. Song, P. Zhu, B. Zhang, Y. Tao, X. Xu, F. Li, K. Wu, J. Liang, D. Shao, H. Wu, X. Ye, C. Ye, R. Wu, M. Jian, Y. Chen, W. Xie, R. Zhang, L. Chen, X. Liu, X. Yao, H. Zheng, C. Yu, Q.

Li, Z. Gong, M. Mao, X. Yang, L. Yang, J. Li, W. Wang, Z. Lu, N. Gu, G. Laurie, L. Bolund, K. Kristiansen, J. Wang, H. Yang, Y. Li and X. Zhang (2012). "Single-cell exome sequencing and monoclonal evolution of a JAK2-negative myeloproliferative neoplasm." Cell **148**(5): 873-885.

Hsu, F., T. Nielsen, A. Alkushi, B. Dupuis, D. Huntsman, C. Liu, M. van de Rijn and C. Gilks (2002). "Tissue microarrays are an effective quality assurance tool for diagnostic immunohistochemistry." Mod Pathol **15**(12): 1374-1380.

Huang, E. H., M. J. Hynes, T. Zhang, C. Ginestier, G. Dontu, H. Appelman, J. Z. Fields, M. S. Wicha and B. M. Boman (2009). "Aldehyde dehydrogenase 1 is a marker for normal and malignant human colonic stem cells (SC) and tracks SC overpopulation during colon tumorigenesis." Cancer Res **69**(8): 3382-3389.

Huang, F., A. Greer, W. Hurlburt, X. Han, R. Hafezi, G. M. Wittenberg, K. Reeves, J. Chen, D. Robinson, A. Li, F. Y. Lee, M. M. Gottardis, E. Clark, L. Helman, R. M. Attar, A. Dongre and J. M. Carboni (2009). "The mechanisms of differential sensitivity to an insulin-like growth factor-1 receptor inhibitor (BMS-536924) and rationale for combining with EGFR/HER2 inhibitors." Cancer Res **69**(1): 161-170.

Huang, H. J., L. S. Angelo, J. Rodon, M. Sun, K. P. Kuenkele, H. A. Parsons, J. C. Trent and R. Kurzrock (2011). "R1507, an anti-insulin-like growth factor-1 receptor (IGF-1R) antibody, and EWS/FLI-1 siRNA in Ewing's sarcoma: convergence at the IGF/IGFR/Akt axis." PLoS One **6**(10): e26060.

Huang, H. Y., P. B. Illei, Z. Zhao, M. Mazumdar, A. G. Huvos, J. H. Healey, L. H. Wexler, R. Gorlick, P. Meyers and M. Ladanyi (2005). "Ewing sarcomas with p53 mutation or p16/p14ARF homozygous deletion: a highly lethal subset associated with poor chemoresponse." J Clin Oncol **23**(3): 548-558.

Hudler, P., N. Kocevar and R. Komel (2014). "Proteomic Approaches in Biomarker Discovery: New Perspectives in Cancer Diagnostics." ScientificWorldJournal **2014**: 260348.

Hughes, P., D. Marshall, Y. Reid, H. Parkes and C. Gelber (2007). "The costs of using unauthenticated, over-passaged cell lines: how much more data do we need?" Biotechniques **43**(5): 575, 577-578, 581-572 passim.

Iida, K., J. Fukushi, Y. Matsumoto, Y. Oda, Y. Takahashi, T. Fujiwara, Y. Fujiwara-Okada, M. Hatano, A. Nabashima, S. Kamura and Y. Iwamoto (2013). "miR-125b develops chemoresistance in Ewing sarcoma/primitive neuroectodermal tumor." Cancer Cell Int **13**(1): 21.

Irish, J. M., R. Hovland, P. O. Krutzik, O. D. Perez, Ø. Bruserud, B. T. Gjertsen and G. P. Nolan (2004). "Single cell profiling of potentiated phospho-protein networks in cancer cells." Cell **118**(2): 217-228.

Joseph, E. W., C. A. Pratilas, P. I. Poulikakos, M. Tadi, W. Wang, B. S. Taylor, E. Halilovic, Y. Persaud, F. Xing, A. Viale, J. Tsai, P. B. Chapman, G. Bollag, D. B. Solit and N. Rosen (2010). "The RAF inhibitor PLX4032 inhibits ERK signaling and tumor cell proliferation in a V600E BRAF-selective manner." Proc Natl Acad Sci U S A **107**(33): 14903-14908.

Juergens, C., C. Weston, I. Lewis, J. Whelan, M. Paulussen, O. Oberlin, J. Michon, A. Zoubek, H. Juergens and A. Craft (2006). "Safety assessment of intensive induction with vincristine, ifosfamide, doxorubicin, and etoposide (VIDE) in the treatment of Ewing tumors in the EURO-E.W.I.N.G. 99 clinical trial." Pediatr Blood Cancer **47**(1): 22-29.

Juergens, H., N. C. Daw, B. Geoerger, S. Ferrari, M. Villarroel, I. Aerts, J. Whelan, U. Dirksen, M. L. Hixon, D. Yin, T. Wang, S. Green, L. Paccagnella and A. Gualberto (2011). "Preliminary efficacy of the anti-insulin-like growth factor type 1 receptor antibody figitumumab in patients with refractory Ewing sarcoma." J Clin Oncol **29**(34): 4534-4540.

Juergens, H., N. C. Daw, B. Geoerger, S. Ferrari, M. Villarroel, I. Aerts, J. Whelan, U. Dirksen, M. L. Hixon, D. Yin, T. Wang, S. Green, L. Paccagnella and A. Gualberto (2011). "Preliminary efficacy of the anti-insulin-like growth factor type 1 receptor antibody figitumumab in patients with refractory Ewing sarcoma." J Clin Oncol **29**(34): 4534-4540.

Kallioniemi, A., T. Visakorpi, R. Karhu, D. Pinkel and O. P. Kallioniemi (1996). "Gene Copy Number Analysis by Fluorescence in Situ Hybridization and Comparative Genomic Hybridization." Methods **9**(1): 113-121.

Kamalakaran, S., V. Varadan, A. Janevski, N. Banerjee, D. Tuck, W. R. McCombie, N. Dimitrova and L. N. Harris (2013). "Translating next generation sequencing to practice: Opportunities and necessary steps." Mol Oncol **7**(4): 743-755.

Kanagal-Shamanna, R., B. P. Portier, R. R. Singh, M. J. Routbort, K. D. Aldape, B. A. Handal, H. Rahimi, N. G. Reddy, B. A. Barkoh, B. M. Mishra, A. V. Paladugu, J. H. Manekia, N. Kalhor, S. R. Chowdhuri, G. A. Staerkel, L. J. Medeiros, R. Luthra and K. P. Patel (2013). "Next-generation sequencing-based multi-gene mutation profiling of solid tumors using fine needle aspiration samples: promises and challenges for routine clinical diagnostics." Mod Pathol.

Kanai, Y. (2010). "Genome-wide DNA methylation profiles in precancerous conditions and cancers." Cancer Sci **101**(1): 36-45.

Kass, M., A. Witkin and T. D (1988). Snakes: active contour models. Int J Comput Vis. **4:** 321-331.

Katayama, R., T. M. Khan, C. Benes, E. Lifshits, H. Ebi, V. M. Rivera, W. C. Shakespeare, A. J. Iafrate, J. A. Engelman and A. T. Shaw (2011). "Therapeutic strategies to overcome crizotinib resistance in non-small cell lung cancers harboring the fusion oncogene EML4-ALK." Proc Natl Acad Sci U S A **108**(18): 7535-7540.

Kauer, M., J. Ban, R. Kofler, B. Walker, S. Davis, P. Meltzer and H. Kovar (2009). "A molecular function map of Ewing's sarcoma." PLoS One **4**(4): e5415.

Kent, W. J. (2002). "BLAT--the BLAST-like alignment tool." Genome Res **12**(4): 656-664.

Keysar, S. B. and A. Jimeno (2010). "More than markers: biological significance of cancer stem cell-defining molecules." Mol Cancer Ther **9**(9): 2450-2457.

Kinsey, M., R. Smith, A. Iyer, E. McCabe and S. Lessnick (2009). "EWS/FLI and its downstream target NR0B1 interact directly to modulate transcription and oncogenesis in Ewing's sarcoma." Cancer Res **69**(23): 9047-9055.

Kovar, H., D. Aryee, G. Jug, C. Henöckl, M. Schemper, O. Delattre, G. Thomas and H. Gadner (1996). "EWS/FLI-1 antagonists induce growth inhibition of Ewing tumor cells in vitro." Cell Growth Differ **7**(4): 429-437.

Kreso, A., C. A. O'Brien, P. van Galen, O. I. Gan, F. Notta, A. M. Brown, K. Ng, J. Ma, E. Wienholds, C. Dunant, A. Pollett, S. Gallinger, J. McPherson, C. G. Mullighan, D. Shibata and J. E. Dick (2013). "Variable clonal repopulation dynamics influence chemotherapy response in colorectal cancer." Science **339**(6119): 543-548.

Krzywinski, M., J. Schein, I. Birol, J. Connors, R. Gascoyne, D. Horsman, S. J. Jones and M. A. Marra (2009). "Circos: an information aesthetic for comparative genomics." Genome Res **19**(9): 1639-1645.

Krüger, S., M. Emig, P. Lohse, G. Ehninger, A. Hochhaus and H. K. Schackert (2006). "The c-kit (CD117) sequence variation M541L, but not N564K, is frequent in the general population, and is not associated with CML in Caucasians." Leukemia **20**(2): 354-355; discussion 356-357.

Kurmasheva, R. T., L. Dudkin, C. Billups, L. V. Debelenko, C. L. Morton and P. J. Houghton (2009). "The insulin-like growth factor-1 receptor-targeting antibody, CP-751,871, suppresses tumor-derived VEGF and synergizes with rapamycin in models of childhood sarcoma." Cancer Res **69**(19): 7662-7671.

Kwak, E. L., Y. J. Bang, D. R. Camidge, A. T. Shaw, B. Solomon, R. G. Maki, S. H. Ou, B. J. Dezube, P. A. Jänne, D. B. Costa, M. Varella-Garcia, W. H. Kim, T. J. Lynch, P. Fidias, H. Stubbs, J. A. Engelman, L. V. Sequist, W. Tan, L. Gandhi, M. Mino-Kenudson, G. C. Wei, S. M. Shreeve, M. J. Ratain, J. Settleman, J. G. Christensen, D. A. Haber, K. Wilner, R. Salgia, G. I. Shapiro, J. W. Clark and A. J. Iafrate (2010). "Anaplastic lymphoma kinase inhibition in non-small-cell lung cancer." N Engl J Med **363**(18): 1693-1703.

Ladenstein, R., U. Pötschger, M. C. Le Deley, J. Whelan, M. Paulussen, O. Oberlin, H. van den Berg, U. Dirksen, L. Hjorth, J. Michon, I. Lewis, A. Craft and H. Jürgens (2010). "Primary disseminated multifocal Ewing sarcoma: results of the Euro-EWING 99 trial." J Clin Oncol **28**(20): 3284-3291.

Landi, D., F. Gemignani, B. Pardini, A. Naccarati, S. Garritano, P. Vodicka, L. Vodickova, F. Canzian, J. Novotny, R. Barale and S. Landi (2012). "Identification of candidate genes carrying polymorphisms associated with the risk of colorectal cancer by analyzing the colorectal mutome and microRNAome." Cancer **118**(19): 4670-4680.

Langmead, B., C. Trapnell, M. Pop and S. L. Salzberg (2009). "Ultrafast and memory-efficient alignment of short DNA sequences to the human genome." Genome Biol **10**(3): R25.

Lanigan, T. M., A. Liu, Y. Z. Huang, L. Mei, B. Margolis and K. L. Guan (2003). "Human homologue of Drosophila CNK interacts with Ras effector proteins Raf and Rlf." FASEB J **17**(14): 2048-2060.

Le Deley, M., O. Delattre, K. Schaefer, S. Burchill, G. Koehler, P. Hogendoorn, T. Lion, C. Poremba, J. Marandet, S. Ballet, G. Pierron, S. Brownhill, M. Nesslböck, A. Ranft, U. Dirksen, O. Oberlin, I. Lewis, A. Craft, H. Jürgens and H. Kovar (2010). "Impact of EWS-ETS fusion type on disease progression in Ewing's sarcoma/peripheral primitive neuroectodermal tumor: prospective results from the cooperative Euro-E.W.I.N.G. 99 trial." J Clin Oncol **28**(12): 1982-1988.

Le Magnen, C., L. Bubendorf, C. A. Rentsch, C. Mengus, J. Gsponer, T. Zellweger, M. Rieken, G. N. Thalmann, M. G. Cecchini, M. Germann, A. Bachmann, S. Wyler, M. Heberer and G. C. Spagnoli (2013). "Characterization and Clinical Relevance of ALDHbright Populations in Prostate Cancer." Clin Cancer Res.

Leacock, S. W., A. N. Basse, G. L. Chandler, A. M. Kirk, D. Rakheja and J. F. Amatruda (2012). "A zebrafish transgenic model of Ewing's sarcoma reveals conserved mediators of EWS-FLI1 tumorigenesis." Dis Model Mech **5**(1): 95-106.

Levin, J. Z., M. F. Berger, X. Adiconis, P. Rogov, A. Melnikov, T. Fennell, C. Nusbaum, L. A. Garraway and A. Gnirke (2009). "Targeted next-generation sequencing of a cancer transcriptome enhances detection of sequence variants and novel fusion transcripts." Genome Biol **10**(10): R115.

Levine, A. J. and M. Oren (2009). "The first 30 years of p53: growing ever more complex." Nat Rev Cancer **9**(10): 749-758.

Lim, J., M. Zhou, T. D. Veenstra and D. K. Morrison (2010). "The CNK1 scaffold binds cytohesins and promotes insulin pathway signaling." Genes Dev **24**(14): 1496-1506.

Lin, P., M. Pandey, F. Jin, S. Xiong, M. Deavers, J. Parant and G. Lozano (2008). "EWS-FLI1 induces developmental abnormalities and accelerates sarcoma formation in a transgenic mouse model." Cancer Res **68**(21): 8968-8975.

Lin, P. P., M. K. Pandey, F. Jin, S. Xiong, M. Deavers, J. M. Parant and G. Lozano (2008). "EWS-FLI1 induces developmental abnormalities and accelerates sarcoma formation in a transgenic mouse model." Cancer Res **68**(21): 8968-8975.

Liu, C., J. Yao, I. de Belle, R. P. Huang, E. Adamson and D. Mercola (1999). "The transcription factor EGR-1 suppresses transformation of human fibrosarcoma HT1080 cells by coordinated induction of transforming growth factor-beta1, fibronectin, and plasminogen activator inhibitor-1." J Biol Chem **274**(7): 4400-4411.

Liu, L., P. L. Channavajhala, V. R. Rao, I. Moutsatsos, L. Wu, Y. Zhang, L. L. Lin and Y. Qiu (2009). "Proteomic characterization of the dynamic KSR-2 interactome, a signaling scaffold complex in MAPK pathway." Biochim Biophys Acta **1794**(10): 1485-1495.

Lizard-Nacol, S., G. Lizard, E. Justrabo and C. Turc-Carel (1989). "Immunologic characterization of Ewing's sarcoma using mesenchymal and neural markers." Am J Pathol **135**(5): 847-855.

Lopez-Guerrero, J. A., I. Machado, K. Scotlandi, R. Noguera, A. Pellin, S. Navarro, M. Serra, S. Calabuig-Farinas, P. Picci and A. Llombart-Bosch (2011). "Clinicopathological significance of cell cycle regulation markers in a large series of genetically confirmed Ewing's sarcoma family of tumors." Int J Cancer **128**(5): 1139-1150.

Lovly, C. M. and A. T. Shaw (2014). "Molecular pathways: resistance to kinase inhibitors and implications for therapeutic strategies." Clin Cancer Res **20**(9): 2249-2256.

Lynch, T. J., D. W. Bell, R. Sordella, S. Gurubhagavatula, R. A. Okimoto, B. W. Brannigan, P. L. Harris, S. M. Haserlat, J. G. Supko, F. G. Haluska, D. N. Louis, D. C. Christiani, J. Settleman and D. A. Haber (2004). "Activating mutations in the epidermal growth factor receptor underlying responsiveness of non-small-cell lung cancer to gefitinib." N Engl J Med **350**(21): 2129-2139.

Mackintosh, C., J. L. Ordonez, D. J. Garcia-Dominguez, V. Sevillano, A. Llombart-Bosch, K. Szuhai, K. Scotlandi, M. Alberghini, R. Sciot, F. Sinnaeve, P. C. Hogendoorn, P. Picci, S. Knuutila, U. Dirksen, M. Debiec-Rychter, K. L. Schaefer and E. de Alava (2012). "1q gain and CDT2 overexpression underlie an aggressive and highly proliferative form of Ewing sarcoma." Oncogene **31**(10): 1287-1298.

Mackintosh, C., J. L. Ordóñez, D. J. García-Domínguez, V. Sevillano, A. Llombart-Bosch, K. Szuhai, K. Scotlandi, M. Alberghini, R. Sciot, F. Sinnaeve, P. C. Hogendoorn, P. Picci, S. Knuutila, U. Dirksen, M. Debiec-Rychter, K. L. Schaefer and E. de Álava (2012). "1q gain and CDT2 overexpression underlie an aggressive and highly proliferative form of Ewing sarcoma." Oncogene **31**(10): 1287-1298.

Maher, C. A., N. Palanisamy, J. C. Brenner, X. Cao, S. Kalyana-Sundaram, S. Luo, I. Khrebtukova, T. R. Barrette, C. Grasso, J. Yu, R. J. Lonigro, G. Schroth, C. Kumar-Sinha and A. M. Chinnaiyan (2009). "Chimeric transcript discovery by paired-end transcriptome sequencing." Proc Natl Acad Sci U S A **106**(30): 12353-12358.

Malempati, S., B. Weigel, A. M. Ingle, C. H. Ahern, J. M. Carroll, C. T. Roberts, J. M. Reid, S. Schmechel, S. D. Voss, S. Y. Cho, H. X. Chen, M. D. Krailo, P. C. Adamson and S. M. Blaney (2012). "Phase I/II trial and pharmacokinetic study of cixutumumab in pediatric patients with refractory solid tumors and Ewing sarcoma: a report from the Children's Oncology Group." J Clin Oncol **30**(3): 256-262.

Malpica, N., C. O. de Solórzano, J. J. Vaquero, A. Santos, I. Vallcorba, J. M. García-Sagredo and F. del Pozo (1997). "Applying watershed algorithms to the segmentation of clustered nuclei." Cytometry **28**(4): 289-297.

Manara, M. C., S. Perdichizzi, M. Serra, R. Pierini, S. Benini, C. M. Hattinger, A. Astolfi, R. Bagnati, M. D'Incalci, P. Picci and K. Scotlandi (2005). "The molecular mechanisms responsible for resistance to ET-743 (Trabectidin; Yondelis) in the Ewing's sarcoma cell line, TC-71." Int J Oncol **27**(6): 1605-1616.

Margulies, M., M. Egholm, W. E. Altman, S. Attiya, J. S. Bader, L. A. Bemben, J. Berka, M. S. Braverman, Y. J. Chen, Z. Chen, S. B. Dewell, L. Du, J. M. Fierro, X. V. Gomes, B. C. Godwin, W. He, S. Helgesen, C. H. Ho, G. P. Irzyk, S. C. Jando, M. L. Alenquer, T. P. Jarvie, K. B. Jirage, J. B. Kim, J. R. Knight, J. R. Lanza, J. H. Leamon, S. M. Lefkowitz, M. Lei, J. Li, K. L. Lohman, H. Lu, V. B. Makhijani, K. E. McDade, M. P. McKenna, E. W. Myers, E. Nickerson, J. R. Nobile, R. Plant, B. P. Puc, M. T. Ronan, G. T. Roth, G. J. Sarkis, J. F. Simons, J. W. Simpson, M. Srinivasan, K. R. Tartaro, A. Tomasz, K. A. Vogt, G. A. Volkmer, S. H. Wang, Y. Wang, M. P. Weiner, P. Yu, R. F. Begley and J. M. Rothberg (2005). "Genome sequencing in microfabricated high-density picolitre reactors." Nature **437**(7057): 376-380.

Martins, A. S., C. Mackintosh, D. H. Martín, M. Campos, T. Hernández, J. L. Ordóñez and E. de Alava (2006). "Insulin-like growth factor I receptor pathway inhibition by ADW742, alone or in combination with imatinib, doxorubicin, or vincristine, is a novel therapeutic approach in Ewing tumor." Clin Cancer Res **12**(11 Pt 1): 3532-3540.

Martínez-Ramírez, A., S. Rodríguez-Perales, B. Meléndez, B. Martínez-Delgado, M. Urioste, J. C. Cigudosa and J. Benítez (2003). "Characterization of the A673 cell line (Ewing tumor) by molecular cytogenetic techniques." Cancer Genet Cytogenet **141**(2): 138-142.

McCabe, N., N. C. Turner, C. J. Lord, K. Kluzek, A. Bialkowska, S. Swift, S. Giavara, M. J. O'Connor, A. N. Tutt, M. Z. Zdzienicka, G. C. Smith and A. Ashworth (2006). "Deficiency in the repair of DNA damage by homologous recombination and sensitivity to poly(ADP-ribose) polymerase inhibition." Cancer Res **66**(16): 8109-8115.

McCubrey, J. A., L. S. Steelman, W. H. Chappell, S. L. Abrams, E. W. Wong, F. Chang, B. Lehmann, D. M. Terrian, M. Milella, A. Tafuri, F. Stivala, M. Libra, J. Basecke, C. Evangelisti, A. M. Martelli and R. A. Franklin (2007). "Roles of the Raf/MEK/ERK pathway in cell growth, malignant transformation and drug resistance." Biochim Biophys Acta **1773**(8): 1263-1284.

McKeon, C., C. Thiele, R. Ross, M. Kwan, T. Triche, J. Miser and M. Israel (1988). "Indistinguishable patterns of protooncogene expression in two distinct but closely related tumors: Ewing's sarcoma and neuroepithelioma." Cancer Res **48**(15): 4307-4311.

Menear, K. A., C. Adcock, R. Boulter, X. L. Cockcroft, L. Copsey, A. Cranston, K. J. Dillon, J. Drzewiecki, S. Garman, S. Gomez, H. Javaid, F. Kerrigan, C. Knights, A. Lau, V. M. Loh, I. T. Matthews, S. Moore, M. J. O'Connor, G. C. Smith and N. M. Martin (2008). "4-[3-(4-cyclopropanecarbonylpiperazine-1-carbonyl)-4-fluorobenzyl]-2H-phthalazin-1-one: a novel bioavailable inhibitor of poly(ADP-ribose) polymerase-1." J Med Chem **51**(20): 6581-6591.

Merchant, M. S., C. W. Woo, C. L. Mackall and C. J. Thiele (2002). "Potential use of imatinib in Ewing's Sarcoma: evidence for in vitro and in vivo activity." J Natl Cancer Inst **94**(22): 1673-1679.

Metzker, M. L. (2010). "Sequencing technologies - the next generation." Nat Rev Genet **11**(1): 31-46.

Milojkovic, D. and J. Apperley (2009). "Mechanisms of Resistance to Imatinib and Second-Generation Tyrosine Inhibitors in Chronic Myeloid Leukemia." Clin Cancer Res **15**(24): 7519-7527.

Minsky, M. (1988). Memoir on Inventing the Confocal Scanning Microscopy. Scanning. **10:** 128-138.

Miyagawa, Y., H. Okita, H. Nakaijima, Y. Horiuchi, B. Sato, T. Taguchi, M. Toyoda, Y. Katagiri, J. Fujimoto, J. Hata, A. Umezawa and N. Kiyokawa (2008). "Inducible expression of chimeric EWS/ETS proteins confers Ewing's family tumor-like phenotypes to human mesenchymal progenitor cells." Mol Cell Biol **28**(7): 2125-2137.

Moller, D. E., A. Yokota, J. F. Caro and J. S. Flier (1989). "Tissue-specific expression of two alternatively spliced insulin receptor mRNAs in man." Mol Endocrinol **3**(8): 1263-1269.

Molofsky, A. V., R. Pardal, T. Iwashita, I. K. Park, M. F. Clarke and S. J. Morrison (2003). "Bmi-1 dependence distinguishes neural stem cell self-renewal from progenitor proliferation." Nature **425**(6961): 962-967.

Momand, J., D. Jung, S. Wilczynski and J. Niland (1998). "The MDM2 gene amplification database." Nucleic Acids Res **26**(15): 3453-3459.

Moreb, J. S. (2008). "Aldehyde dehydrogenase as a marker for stem cells." Curr Stem Cell Res Ther **3**(4): 237-246.

Morin, R., M. Bainbridge, A. Fejes, M. Hirst, M. Krzywinski, T. Pugh, H. McDonald, R. Varhol, S. Jones and M. Marra (2008). "Profiling the HeLa S3 transcriptome using randomly primed cDNA and massively parallel short-read sequencing." Biotechniques **45**(1): 81-94.

Morris, S. W., M. N. Kirstein, M. B. Valentine, K. G. Dittmer, D. N. Shapiro, D. L. Saltman and A. T. Look (1994). "Fusion of a kinase gene, ALK, to a nucleolar protein gene, NPM, in non-Hodgkin's lymphoma." Science **263**(5151): 1281-1284.

Mortazavi, A., B. A. Williams, K. McCue, L. Schaeffer and B. Wold (2008). "Mapping and quantifying mammalian transcriptomes by RNA-Seq." Nat Methods **5**(7): 621-628.

Muteeb, G. and R. Sen (2010). "Random mutagenesis using a mutator strain." Methods Mol Biol **634**: 411-419.

Nagase, T., N. Seki, K. Ishikawa, A. Tanaka and N. Nomura (1996). "Prediction of the coding sequences of unidentified human genes. V. The coding sequences of 40 new genes (KIAA0161-KIAA0200) deduced by analysis of cDNA clones from human cell line KG-1." DNA Res **3**(1): 17-24.

Navin, N. E. and J. Hicks (2010). "Tracing the tumor lineage." Mol Oncol **4**(3): 267-283.

Neumeister, V. M., V. Anagnostou, S. Siddiqui, A. M. England, E. R. Zarrella, M. Vassilakopoulou, F. Parisi, Y. Kluger, D. G. Hicks and D. L. Rimm (2012). "Quantitative

assessment of effect of preanalytic cold ischemic time on protein expression in breast cancer tissues." J Natl Cancer Inst **104**(23): 1815-1824.

Niedan, S., M. Kauer, D. N. Aryee, R. Kofler, R. Schwentner, A. Meier, U. Pötschger, U. Kontny and H. Kovar (2013). "Suppression of FOXO1 is responsible for a growth regulatory repressive transcriptional sub-signature of EWS-FLI1 in Ewing sarcoma." Oncogene.

O'Neill, R. A., A. Bhamidipati, X. Bi, D. Deb-Basu, L. Cahill, J. Ferrante, E. Gentalen, M. Glazer, J. Gossett, K. Hacker, C. Kirby, J. Knittle, R. Loder, C. Mastroieni, M. Maclaren, T. Mills, U. Nguyen, N. Parker, A. Rice, D. Roach, D. Suich, D. Voehringer, K. Voss, J. Yang, T. Yang and P. B. Vander Horn (2006). "Isoelectric focusing technology quantifies protein signaling in 25 cells." Proc Natl Acad Sci U S A **103**(44): 16153-16158.

Okada, T., K. Tanaka, F. Nakatani, R. Sakimura, T. Matsunobu, X. Li, M. Hanada, T. Nakamura, Y. Oda, M. Tsuneyoshi and Y. Iwamoto (2006). "Involvement of P-glycoprotein and MRP1 in resistance to cyclic tetrapeptide subfamily of histone deacetylase inhibitors in the drug-resistant osteosarcoma and Ewing's sarcoma cells." Int J Cancer **118**(1): 90-97.

Olmos, D., S. Postel-Vinay, L. R. Molife, S. H. Okuno, S. M. Schuetze, M. L. Paccagnella, G. N. Batzel, D. Yin, K. Pritchard-Jones, I. Judson, F. P. Worden, A. Gualberto, M. Scurr, J. S. de Bono and P. Haluska (2010). "Safety, pharmacokinetics, and preliminary activity of the anti-IGF-1R antibody figitumumab (CP-751,871) in patients with sarcoma and Ewing's sarcoma: a phase 1 expansion cohort study." Lancet Oncol **11**(2): 129-135.

Olshen, A. B., E. S. Venkatraman, R. Lucito and M. Wigler (2004). "Circular binary segmentation for the analysis of array-based DNA copy number data." Biostatistics **5**(4): 557-572.

Ottaviano, L., K. L. Schaefer, M. Gajewski, W. Huckenbeck, S. Baldus, U. Rogel, C. Mackintosh, E. de Alava, O. Myklebost, S. H. Kresse, L. A. Meza-Zepeda, M. Serra, A. M. Cleton-Jansen, P. C. Hogendoorn, H. Buerger, T. Aigner, H. E. Gabbert and C. Poremba (2010). "Molecular characterization of commonly used cell lines for bone tumor research: a trans-European EuroBoNet effort." Genes Chromosomes Cancer **49**(1): 40-51.

Owen, L., A. Kowalewski and S. Lessnick (2008). "EWS/FLI mediates transcriptional repression via NKX2.2 during oncogenic transformation in Ewing's sarcoma." PLoS One **3**(4): e1965.

Ozvegy-Laczka, C., J. Cserepes, N. B. Elkind and B. Sarkadi (2005). "Tyrosine kinase inhibitor resistance in cancer: role of ABC multidrug transporters." Drug Resist Updat **8**(1-2): 15-26.

Pappo, A. S., S. R. Patel, J. Crowley, D. K. Reinke, K. P. Kuenkele, S. P. Chawla, G. C. Toner, R. G. Maki, P. A. Meyers, R. Chugh, K. N. Ganjoo, S. M. Schuetze, H. Juergens, M. G. Leahy, B. Geoerger, R. S. Benjamin, L. J. Helman and L. H. Baker (2011). "R1507, a monoclonal antibody to the insulin-like growth factor 1 receptor, in patients with recurrent or refractory Ewing sarcoma family of tumors: results of a phase II Sarcoma Alliance for Research through Collaboration study." J Clin Oncol **29**(34): 4541-4547.

Pappo, A. S., S. R. Patel, J. Crowley, D. K. Reinke, K. P. Kuenkele, S. P. Chawla, G. C. Toner, R. G. Maki, P. A. Meyers, R. Chugh, K. N. Ganjoo, S. M. Schuetze, H. Juergens, M. G. Leahy, B. Geoerger, R. S. Benjamin, L. J. Helman and L. H. Baker (2011). "R1507, a monoclonal antibody to the insulin-like growth factor 1 receptor, in patients with recurrent or refractory Ewing sarcoma family of tumors: results of a phase II Sarcoma Alliance for Research through Collaboration study." J Clin Oncol **29**(34): 4541-4547.

Parkin, D., C. Stiller and J. Nectoux (1993). "International variations in the incidence of childhood bone tumours." Int J Cancer **53**(3): 371-376.

Pavlicek, A., M. E. Lira, N. V. Lee, K. A. Ching, J. Ye, J. Cao, S. J. Garza, K. E. Hook, M. Ozeck, S. T. Shi, J. Yuan, X. Zheng, P. A. Rejto, J. L. Kan and J. G. Christensen (2013). "Molecular Predictors of Sensitivity to the Insulin-like Growth Factor 1 Receptor Inhibitor, Figitumumab (CP-751,871)." Mol Cancer Ther.

Pawley, J. Points, pixels, and gray levels: digitizing image data. Handbook of Biological Confocal Microscopy, Springer-Verlag New York**:** 59-70.

Pelkmans, L. (2012). "Cell Biology. Using cell-to-cell variability--a new era in molecular biology." Science **336**(6080): 425-426.

Peter, M., J. Couturier, H. Pacquement, J. Michon, G. Thomas, H. Magdelenat and O. Delattre (1997). "A new member of the ETS family fused to EWS in Ewing tumors." Oncogene **14**(10): 1159-1164.

Peto, J., N. Collins, R. Barfoot, S. Seal, W. Warren, N. Rahman, D. F. Easton, C. Evans, J. Deacon and M. R. Stratton (1999). "Prevalence of BRCA1 and BRCA2 gene mutations in patients with early-onset breast cancer." J Natl Cancer Inst **91**(11): 943-949.

Pitts, T. M., A. C. Tan, G. N. Kulikowski, J. J. Tentler, A. M. Brown, S. A. Flanigan, S. Leong, C. D. Coldren, F. R. Hirsch, M. Varella-Garcia, C. Korch and S. G. Eckhardt (2010). "Development of an integrated genomic classifier for a novel agent in colorectal cancer: approach to individualized therapy in early development." Clin Cancer Res **16**(12): 3193-3204.

Ponti, D., A. Costa, N. Zaffaroni, G. Pratesi, G. Petrangolini, D. Coradini, S. Pilotti, M. A. Pierotti and M. G. Daidone (2005). "Isolation and in vitro propagation of tumorigenic breast cancer cells with stem/progenitor cell properties." Cancer Res **65**(13): 5506-5511.

Postel-Vinay, S., A. S. Véron, F. Tirode, G. Pierron, S. Reynaud, H. Kovar, O. Oberlin, E. Lapouble, S. Ballet, C. Lucchesi, U. Kontny, A. González-Neira, P. Picci, J. Alonso, A. Patino-Garcia, B. B. de Paillerets, K. Laud, C. Dina, P. Froguel, F. Clavel-Chapelon, F. Doz, J. Michon, S. J. Chanock, G. Thomas, D. G. Cox and O. Delattre (2012). "Common variants near TARDBP and EGR2 are associated with susceptibility to Ewing sarcoma." Nat Genet **44**(3): 323-327.

Potikyan, G., K. France, M. Carlson, J. Dong, S. Nelson and C. Denny (2008). "Genetically defined EWS/FLI1 model system suggests mesenchymal origin of Ewing's family tumors." Lab Invest **88**(12): 1291-1302.

Potratz, J. C., D. N. Saunders, D. H. Wai, T. L. Ng, S. E. McKinney, J. M. Carboni, M. M. Gottardis, T. J. Triche, H. Jürgens, M. N. Pollak, S. A. Aparicio and P. H. Sorensen (2010). "Synthetic lethality screens reveal RPS6 and MST1R as modifiers of insulin-like growth factor-1 receptor inhibitor activity in childhood sarcomas." Cancer Res **70**(21): 8770-8781.

Poulikakos, P. I. and N. Rosen (2011). "Mutant BRAF melanomas--dependence and resistance." Cancer Cell **19**(1): 11-15.

Prieur, A., F. Tirode, P. Cohen and O. Delattre (2004). "EWS/FLI-1 silencing and gene profiling of Ewing cells reveal downstream oncogenic pathways and a crucial role for repression of insulin-like growth factor binding protein 3." Mol Cell Biol **24**(16): 7275-7283.

Rajalingam, K., R. Schreck, U. R. Rapp and S. Albert (2007). "Ras oncogenes and their downstream targets." Biochim Biophys Acta **1773**(8): 1177-1195.

Redmond, K. M., T. R. Wilson, P. G. Johnston and D. B. Longley (2008). "Resistance mechanisms to cancer chemotherapy." Front Biosci **13**: 5138-5154.

Riggi, N., L. Cironi, P. Provero, M. Suvà, K. Kaloulis, C. Garcia-Echeverria, F. Hoffmann, A. Trumpp and I. Stamenkovic (2005). "Development of Ewing's sarcoma from primary bone marrow-derived mesenchymal progenitor cells." Cancer Res **65**(24): 11459-11468.

Riggi, N., L. Cironi, M. Suvà and I. Stamenkovic (2007). "Sarcomas: genetics, signalling, and cellular origins. Part 1: The fellowship of TET." J Pathol **213**(1): 4-20.

Riggi, N., M. Suvà, C. De Vito, P. Provero, J. Stehle, K. Baumer, L. Cironi, M. Janiszewska, T. Petricevic, D. Suvà, S. Tercier, J. Joseph, L. Guillou and I. Stamenkovic (2010). "EWS-FLI-1 modulates miRNA145 and SOX2 expression to initiate mesenchymal stem cell reprogramming toward Ewing sarcoma cancer stem cells." Genes Dev **24**(9): 916-932.

Riggi, N., M. Suvà, D. Suvà, L. Cironi, P. Provero, S. Tercier, J. Joseph, J. Stehle, K. Baumer, V. Kindler and I. Stamenkovic (2008). "EWS-FLI-1 expression triggers a Ewing's sarcoma initiation program in primary human mesenchymal stem cells." Cancer Res **68**(7): 2176-2185.

Rikhof, B., S. de Jong, A. Suurmeijer, C. Meijer and W. van der Graaf (2009). "The insulin-like growth factor system and sarcomas." J Pathol **217**(4): 469-482.

Riley, R., S. Burchill, K. Abrams, D. Heney, A. Sutton, D. Jones, P. Lambert, B. Young, A. Wailoo and I. Lewis (2003). "A systematic review of molecular and biological markers in tumours of the Ewing's sarcoma family." Eur J Cancer **39**(1): 19-30.

Roundhill, E. and S. Burchill (2013). "Membrane expression of MRP-1, but not MRP-1 splicing or Pgp expression, predicts survival in patients with ESFT." Br J Cancer **109**(1): 195-206.

Saini, M., A. N. Jha, A. Abrari and S. Ali (2012). "Expression of proto-oncogene KIT is up-regulated in subset of human meningiomas." BMC Cancer **12**: 212.

Sandison, D. and W. Webb (1994). Background rejection and signal-to-noise optimization in the confocal and alternative fluorescence microscopes. Applied Optics. **33:** 603-610.

Sanger, F., S. Nicklen and A. R. Coulson (1977). "DNA sequencing with chain-terminating inhibitors." Proc Natl Acad Sci U S A **74**(12): 5463-5467.

Santo, E. E., M. E. Ebus, J. Koster, J. H. Schulte, A. Lakeman, P. van Sluis, J. Vermeulen, D. Gisselsson, I. Øra, S. Lindner, P. G. Buckley, R. L. Stallings, J. Vandesompele, A. Eggert, H. N. Caron, R. Versteeg and J. J. Molenaar (2012). "Oncogenic activation of FOXR1 by 11q23 intrachromosomal deletion-fusions in neuroblastoma." Oncogene **31**(12): 1571-1581.

Sapkota, Y., J. R. Mackey, R. Lai, C. Franco-Villalobos, S. Lupichuk, P. J. Robson, K. Kopciuk, C. E. Cass, Y. Yasui and S. Damaraju (2013). "Assessing SNP-SNP interactions among DNA repair, modification and metabolism related pathway genes in breast cancer susceptibility." PLoS One **8**(6): e64896.

Schubert, W., B. Bonnekoh, A. J. Pommer, L. Philipsen, R. Bockelmann, Y. Malykh, H. Gollnick, M. Friedenberger, M. Bode and A. W. Dress (2006). "Analyzing proteome topology and function by automated multidimensional fluorescence microscopy." Nat Biotechnol **24**(10): 1270-1278.

Schutte, M., R. H. Hruban, J. Geradts, R. Maynard, W. Hilgers, S. K. Rabindran, C. A. Moskaluk, S. A. Hahn, I. Schwarte-Waldhoff, W. Schmiegel, S. B. Baylin, S. E. Kern and J. G. Herman (1997). "Abrogation of the Rb/p16 tumor-suppressive pathway in virtually all pancreatic carcinomas." Cancer Res **57**(15): 3126-3130.

Scotlandi, K., S. Benini, P. Nanni, P. L. Lollini, G. Nicoletti, L. Landuzzi, M. Serra, M. C. Manara, P. Picci and N. Baldini (1998). "Blockage of insulin-like growth factor-I receptor inhibits the growth of Ewing's sarcoma in athymic mice." Cancer Res **58**(18): 4127-4131.

Scotlandi, K., S. Benini, M. Sarti, M. Serra, P. Lollini, D. Maurici, P. Picci, M. Manara and N. Baldini (1996). "Insulin-like growth factor I receptor-mediated circuit in Ewing's sarcoma/peripheral neuroectodermal tumor: a possible therapeutic target." Cancer Res **56**(20): 4570-4574.

Scotlandi, K., S. Perdichizzi, M. C. Manara, M. Serra, S. Benini, V. Cerisano, R. Strammiello, M. Mercuri, G. Reverter-Branchat, G. Faircloth, M. D'Incalci and P. Picci (2002). "Effectiveness of Ecteinascidin-743 against drug-sensitive and -resistant bone tumor cells." Clin Cancer Res **8**(12): 3893-3903.

Scotlandi, K., D. Remondini, G. Castellani, M. C. Manara, F. Nardi, L. Cantiani, M. Francesconi, M. Mercuri, A. M. Caccuri, M. Serra, S. Knuutila and P. Picci (2009). "Overcoming resistance to conventional drugs in Ewing sarcoma and identification of molecular predictors of outcome." J Clin Oncol **27**(13): 2209-2216.

Seddon, B. and J. Whelan (2008). "Emerging chemotherapeutic strategies and the role of treatment stratification in Ewing sarcoma." Paediatr Drugs **10**(2): 93-105.

Sengupta, A., M. Rahman, S. Mateo-Lozano, O. M. Tirado and V. Notario (2013). "The dual inhibitory effect of thiostrepton on FoxM1 and EWS/FLI1 provides a novel therapeutic option for Ewing's sarcoma." Int J Oncol **43**(3): 803-812.

Shah, N. P., J. M. Nicoll, B. Nagar, M. E. Gorre, R. L. Paquette, J. Kuriyan and C. L. Sawyers (2002). "Multiple BCR-ABL kinase domain mutations confer polyclonal resistance to the tyrosine kinase inhibitor imatinib (STI571) in chronic phase and blast crisis chronic myeloid leukemia." Cancer Cell **2**(2): 117-125.

Shah, N. P., C. Tran, F. Y. Lee, P. Chen, D. Norris and C. L. Sawyers (2004). "Overriding imatinib resistance with a novel ABL kinase inhibitor." Science **305**(5682): 399-401.

Sharma, S. V., D. Y. Lee, B. Li, M. P. Quinlan, F. Takahashi, S. Maheswaran, U. McDermott, N. Azizian, L. Zou, M. A. Fischbach, K. K. Wong, K. Brandstetter, B. Wittner, S. Ramaswamy, M. Classon and J. Settleman (2010). "A chromatin-mediated reversible drug-tolerant state in cancer cell subpopulations." Cell **141**(1): 69-80.

Shinawi, M. and S. W. Cheung (2008). "The array CGH and its clinical applications." Drug Discov Today **13**(17-18): 760-770.

Shukla, S., Z. S. Chen and S. V. Ambudkar (2012). "Tyrosine kinase inhibitors as modulators of ABC transporter-mediated drug resistance." Drug Resist Updat **15**(1-2): 70-80.

Siddle, K. (2011). "Signalling by insulin and IGF receptors: supporting acts and new players." J Mol Endocrinol **47**(1): R1-10.

Sircoulomb, F., I. Bekhouche, P. Finetti, J. Adélaïde, A. Ben Hamida, J. Bonansea, S. Raynaud, C. Innocenti, E. Charafe-Jauffret, C. Tarpin, F. Ben Ayed, P. Viens, J. Jacquemier, F. Bertucci, D. Birnbaum and M. Chaffanet (2010). "Genome profiling of ERBB2-amplified breast cancers." BMC Cancer **10**: 539.

Slamon, D. J., W. Godolphin, L. A. Jones, J. A. Holt, S. G. Wong, D. E. Keith, W. J. Levin, S. G. Stuart, J. Udove and A. Ullrich (1989). "Studies of the HER-2/neu proto-oncogene in human breast and ovarian cancer." Science **244**(4905): 707-712.

Slamon, D. J., B. Leyland-Jones, S. Shak, H. Fuchs, V. Paton, A. Bajamonde, T. Fleming, W. Eiermann, J. Wolter, M. Pegram, J. Baselga and L. Norton (2001). "Use of chemotherapy plus a monoclonal antibody against HER2 for metastatic breast cancer that overexpresses HER2." N Engl J Med **344**(11): 783-792.

Smith, R., L. A. Owen, D. J. Trem, J. S. Wong, J. S. Whangbo, T. R. Golub and S. L. Lessnick (2006). "Expression profiling of EWS/FLI identifies NKX2.2 as a critical target gene in Ewing's sarcoma." Cancer Cell **9**(5): 405-416.

Smolen, G. A., R. Sordella, B. Muir, G. Mohapatra, A. Barmettler, H. Archibald, W. J. Kim, R. A. Okimoto, D. W. Bell, D. C. Sgroi, J. G. Christensen, J. Settleman and D. A. Haber (2006). "Amplification of MET may identify a subset of cancers with extreme sensitivity to the selective tyrosine kinase inhibitor PHA-665752." Proc Natl Acad Sci U S A **103**(7): 2316-2321.

Soda, M., Y. L. Choi, M. Enomoto, S. Takada, Y. Yamashita, S. Ishikawa, S. Fujiwara, H. Watanabe, K. Kurashina, H. Hatanaka, M. Bando, S. Ohno, Y. Ishikawa, H. Aburatani, T. Niki, Y. Sohara, Y. Sugiyama and H. Mano (2007). "Identification of the transforming EML4-ALK fusion gene in non-small-cell lung cancer." Nature **448**(7153): 561-566.

Solomon, D. A., T. Kim, L. A. Diaz-Martinez, J. Fair, A. G. Elkahloun, B. T. Harris, J. A. Toretsky, S. A. Rosenberg, N. Shukla, M. Ladanyi, Y. Samuels, C. D. James, H. Yu, J. S. Kim and T. Waldman (2011). "Mutational inactivation of STAG2 causes aneuploidy in human cancer." Science **333**(6045): 1039-1043.

Sorensen, P. H., S. L. Lessnick, D. Lopez-Terrada, X. F. Liu, T. J. Triche and C. T. Denny (1994). "A second Ewing's sarcoma translocation, t(21;22), fuses the EWS gene to another ETS-family transcription factor, ERG." Nat Genet **6**(2): 146-151.

Sprouffske, K., L. M. Merlo, P. J. Gerrish, C. C. Maley and P. D. Sniegowski (2012). "Cancer in light of experimental evolution." Curr Biol **22**(17): R762-771.

Srivastava, R. K., A. R. Srivastava and Y. S. Cho-Chung (1998). "Synergistic effects of 8-chlorocyclic-AMP and retinoic acid on induction of apoptosis in Ewing's sarcoma CHP-100 cells." Clin Cancer Res **4**(3): 755-761.

Staege, M., C. Hutter, I. Neumann, S. Foja, U. Hattenhorst, G. Hansen, D. Afar and S. Burdach (2004). "DNA microarrays reveal relationship of Ewing family tumors to both endothelial and fetal neural crest-derived cells and define novel targets." Cancer Res **64**(22): 8213-8221.

Stephens, P. J., D. J. McBride, M. L. Lin, I. Varela, E. D. Pleasance, J. T. Simpson, L. A. Stebbings, C. Leroy, S. Edkins, L. J. Mudie, C. D. Greenman, M. Jia, C. Latimer, J. W. Teague, K. W. Lau, J. Burton, M. A. Quail, H. Swerdlow, C. Churcher, R. Natrajan, A. M. Sieuwerts, J. W. Martens, D. P. Silver, A. Langerød, H. E. Russnes, J. A. Foekens, J. S. Reis-Filho, L. van 't Veer, A. L. Richardson, A. L. Børresen-Dale, P. J. Campbell, P. A. Futreal and M. R. Stratton (2009). "Complex landscapes of somatic rearrangement in human breast cancer genomes." Nature **462**(7276): 1005-1010.

Stiller, C., S. Bielack, G. Jundt and E. Steliarova-Foucher (2006). "Bone tumours in European children and adolescents, 1978-1997. Report from the Automated Childhood Cancer Information System project." Eur J Cancer **42**(13): 2124-2135.

Stratton, J. F., S. A. Gayther, P. Russell, J. Dearden, M. Gore, P. Blake, D. Easton and B. A. Ponder (1997). "Contribution of BRCA1 mutations to ovarian cancer." N Engl J Med **336**(16): 1125-1130.

Sugita, T., H. Aya, M. Ueno, T. Ishizuka and K. Kawashima (1997). "Characterization of molecularly cloned human 5-aminoimidazole-4-carboxamide ribonucleotide transformylase." J Biochem **122**(2): 309-313.

Suh, C. H., N. G. Ordóñez, J. Hicks and B. Mackay (2002). "Ultrastructure of the Ewing's sarcoma family of tumors." Ultrastruct Pathol **26**(2): 67-76.

Sultan, M., M. H. Schulz, H. Richard, A. Magen, A. Klingenhoff, M. Scherf, M. Seifert, T. Borodina, A. Soldatov, D. Parkhomchuk, D. Schmidt, S. O'Keeffe, S. Haas, M. Vingron, H. Lehrach and M. L. Yaspo (2008). "A global view of gene activity and alternative splicing by deep sequencing of the human transcriptome." Science **321**(5891): 956-960.

Suvà, M. L., N. Riggi, J. C. Stehle, K. Baumer, S. Tercier, J. M. Joseph, D. Suvà, V. Clément, P. Provero, L. Cironi, M. C. Osterheld, L. Guillou and I. Stamenkovic (2009). "Identification of cancer stem cells in Ewing's sarcoma." Cancer Res **69**(5): 1776-1781.

Szakács, G., J. P. Annereau, S. Lababidi, U. Shankavaram, A. Arciello, K. J. Bussey, W. Reinhold, Y. Guo, G. D. Kruh, M. Reimers, J. N. Weinstein and M. M. Gottesman (2004). "Predicting drug sensitivity and resistance: profiling ABC transporter genes in cancer cells." Cancer Cell **6**(2): 129-137.

Szakács, G., J. K. Paterson, J. A. Ludwig, C. Booth-Genthe and M. M. Gottesman (2006). "Targeting multidrug resistance in cancer." Nat Rev Drug Discov **5**(3): 219-234.

Takahasi, K. R., Y. Sakuraba and Y. Gondo (2007). "Mutational pattern and frequency of induced nucleotide changes in mouse ENU mutagenesis." BMC Mol Biol **8**: 52.

Takigami, I., T. Ohno, Y. Kitade, A. Hara, A. Nagano, G. Kawai, M. Saitou, A. Matsuhashi, K. Yamada and K. Shimizu (2011). "Synthetic siRNA targeting the breakpoint of EWS/Fli-1 inhibits growth of Ewing sarcoma xenografts in a mouse model." Int J Cancer **128**(1): 216-226.

Tallman, M. S., J. W. Andersen, C. A. Schiffer, F. R. Appelbaum, J. H. Feusner, W. G. Woods, A. Ogden, H. Weinstein, L. Shepherd, C. Willman, C. D. Bloomfield, J. M. Rowe and P. H. Wiernik (2002). "All-trans retinoic acid in acute promyelocytic leukemia: long-term outcome and prognostic factor analysis from the North American Intergroup protocol." Blood **100**(13): 4298-4302.

Tap, W. D., G. Demetri, P. Barnette, J. Desai, P. Kavan, R. Tozer, P. W. Benedetto, G. Friberg, H. Deng, I. McCaffery, I. Leitch, S. Badola, S. Chang, M. Zhu and A. Tolcher (2012). "Phase II study of ganitumab, a fully human anti-type-1 insulin-like growth factor receptor antibody, in patients with metastatic Ewing family tumors or desmoplastic small round cell tumors." J Clin Oncol **30**(15): 1849-1856.

Therrien, M., A. M. Wong and G. M. Rubin (1998). "CNK, a RAF-binding multidomain protein required for RAS signaling." Cell **95**(3): 343-353.

Thompson, A., M. Teitell, A. Arvand and C. Denny (1999). "Divergent Ewing's sarcoma EWS/ETS fusions confer a common tumorigenic phenotype on NIH3T3 cells." Oncogene **18**(40): 5506-5513.

Tirode, F., K. Laud-Duval, A. Prieur, B. Delorme, P. Charbord and O. Delattre (2007). "Mesenchymal stem cell features of Ewing tumors." Cancer Cell **11**(5): 421-429.

Torchia, E., K. Boyd, J. Rehg, C. Qu and S. Baker (2007). "EWS/FLI-1 induces rapid onset of myeloid/erythroid leukemia in mice." Mol Cell Biol **27**(22): 7918-7934.

Torchia, E. C., S. Jaishankar and S. J. Baker (2003). "Ewing tumor fusion proteins block the differentiation of pluripotent marrow stromal cells." Cancer Res **63**(13): 3464-3468.

Toretsky, J., T. Kalebic, V. Blakesley, D. LeRoith and L. Helman (1997). "The insulin-like growth factor-I receptor is required for EWS/FLI-1 transformation of fibroblasts." J Biol Chem **272**(49): 30822-30827.

Turc-Carel, C., I. Philip, M. Berger, T. Philip and G. Lenoir (1983). "[Chromosomal translocation (11; 22) in cell lines of Ewing's sarcoma]." C R Seances Acad Sci III **296**(23): 1101-1103.

Turtoi, A., A. Blomme, D. Debois, J. Somja, D. Delvaux, G. Patsos, E. Di Valentin, O. Peulen, E. N. Mutijima, E. De Pauw, P. Delvenne, O. Detry and V. Castronovo (2013). "Organized proteomic heterogeneity in colorectal cancer liver metastases and implications for therapies." Hepatology.

Ulahannan, D., M. B. Kovac, P. J. Mulholland, J. B. Cazier and I. Tomlinson (2013). "Technical and implementation issues in using next-generation sequencing of cancers in clinical practice." Br J Cancer.

Ulanet, D. B., D. L. Ludwig, C. R. Kahn and D. Hanahan (2010). "Insulin receptor functionally enhances multistage tumor progression and conveys intrinsic resistance to IGF-1R targeted therapy." Proc Natl Acad Sci U S A **107**(24): 10791-10798.

van Maldegem, A. M., P. C. Hogendoorn and A. B. Hassan (2012). "The clinical use of biomarkers as prognostic factors in Ewing sarcoma." Clin Sarcoma Res **2**(1): 7.

Vandesompele, J., K. De Preter, F. Pattyn, B. Poppe, N. Van Roy, A. De Paepe and F. Speleman (2002). "Accurate normalization of real-time quantitative RT-PCR data by geometric averaging of multiple internal control genes." Genome Biol **3**(7): RESEARCH0034.

Vogelstein, B. and K. W. Kinzler (2004). "Cancer genes and the pathways they control." Nat Med **10**(8): 789-799.

von Bubnoff, N., D. R. Veach, H. van der Kuip, W. E. Aulitzky, J. Sänger, P. Seipel, W. G. Bornmann, C. Peschel, B. Clarkson and J. Duyster (2005). "A cell-based screen for resistance of Bcr-Abl-positive leukemia identifies the mutation pattern for PD166326, an alternative Abl kinase inhibitor." Blood **105**(4): 1652-1659.

Waters, J. and S. JR (2008). Interpreting Fluorescence Microscopy Images and Measurements. Cell Press**:** 37-42.

Webb, T. R., J. Slavish, R. E. George, A. T. Look, L. Xue, Q. Jiang, X. Cui, W. B. Rentrop and S. W. Morris (2009). "Anaplastic lymphoma kinase: role in cancer pathogenesis and small-molecule inhibitor development for therapy." Expert Rev Anticancer Ther **9**(3): 331-356.

Weir, B. A., M. S. Woo, G. Getz, S. Perner, L. Ding, R. Beroukhim, W. M. Lin, M. A. Province, A. Kraja, L. A. Johnson, K. Shah, M. Sato, R. K. Thomas, J. A. Barletta, I. B. Borecki, S. Broderick, A. C. Chang, D. Y. Chiang, L. R. Chirieac, J. Cho, Y. Fujii, A. F. Gazdar, T. Giordano, H. Greulich, M. Hanna, B. E. Johnson, M. G. Kris, A. Lash, L. Lin, N. Lindeman, E. R. Mardis, J. D. McPherson, J. D. Minna, M. B. Morgan, M. Nadel, M. B. Orringer, J. R. Osborne, B.

Ozenberger, A. H. Ramos, J. Robinson, J. A. Roth, V. Rusch, H. Sasaki, F. Shepherd, C. Sougnez, M. R. Spitz, M. S. Tsao, D. Twomey, R. G. Verhaak, G. M. Weinstock, D. A. Wheeler, W. Winckler, A. Yoshizawa, S. Yu, M. F. Zakowski, Q. Zhang, D. G. Beer, I. I. Wistuba, M. A. Watson, L. A. Garraway, M. Ladanyi, W. D. Travis, W. Pao, M. A. Rubin, S. B. Gabriel, R. A. Gibbs, H. E. Varmus, R. K. Wilson, E. S. Lander and M. Meyerson (2007). "Characterizing the cancer genome in lung adenocarcinoma." Nature **450**(7171): 893-898.

Weisberg, E., P. W. Manley, W. Breitenstein, J. Brüggen, S. W. Cowan-Jacob, A. Ray, B. Huntly, D. Fabbro, G. Fendrich, E. Hall-Meyers, A. L. Kung, J. Mestan, G. Q. Daley, L. Callahan, L. Catley, C. Cavazza, M. Azam, A. Mohammed, D. Neuberg, R. D. Wright, D. G. Gilliland and J. D. Griffin (2005). "Characterization of AMN107, a selective inhibitor of native and mutant Bcr-Abl." Cancer Cell **7**(2): 129-141.

Witkiewicz, A. K., K. E. Knudsen, A. P. Dicker and E. S. Knudsen (2011). "The meaning of p16(ink4a) expression in tumors: functional significance, clinical associations and future developments." Cell Cycle **10**(15): 2497-2503.

Xu, X., Y. Hou, X. Yin, L. Bao, A. Tang, L. Song, F. Li, S. Tsang, K. Wu, H. Wu, W. He, L. Zeng, M. Xing, R. Wu, H. Jiang, X. Liu, D. Cao, G. Guo, X. Hu, Y. Gui, Z. Li, W. Xie, X. Sun, M. Shi, Z. Cai, B. Wang, M. Zhong, J. Li, Z. Lu, N. Gu, X. Zhang, L. Goodman, L. Bolund, J. Wang, H. Yang, K. Kristiansen, M. Dean and Y. Li (2012). "Single-cell exome sequencing reveals single-nucleotide mutation characteristics of a kidney tumor." Cell **148**(5): 886-895.

Xu, X., Y. Hou, X. Yin, L. Bao, A. Tang, L. Song, F. Li, S. Tsang, K. Wu, H. Wu, W. He, L. Zeng, M. Xing, R. Wu, H. Jiang, X. Liu, D. Cao, G. Guo, X. Hu, Y. Gui, Z. Li, W. Xie, X. Sun, M. Shi, Z. Cai, B. Wang, M. Zhong, J. Li, Z. Lu, N. Gu, X. Zhang, L. Goodman, L. Bolund, J. Wang, H. Yang, K. Kristiansen, M. Dean and Y. Li (2012). "Single-cell exome sequencing reveals single-nucleotide mutation characteristics of a kidney tumor." Cell **148**(5): 886-895.

Yang, M., R. Zhang, M. Yan, Z. Ye, W. Liang and Z. Luo (2010). "Detection and characterization of side population in Ewing's sarcoma SK-ES-1 cells in vitro." Biochem Biophys Res Commun **391**(1): 1062-1066.

Yao, I., Y. Hata, N. Ide, K. Hirao, M. Deguchi, H. Nishioka, A. Mizoguchi and Y. Takai (1999). "MAGUIN, a novel neuronal membrane-associated guanylate kinase-interacting protein." J Biol Chem **274**(17): 11889-11896.

Yap, T. A., M. Gerlinger, P. A. Futreal, L. Pusztai and C. Swanton (2012). "Intratumor heterogeneity: seeing the wood for the trees." Sci Transl Med **4**(127): 127ps110.

Yotov, W. V. and R. St-Arnaud (1996). "Differential splicing-in of a proline-rich exon converts alphaNAC into a muscle-specific transcription factor." Genes Dev **10**(14): 1763-1772.

Yuan, T. L., G. Wulf, L. Burga and L. C. Cantley (2011). "Cell-to-cell variability in PI3K protein level regulates PI3K-AKT pathway activity in cell populations." Curr Biol **21**(3): 173-183.

Zeng, X., H. Zhang, A. Oh, Y. Zhang and D. Yee (2011). "Enhancement of doxorubicin cytotoxicity of human cancer cells by tyrosine kinase inhibition of insulin receptor and type I IGF receptor." Breast Cancer Res Treat.

Zhang, S., F. Wang, J. Keats, X. Zhu, Y. Ning, S. D. Wardwell, L. Moran, Q. K. Mohemmad, R. Anjum, Y. Wang, N. I. Narasimhan, D. Dalgarno, W. C. Shakespeare, J. J. Miret, T. Clackson and V. M. Rivera (2011). "Crizotinib-resistant mutants of EML4-ALK identified through an accelerated mutagenesis screen." Chem Biol Drug Des **78**(6): 999-1005.

Ziogas, A., K. Moelling and G. Radziwill (2005). "CNK1 is a scaffold protein that regulates Src-mediated Raf-1 activation." J Biol Chem **280**(25): 24205-24211.

Zoubek, A., B. Dockhorn-Dworniczak, O. Delattre, H. Christiansen, F. Niggli, I. Gatterer-Menz, T. Smith, H. Jürgens, H. Gadner and H. Kovar (1996). "Does expression of different EWS chimeric transcripts define clinically distinct risk groups of Ewing tumor patients?" J Clin Oncol **14**(4): 1245-1251.